

**Establishment and regulation
of polar growth in *Streptomyces***

By

Antje Marie Hempel

2012

John Innes Centre
Department of Molecular Microbiology
Norwich Research Park, Colney Lane, Norwich NR4 7UH
United Kingdom

**Thesis submitted to the University of East Anglia for the degree of
Doctor of Philosophy**

©This copy of the Thesis has been supplied on condition that anyone who consults it is understood to recognise that its copyright rests with the author and that neither quotation from this thesis, nor any information derived therefrom, may be published without the author's prior, written consent.

Acknowledgements

It was a fantastic experience to work in the productive and stimulating environment of the John Innes Centre and I would like to express my sincere thanks to all people, who have turned these 3.5 years into such a wonderful time.

First of all, I would like to thank Prof. Dr. Mark Buttner, John Innes Centre, and Dr. Klas Flärdh, Lund University, Sweden, for being such fantastic supervisors and mentors. Thank you very much for your guidance, encouragement and support during these past years and into my next career stage. Mark, thank you very much for everything, for the freedom to continue to work on a project I love and your constant support during the good and the “not-so-good” times of the past years. It was a tremendous joy and pleasure to work in your group and I am very sad to leave – without even entering the hot lab once! All this would not have happened if it was not for you, Klas. You introduced me to the *Streptomyces* world during my Master project in your lab and I am very grateful to you that you allowed me to take the DivIVA phosphorylation story with me to Norwich to finish it up. Now I am ready to leave this *Streptomyces* world with “a laughing and a crying eye” (as Germans would say). It was truly a fantastic time and I will miss you and *Streptomyces* very much.

I would like to thank my supervisory committee, Prof. Dr. Martin Howard and Prof. Dr. Liam Dolan, as well as Prof. Dr. Mervyn Bibb, Prof. Dr. Keith Chater and Prof. Dr. Sir David Hopwood for fruitful discussions and invaluable advice during the course of my PhD project.

Furthermore, I would like to thank our collaborators for essential experimental and technical support: Dr. Gerhard Saalbach and Dr. Mike Naldrett for help with mass spectrometry and proteomics; Dr. David Richards for a very exciting trip into biophysics; Dr. Virginie Molle and Jade Leiba for an incredible journey into the depth of protein phosphorylation; Dr. Stuart Cantlay for experimental support; Dr. Grant Calder for microscopy support.

I would like to thank the media kitchen staff for their hard work. It has been such a luxury to have all the media ready-made on the shelf or as a special order.

I would also like to thank past and present members of the *Streptomyces* group on and the Department of Molecular Microbiology for such a great time. Many, many thanks to Maureen Bibb for all your help and advice – inside and outside John Innes – and an always open ear. Now to you the cheering crowd: Emma Sherwood, my bench mates Tung Le and Matt Bush, Mahmoud Al-Bassam, Govind Chandra, Ngat Tran, Juan-Pablo Gomez-Escribano, Jason Terpolilli, Anyarat Thanapipatsiri (Jip), Jeremy Thornton, Morgan Feeney, Jürgen Prell, Chris den Hengst, Robert Bell, Jennifer Parker, Lucy Foulston and Jan Claessen and many more; thank you so much for useful discussions and technical help, friendship inside and outside the lab and of course the never-ending highly competitive *Streptomyces* badminton tournaments. I would like to thank my friends at the Biologihuset in Lund, Sweden: Jessica Larsson, Sebastian and Lisa Wasserström, Paola Salerno and Stuart Cantlay.

I am very grateful about the generous funding from the *Streptomyces* industrial account, the Biotechnology and Biological Sciences Research Council (BBSRC) Institute Strategic Programme Grant “Understanding and Exploiting Plant and Microbial Secondary Metabolism” (BB/J004596/1), the John Innes Foundation and Hardship Fund. Thank you very much.

Finally, I would like to thank my friends and my family for their constant help and support during the last years. Markus, over the years we have lived everywhere in Europe, but in England we had the most wonderful time of all. Without your love and patience and your endless support, our life would have never turned out the way it did and especially the past months would have been impossible to achieve. My dear little Johann; you are still so tiny, but you have been a textbook baby all the way through. Markus and Johann, you are both wonderful and I love you both!

This thesis is especially dedicated to the loving memory of
my grandmother, Marie Wollkopf (1910 – 2010) and
my grandfather-in-law, Werner Auerswald (1919 – 2012).

Antje Marie Hempel

Abstract

A fundamental question in developmental biology is how cells establish polarity, and most strikingly how cells grow polarly. From neuronal dendrites and root hairs to bud emergence and elongation of yeast, broadly conserved pathways control cell polarity in eukaryotes. In contrast, virtually nothing is known about the regulatory mechanisms controlling polar cell growth in prokaryotes. In evolutionary terms, the most ancient form of polar growth is found in the branching hyphae of the filamentous bacteria *Streptomyces*, and it is clear that the essential coiled-coil protein DivIVA, which forms part of a tip-organising, multi-protein polarisome complex, plays a key role in the control of cell polarity, apical growth and hyphal branching in *Streptomyces coelicolor*. I identified and characterised two regulatory mechanisms, both reminiscent of aspects of cell polarity control in eukaryotes.

First, I show that the mechanistic basis of branch-site selection during hyphal growth in *Streptomyces* is a novel polarisome splitting mechanism, in which the apical tip polarisome splits to leave behind a small daughter polarisome on the lateral membrane as the tip grows away. This daughter polarisome gradually grows in size, and ultimately initiates the outgrowth of a new branch.

Second, I show that the Ser/Thr protein kinase AfsK is part of an apparatus that controls the polarisome complex at the hyphal tip. Activated AfsK directly phosphorylates DivIVA and profoundly alters the subcellular localisation of DivIVA to establish multiple new sites of polar growth. Thereby, AfsK modulates apical growth and lateral branching during normal growth and cell wall stress. I suggest that this is part of a stress response that provides *Streptomyces* with a mechanism to dismantle the apical growth apparatus at established hyphal tips that encounter problems with cell wall synthesis (for example through exposure to an antibiotic or by hitting a physical obstacle in the soil) and instead direct emergence of new branches elsewhere along the hyphae.

Publications (see Appendix)

Richards, D. M., A. M. Hempel*, K. Flärdh, M. J. Buttner & M. Howard, (2012)
Mechanistic basis of branch-site selection in filamentous bacteria. *PLoS Comput Biol* **8**: e1002423. *Joint first authors

Hempel, A. M., S. Cantlay, V. Molle, S. Wang, M. J. Naldrett, J. L. Parker, D. M. Richards, Y. G. Jung, M. J. Buttner, and K. Flärdh (2012). A Ser/Thr protein kinase regulates polar growth and hyphal branching in the filamentous bacteria *Streptomyces*. *Proc Natl Acad Sci USA* **109**: e2371-2379.

Table of Contents

Index of Tables, Figures and Equations	11
Abbreviations	15
Chapter 1 – Introduction	17
1.1 Cell polarity is universal in the kingdom of life	18
1.2 The complex life cycle of <i>Streptomyces</i>	19
1.2.1 General information about <i>Streptomyces</i> and its genome	19
1.2.2 The <i>Streptomyces</i> life cycle	20
1.3 Different modes of cell growth in bacteria	23
1.4 The bacterial cell wall	25
1.4.1 Cell wall composition of Gram-positive and Gram-negative bacteria	26
1.4.2 Peptidoglycan synthesis	28
1.4.3 Cell wall stress	30
1.5 The role of the bacterial cytoskeleton in cell wall growth	33
1.6 A special case: Polar growth in Actinobacteria	37
1.6.1 Polar growth in Actinobacteria is independent of MreB	37
1.6.2 A bacterial polarisome complex orchestrates apical growth	38
1.6.3 How is the polarity determinant DivIVA targeted to hyphal tips?	39
1.6.4 How is apical growth regulated?	44
1.6.5 What is the cell polarity system directing?	50
1.7 Aim of this thesis	52

Chapter 2 – Material and Methods	53
2.1 Bacterial strains and plasmids.....	55
2.1.1 <i>E. coli</i> strains	55
2.1.2 <i>S. coelicolor</i> strains	55
2.1.3 Plasmids	57
2.2 Growth conditions and storage of bacterial strains	58
2.2.1 <i>E. coli</i> strains	58
2.2.2 <i>S. coelicolor</i> strains	59
2.3 Culture media and antibiotics.....	60
2.3.1 Antibiotic concentrations for <i>E. coli</i> and <i>S. coelicolor</i>	60
2.3.2 Solid media	61
2.3.3 Liquid media	62
2.4 General Molecular Biology Methods.....	63
2.4.1 Plasmid DNA isolation from <i>E. coli</i>	63
2.4.2 Genomic DNA isolation from <i>S. coelicolor</i>	63
2.4.3 Agarose gel electrophoresis	64
2.4.4 DNA extraction from agarose gels	64
2.4.5 DNA digestion with restriction enzymes	64
2.4.6 Ligation	64
2.4.7 Preparation and transformation of electro-competent <i>E. coli</i>	65
2.4.8 Preparation and transformation of chemically competent <i>E. coli</i>	65
2.4.9 Interspecies conjugation from <i>E. coli</i> to <i>S. coelicolor</i>	66
2.5 PCR and Sanger sequencing	67
2.5.1 Oligonucleotides	67
2.5.2 General PCR	67
2.5.3 PCR for ABI-automated sequencing	68
2.6 Construction of plasmids and PCR-targeted mutagenesis	68
2.6.1 Construction of <i>S. coelicolor</i> kinase mutants	68
2.6.2 Complementation of the <i>afsK</i> mutant	69
2.6.3 Construction of an AfsK-mCherry fusion	69

Table of Contents

2.6.4	Construction of an allele encoding a constitutively active form of AfsK	70
2.6.5	Construction of pIJ10550	70
2.6.6	Construction of a <i>FLAG-divIVA</i> allele introducing two additional trypsin cleavage sites in the C-terminus	70
2.7	Protein experiments	71
2.7.1	Preparation of <i>S. coelicolor</i> cell extracts	71
2.7.2	Determination of protein concentration	72
2.7.3	Immunoprecipitation of FLAG-DivIVA	72
2.7.4	<i>In vitro</i> dephosphorylation of immunoprecipitated DivIVA	72
2.7.5	SDS-PAGE	73
2.7.6	ProQ-Diamond Staining of SDS-PA gels	73
2.7.7	Immunoblotting	74
2.7.8	<i>In vitro</i> phosphorylation of DivIVA	74
2.8	Proteomics	75
2.8.1	MALDI-ToF	75
2.8.2	Nano-HPLC MALDI-ToF	76
2.9	Microscopy	77
2.9.1	Light microscopy	77
2.9.2	Analysis of hyphal branching data from still images	78
2.9.3	Time-lapse microscopy	79
Chapter 3 – Mechanistic basis of branch-site selection in <i>Streptomyces</i>		80
3.1	Introduction	82
3.2	Lateral polarisomes arise from splitting of apical polarisomes	83
3.3	Measurements of hyphal growth and lateral branching	86
3.3.1	Tip growth speed	86
3.3.2	Controlling for biases	88
3.4	How far behind the hyphal tip do new branches form	89

3.5	Development of a minimal mathematical model describing the growth of polarisomes	91
3.6	The tip-to-branch distribution is regulated by one aspect of polarisome splitting	95
3.7	Verifying a prediction of the model concerning the tip-to-branch distribution	97
3.8	A different aspect of the polarisome splitting mechanism regulates the branch-to-branch distance	100
3.9	Full model: curvature-dependent polarisome splitting	104
3.10	Discussion	105
3.11	Summary Points	109

Chapter 4 – Polar growth in *Streptomyces* is regulated by a

	Ser/Thr protein kinase	110
4.1	Introduction	112
4.2	DivIVA phosphorylation increases dramatically when cell wall synthesis is blocked	113
4.3	Increased DivIVA phosphorylation upon cell envelope stress is not part of a general stress response	118
4.4	The C-terminal region of DivIVA is the target of multiple phosphorylations	120
4.5	DivIVA is not phosphorylated by PASTA-domain containing Ser/Thr protein kinases	123
4.6	The DivIVA protein kinase is AfsK	125
4.7	DivIVA is phosphorylated by AfsK <i>in vitro</i>	130
4.8	The AfsK kinase co-localises with its substrate DivIVA at the tips of growing vegetative hyphae	132
4.9	AfsK regulates the branching of growing hyphae	135

Table of Contents

4.10	Constitutively active AfsK mutant protein profoundly affects apical growth, DivIVA localisation, and hyphal branching	141
4.11	Discussion	146
4.12	Summary Points	150
Chapter 5 – Systematic characterisation of the Ser/Thr phosphorylation sites of the <i>Streptomyces</i> polarity determinant DivIVA using a combination of nano-LC and high-accuracy mass spectrometry		151
5.1	Introduction	153
5.2	MALDI-ToF mass spectrometric analysis of DivIVA phosphorylation	153
5.3	Introduction of two additional trypsin cleavage sites into the 7.2 kDa C-terminal peptide	157
5.4	Mapping the phosphorylation sites in the DivIVA C-terminus	159
5.5	Discussion and Conclusion	175
5.6	Summary Points	178
Chapter 6 – Discussion		179
References		184
Publications		201

Index of Tables, Figures and Equations

Chapter 1 – Introduction

Figure 1.1 Schematic representation of the complex developmental life cycle of <i>S. coelicolor</i>	22
Figure 1.2 Different modes of cell wall growth	24
Figure 1.3 Schematic of the different cell wall composition of Gram-negative and Gram-positive bacteria	27
Figure 1.4 Schematic of the important steps of peptidoglycan biosynthesis and inhibition of individual steps by antibiotics	29
Figure 1.5 The σ^E -CseABC signal transduction system in <i>S. coelicolor</i>	32
Figure 1.6 Prokaryotic MreB and FtsZ are structural homologues of the eukaryotic cytoskeletal elements actin and tubulin	35
Figure 1.7 Simple illustration of the assembly of the set of components of the cell wall biosynthetic machinery specific for cell elongation and division	36
Figure 1.8 Comparison of selected DivIVA homologues from different Gram-positive bacteria	43
Figure 1.9 Overview of 34 predicted Ser/Thr protein kinases in <i>S. coelicolor</i>	48
Figure 1.10 AfsR signal transduction cascade influences secondary metabolism in <i>S. coelicolor</i>	49

Chapter 2 – Material and Methods

Table 2.1 <i>E. coli</i> K12 strains used in this study	55
Table 2.2 <i>S. coelicolor</i> A3(2) strains used in this study	55
Table 2.3 Plasmids used in this study	57

Table 2.4 Antibiotic concentrations used in this study	60
Table 2.5 Solid media used in this study	61
Table 2.6 Liquid media used in this study	62
Table 2.7 Oligonucleotide primers used in this study	67
 Chapter 3 – Mechanistic basis of branch-site selection in <i>Streptomyces</i>	
Figure 3.1 Evidence of polarisome splitting, growth of polarisomes and emergence of branches, in fluorescence-imaged <i>S. coelicolor</i> expressing <i>divIVA-egfp</i>	85
Figure 3.2 Tip growth speed against time for established hyphae and newly formed branches from time-lapse imaging of <i>Streptomyces</i> hyphae	87
Figure 3.3 Histogram of tip-to-branch distribution of the experimental data at 80 μm trim	90
Equation 1	93
Table 3.1 Main parameters and their values	94
Figure 3.4 Comparison of histograms of tip-to-branch distribution between minimal model and experimental data at 80 μm trim	96
Figure 3.5 Comparison of tip-to-branch distribution at small distances between minimal model and experimental data at 80 μm trim	98
Figure 3.6 Example of branch development at almost zero distance from the hyphal tip in fluorescence-imaged <i>S. coelicolor</i> expressing <i>divIVA-egfp</i> ..	99
Equation 2	102
Figure 3.7 Comparison of histograms of the branch-to-branch distribution between minimal model and experimental data at 80 μm trim	103
Figure 3.8 Schematic of colony morphology for various values of the binding parameter (β)	107
Figure 3.9 Two very different aspects of polarisome splitting regulate branch development in <i>Streptomyces</i>	108

Chapter 4 – Polar growth in *Streptomyces* is regulated by a Ser/Thr protein kinase

Figure 4.1 DivIVA is post-translationally regulated by phosphorylation	115
Figure 4.2 DivIVA is subject to increased phosphorylation specifically upon inhibition of cell wall synthesis	117
Figure 4.3 Increased DivIVA phosphorylation is not part of a general stress response	119
Figure 4.4 <i>S. coelicolor</i> DivIVA is multiply phosphorylated in the C-terminal region	121
Figure 4.5 DivIVA is not phosphorylated by PASTA domain-containing Ser/Thr protein kinases	124
Table 4.1 Overview of the 17 predicted Ser/Thr protein kinases in <i>S. coelicolor</i> that were tested for their involvement DivIVA phosphorylation	126
Figure 4.6 DivIVA is not phosphorylated by several Ser/Thr protein kinases	127
Figure 4.7 The DivIVA kinase is AfsK	128
Figure 4.8 <i>In vitro</i> phosphorylation of DivIVA by AfsK	131
Figure 4.9 The DivIVA kinase AfsK localises to hyphal tips	133
Figure 4.10 The <i>afsK</i> mutant has a branching phenotype	137
Figure 4.11 The branch-to-branch distance in the <i>afsK</i> mutant is unchanged	139
Figure 4.12 Histogram comparing the mathematical model and experimental data of the tip-to-branch distribution of the <i>afsK</i> mutant with a trim length of 80µm	140
Figure 4.13 Engineered expression of a constitutively active version of the AfsK kinase induces high levels of DivIVA phosphorylation and profoundly affects hyphal tip extension and branching	144

Figure 4.14 Communication between the polarity determinant DivIVA and the cell wall biosynthetic machinery in *Streptomyces* is bidirectional149

Chapter 5 – Systematic characterisation of the Ser/Thr phosphorylation sites of the *Streptomyces* polarity determinant DivIVA using a combination of nano-LC and high-accuracy mass spectrometry

Figure 5.1 *S. coelicolor* DivIVA is multiply phosphorylated in the C-terminus155

Figure 5.2 Schematic of the site-directed mutagenesis to introduce two additional trypsin cleavage sites in the DivIVA C-terminus158

Table 5.1 Overview of initial Mascot results identifying various phosphopeptides and possible phosphorylation sites in the DivIVA C-terminus160

Figure 5.3 Identification of the phosphorylation sites on peptide QLETQADDSLAPPR (amino acids 301 to 314)163

Table 5.2 Scaffold/Ascore results of the XIC of $m/z = 810.8669$ of the QLETQADDSLAPPR (amino acids 301 to 314) phosphopeptide isoforms165

Figure 5.4 Identification of the phosphorylation site on peptide TPATASLPPSPAPSMAPAGASAPSYGGNR (amino acids 315 to 343)167

Table 5.3 Scaffold/Ascore results identifying the phosphorylated residues in the extracted ion chromatogram of $m/z = 921.0932$ of TPATASLPPSPAPSMAPAGASAPSYGGNR (amino acids 315 to 343)169

Figure 5.5 Identification of the phosphorylation sites on peptide SMGGGPGQSGPSYGGQR (amino acids 344 to 360)171

Table 5.4 Scaffold/Ascore results identifying the phosphorylated residues in the extracted ion chromatogram of $m/z = 830.0932$ of SMGGGPGQSGPSYGGQR (amino acids 344 to 360)173

Figure 5.6 Overview schematic of the five identified phosphorylation sites in the tryptic peptides of the DivIVA C-terminus177

Abbreviations

aa	Amino acid
Apra	Apramycin
ATP	Adenosine-triphosphate
Carb	Carbenicillin
C-terminal	Carboxy-terminal
Da	Dalton
DIC	Differential interference contrast
DMSO	Dimethylsulphoxide
DNA	Deoxyribonucleic acid
dNTP	Deoxynucleoside triphosphate
DTT	Dithiothreitol
EDTA	Ethylene diamine tetraacetic acid
EGTA	Ethylene glycol tetraacetic acid
EGFP	Enhanced green fluorescence protein
FLAG	Polypeptide protein tag (N-DYKDDDDK-C)
HPLC	High Pressure Liquid chromatography
Hyg	Hygromycin
Hz	Hertz
Kan	Kanamycin
kDa	Kilodalton
LC	Liquid chromatography
MALDI-ToF	Matrix-assisted laser desorption ionisation time-of-flight
MS	Mass spectrometry
m/z	Mass-to-charge ratio
N-terminal	Amino-terminal
OD	Optical density
PCR	Polymerase chain reaction
PEG	Polyethylene glycol

Abbreviations

PPase	Protein phosphatase
rpm	Revolutions per minute
SDS	Sodium dodecyl sulphate
Spec	Spectinomycin
TFA	Trifluoroacetic acid
Thio	Thiostrepton
Tris	Tris(hydroxymethyl)aminomethane
UV	Ultraviolet
X-gal	5-bromo-4-chloro-indolyl- β -D-galactopyranoside
XIC	Extracted ion chromatogram

Chapter 1

Introduction

1.1	Cell polarity in the kingdom of life	18
1.2	The complex life cycle <i>Streptomyces</i>	19
1.2.1	General information about <i>Streptomyces</i> and its genome	19
1.2.2	The <i>Streptomyces</i> life cycle	20
1.3	Different modes of cell growth in bacteria	23
1.4	The bacterial cell wall	25
1.4.1	Cell wall composition of Gram-positive and Gram-negative bacteria	26
1.4.2	Peptidoglycan synthesis	28
1.4.3	Cell wall stress	30
1.5	The role of the bacterial cytoskeleton in cell wall growth	33
1.6	A special case: Polar growth in Actinobacteria	37
1.6.1	Polar growth in Actinobacteria is independent of MreB	37
1.6.2	A bacterial polarisome complex orchestrates apical growth	38
1.6.3	How is the polarity determinant DivIVA targeted to hyphal tips? ...	39
1.6.4	How is apical growth regulated?	44
1.6.5	What is the cell polarity system directing?	50
1.7	Aims of this thesis	52

1.1 Cell polarity is universal in the kingdom of life

A fundamental question in developmental biology is how cells establish polarity. It typically involves the initial deposition of a landmark protein at a cellular locus, followed by reinforcement of the polarisation mark by assembly of larger multiprotein complexes. In eukaryotes these complexes include broadly conserved proteins involved in the re-organisation and polarisation of the cytoskeleton and other cellular constituents (McCaffrey & Macara, 2009; Nelson, 2003). Among the most pronounced cases of cell polarity are those where growth or extension of the cell is targeted to a specific subcellular site, resulting in polar or apical growth. Important examples of polarised growth in eukaryotic cells include neuronal dendrites in animals, and root hairs and pollen tubes in plants.

Filamentous fungi and yeasts also undergo polar growth, although the hyphal tip growth of filamentous fungi is different from budding in the yeast *Saccharomyces cerevisiae* (reviewed by Steinberg, 2007). Filamentous fungi form hyphae, which consist of a chain of elongated cells that extend at the apex of the tip cell. Growth of fungal hyphae is mediated by the physical properties of the cell turgor and cytoskeleton-based polar exocytosis at the hyphal tip driven by several different motor proteins (kinesins and myosins) and cytoplasmic expansion forces. This pushes the cytoplasm against the flexible apical wall, which resists the internal turgor pressure and so maintains the hyphal shape. The organising centre for hyphal growth and morphogenesis is called the “Spitzenkörper”, which is present in all growing hyphal tips, at hyphal branch points and during spore germination. The Spitzenkörper is part of the endomembrane system in fungi with a complex structure: it contains small vesicles organised around a core area that contains a dense meshwork of actin filaments and several polysomes (complexes of multiple ribosomes bound to and translating a single mRNA). Microtubules extend into and through the Spitzenkörper. Although hyphal growth in fungi has been a hot topic in fungal research for many years, the underlying mechanisms are still not fully understood.

In evolutionary terms, one of the most ancient forms of polarised growth is found in bacteria, and most strikingly in the filamentous bacteria *Streptomyces*.

1.2 The complex life cycle of *Streptomyces*

1.2.1 General information about *Streptomyces* and its genome

Streptomycetes belong to the phylum Actinobacteria, which are Gram-positive bacteria with a high GC-content (63-78%) in their DNA. Actinobacteria are ubiquitous in nature, most especially in soil habitats. Actinobacteria show substantial physiological and morphological variety, including obligate aerobes and anaerobes, spore-forming filamentous bacteria, as well as rod- or club-shaped bacteria. For humankind, the major order *Actinomycetales*, often called Actinomycetes, are of particular importance since they include various pathogenic species as well as organisms of industrial importance. One of the best-known representatives is the intracellular pathogen *M. tuberculosis*, which causes tuberculosis.

The genus *Streptomyces* is represented by more than 500 species. Major characteristics include the formation of a hyphal mycelium and dispersal by means of spores. Many *Streptomyces* species are of importance for human and veterinary medicine because they produce antibiotics and a wide range of other secondary metabolites, the production of which coincides with the onset of morphological differentiation. Industrial large-scale fermentations are especially complicated because of the mycelial growth habit of these organisms. In contrast, *Streptomyces scabies* is a plant pathogen causing the economically important potato disease common scab.

Streptomyces coelicolor A3(2) is a member of the soil-dwelling group of filamentous Actinobacteria. It has been the most developed model organism among the Actinomycetes and is nowadays particularly interesting for the field of prokaryotic development (Hopwood, 1999; Kieser *et al.*, 2000; Hopwood, 2007). *Streptomyces coelicolor* is the organism that was studied in this thesis. Its linear chromosome of 8.7 Mb was one of the first bacterial genomes to be sequenced and has many unusual features for a bacterial genome (Bentley *et al.*, 2002; Hopwood, 2006). The genome contains 7,825 predicted genes, which is one of the largest number of genes found in a bacterium so far, including more than 20 secondary metabolite clusters. The *S. coelicolor* chromosome also shows a

distinct organisation: The origin of replication (*oriC*) is localised in the centre of the chromosome, surrounded by a ‘core’ of mainly ‘housekeeping’ genes for essential functions like DNA replication, transcription, translation, amino acid biosynthesis and morphological development. In contrast, the two ‘arms’ of the chromosome contain non-essential genes and inverted repeats. The *S. coelicolor* genome has a vast number of duplicated gene sets that are thought to operate in specialised cell types or ‘tissues’ during the different phases of colony development. 965 genes (12.3%) encode regulatory proteins, likely to be involved in sensing and responding to external stimuli and stresses in the soil habitat.

1.2.2 The *Streptomyces* life cycle

The life cycle of *S. coelicolor* is very complex and comparable to that of filamentous fungi (**Figure 1.1**; reviewed for example by Chater, 1998; Chater, 2001; Flärdh & Buttner, 2009; McCormick & Flärdh, 2012). Under optimal growth conditions, the life cycle is completed within four to five days. It starts with growth as tubular filaments called hyphae, which extend and branch to produce a vegetative mycelium. From a mycelium of vegetative substrate hyphae, new branches coated with a hydrophobic sheath break surface tension at the air-water interface and grow into the air by tip extension to form an aerial mycelium. This marks the onset of morphological differentiation in *Streptomyces*.

Subsequently, aerial hyphae stop growing and initiate sporulation. Initially, multiple, regularly spaced sporulation septa form synchronously over a distance of up to 50 μm , subdividing the sporogenic apical cell at 1 – 2 μm intervals into dozens of box-like, unigenomic prespore compartments. The spore walls then thicken, the spores become rounded, and a spore pigment is deposited, which is grey-brown in *S. coelicolor*. Eventually, mature, desiccation-resistant spores are released to begin the life-cycle again. Under optimal growth conditions, spore germination is triggered and one or two germ tubes emerge and grow by tip extension. Hyphae increase exponentially in number by branching during growth of a substrate mycelium.

Morphological development is well-studied genetically and requires the activities of two sets of developmental regulators: the *bld* and *whi* genes. *bld* mutants form a substrate mycelium, but they are unable to make an aerial mycelium, and so they completely lack the characteristic fuzzy appearance of wild-type colonies and instead look “bald”. In contrast, *whi* mutants form aerial hyphae in the normal way, but these hyphae fail to differentiate into mature chains of pigmented spores, and therefore these mutants have a “white” appearance.

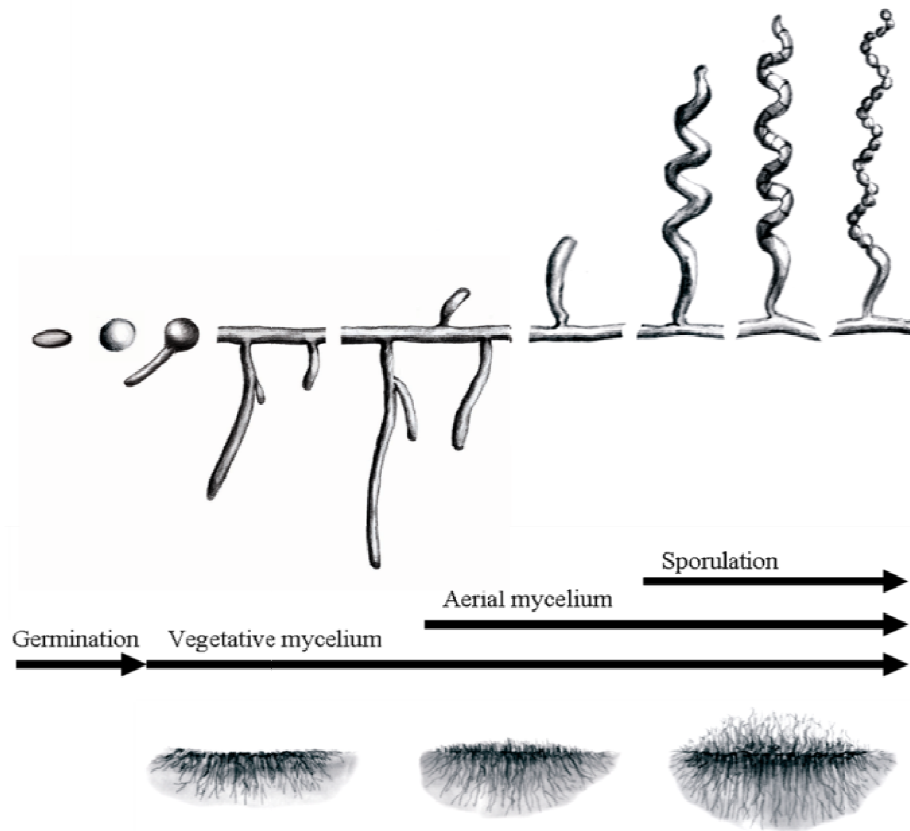


Figure 1.1 Schematic representation of the complex developmental life cycle of *S. coelicolor*.

The major growth stages are illustrated from spore germination and vegetative growth to formation of aerial hyphae, morphological differentiation and finally sporulation. Adapted from Chater (1998, 2000) and Wollkopf (2007).

1.3 Different modes of cell growth in bacteria

In virtually all bacteria, cell division occurs through new cell wall synthesis. In diverse well-studied rod-shaped bacteria like *Bacillus subtilis* and *Escherichia coli*, cell wall synthesis is spatially and temporally highly regulated. The cell division septum divides the cell and creates two new cell poles. Thereafter, elongation of the cell and acquisition of the rod shape occurs in two distinct ways. New cell wall precursors are inserted in a dispersed fashion into the lateral cell wall (highlighted in red in **Figure 1.2A**), while the cell poles remain inert, with no sign of new incorporation or turnover of existing cell wall material (de Pedro *et al.*, 1997). This is sometimes referred to as zonal or non-polar growth. In addition, (Daniel & Errington, 2003) showed that fluorescently labelled vancomycin binds to new cell wall material, thereby marking the sites of active cell wall synthesis. Importantly, using this technique, they showed that cell wall growth in *B. subtilis* occurs in defined helical bands and that, during cell division, new cell wall material is inserted at the division site.

Cell wall growth in cocci such as *Staphylococcus aureus* occurs solely through cell division, in which new cell wall material that builds the division septum ultimately forms a hemisphere of the cell wall in each daughter cell (**Figure 1.2A**).

In stark contrast, cell elongation in the rod-shaped Actinobacteria *Corynebacterium glutamicum* and *Mycobacterium tuberculosis* is accomplished by polar growth, which means that the cell wall is synthesised at the cell poles, while the lateral wall appears inert. Similarly, hyphae of *Streptomyces coelicolor* extend by incorporating new cell wall material at the hyphal tips and develop new lateral branches that also grow by tip extension (**Figure 1.2A and B**; Flårdh, 2003a).

Recently, the Brun lab has shown that the rod-shaped bacterium *Agrobacterium tumefaciens*, a member of the Alphaproteobacterial order Rhizobiales, and also the closely related *Sinorhizobium meliloti*, *Brucella abortus*, and *Ochrobactrum anthropi* grow unidirectionally from the new pole generated after cell division (Brown *et al.*, 2011 and 2012).

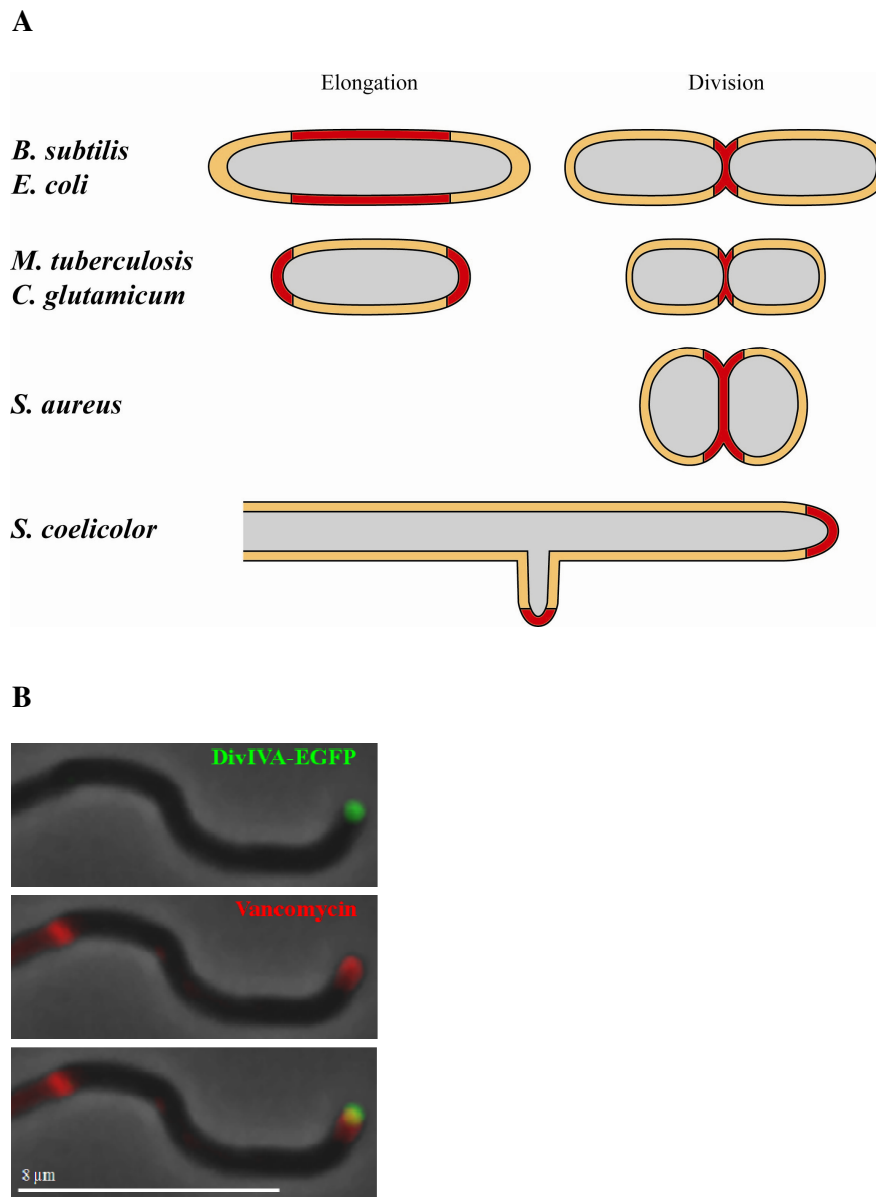


Figure 1.2 Different modes of cell wall growth.

(A) Sites of nascent cell wall synthesis are indicated in red in *B. subtilis*, *E. coli*, *M. tuberculosis*, *C. glutamicum*, *S. aureus* and *S. coelicolor*. (B) Polar localisation of DivIVA-EGFP to hyphal tips. Staining of nascent cell wall synthesis at hyphal tips and cell division septa in *S. coelicolor* using fluorescently-labelled vancomycin. Size bar, 8 μ m.

1.4 The bacterial cell wall

In most bacteria, cell shape, integrity, growth and division is maintained by the cell wall, which also gives the cells mechanical strength to resist osmotic pressure and environmental threats. In order to do that, the cell wall is very dynamic, cycling between biosynthesis, assembly, maturation, and disassembly and recycling

Most bacterial cells are surrounded by a cell wall. However, there are bacteria that lack one yet still retain distinct diverse morphologies. Members of the Mollicutes, for example including mycoplasmas and spiroplasmas, have the simplest genomes of any self-replicating, free-living bacteria described to date. However, they only have a cholesterol-containing membrane and they seem to govern their defined shapes through internal cytoskeletal structures (Trachtenberg, 1998). In addition, cell wall-deficient derivatives of common bacteria are called L-forms. They can still grow and proliferate and have been studied for decades in the attempt to understand their importance in antibiotic resistance and pathogenesis (see recent work on *B. subtilis* L-forms: Leaver *et al.*, 2009; Dominguez-Cuevas *et al.*, 2012).

The bacterial cell wall looks like a mesh sacculus that surrounds the cytoplasm and the membrane and is mainly composed of parallel glycan chains, which are cross-linked by short peptides. Each chain is a polymer of alternating covalently β -1,4-linked *N*-acetyl glucosamine (GlcNAc) and *N*-acetyl muramic acid (MurNAc). The number of disaccharide units in the glycan chains varies between different bacterial species.

Already in 1884, the Danish microbiologist Hans Christian Gram developed a simple staining method using crystal-violet dye to differentiate between two major bacterial classes. This method was historically used as the standard procedure for bacterial classification. His method is based on the chemical and physical properties of the bacterial cell wall.

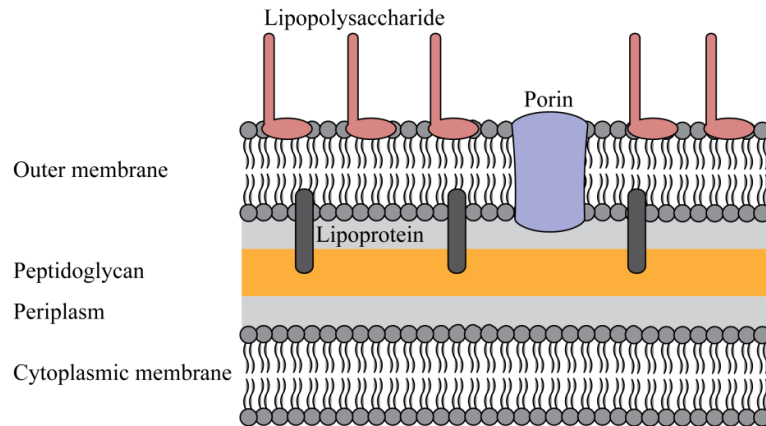
1.4.1 Cell wall composition of Gram-negative and Gram-positive bacteria

The cell wall composition in Gram-negative and Gram-positive bacteria is very different (**Figure 1.3**; Cabeen & Jacobs-Wagner, 2005; Jordan *et al.*, 2008).

Gram-negative bacteria have a much thinner but more complex cell wall, which does not retain the Gram stain. It is composed of a single peptidoglycan layer located within a periplasmic space that is created between the inner and outer membranes. The outer membrane has a complex structure that includes porins, which allow the passage of small hydrophilic molecules across the membrane, phospholipids, lipoproteins and lipopolysaccharide molecules extend into the extra-cellular space. Thereby, the outer membrane forms a permeability barrier that controls the traffic of large molecules into the cell. For that reason, glycopeptide antibiotics are not effective on Gram-negative bacteria, because they simply cannot penetrate the outer membrane.

In contrast, Gram-positive bacteria have a very thick cell wall (20 – 80 nm), which retains the Gram stain and consists of a multi-layered peptidoglycan sheath outside of the cytoplasmic membrane. Characteristically, these cell walls contain very little lipids, but instead high concentrations of teichoic and lipoteichoic acids and proteins. Teichoic acids are predominantly linked to and are embedded in the peptidoglycan layer. Lipoteichoic acids span the peptidoglycan layer and extend into the cytoplasmic membrane. These anionic polysaccharides have vital roles in cell growth, morphology and division. The composition of the Gram-positive cell wall varies quite substantially between organisms.

Gram-negative bacteria



Gram-positive bacteria

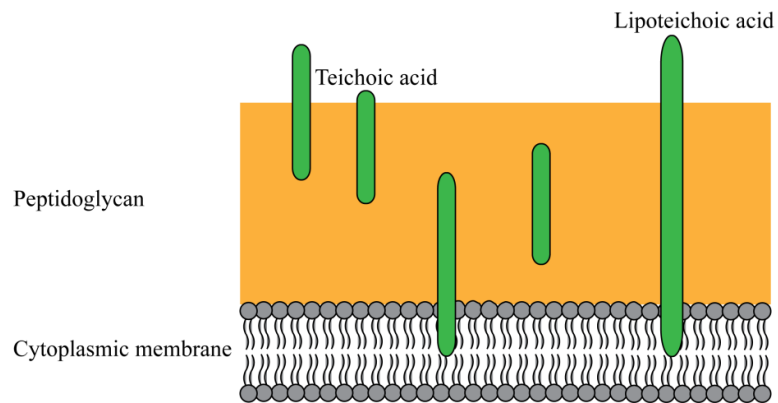


Figure 1.3 Schematic of the different cell wall composition of Gram-negative and Gram-positive bacteria.

Schematic was modified from Cabeen & Jacobs-Wagner (2005).

1.4.2 Peptidoglycan synthesis

Peptidoglycan is the main component of Gram-positive cell walls. The growth of the peptidoglycan sacculus is a very dynamic process under tight spatiotemporal regulation and cytoskeletal and cytoplasmic proteins have central functions for determining the structure and shape of the peptidoglycan sacculus.

Peptidoglycan synthesis requires mainly two sets of enzymes, synthases, the “makers”, which make peptidoglycan and attach it to the existing peptidoglycan sacculus, and hydrolases, the “breakers”, which cleave the sacculus to allow insertion of newly synthesised peptidoglycan. It occurs in four main steps that are located in different parts of the bacterial cell (**Figure 1.4**). First, the soluble nucleotide precursors UDP-*N*-acetyl-glucosamine (UDP-GlcNAc) and UDP-*N*-acetyl-muramic acid (UDP-MurNAc) are synthesised in the cytoplasm (Barreteau *et al.*, 2008). UDP-GlcNAc and UDP-MurNAc are the building blocks for the peptidoglycan backbone. Second, at the inner leaflet of the membrane the nucleotide precursors are assembled with undecaprenyl phosphate to form the lipid-anchored monomeric disaccharide-pentapeptide subunit called lipid II. Lipid II is then flipped across the cytoplasmic membrane, maybe mediated by FtsW-RodA (Bouhss *et al.*, 2008; Mohammadi *et al.*, 2011). Third, glycosyltransferases polymerise lipid II and thereby release the undecaprenyl phosphate, which cycles back to the cytoplasm. The resulting glycan chains are inserted into the peptidoglycan cell wall. Fourth, the glycan chains are cross-linked by transpeptidases (Vollmer *et al.*, 2008). The nature of the peptidoglycan cross-links varies between bacteria.

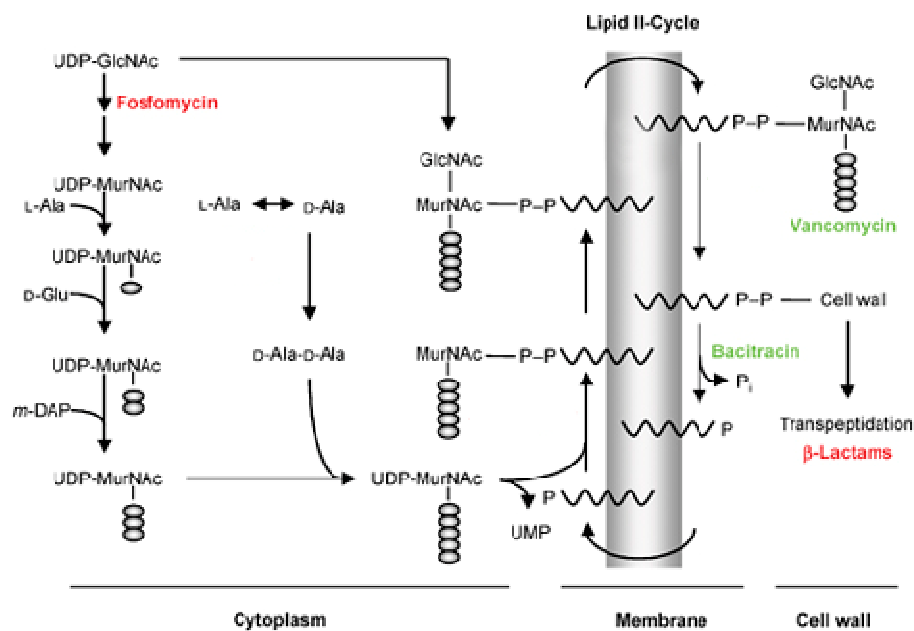


Figure 1.4 Schematic of the important steps of peptidoglycan biosynthesis and inhibition of individual steps by antibiotics (Modified from Jordan *et al.*, 2008).

Comments: GlcNAc, *N*-acetyl-glucosamine; MurNAc, *N*-acetyl-muramic acid. Amino acids are illustrated as small grey circles, undecaprenol is illustrated as waved lines. Some antibiotics inhibit steps in peptidoglycan synthesis by sequestering the substrate of the given step (marked in green) or by inhibiting the corresponding enzymatic function (marked in red).

1.4.3 Cell wall stress

Bacteria need to modify the cell envelope in response to changes in their surrounding environment, including cell envelope stress caused by antibiotics. Several clinically relevant antibiotics target specifically the bacterial cell wall, inhibiting peptidoglycan synthesis by either mimicking or binding to a substrate or directly inhibiting an enzymatic function. Here I give a brief overview of antibiotics that were used later in this study (**Figure 1.4**). Phosphomycin (fosfomycin), bacitracin and penicillin G are all substrate-mimicking antibiotics. Phosphomycin is a structural analogue of the substrate of MurA and thereby inhibits its enzymatic function (Jordan *et al.*, 2008). MurA catalyses the first committed step of peptidoglycan biosynthesis, the transfer of enolpyruvate from phosphoenolpyruvate to the 3'-hydroxyl group of UDP-N-acetylglucosamine. Bacitracin is a cyclic, non-ribosomally synthesised peptide antibiotic that binds to undecaprenyl phosphate, the membrane carrier of lipid II, thereby preventing the recycling of the lipid II carrier (Bugg & Walsh, 1992). β -lactam antibiotics like penicillins (Penicillin G was used in this study), act as pseudosubstrates of the transpeptidase enzyme that catalyses the glycan cross-linking (Jordan *et al.*, 2008). In contrast, vancomycin is a glycopeptide that binds directly to the D-alanyl-D-alanine (D-Ala-D-Ala) terminus of the lipid II substrate on the outside of the cytoplasmic membrane. This binding blocks cell wall synthesis, principally by denying transpeptidase access to its substrate, thereby preventing formation of the peptide cross-links between polysaccharide strands that give the cell wall its rigidity (Arthur *et al.*, 1992).

In general, cell envelope stress responses are orchestrated by two-component signal transduction systems or extracytoplasmic function (ECF) sigma factor/anti-sigma factor pairs, both usually consisting of a stress sensor membrane protein and a cytoplasmic regulator (recently reviewed by Jordan *et al.*, 2008). Two-component systems comprise a sensor kinase and a cognate response regulator. In the absence of the stimulus the kinase is inactive and the regulator is unphosphorylated. When the stimulus is present, the sensor kinase auto-phosphorylates on a His residue and the phosphate is transferred onto the response regulator, leading to its activation. In contrast, in the absence of the signal, an

anti-sigma factor binds tightly to the sigma factor to sequester it from core RNA polymerase. But upon signal perception, it releases the sigma factor, allowing holoenzyme formation and transcription of the target regulon. The response to cell envelope stress conditions is well studied in *B. subtilis*. There at least three of the seven encoded ECF sigma factors (σ^M , σ^X , σ^W) are involved in the response of *B. subtilis* to cell envelope stress conditions.

In streptomycetes, the σ^E -CseABC signal transduction system senses and responds to changes in cell wall integrity (**Figure 1.5**, Hong *et al.*, 2002). Unusually, this system involves both a two-component system and an ECF sigma factor (but no known anti-sigma factor). It consists of four proteins encoded in an operon; the RNA polymerase sigma factor σ^E , an extracytoplasmic lipoprotein CseA, the response regulator CseB and the sensor kinase CseC (Cse stands for control of sigma E). Upon signal perception, CseC activates CseB via phosphorylation and thereby expression of the *sigE-cseABC* operon is stimulated. These signals may include cell wall precursors or breakdown products since the expression of σ^E is induced in response to stress signals from the cell envelope (Hong *et al.*, 2002; Hutchings *et al.*, 2006). Among the treatments that induce the σ^E -CseABC system are antibiotics that inhibit intermediate and late steps in peptidoglycan synthesis. The target regulon of σ^E consists of approximately 59 genes, which are involved in cell wall synthesis and remodelling, determination of cell shape and transcriptional regulation (Hong *et al.*, 2002; Tran, 2010). Thus σ^E is a key regulator of cell envelope stress in *S. coelicolor*, and σ^E itself is proteolytically regulated by ClpXP degradation (Tran, 2010). The lipoprotein CseA is proposed to somehow modulate the signal sensing of CseC and thereby to negatively regulate the *sigE* promoter (Hutchings *et al.*, 2006).

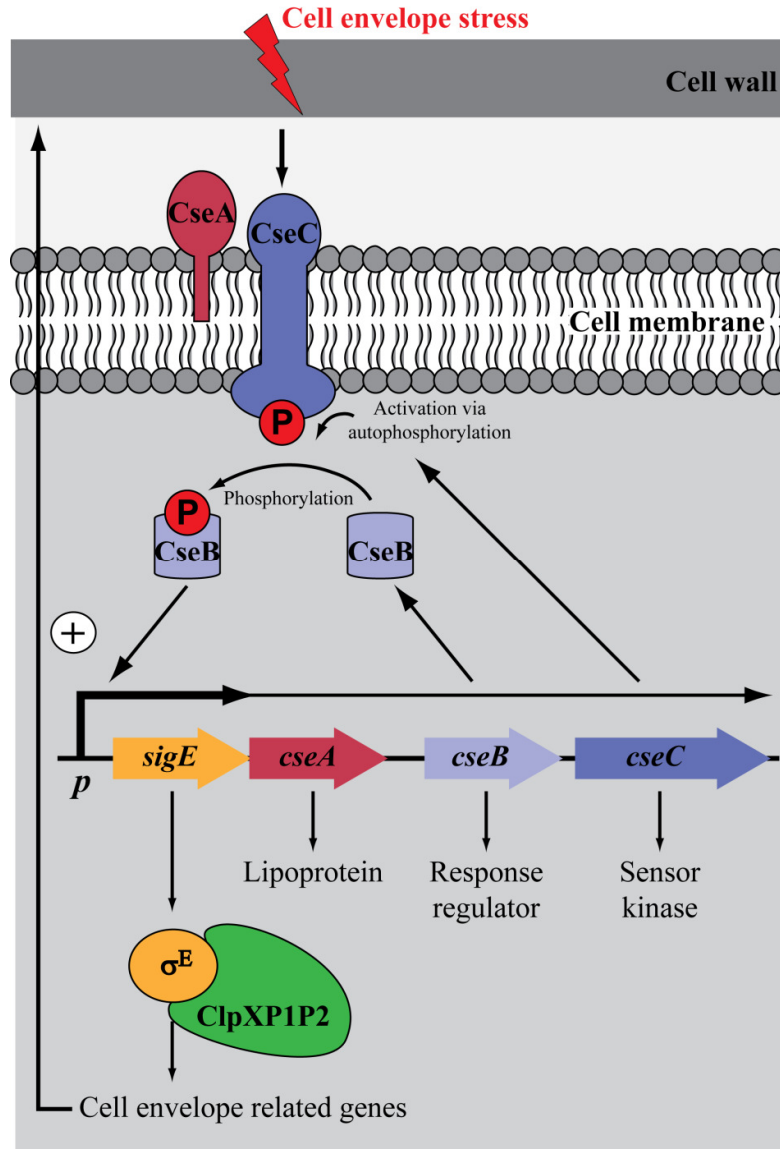


Figure 1.5 The σ^E -CseABC signal transduction system in *S. coelicolor*.

1.5 The role of the bacterial cytoskeleton in cell wall growth

Three cytoskeletal systems are found in eukaryotes that consist of microfilaments (actin), microtubules (tubulin) and intermediate filaments. Major functions of these systems are the maintenance of cell shape and integrity as well as transport processes, motility, chromosome segregation, signal transduction and cytokinesis.

For many years the prevailing view was that bacteria had no cytoskeleton and instead maintained their cell shape solely by the cell wall functioning as an exoskeleton. More recently, homologues of all three eukaryotic cytoskeletal elements have been found in bacteria (Carballido-Lopez & Errington, 2003; Löwe *et al.*, 2004; Amos *et al.*, 2004; Cabeen & Jacobs-Wagner, 2005; Shih & Rothfield, 2006; Graumann, 2007). Although the eukaryotic and bacterial homologues are very divergent at the amino acid sequence level, the crystal structures of bacterial MreB and FtsZ unambiguously demonstrate that eukaryotic actin and tubulin have bacterial origins (Löwe & Amos, 1998; van den Ent *et al.*, 2001b; **Figure 1.6**).

Pioneering work from Jeff Errington's lab and others showed that bacterial cells have a functional cytoskeleton and that this bacterial cytoskeleton guides peptidoglycan synthesis and insertion in the different phases of the cell cycle (Jones *et al.*, 2001; Carballido-Lopez & Errington, 2003; Carballido-Lopez, 2006; **Figure 1.7**). There are also multiple lines of evidence that the cell wall synthesis machinery The actin-like rod-shape-determining protein MreB directs the elongation of newly divided cells by inserting peptidoglycan into multiple sites in the lateral cell wall ('dispersed' elongation). Upon cell division, the tubulin-like cell division protein FtsZ forms a cytokinetic ring at midcell. This directs the 'preseptal' phase of cell elongation, which is followed by 'constrictive' septum synthesis, cell division and daughter cell separation. The role of the bacterial tubulin homologue FtsZ as an essential cell division protein was shown in *e.g.* *E. coli*, *B. subtilis* and *Caulobacter crescentus* (reviewed by Margolin, 2005). It defines the cell division plane and directs formation of the division septum.

The actin homologue MreB has been recognised as a protein with a unique function in rod-shaped bacteria. Depletion of MreB in *E. coli* resulted in spherical

or irregularly shaped cells (Kruse *et al.*, 2005). In *B. subtilis*, there are three MreB homologues, MreB, Mbl (MreB-like) and MreBH. These proteins form helical cable-like structures and appear to co-localise with MreB *in vivo* (Carballido-Lopez *et al.*, 2006). Cells with a disrupted *mbl* gene have a distorted morphology with irregular bends, twists and bulges. Until very recently, the current view was that the helical MreB cytoskeleton is static and involved in organising how new material is inserted into the lateral cell wall during elongation of rod-shaped bacteria like *E. coli*, *B. subtilis*, and *C. crescentus*. Two ground-breaking studies have changed this dogma in 2012 by demonstrating that MreB does not form a helix and previous results were largely artefactual. Instead, the cell wall synthesis machinery may move uncoordinated and circumferential (in relation to the cell) along peripheral tracks and this movement then forms rings of new cell wall material, which then drives the motion of the MreB filaments (Dominguez-Escobar *et al.*, 2011; Garner *et al.*, 2011). In the light of these new studies, it remains to be shown what the biological role of MreB is. Dominguez-Escobar *et al.* (2011) proposed two models; MreB might just act as a passive scaffold of cell wall synthesis activities in the cell or, alternatively, MreB might actively restrict the diffusion these cell wall elongation complexes to ensure correctly oriented movement within the membrane. Strikingly, most rod-shaped or elongated bacteria contain *mreB* genes while coccoid bacteria tend to lack *mreB*.

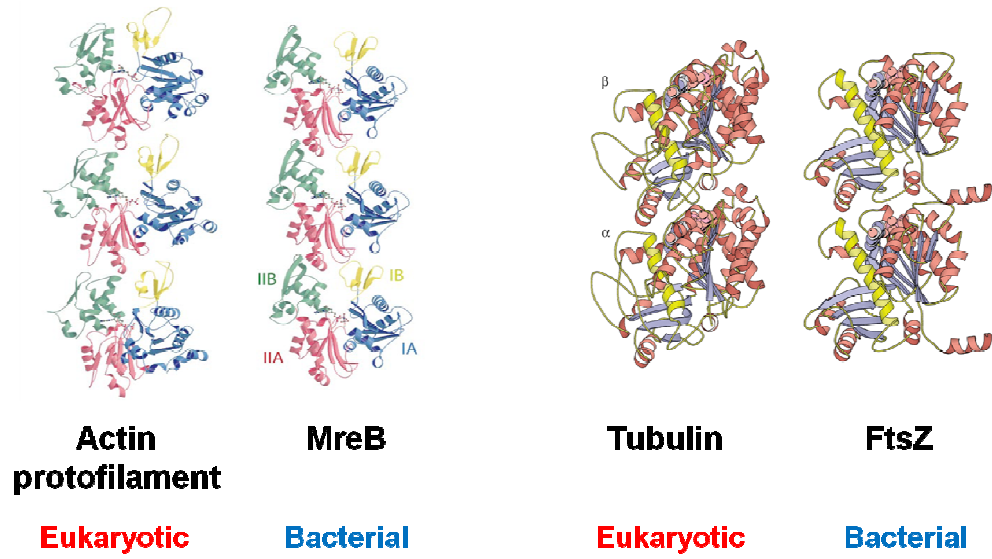


Figure 1.6 Prokaryotic MreB and FtsZ are structural homologues of the eukaryotic cytoskeletal elements actin and tubulin (van den Ent *et al.*, 2001a).

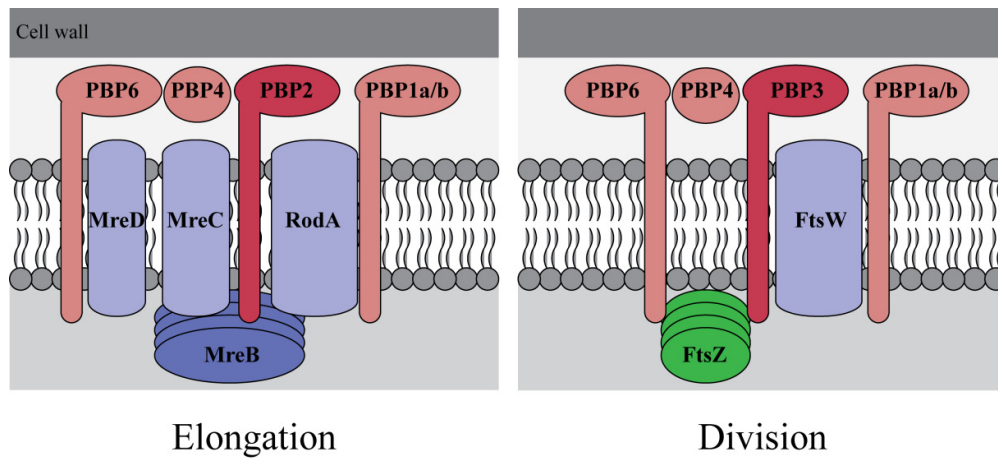


Figure 1.7 Simplified illustration of the assembly of the set of components of the cell wall biosynthetic machinery specific for cell elongation and division (modified from Cabeen & Jacobs-Wagner, 2005).

This model derived from multiple lines of evidence in different bacterial species.

1.6 A special case: Polar growth in Actinobacteria

1.6.1 Polar growth in Actinobacteria is independent of MreB

A deviation from the generalisation arising from the studies on *e.g.* *E. coli* and *B. subtilis* is presented by the rod-shaped Actinobacteria, such as *Corynebacterium* and *Mycobacterium*, in which *mreB* is absent and cell wall growth occurs at the poles (Daniel & Errington, 2003; Chauhan *et al.*, 2006). In Actinobacteria, MreB is only conserved in those species that develop a sporulating aerial mycelium (Mazza *et al.*, 2006). *S. coelicolor* contains two *mreB* genes that, in contrast to other bacteria, seem to be involved only in spore wall synthesis and are not required for tip extension in vegetative or aerial hyphae (Mazza *et al.*, 2006). Thus it is clear that the mechanism underlying polarised growth in Actinobacteria is different from the *mreB*-dependent elongation of bacteria like *E. coli* and *B. subtilis*. Hyphal tip extension and branching are also independent of *ftsZ*, which is a non-essential gene in *S. coelicolor* (McCormick *et al.*, 1994; Mazza *et al.*, 2006). However, as it is described in more detail later, it is clear that DivIVA plays a key role in coordinating polar growth in Actinobacteria, as several studies in *Streptomyces*, *Corynebacterium* and *Mycobacterium* have shown. However, numerous questions remain to be answered concerning how apical growth is organised in general; how the cell wall biosynthetic machinery is recruited to the hyphal tip; and how is cell polarity re-oriented and new sites of cell wall growth established during branching?

1.6.2 A bacterial polarisome complex orchestrates apical growth

Previous work demonstrated that DivIVA accumulates at the tips of growing vegetative hyphae in *S. coelicolor* and has a strong effect on tip extension and cell shape when over-expressed or partially depleted (Flärdh, 2003a). Live cell imaging of *Streptomyces* hyphae has been used to monitor the dynamics and subcellular distribution of functional DivIVA-EGFP fusion proteins. A small focus of DivIVA precedes visible branch outgrowth suggesting it marks the site where new cell wall synthesis will occur (Hempel *et al.*, 2008). The location along the lateral wall at which new branch points form is not entirely random; there is a marked preference for new branches to emerge from the outer curvature of bent or curved hyphae (Hempel *et al.*, 2008), but the mechanism underlying this preference remains unclear. In *S. coelicolor*, *divIVA* is essential and the DivIVA protein is the first clear example of a protein associated with polar tip extension (Flärdh, 2003a). No role in cell division has been established to date.

Studies in other Actinomycetes showed that *C. glutamicum divIVA* and *M. smegmatis divIVA* are also essential genes and the proteins are involved in polarised growth and cell shape determination (Ramos *et al.*, 2003; Nguyen *et al.*, 2007; Letek *et al.*, 2008). Interestingly, depletion of DivIVA in *C. glutamicum* led to a loss of rod-shape and polar growth and resulted in growth as coccoid cells (Letek *et al.*, 2008). Heterologous expression of *divIVA* genes from *Streptomyces* and *Mycobacterium* in *C. glutamicum* depletion strains could restore polarised growth, while *divIVA* from *B. subtilis* and *Streptococcus pneumoniae* could not. Surprisingly, heterologous expression of other *divIVA* homologues in *Streptomyces* was always lethal (Letek *et al.*, 2009).

Additional components are likely to be involved, together forming a tip-organising complex, which we term bacterial polarisome, by functional analogy with the polarisome complex that directs cell polarity in yeasts and filamentous fungi (Moosely & Goode, 2006). These additional components are likely to include Scy (*Streptomyces* cytoskeletal protein; SCO5397; 1326 amino acids; Walshaw *et al.*, 2010) and the intermediate filament protein FilP (filament-forming protein; SCO5396; 310 amino acids; Bagchi *et al.*, 2008)). Overall, all three proteins (DivIVA, Scy and FilP) have a very similar domain organisation;

two coiled-coil domains separated by a flexible linker. Scy and FilP are encoded by genes lying adjacent to each other on the *S. coelicolor* chromosome. Both genes are non-essential, however the effect of deletion on hyphal growth rate and morphology is strong. FilP was shown to form long intermediate-filament-like filaments *in vitro* and *in vivo* (Bagchi *et al.*, 2008). FilP-EGFP fusion proteins formed filaments in growing hyphae, which are often associated with the hyphal tip. Interestingly, in *C. glutamicum* another coiled-coil, filament-forming protein, RsmP, was identified to be essential for polar growth (Fiuza *et al.*, 2010).

1.6.3 How is the polarity determinant DivIVA targeted to hyphal tips?

Apart from DivIVA, various bacterial proteins are known to localise exclusively to the cell pole and determine cell polarity, thus defining the cell pole as a specialised compartment. Because active transport mechanisms delivering proteins to the pole are not known in bacteria and no physical barrier separates the pole from the rest of the cell, the key question is how the polarity determinants are targeted to the cell pole, and in the case of *Streptomyces*, how in particular DivIVA is targeted to the hyphal tip.

DivIVA is not confined exclusively to Actinobacteria. Homologues are found in a range of Gram-positive bacteria with the *divIVA* gene typically being located downstream of a cluster of cell division genes (*ftsZ*, *ftsQ*, *ftsW*) (Flårdh, 2003a). Its sequence is quite conserved across these homologues (**Figure 1.8A**). Based on the available data, DivIVA seems to serve a variety of functions related to cell polarity across different bacteria.

DivIVA homologues share sequence conservation in particular in the N-terminal and the C-terminal part of the protein, followed by sequences with low similarity that adopt a coiled-coil conformation with two coiled-coiled domains separated by a flexible linker (Edwards & Errington, 1997; Edwards *et al.*, 2000; Oliva *et al.*, 2010; **Figure 1.8A**). A direct comparison of the domain organisation of *S. coelicolor* versus *B. subtilis* DivIVA is shown in **Figure 1.8B**. *S. coelicolor* DivIVA, which has a predicted size of 41 kDa, was shown to be primarily

cytoplasmic and to exist as high-molecular-weight multimeric complexes *in vivo* (Wang *et al.*, 2009). The two coiled-coil domains are separated by a proline-glutamine-glycine (PQG)-rich segment. The PQG-rich segment and most of the C-terminal segment are only present in streptomycetes and both are not essential for DivIVA function (Wang *et al.*, 2009). Purified DivIVA oligomerises and assembles into filamentous structures *in vitro*. These filaments were found to be of variable length with a diameter of approximately 2 nm. The *Bacillus*, *Mycobacterium* and *Enterococcus* DivIVAs have also been shown to oligomerise and form various higher order structures (Muchova *et al.*, 2002a, Muchova *et al.*, 2002b; Stahlberg *et al.*, 2004; Nguyen *et al.*, 2007; Rigden *et al.*, 2008).

Among the DivIVA proteins from different bacteria, the function of *B. subtilis* DivIVA is mechanistically the best understood. In *B. subtilis*, *divIVA* is not essential and plays two distinct roles, in division-site selection and in chromosome segregation. During cell division, DivIVA is targeted to the cell poles where it sequesters the cell division inhibitors MinCD via MinJ (Bramkamp *et al.*, 2008; Lenarcic *et al.*, 2009). This allows FtsZ ring assembly only at midcell. During sporulation, DivIVA is involved in the attachment of the chromosomes to the cell poles through interaction with RacA (Edwards *et al.*, 2000; Thomaidis *et al.*, 2001; Errington, 2001). Recently, it has become clear that *B. subtilis* DivIVA appears to recognise and preferentially assemble at negatively curved membrane surfaces (Lenarcic *et al.*, 2009; Ramamurthi & Losick, 2009; Eswaramoorthy *et al.*, 2012). Although *B. subtilis* DivIVA serves a very different function, the characteristic that it shares with *Streptomyces* DivIVA is polar targeting.

Through a collaborative effort between the groups of Leendert Hamoen and Jan Löwe, the crystal structure of *Bacillus* DivIVA has been solved (Oliva *et al.*, 2010). This work showed that the first coiled-coil domain forms a parallel dimer and the conserved 20 amino acid N-terminus folds back on this dimer. This forms a crossed-loop structure with a phenylalanine (Phe17) and an arginine (Arg18) exposed, of which Phe17 is thought to interact with the membrane. Although this particular phenylalanine is not conserved in *S. coelicolor* DivIVA, there is a leucine (Leu18) in close proximity, which could be interesting to investigate. Previous studies have shown that the N-terminus in *S. coelicolor* and *C.*

glutamicum is essential for the function and the localisation of DivIVA (Wang *et al.*, 2009; Letek *et al.*, 2009). The crystal structure of *Bacillus* DivIVA shows that the C-terminus forms a tetrameric structure that consist of two parallel dimers of the second coiled-coil domain, suggesting a “molecular bridging” model (Oliva *et al.*, 2010; **Figure 1.8C**).

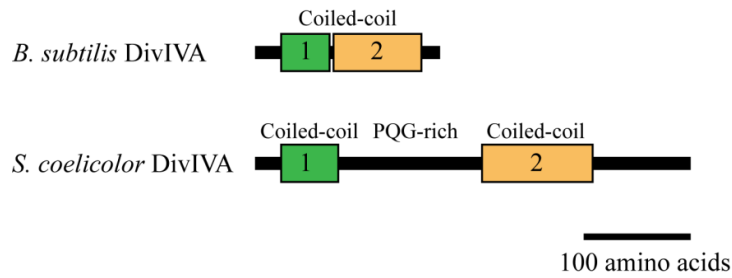
Affinity for membranes with a high degree of negative curvature might be sufficient to explain the oligomerisation of *Streptomyces* DivIVA at the cell poles, but it cannot explain the localisation of small DivIVA foci along the lateral wall preceding branch development. There, the degree of negative curvature is minimal and may therefore contribute to the stabilisation of the DivIVA cluster, but it is unlikely to determine the initial site selection. Determining the mechanism underlying the placement of DivIVA foci is critical for understanding how cell polarity is established and branch development is initiated in *Streptomyces*.

Chapter 1 – Introduction

A

		1	110
Hsub	(1)	HELTPEADVHIVAFSKPPIGKGYRDEVDAPFLILVEKILTRLLR	
Htub	(1)	HELTPEADVHIVAFSKPPIGKGYRDEVDAPFLILVEKILTRLLR	ENSLINQRIWELDQELAAQGGAG
Scu	(1)	HELTPEADVHIVAFSKPPIGKGYRDEVDAPFLILVEKILTRLLR	ENSLINQRIWELDQELAAQGGAG
Scab	(1)	HELTPEADVHIVAFSKPPIGKGYRDEVDAPFLILVEKILTRLLR	ENSLINQRIWELDQELAAQGGAG
Sav	(1)	HELTPEADVHIVAFSKPPIGKGYRDEVDAPFLILVEKILTRLLR	ENSLINQRIWELDQELAAQGGAG
Sven	(1)	HELTPEADVHIVAFSKPPIGKGYRDEVDAPFLILVEKILTRLLR	ENSLINQRIWELDQELAAQGGAG
Sgr	(1)	HELTPEADVHIVAFSKPPIGKGYRDEVDAPFLILVEKILTRLLR	ENSLINQRIWELDQELAAQGGAG
		111	220
Hsub	(42)	-----KRT-----ELEAKVKKLDERIG	
Htub	(68)	---V---TEQATQATPAYEPEKGPAPAAVWSGHWEE-----QALKARVLSLQDTADRIEFT	
Scu	(85)	---GQGGPQQGGHPQQGHRGSGAPVEMISGPPQQ-----HGGHGGPQLPSGAPQLPAGPG---GQGGPQG---PQHNGQG---PQHNGQGSGP	
Scab	(109)	---GQGGPQQGGHPQQGHRGSGAPVEMISGPPQQ-----HGGHGGPQLPSGAPQLPAGPG---GQGGPQG---PQHNGQG---PQHNGQGSGP	
Sav	(67)	---GHRKPEQQDQDQGGHRGSGAPVEMISGPPQQG---GEGGPPQLPSGAPQLPAGPG---GQGGPQG---PQHNGQG---PQHNGQGSGP	
Sven	(67)	---GHRKPEQQDQDQGGHRGSGAPVEMISGPPQQG---GEGGPPQLPSGAPQLPAGPG---GQGGPQG---PQHNGQG---PQHNGQGSGP	
Sgr	(70)	---GHRKPEQQDQDQGGHRGSGAPVEMISGPPQQG---GEGGPPQLPSGAPQLPAGPG---GQGGPQG---PQHNGQG---PQHNGQGSGP	
		221	330
Hsub	(59)	-----HFAWIEGSLAKSLLVAQQAARDVWRKNSQKSAKLTIVKAKKMAADRIEBSLSK	
Htub	(121)	-----AKASDRKHLADARAWAQITLGEARRTADATFAEARAGADAWLADAGERSBAQLAQCEKADATQADAEKRBSEIDNGITPQQ	
Scu	(166)	---H---GQGGPQGSGG---PQGGPQGSGGSGGPPGGG---GPGGISAARVLSLAQQTADQATAEARSKANKIVGEARSRANGLERDARAKADALERDQEKHRVANGSTLSA	
Scab	(194)	---GQGGPQGSGGSGG---PQGGPQGSGGSGGPPGGG---GPGGISAARVLSLAQQTADQATAEARSKANKIVGEARSRANGLERDARAKADALERDQEKHRVANGSTLSA	
Sav	(173)	---GQGGPQGSGGSGG---PQGGPQGSGGSGGPPGGG---GPGGISAARVLSLAQQTADQATAEARSKANKIVGEARSRANGLERDARAKADALERDQEKHRVANGSTLSA	
Sven	(145)	---GQGGPQGSGGSGG---PQGGPQGSGGSGGPPGGG---GPGGISAARVLSLAQQTADQATAEARSKANKIVGEARSRANGLERDARAKADALERDQEKHRVANGSTLSA	
Sgr	(154)	---GQGGPQGSGGSGG---PQGGPQGSGGSGGPPGGG---GPGGISAARVLSLAQQTADQATAEARSKANKIVGEARSRANGLERDARAKADALERDQEKHRVANGSTLSA	
		331	440
Hsub	(111)	SRKLAHELEKIKKQSKVETKRFQHLDEAQDILKEDWDHILLEYVDVFEKKE	
Htub	(202)	HAVLEGRILQLRFFPEREYRRLKSYLRSQLRQLSTQAUISLAPPKRFBAASLPPSA---PSMAFAGASAPSYGGGQ---HGGGPG---QSGPSYGGQQHSFANT	
Scu	(270)	HAVLEGRILQLRFFPEREYRRLKSYLRSQLRQLSTQAUISLAPPKRFBAASLPPSA---PSMAFAGASAPSYGGGQ---HGGGPG---QSGPSYGGQQHSFANT	
Scab	(304)	HAVLEGRILQLRFFPEREYRRLKSYLRSQLRQLSTQAUISLAPPKRFBAASLPPSA---PSMAFAGASAPSYGGGQ---HGGGPG---QSGPSYGGQQHSFANT	
Sav	(281)	HAVLEGRILQLRFFPEREYRRLKSYLRSQLRQLSTQAUISLAPPKRFBAASLPPSA---PSMAFAGASAPSYGGGQ---HGGGPG---QSGPSYGGQQHSFANT	
Sven	(237)	HAVLEGRILQLRFFPEREYRRLKSYLRSQLRQLSTQAUISLAPPKRFBAASLPPSA---PSMAFAGASAPSYGGGQ---HGGGPG---QSGPSYGGQQHSFANT	
Sgr	(246)	HAVLEGRILQLRFFPEREYRRLKSYLRSQLRQLSTQAUISLAPPKRFBAASLPPSA---PSMAFAGASAPSYGGGQ---HGGGPG---QSGPSYGGQQHSFANT	
		441	471
Hsub	(165)	-----	
Htub	(261)	-----	
Scu	(368)	QENAPVIRPQGPSHMGQAPSINRGFLIDRDM	
Scab	(411)	QENAPVIRPQGPSHMGQAPSINRGFLIDRDM	
Sav	(379)	QENAPVIRPQGPSHMGQAPSINRGFLIDRDM	
Sven	(334)	QENAPVIRPQGPSHMGQAPSINRGFLIDRDM	
Sgr	(353)	QENAPVIRPQGPSHMGQAPSINRGFLIDRDM	

B



C

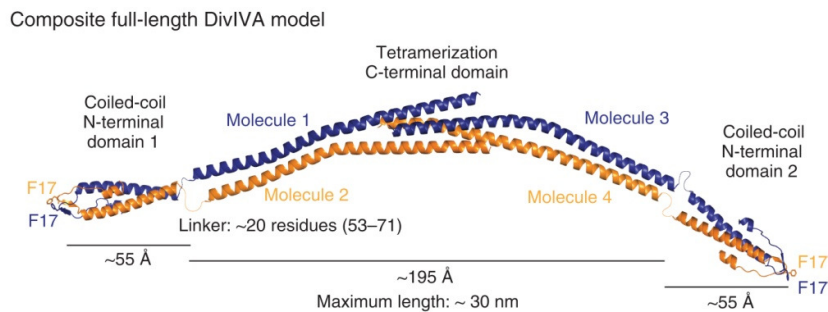


Figure 1.8 Comparison of selected DivIVA homologues from different Gram-positive bacteria.

(A) Alignment of DivIVA from *B. subtilis* (Bsub, CAB6818), followed by *M. tuberculosis* (Mtub, CAA54385) and 5 *Streptomyces* species: *S. coelicolor* (Sco, SCO2077), *S. scabies* (Scab, SCAB68081), *S. avermitilis* (Sav, SAV6129), *S. venezuelae* (Sven, SMDO2922), *S. griseus* (Sgr, SGR5428). The alignment was generated using VectorNTI and identical amino acids were coloured in red, conserved amino acids in blue and similar amino acids in green. (B) Domain organisation in *B. subtilis* and *S. coelicolor* DivIVA. (C) Composite model of *B. subtilis* DivIVA based on the crystal structures of the N- and C-terminal domains (Oliva *et al.*, 2010).

1.6.4 How is apical growth regulated?

Given that *Streptomyces* hyphae grow polarly at hyphal tips and establish new sites of polar growth along the lateral wall to develop into branches, the precise regulation of polarity is crucial to the filamentous growth habit of the organism. Therefore, the organism must have mechanisms to modulate not only where but also when new sites of cell wall growth are established along the hyphae, for example when hyphae run into an obstacle in the soil.

One way to regulate polar growth is by post-translational modifications such as protein phosphorylation. Protein phosphorylation is the most widespread type of post-translational modification used in signal transduction and control of protein activity and has been studied since the beginning of the 20th century. Phosphorylation affects many basic cellular processes, including metabolism, growth, division, differentiation, motility, cellular transport processes, muscle contraction, immunity, learning and memory (reviewed by Ubersax & Ferrel, 2007). In eukaryotes, the vast majority of protein phosphorylation occurs on serine and threonine residues.

Ser/Thr protein kinases function as molecular switches that are either in the inactive or active conformation and the transition between these two activity states is tightly regulated by various mechanisms such as the binding of effector molecules or subcellular location. The kinase catalytic domain is characterised by specific conserved motifs and invariant residues, which directly or indirectly position the phosphate donor ATP molecule and the protein substrate for catalysis (Hanks & Hunter, 1995). The kinases become activated by autophosphorylation of one or two Ser/Thr residues in the activation loop or by transphosphorylation of the activation loop by another kinase. Phosphorylation of this activation loop stimulates a stable, active protein conformation and thereby promotes substrate binding and phosphorylation (Nolen *et al.*, 2004).

Despite the prominent roles of Ser/Thr protein kinases in eukaryotic signal transduction, the importance of bacterial Ser/Thr protein kinases was for a long time largely overlooked, and overshadowed by the histidine kinases that target response regulators in conventional bacterial two-component signal transduction

systems (Stock *et al.*, 2000). The first description of a bacterial phosphoprotein in *E. coli*, isocitrate dehydrogenase, dates back to 1979 (Garnak & Reeves, 1979) and the first bacterial serine/threonine protein kinase, Pkn1 (required for normal development in *Myxococcus xanthus*), was characterised in 1991 (Munoz-Dorado *et al.*, 1991). However, it is now clear, for example from genomics and phosphoproteomics, that Ser/Thr protein kinases are extensively used by bacteria in a variety of regulatory roles (for a recent review, see Pereira *et al.*, 2011). For example, in *B. subtilis* the Ser/Thr protein kinase PrkC controls germination of spores in response to muropeptides released from bacterial cell walls, and in *Streptococcus pneumoniae* the Ser/Thr protein kinase StkP is involved in coordination of growth and cell division (Shah *et al.*, 2008a; Beilharz *et al.*, 2012; Fleurie *et al.*, 2012). These two bacterial species have only two and one Ser/Thr protein kinases, respectively, but the phylogenetic distribution of Ser/Thr protein kinases among bacterial taxa is uneven; some groups encode only a few per genome while others have dozens of Ser/Thr protein kinase genes, or in some cases even hundreds (Galperin *et al.*, 2010).

The Actinobacteria are an ancient and deeply branching bacterial phylum, in which Ser/Thr protein kinases are particularly widespread and abundant (Petrickova & Petricek, 2003; Molle & Kremer, 2010; Pereira *et al.*, 2011; Prisic *et al.*, 2010). For example, *M. tuberculosis* encodes 11 Ser/Thr protein kinases, two of which are the PASTA-domain containing kinases PknA and PknB (PASTA for penicillin-binding protein and Ser/Thr kinase associated).

PknB in *Mycobacterium* is the best studied example of a bacterial Ser/Thr protein kinase and the first kinase for which the crystal structure was solved (Ortiz-Lombardia *et al.*, 2003; Young *et al.*, 2003). PASTA-domain containing Ser/Thr protein kinases have one or more extracellular sensor domains containing the PASTA-motif. In the current model, the binding of a ligand molecule to the extracellular PASTA domains of two or more PknB kinase monomers changes the conformation of the intracellular kinase domains, bringing them closer together and leading to autophosphorylation and activation of the kinase. Activated kinases can then either directly phosphorylate their target or activate a soluble kinase, which in turn phosphorylates the target. In *M. tuberculosis*, both PASTA-domain

containing Ser/Thr protein kinases PknA and PknB have been shown to phosphorylate the DivIVA orthologue Wag31 (also called Ag84) on T73 between the two coiled coil domains (Kang *et al.*, 2005). This site is not conserved in *Streptomyces* DivIVA. Wag31 phosphorylation is not essential, but it seems to influence the growth rate. A phospho-ablative mutant Wag31 T73A grows much slower than the wild type (Kang *et al.*, 2008). In contrast, a phospho-mimetic mutant Wag31 T73E appears to have increased peptidoglycan and lipid biosynthesis (Hamasha *et al.*, 2010). Ser/Thr protein kinases PknA and PknB have clear effects on cell shape determination and *pknB* is an essential gene. Previous work suggested that PknA and PknB, directly or indirectly, affect cell wall integrity in *M. tuberculosis*, raising the possibility that they sense unlinked peptidoglycan via their PASTA domains and play a role in directing the cell wall biosynthetic machinery (Urabe & Ogawara, 1995; Jones & Dyson, 2006; Jung, 2007). This hypothesis concerning the role of PASTA domains has now been confirmed by studies on the *B. subtilis* PASTA-domain containing Ser/Thr protein kinase PrkC, which senses muropeptides and signals spores to exit dormancy (Shah *et al.*, 2008; Dworkin & Shah, 2010).

Recent work in *C. glutamicum* suggests that Ser/Thr phosphorylation of the coiled coil protein RsmP modulates its assembly dynamics and localisation and thereby might influence the regulation of growth at the cell poles (Fiuza *et al.*, 2010).

S. coelicolor encodes at least 34 Ser/Thr protein kinases (**Figure 1.9**; Petrickova & Petricek, 2003) and a recent phosphoproteomic survey detected at least 40 phosphoproteins (Parker *et al.*, 2010a; Parker *et al.*, 2010b), most of them being phosphorylated on serines and threonines, but the number of substrates is anticipated to be much larger, underlining both the fundamental importance of actinobacterial Ser/Thr protein kinases, but also the need for improved understanding of their substrates and biological functions.

There is no in-depth knowledge of any Ser/Thr protein kinases in *Streptomyces*, and almost the only ones that have been studied are AfsL (SCO4377), AfsK (SCO4423) and PkaG (SCO4487), worked on by Horinouchi and colleagues since the 1980s, mostly in *S. griseus* and *S. lividans*. These three kinases are implicated in a signal transduction pathway involved in secondary metabolism (**Figure 1.10**)

(reviewed by Umeyama *et al.*, 2002). In brief, AfsL, AfsK and PkaG are proposed to sense some undefined environmental or nutritional condition, leading to phosphorylation of the regulatory protein AfsR (SCO4426). Phosphorylated AfsR then activates transcription of *afsS* (SCO4425), and AfsS in turn activates expression of several secondary metabolite gene clusters, including those for actinorhodin and undecylprodigiosin.

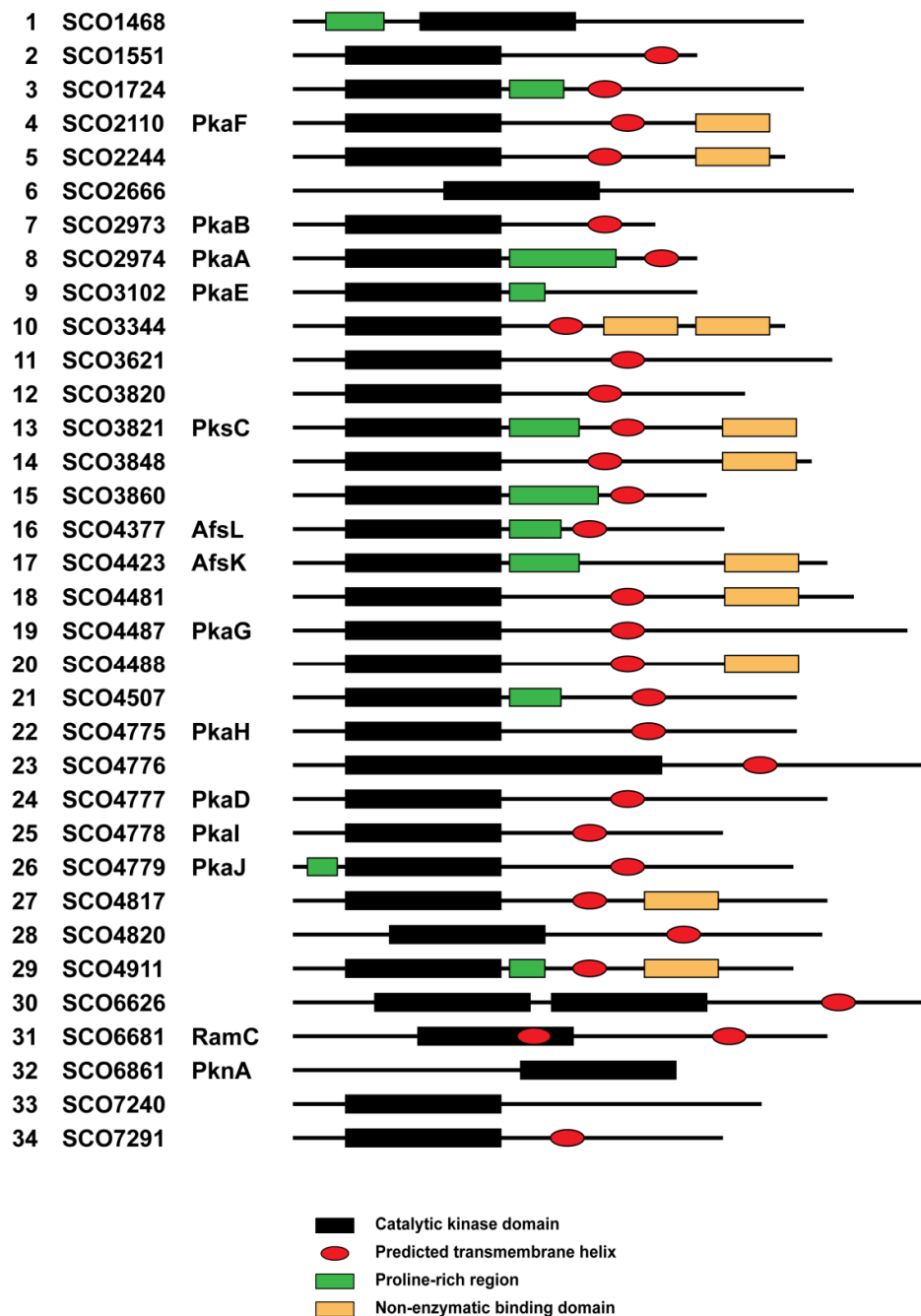


Figure 1.9 Overview of 34 predicted Ser/Thr protein kinases in *S. coelicolor*.

Figure modified from Petrickova & Petricek (2003).

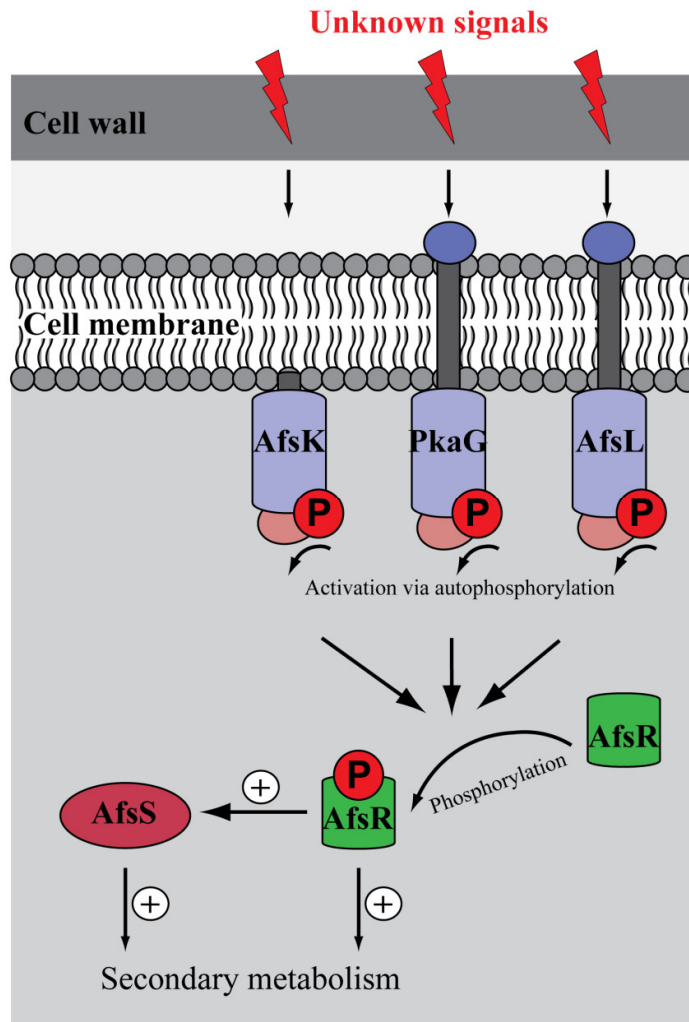


Figure 1.10 AfsR signal transduction cascade influences secondary metabolism in *S. coelicolor*.

1.6.5 What is the cell polarity system directing?

Not much is known about which processes are directed by the cell polarity system in *Streptomyces* and how this is achieved mechanistically, but there is evidence of at least four areas that seem to be directed or at least linked to cell polarity; polar cell wall synthesis, polar secretion of cellulose and assembly of fimbriae, nucleoid migration and DNA transfer by means of conjugation.

In the current view it is assumed that the polarisome complex directs the cell wall biosynthetic machinery that extends hyphae and forms new branches (Hempel *et al.*, 2008). Although interaction with specific members of the *Streptomyces* cell wall biosynthetic machinery remain to be confirmed, it has been shown for the DivIVA homologue Wag 31 in *M. tuberculosis* that it interacts with PBP3 (encoded by *ftsI*), although this interaction may not to be essential for cell growth (Mukherjee *et al.*, 2009).

Recently, an *in silico* analysis of the *S. coelicolor* genome identified 56 candidate cell wall hydrolase genes. Cell wall hydrolase enzymes are known to remodel the cell wall by incorporating newly synthesised peptidoglycan thereby accommodating changes in cell shape. Two of these hydrolase genes are predicted to encode a lytic transglycosylase (SwLB), and an endopeptidase (SwIC) and have been shown to play a role in formation and development of lateral branches (Haiser *et al.*, 2009).

Cellular architecture is strongly influenced by the deposition of β -glucan-containing polysaccharides produced by cellulose synthase and synthase-like enzymes. A recent *Streptomyces* study speculates that the polar localised cellulose synthase-like protein CslA may couple extracellular and cytoskeletal components to control tip growth and morphological development (Xu *et al.*, 2008). Bacterial two-hybrid analysis showed that CslA directly interacts with DivIVA, although an *in vivo* interaction and the mechanism of action remains to be investigated. Remarkably, a recent study by (de Jong *et al.*, 2009) suggests that cellulose may play a role in attachment of hyphae to surfaces by cellulose-anchored amyloid fimbriae.

As most cell division genes in *Streptomyces* are not essential for vegetative growth, only occasional cell division is taking place in vegetative hyphae and the

chromosomes remain uncondensed and unsegregated (McCormick, 2009). Yet, during hyphal growth these chromosomes have to replicate, segregate and move forward towards the hyphal tips and into newly developing branches in order to ensure efficient hyphal growth (Flärdh, 2003b). With the development of new microscopical tools, recent advances have shown that replisomes assemble close to the hyphal tips and follow the hyphal tip at a speed similar to the tip growth speed (Wolanski *et al.*, 2011). Replication occurs asynchronously and only specifically selected chromosomes are replicated (Ruban-Osmialowska *et al.*, 2006). Branch formation seem dependent on the presence of a replisome (Wolanski *et al.*, 2011). However, the molecular mechanism driving nucleoid migration remains mysterious.

A recent report suggests that *Streptomyces* have adapted the FtsK/SpoIIIE system known to drive chromosome segregation during cell division to transfer plasmid DNA between two distinct *Streptomyces* hyphae (Vogelmann *et al.*, 2011). This involves the protein TraB that covalently binds to double-stranded DNA of the circular plasmid before forming a pore in the cell envelope and subsequent DNA translocation during conjugation. TraB was also shown to be polarly localised suggesting that the hyphal tips are the actual sites of cell contact and DNA transfer (Vogelmann *et al.*, 2011).

1.7 Aims of this thesis

Streptomyces and other members of the phylum Actinobacteria grow in a polarised fashion. Filamentous *Streptomyces* in particular form a branched hyphal network, which shows striking analogy to the growth habit of filamentous fungi. In evolutionary terms, *Streptomyces* probably represent the most ancient form of polar growth known. Cell polarity, apical growth and hyphal branching are orchestrated by a multi-protein polarisome complex at the hyphal tips. The essential coiled-coil protein DivIVA is a key component of the polarisome complex, and forms distinct foci at the tips of established hyphae and along the lateral wall preceding the initiation of branch development.

The aims of this thesis were to investigate how new branch sites are selected in *Streptomyces* and how polar growth and lateral branching are regulated at the molecular level.

Chapter 2

Materials and Methods

2.1	Bacterial strains and plasmids	53
2.1.1	<i>E. coli</i> strains	55
2.1.2	<i>S. coelicolor</i> strains	55
2.1.3	Plasmids	57
2.2	Growth conditions and storage of bacterial strains	58
2.2.1	<i>E. coli</i> strains	58
2.2.2	<i>S. coelicolor</i> strains	59
2.3	Culture media and antibiotics	60
2.3.1	Antibiotic concentrations for <i>E. coli</i> and <i>S. coelicolor</i>	60
2.3.2	Solid media	61
2.3.3	Liquid media	62
2.4	General Molecular Biology Methods	63
2.4.1	Plasmid DNA isolation from <i>E. coli</i>	63
2.4.2	Genomic DNA isolation from <i>S. coelicolor</i>	63
2.4.3	Agarose gel electrophoresis	64
2.4.4	DNA extraction from agarose gels	64
2.4.5	DNA digestion with restriction enzymes	64
2.4.6	Ligation	64
2.4.7	Preparation and transformation of electro-competent <i>E. coli</i>	65
2.4.8	Preparation and transformation of chemically competent <i>E. coli</i>	65
2.4.9	Interspecies conjugation from <i>E. coli</i> to <i>S. coelicolor</i>	66
2.5	PCR and Sanger sequencing	67
2.5.1	Oligonucleotides	67
2.5.2	General PCR	67
2.5.3	PCR for ABI-automated sequencing	68

2.6	Construction of plasmids and PCR-targeted mutagenesis	68
2.6.1	Construction of <i>S. coelicolor</i> kinase mutants	68
2.6.2	Complementation of the <i>afsK</i> mutant	69
2.6.3	Construction of an AfsK-mCherry fusion	69
2.6.4	Construction of an allele encoding a constitutively active form of AfsK	70
2.6.5	Construction of pIJ10550	70
2.6.6	Construction of a <i>FLAG-divIVA</i> allele introducing two additional trypsin cleavage sites in the C-terminus	70
2.7	Protein experiments	71
2.7.1	Preparation of <i>S. coelicolor</i> cell extracts	71
2.7.2	Determination of protein concentration	72
2.7.3	Immunoprecipitation of FLAG-DivIVA	72
2.7.4	<i>In vitro</i> dephosphorylation of immunoprecipitated DivIVA	72
2.7.5	SDS-PAGE	73
2.7.6	ProQ-Diamond Staining of SDS-PA gels	73
2.7.7	Immunoblotting	74
2.7.8	<i>In vitro</i> phosphorylation of DivIVA	74
2.8	Proteomics	75
2.8.1	MALDI-ToF	75
2.8.2	Nano-HPLC MALDI-ToF	76
2.9	Microscopy	77
2.9.1	Light microscopy	77
2.9.2	Analysis of hyphal branching data from still images	78
2.9.2	Time-lapse microscopy	79

2.1 Bacterial strains and plasmids

2.1.1 *E. coli* strains

Table 2.1 *E. coli* K12 strains used in this study.

<i>E. coli</i> strain	Genotype	Reference
DH5 α	F' <i>supE44</i> Δ <i>lacU169</i> (Φ 80 <i>lacZ</i> Δ <i>M15</i>) <i>hsdR17</i> <i>recA1</i> <i>endA1</i> <i>gyrA96</i> <i>thi-1</i> <i>relA1</i>	Hanahan, 1983
ET12567/pUZ8002	F' <i>dam13::Tn9</i> <i>dcm6</i> <i>hsdM</i> <i>hsdR</i> <i>recF143::Tn10</i> <i>galK2</i> <i>galT22</i> <i>ara-14</i> <i>lacY1</i> <i>xyl-5</i> <i>leuB6</i> <i>thi-1</i> <i>tonA31</i> <i>rpsL</i> <i>hisG4</i> <i>tsx-78</i> <i>mtl-1</i> <i>glnV44</i> , Chl ^R , Tet ^R ; carries RK2 derivative with defective <i>oriT</i> for plasmid mobilisation, Kan ^R	Flett <i>et al.</i> , 1997

2.1.2 *S. coelicolor* strains

Table 2.2 *S. coelicolor* A3(2) strains used in this study.

<i>S. coelicolor</i> strain	Genotype	Reference
M145	Prototrophic, SCP1 ⁻ SCP2 ⁻	Kieser <i>et al.</i> , 2000
M600	Prototrophic, SCP1 ⁻ SCP2 ⁻	Kieser <i>et al.</i> , 2000
J2130	M600 Δ <i>SCO3356</i>	Paget <i>et al.</i> 1999a
J3376	M600 Δ <i>SCO2110</i> (inframe)	Jung, 2007
J3377	M600 Δ <i>SCO3821</i> (inframe)	Jung, 2007
J3378	M600 Δ <i>SCO3848</i> (inframe)	Jung, 2007
J3379	M600 Δ <i>SCO2110</i> (inframe) Δ <i>SCO3821</i> (inframe)	Jung, 2007
J3381	M600 Δ <i>SCO3821</i> (inframe) Δ <i>SCO3848</i> (inframe)	Jung, 2007
J3382	M600 Δ <i>SCO2110</i> (inframe) Δ <i>SCO3848</i> (inframe)	Jung, 2007
J3385	M600 Δ <i>SCO3821</i> (inframe) Δ <i>SCO3848</i> (inframe) Δ <i>SCO2110::apr</i> (Apra ^R)	Jung, 2007

Chapter 2 – Material and Methods

K112	M145 <i>divIVA_{SC}⁺::pKF59[Φ(<i>divIVA_{SC}-egfp</i>)]</i>	Flårdh, 2003a
K128	M600 <i>attB_{pSAM2}::pKF67[tipAp-FLAG-divIVA]</i>	This work
K120	M145 <i>attB_{pSAM2}::pKF67[tipAp-FLAG-divIVA]</i>	Wang <i>et al.</i> , 2009
K324	M600 <i>ΔafsK::apr attB_{φBT1}::pKF252[divIVA-egfp]</i>	Stuart Cantlay
K325	M600 <i>attB_{φBT1}::pKF252[divIVA-egfp]</i>	Stuart Cantlay
K326	M600 <i>attB_{φC31}::pKF255[afsK-mCherry]</i>	Stuart Cantlay
K327	M600 <i>ΔafsK::apr attB_{φC31}::pKF255[afsK-mCherry]</i>	Stuart Cantlay
K330	M600 <i>attB_{φBT1}::pKF252[divIVA-egfp]</i> <i>attB_{φC31}::pKF255[afsK-mCherry]</i>	Stuart Cantlay
K335	M600 <i>attB_{φC31}::pKF275[tipAp-afsK (T165D T168D)]</i>	Stuart Cantlay
K336	M600 <i>attB_{φC31}::pIJ6902[tipAp]</i>	Stuart Cantlay
K338	M600 <i>attB_{φBT1}::pKF252[divIVA-egfp]</i> <i>attB_{φC31}::pKF275[tipAp-afsK (T165D T168D)]</i>	Stuart Cantlay
K339	M600 <i>attB_{φBT1}::pKF252[divIVA-egfp]</i> <i>attB_{φC31}::pIJ6902 [tipAp]</i>	Stuart Cantlay
M523	M600 <i>ΔafsR (inframe)</i>	Floriano & Bibb, 1996
M1101	M600 <i>ΔafsK::apr (Apra^R)</i>	Parker, 2010b
M1103	M600 <i>ΔSCO1468::apr (Apra^R)</i>	Parker, 2010b
M1104	M600 <i>ΔSCO2244::apr (Apra^R)</i>	Parker, 2010b
M1105	M600 <i>ΔSCO3102::apr (Apra^R)</i>	Parker, 2010b
M1106	M600 <i>ΔSCO3820-3821::apr (Apra^R)</i>	Parker, 2010b
M1107	M600 <i>ΔSCO4487-4488::apr (Apra^R)</i>	Parker, 2010b
M1108	M600 <i>ΔSCO4507::apr (Apra^R)</i>	Parker, 2010b
M1109	M600 <i>ΔSCO4775-4779::apr (Apra^R)</i>	Parker, 2010b
M1111	M600 <i>ΔSCO7240::apr (Apra^R)</i>	Parker, 2010b
M1117	M600 <i>ermEp* afsK</i>	Parker, 2010b

2.1.3 Plasmids

Table 2.3 Plasmids used in this study.

Plasmid	Genotype	Reference
pGEX(M)_AfsK	<i>afsK</i> (1-331 kinase domain) amplified with VM712 and VM739, digested and cloned with <i>Bam</i> HI and <i>Hind</i> III into pGEX(M)	Virginie Molle, Hempel <i>et al.</i> , 2012
pGEX(M)_DivIVA	<i>divIVA</i> amplified with VM748 and VM749, digested and cloned with <i>Bam</i> HI and <i>Hind</i> III into pGEX(M)	Virginie Molle, Hempel <i>et al.</i> , 2012
pIJ773	Source of the <i>FRT-apr-oriT-FRT</i> cassette (Apra ^R)	Gust <i>et al.</i> , 2003
pIJ6902	Mobilisable vector that integrates at <i>attB</i> _{ϕC31} in <i>S. coelicolor</i> , carries thiostrepton-inducible promoter <i>tipAp</i> (Apra ^R , Thio ^R)	Huang <i>et al.</i> , 2005
pIJ10550	Mobilisable vector that integrates at <i>attB</i> _{ϕC31} in <i>S. coelicolor</i> , carries thiostrepton-inducible promoter <i>tipAp</i> (Vio ^R , Thio ^R)	This work
pIJ10551	<i>afsK</i> amplified with phosphorylated primers <i>afsK</i> fwd and <i>afsK</i> rev, which introduced <i>Nde</i> I and <i>Hind</i> III restriction sites, cloned in <i>Sma</i> I site of pUC19 (Carb ^R)	This work
pIJ10552	<i>FLAG-divIVA</i> amplified with phosphorylated primers KF478 and KF86, which introduced <i>Nde</i> I restriction at ATG start site, cloned in <i>Sma</i> I site of pUC19 (Carb ^R)	This work
pIJ10553	Site-directed mutagenesis of pIJ10552 using phosphorylated primers AH13/14 and AH15/16, which introduced Q343R and Q360R (Carb ^R)	This work
pIJ10554	FLAG- <i>divIVA</i> (Q343R Q360R) cloned into pIJ10550 (Vio ^R)	This work
pKF210	Mobilizable vector that integrates at <i>attB</i> _{ϕC31} in <i>S. coelicolor</i> , carries promoterless <i>mCherry</i> gene (Apra ^R , Thio ^R)	Flärdh, unpublished
pKF59	Plasmid carrying <i>divIVA-egfp</i> fusion (Kan ^R)	Flärdh, 2003a

pKF67	<i>FLAG-divIVA</i> in pPM927 (Spec ^R)	Wang <i>et al.</i> , 2009
pKF252	<i>divIVA-egfp</i> , excised from pKF59 with <i>XbaI</i> and <i>NsiI</i> and cloned into <i>AvrII-NsiI</i> -cut pMS82 (Hyg ^R)	Stuart Cantlay, Hempel <i>et al.</i> , 2012
pKF255	<i>afsK</i> amplified with KF547 and KF548, digested and cloned with <i>BamHI</i> and <i>NdeI</i> into pKF210 to create an <i>afsK-mCherry</i> fusion (Apra ^R)	Stuart Cantlay, Hempel <i>et al.</i> , 2012
pKF275	<i>afsK</i> (T165D, T168D) allele cloned into pIJ6902 under control of <i>tipAp</i> (Apra ^R , Thio ^R)	Stuart Cantlay, Hempel <i>et al.</i> , 2012
pMS82	Mobilizable vector that integrates at <i>attB_{φBT}</i> in <i>S. coelicolor</i> (Hyg ^R)	Gregory <i>et al.</i> , 2003
pPM927	integrating <i>S. coelicolor</i> vector at <i>attB_{pSAM2}</i> containing <i>tipA</i> promoter (Spec ^R)	Smokvina <i>et al.</i> , 1990
pSET152	Plasmid cloning vector for the conjugal transfer of DNA from <i>E. coli</i> to <i>Streptomyces</i> spp. Integrates site-specifically at the <i>attB_{φC31}</i> attachment site (Apra ^R)	Bierman <i>et al.</i> , 1992
pUC19	<i>E. coli</i> multicopy cloning vector with <i>lacZ</i> selection (Carb ^R)	Yanisch-Perron <i>et al.</i> , 1985
pUZ8002	Non-transmissible <i>oriT</i> -mobilising plasmid (Kan ^R)	Paget <i>et al.</i> 1999a

2.2 Growth conditions and storage of bacterial strains

Unless stated otherwise, media preparations, culture conditions and antibiotic concentrations followed in general previous descriptions for *E. coli* (Sambrook & Russel, 2001) and *Streptomyces* (Kieser *et al.*, 2000). When required, X-gal was added to a final concentration of 40 µg/ml. For details see Materials and Methods section 2.3.

2.2.1 *E. coli* strains

In general, *E. coli* strains were cultured on solid or in liquid medium containing the appropriate antibiotics and incubated overnight at 37°C. Glycerol stocks were made from fresh overnight cultures by adding 40% (v/v) to an equal volume of culture and storing at -80°C.

2.2.2 *S. coelicolor* strains

In general, *Streptomyces* strains were grown on soya flour mannitol medium (SFM) containing the appropriate antibiotics and incubated at 30°C for 4 to 5 days. For spore preparation, *Streptomyces* strains were streaked to obtain a confluent lawn and incubated at 30°C for about 6 days. *Streptomyces* spores were harvested as described by Kieser *et al.* (2000) and stored in 20% glycerol at -20°C and -80°C. The viable spore concentration was determined by plating out a dilution series on SFM plates.

To inoculate *Streptomyces* liquid cultures, approximately 5×10^8 spores (per 25 ml final liquid culture volume) were pregerminated. Spores were pelleted to remove glycerol and resuspended in 5 ml 0.05 M TES pH 8. After a 10-minute heat shock at 50°C, tubes were cooled under tap water. An equal volume of double strength germination medium was added and spores were incubated at 37°C for 2.5 hours with shaking. Germinated spores were spun, inoculated in YEME and allowed to grow at 30°C with shaking at 250 rpm.

For expression of genes from the thiostrepton-inducible promoter, *tipAp*, thiostrepton concentrations between 0.1 and 10 µg/ml were used.

2.3 Culture media and antibiotics

Unless stated otherwise, media preparations followed previous descriptions Sambrook & Russel (2001) for *E. coli* and Kieser *et al.* (2000) for *S. coelicolor*.

2.3.1 Antibiotic concentrations for *E. coli* and *S. coelicolor*

Table 2.4 Antibiotic concentrations used in this study.

Antibiotic	Final concentration in media (µg/ml)
Apramycin (Apra)	50 (<i>E. coli</i>) 25 (<i>S. coelicolor</i>)
Carbenicillin (Carb)	100 (<i>E. coli</i>)
Chloramphenicol (Chlor)	25 (<i>E. coli</i>)
Hygromycin (Hyg)	40 (<i>E. coli</i>) 20 (<i>S. coelicolor</i>)
Kanamycin (Kan)	50 (<i>E. coli</i>) 5 (<i>S. coelicolor</i>)
Nalidixic acid (Nal)	25
Spectinomycin (Spec)	50 (<i>E. coli</i>) 100 (<i>S. coelicolor</i>)
Thiostrepton (Thio)	0.1-10 (<i>S. coelicolor</i>)
Viomycin (Vio)	30

For phosphorylation assays, I determined the minimal inhibitory concentration for various antibiotics. Therefore, *Streptomyces* wild-type hyphae were grown as described in **section 2.2** in YEME in the presence of different antibiotic dilutions. After 20 hours of growth the optical density was measured at 600 nm with a spectrophotometer and plotted against the concentration of antibiotics. For the experiment, I decided on the following final concentration for the experiments: 50 µg/ml bacitracin, 50 µg/ml vancomycin, 600 µg/ml phosphomycin, 200 µg/ml penicillin G, 25 µg/ml novobiocin, 150 µg/ml kanamycin, and 10 µg/ml thiostrepton.

2.3.2 Solid media

Table 2.5 Solid media used in this study.

Medium	Composition		Instructions for preparation
DNA (Difco nutrient agar)	Difco Nutrient Agar	4.6 g	Difco Nutrient Agar was placed in each 250 ml Erlenmeyer flask and distilled water was added. The flasks were closed and autoclaved.
	dH ₂ O to	200 ml	
L-Agar	Agar	10.0 g	The ingredients, except agar, were dissolved in distilled water and 200 ml were poured into 250 ml Erlenmeyer flasks each containing 2 g agar. The flasks were closed and autoclaved.
	Difco Bacto tryptone	10.0 g	
	NaCl	5.0 g	
	Glucose	1.0 g	
	dH ₂ O to	1000 ml	
LB-Agar	Agar	15.0 g	The ingredients, except agar, were dissolved in distilled water, the pH adjusted to 7.5 with NaOH and 200 ml aliquots were dispensed into 250 ml Erlenmeyer flasks containing 2 g agar. The flasks were closed and autoclaved.
	Difco Bacto tryptone	10.0 g	
	Yeast extract	5.0 g	
	NaCl	10.0 g	
	dH ₂ O to	1000 ml	
SFM medium (Soya flour mannitol medium)	Agar	20.0 g	Mannitol was dissolved in water and 200 ml aliquots poured into 250 ml Erlenmeyer flasks each containing 2 g agar and 2 g soya flour. The flasks were autoclaved twice (115°C, 15 minutes), with gentle shaking between the two runs.
	Mannitol	20.0 g	
	Soya flour	20.0 g	
	Tap water to	1000 ml	

2.3.3 Liquid media

Table 2.6 Liquid media used in this study.

Medium	Composition		Instructions for preparation
2× Double strength germination medium	Difco Casaminoacids	10.0	The ingredients were dissolved in distilled water, without CaCl ₂ , and aliquoted and autoclaved. CaCl ₂ was prepared as a 1M solution and autoclaved separately; 100 µl were added to 10 ml medium at time of use.
	Difco yeast extract	10.0	
	CaCl ₂	1.1	
	Glucose	1.0	
	dH ₂ O to	1000 ml	
L (Lennox)-Broth	Difco Bacto tryptone	10.0 g	The ingredients were dissolved in distilled water and aliquots dispensed and autoclaved.
	Difco yeast extract	5.0g	
	NaCl	5.0 g	
	Glucose	1.0 g	
	dH ₂ O to	1000 ml	
LB (Luria-Bertani)-broth	Difco Bacto tryptone	10.0 g	The ingredients were dissolved in distilled water, pH adjusted to 7.0 and aliquots dispensed and autoclaved.
	Difco yeast extract	5.0 g	
	NaCl	10.0 g	
	dH ₂ O to	1000 ml	
SOC	Tryptone	20.0 g	After dissolving the solutes in water, 10 ml 250 mM KCl was added and the pH was adjusted to pH 7 with 5 N NaOH. The volume was then made up to 1000 ml with deionised water and autoclaved. After autoclaving, 20 ml of sterile 1 M glucose and 5 ml of sterile 2 M MgCl ₂ were added.
	Yeast extract	5.0 g	
	NaCl	0.5 g	
	dH ₂ O to	950 ml	
TSB (Tryptone Soya Broth)	Oxoid tryptone soya broth CM129	30.0 g	
	dH ₂ O to	1000 ml	
YEME (Yeast Extract-Malt Extract Medium)	Difco Bacto peptone	3.0 g	After autoclaving MgCl ₂ ·6H ₂ O (2.5 M) to a final concentration of 5 mM (2ml/ l) was added.
	Difco yeast extract	5.0 g	
	Oxoid malt extract	3.0 g	
	Glucose	10.0 g	
	Sucrose	340 g	
	dH ₂ O to	1000 ml	

2xYT	Difco Bacto tryptone	16.0 g	The ingredients were dissolved in distilled water. The pH was adjusted to 7.4 with NaOH before autoclaving in aliquots.
	Difco yeast extract	10.0 g	
	NaCl	5.0 g	
	dH ₂ O to	1000 ml	

2.4 General Molecular Biology Methods

2.4.1 Plasmid isolation from *E. coli*

For high-quality preparations, plasmids were extracted using QIAprep Spin Miniprepkit (Qiagen) according to manufacturer's instructions.

Alternatively, for screening purposes, plasmids were prepared using the method of (Le Gouill *et al.*, 1994). Cells from an 1.5 ml-overnight culture were harvested by centrifugation and resuspended in 100 µl of solution 1 (50 mM glucose, 10 mM EDTA, 25 mM Tris-HCl pH 8, 100 µg/ml ribonuclease A). Then, 200 µl of fresh solution 2 (0.2 N NaOH, 1% SDS) was added and contents mixed gently by inversion, before 200 µl of chloroform was added. After 1 minute of lysis, 150 µl of solution 3 (249 g/l potassium acetate and 50% ml acetic acid) was added and the samples mixed by gentle shaking. After centrifugation at 13,000 rpm for 2 minutes at room temperature, the upper phase was transferred into a clean tube. DNA was precipitated with 95% ethanol, incubated for 10 minutes at -20°C and pelleted at 13,000 rpm for 5 minutes at 4°C. DNA was washed with 75% ethanol and resuspended in water or Tris-EDTA buffer (TE; 10 mM Tris-HCl pH 8, 1 mM EDTA).

2.4.2 Genomic DNA isolation from *S. coelicolor*

For quick preparation of genomic DNA for example used as PCR template for subsequent sequencing, the following protocol was used. A 10 ml-culture of *Streptomyces* was grown overnight in YEME. About 2 ml of mycelium was harvested by centrifugation and the pellet was resuspended in 100 µl P1 QIAprep Spin Miniprepkit (Qiagen) and vortexed. Then 100 µl P2 QIAprep Spin

Miniprepkit (Qiagen) were added and the mixture was boiled for 5 minutes. From a 50 – 200-fold dilution in water, 1 µl was used for a PCR reaction.

2.4.3 Agarose gel electrophoresis

DNA molecules were separated according to the size by gel electrophoresis using 0.5 - 1% agarose gels, 1x Tris-borate-EDTA buffer (TBE; 40 mM Tris-borate, 2 mM Na₂EDTA·H₂O, pH 8.5), and 10x loading buffer (20% Ficoll 400, 0.1 M EDTA pH 8.0, 1% SDS, 0.25% (w/v) bromophenol blue and 0.25% (w/v) xylene cyanol). As a size marker 1 kb DNA ladder (NEB) was used. Gels were stained with ethidium bromide (0.5-1 µg/ml in 1×TBE buffer) and documentation was done with a digital imaging system.

2.4.4 DNA extraction from agarose gels

Restriction fragments were isolated from agarose gels that were run and loaded as described above. Bands were visualised using long-wavelength UV light (310 nm) to minimise nicking of the DNA molecules. Fragments were excised with a razor blade and DNA fragments were then extracted using the QIAquick Gel Extraction Kit (Qiagen). Recovery was determined by agarose gel electrophoresis.

2.4.5 DNA digestion with restriction enzymes

Restriction enzyme digestion of plasmids was carried out according to the enzyme manufacturer's instructions. The reaction volume was usually 20 µl for analytical digests and 50-100 µl for preparative digests. Digests were typically carried out for 1-3 hours at the recommended temperature.

2.4.6 Ligation

Vector and insert DNA were mixed at a molar ratio of 1:2 or 1:3, respectively, with 1/10 volume 10× ligation buffer and 10 U T4 DNA ligase (NEB) in 20 µl total reaction volume. The mixture was incubated at 4°C overnight. The ligated

DNA was used to transform *E. coli* competent cells.

2.4.7 Preparation and transformation of electro-competent *E. coli*

An overnight culture of the desired *E. coli* strain was diluted 50-fold in 50 ml of fresh media and grown at 37°C with shaking to an OD₆₀₀ of 0.5-0.6. After chilling on ice for 5 minutes, the cells were harvested by centrifugation at 3500 rpm for 5 minutes at 4°C. The supernatant was discarded and the pellet resuspended in 50 ml ice-cold water and centrifuged as above. The pellet was resuspended in 50 ml ice-cold water and centrifuged as above. The supernatant was discarded and the pellet was resuspended in the remaining 100 µl 10% glycerol, quickly aliquoted and frozen at -80°C.

For each transformation, 50 µl of cells were quickly thawed and mixed with DNA (maximal 100 ng DNA). Electroporation was carried out in 0.2 cm ice-cold electroporation cuvettes using a BioRad GenePulser II set to: 200 Ω, 25 µF and 2.5 kV. The time constant was typically 4.5-4.9 ms. After addition of 0.8 ml ice cold SOC, cells were incubated at 37°C with shaking for 1 hour before plating. Plates containing the appropriate antibiotic selection were incubated overnight at 37°C.

2.4.8 Preparation and transformation of chemically competent *E. coli*

For quick transformations, a PEG/DMSO one-step procedure was chosen. An overnight culture of the desired *E. coli* strain was diluted 50-fold in 50 ml of fresh media and grown at 37°C with shaking to an OD₆₀₀ of 0.4-0.5. Cells were harvested by centrifugation at 3500 rpm for 5 minutes at 4°C. The supernatant was discarded and the pellet resuspended in one-tenth volume cold TSS. After the cells were incubated on ice for 20 minutes, they were quickly aliquoted and frozen at -80°C. For each transformation, 100-200 µl of cells were quickly thawed and incubated with DNA on ice for 30 minutes (maximal 100 ng DNA). After adding 0.8 ml pre-warmed SOC, cells were incubated at 37°C with shaking for 1 hour before plating.

For high-quality transformation of constructs into DH5 α , frozen commercial competent cells (Invitrogen) were used. Cells were quickly thawed. DNA was added to 25-50 μ l of competent cells, which were incubated on ice for 30 minutes. The suspension was heat-shocked at 42°C for 20 seconds, and then transferred to ice for 2 minutes. 0.8 ml of warm SOC was added to the suspension, which was incubated for 1 hour at 37°C. The transformed cells were plated out on plates containing the appropriate antibiotic selection and incubated at 37°C overnight.

2.4.9 Interspecies conjugation from *E. coli* to *S. coelicolor*

Plasmids were transferred from *E. coli* ET12567/pUZ8002 to *S. coelicolor* using a modified version of the protocol of Flett *et al.* (1997). *E. coli* ET12567/pUZ8002 with the plasmid of interest were grown at 37°C to an OD₆₀₀ of 0.4 to 0.6 in LB, washed twice with LB, and resuspended in 1/10 of the culture volume. For conjugation, 20 μ l of a dense *Streptomyces* spore preparation was mixed with 2x YT to a total volume of 1 ml and 500 μ l *E. coli* suspensions were added. The conjugation mix was centrifuged at low speed for 1 minute, resuspended, and dispersed on several SFM plates containing 10 mM MgCl₂. After 16 to 20 hours at 30°C, the plates were overlaid with 1 ml sterile water containing 0.5 mg nalidixic acid to suppress *E. coli* growth and appropriate antibiotics in 25-fold higher concentrations than the desired final concentration in the plate.

2.5 PCR and Sanger sequencing

2.5.1 Oligonucleotides

Table 2.7 Oligonucleotide primers used in this study.

Name	Sequence (5' – 3') ¹	Restriction site	Template
afsK fwd	aaaaacatatggtggatcagctgacg	<i>NdeI</i>	<i>afsK</i>
afsK rev	ttttaagctttcacgtcgtacgggc	<i>HindIII</i>	<i>afsK</i>
apraDIS	gatcgactgatgcatcagcgggtggagtgcaatgctgattc cggggatccgtcgac		<i>vio</i>
APRAdis	tccaacgcatctcgttctccgctcatgagctcagccaatgtag gctggagctgcttc		<i>vio</i>
KF478	ctggttaaccatgactacaaggacgacgatgacaagat gccggtgacccccgaggac	<i>NdeI</i>	divIVA
KF86	ggtcgacggcgagacggta		divIVA
AH13	ggtcgatggcggcggccgggc		divIVA
AH14	ggtgccgccgtaggacggagc		divIVA
AH15	ggcagatgctccccgcatgacc		divIVA
AH16	gctggccgccgtaggacggacc		divIVA

2.5.2 General PCR

For high-quality PCR reactions Phusion[®] High-Fidelity DNA Polymerase (Finnzymes) and synthetic oligonucleotides primers (Invitrogen or Sigma-Genosys) were used for PCR.

Typically, a reaction mixture contained 1x Phusion buffer, 200 μ M of each of the four dNTPs, 0.02 U/ μ l Phusion[®] High-Fidelity DNA Polymerase (Finnzymes), 1 μ M of each primer, and approx. 50 ng template DNA and 3% DMSO in a final volume of 50 μ l. Oligos were phosphorylated using T4 Polynukleotide kinase (NEB). All PCR products were initially cloned into the dephosphorylated *SmaI*-cut pUC19 and subsequently sequenced before being transferred to the final destination vector.

In general, two-step PCR was favoured. After the initial denaturation at 98°C for 3 minutes, the samples were subjected to 35 cycles of denaturation (98°C, 30

seconds) and annealing - extension (72°C, 30 seconds/ 1kb) and then incubated for 10 minutes at 72°C. In extreme cases (for example amplifying *afsK*), 10% DMSO was used and both, the initial denaturation time and the final extension time increased to 10 minutes.

The PTC-100 Programmable Thermo Controller (MJ Research, Inc.) was used in all PCR reactions. Subsequently, PCR products were purified using Qiagen PCR purification kit (Qiagen) and analysed by agarose gel electrophoresis.

2.5.3 PCR for ABI-automated sequencing

PCR sequencing reactions were prepared by adding 0.2 to 2 µg of plasmid DNA, or 15 to 30 ng of PCR product DNA, 1 to 5 pmol of primer, 0.5 µl of 100% DMSO, 2 µl of 5x sequencing buffer and 1 µl of Big Dye reaction mix (Big Dye Terminator v3.1, Applied Biosystems), and the total volume made up to 10 µl in 200 µl tubes. The PCR program was 25 cycles of 30 seconds at 96°C, 30 seconds at 50°C, and 4 minutes at 60°C. After the PCR, reactions were sent for automated sequencing. Vector NTI Advance 11 (Invitrogen) was used to compile and analyse the sequences.

2.6 Construction of plasmids and PCR-targeted mutagenesis

2.6.1 Construction of *S. coelicolor* kinase mutants

Ser/Thr protein kinase mutants of *S. coelicolor* M600 were generated by Yong-Gyun Jung and Jennifer Parker, Department of Biology, John Innes Centre (Jung, 2007; Parker 2010b; Hempel *et al.*, 2012) for details. In brief, the entire coding sequence of individual genes (*SCO1468*, *SCO2110*, *SCO2244*, *SCO3102*, *SCO3821*, *SCO3848*, *SCO4507*, *SCO7240*), or pairs of adjacent genes (*SCO3820* and *SCO3821*, *SCO4487* and *SCO4488*), or five adjacent genes (*SCO4775*-*SCO4779*) was replaced with an apramycin-resistance cassette (*apr*) deriving

from pIJ773, using the PCR-targeting method of Gust *et al.* (2003). The double and triple mutants corresponding to the three PASTA domain-containing eSTK genes (*SCO2110*, *SCO3821* and *SCO3848*) were built up by converting *apr*-marked mutations into in-frame deletions as described by Gust *et al.* (2003), and then re-using the *apr* cassette to replace the next gene. All Ser/Thr protein kinase mutant strains were verified by PCR and by Southern blot hybridization.

2.6.2 Complementation of the *afsK* mutant

For complementation of the *afsK* mutant, the *afsK* coding sequence and the entire upstream 217 bp intergenic region, which includes the mapped promoter (Lee *et al.*, 2002), was amplified using the primers KF549, which introduced a *SpeI* restriction site, and KF547, allowing the amplified fragment to be digested and ligated into the *EcoRV-SpeI*-cut pMS82. The resulting plasmid, pKF256, was introduced into *S. coelicolor* strains by conjugation and integrated into the chromosome at the ϕ BT1 attachment site. This was done by Stuart Cantlay, Department of Biology, Lund University, Sweden.

2.6.3 Construction of an AfsK-mCherry fusion

In order to fuse AfsK to a fluorescent protein, the *afsK* gene, including the promoter region, was amplified using the primers KF547 and KF548, which introduced *Bam*HI and *Nde*I restriction sites and replaced the stop codon with four glycine codons. This PCR product was ligated into *Bam*HI-*Nde*I-cut pKF210 resulting in an in-frame fusion of *afsK* with *mCherry* connected by a tetra-glycine linker. The resulting plasmid, pKF255, was introduced into *S. coelicolor* strains by conjugation and integrated into the chromosome at the *attB* _{ϕ C31} attachment site. This was done by Stuart Cantlay, Department of Biology, Lund University, Sweden.

2.6.4 Construction of an allele encoding a constitutively active form of AfsK

To create an *afsK* allele that would encode a constitutively active AfsK, site-directed mutagenesis was performed using primers KF658 and KF659 and pIJ10551 as the template. Briefly, the primers led to amplification of the entire plasmid as a linear fragment incorporating the desired mutations (T165D T168D), which were built into primers KF658 and KF659, respectively. The primers were phosphorylated prior to the PCR reaction, and the PCR product was purified and religated. To create an inducible construct, the *afsK* (T165D T168D) allele was cut out from the resulting plasmid, and subcloned into *NdeI-EcoRI*-cut pIJ6902, placing the *afsK* (T165D T168D) allele directly downstream of the thiostrepton-inducible promoter *tipAp* (Huang *et al.*, 2005). The resulting plasmid, pKF275, was introduced into *S. coelicolor* strains by conjugation and integrated into the chromosome at the *attB*_{φC31} attachment site. This was done by Stuart Cantlay, Department of Biology, Lund University, Sweden.

2.6.5 Construction of pIJ10550

The entire coding sequence of the apramycin (*apr*) resistance cassette in pIJ6902 was replaced with a viomycin (*vio*) resistance cassette deriving from pIJ790, using the PCR-targeting method of Gust *et al.* (2003) and primers *apraDIS* and *APRAdis*. The resistance cassette in the resulting vector pIJ10550 was verified by PCR and sequencing.

2.6.6 Construction of a *FLAG-divIVA* allele introducing two additional trypsin cleavage sites in the C-terminus

Initially, *divIVA* was amplified with phosphorylated primers KF478 and KF86, which introduced *NdeI* restriction site and an N-terminal FLAG-tag, and cloned in *SmaI* site of pUC19. This resulted in vector pIJ10552. To create a mutant *FLAG-divIVA* allele that would encode two additional tryptic cleavage sites Q343R and Q360R, site-directed mutagenesis was performed on pIJ10552 using primers

AH13/14 and AH15/16. Briefly, the primers led to amplification of the entire plasmid as a linear fragment incorporating the desired mutations (Q343R Q360R), which were built into the forward primers AH13 and AH15, respectively. The primers were phosphorylated prior to the PCR reaction, and the PCR product was purified and religated. The *FLAG-divIVA* (Q343R Q360R) allele was cut out from the resulting plasmid pIJ10553, and subcloned into *NdeI-BamHI*-cut pIJ10550, placing the *FLAG-divIVA* (Q343R Q360R) allele directly downstream of the thiostrepton-inducible promoter *tipAp* (Huang *et al.*, 2005). The resulting plasmid pIJ10554, was introduced into *S. coelicolor* strains by conjugation and integrated into the chromosome at the *attB_{φC31}* attachment site.

2.7 Protein experiments

2.7.1 Preparation of *S. coelicolor* cell extracts

Hyphae were harvested at 3,000 rpm for 4 minutes, washed twice in 10.3% sucrose and resuspended in appropriate buffer as stated below. Cell lysates were prepared using sonication with Ultrasonic Processor VibraCell™ VC100 (Sonics and Material Incorporated; 5-6 pulses, 8-12 output watts, 10 seconds) or bead beating with Fastprep™ (MP Biomedicals or FP120 BIO101 Thermo Electroporation; 6 times, 6.5 m/s, 30 seconds). After lyses, cell lysates were cleared by centrifugation at 13,000 rpm, 30 minutes at 4°C using a bench centrifuge, if appropriate followed by ultracentrifugation (Sorvall® RC M100, rotor PP80-AT-260, Sorvall DuPont) at 40,000 rpm, 1 hour at 4°C. The supernatant was saved and used for immunoprecipitation or analysed by sodium dodecyl sulphate polyacrylamide electrophoresis (SDS-PAGE) and Western Blotting.

For analysis of phosphorylation, hyphae were resuspended in immunoprecipitation buffer (IP buffer; 100 mM Tris-HCl pH 7.5, 5% glycerol, 50 mM sodium pyrophosphate, 1 mM sodium molybdade, 25 mM sodium fluoride, 25 mM glycerophosphate, 15 mM ethylene glycol tetracetic acid (EGTA), 5 mM

ethylenediaminetetraacetic acid (EDTA), 1% Triton X-100, 150 mM NaCl, 1 mM phenylmethylsulphonyl fluoride (PMSF), 10 μ M leupeptin, 1 nM calyculin A, 1 mM sodium orthovanadate). For mass spectroscopy, cell extracts were prepared in Tris buffered saline (TBS; 25 mM Tris-HCl pH 7.5, 150 mM NaCl) plus complete EDTA-free protease inhibitor cocktail (Roche).

2.7.2 Determination of protein concentration

Protein concentrations were determined using a BioRad D_c Protein Assay Kit (Bio-Rad Laboratories, Incorporated) according to the manufacturer's instruction using bovine serum albumin as protein standard.

2.7.3 Immunoprecipitation of FLAG-DivIVA

Cells were lysed as described in section 2.8 and the cleared lysate used for immunoprecipitation. To prepare the anti-FLAG[®] M2 affinity gel (Sigma-Aldrich Incorporated), an appropriate amount of the resin were either washed three times with IP buffer or with TBS before being mixed with equal amounts of total cell extracts. Mixtures were incubated 30 minutes to overnight at 4°C with gentle shaking. Beads were washed afterwards either three times with IP buffer/ 1 M NaCl and twice with IP buffer/1 mM PMSF or five times with TBS or TBS/ 1% Triton-X100. Bound proteins were eluted with 2x elution buffer (125 mM Tris-HCl pH 8, 4% SDS, 20% glycerol, 0.004% bromophenol blue) and boiling for 3 minutes. Alternatively, bound proteins were eluted by competition with 3x FLAG[®] peptide (Sigma-Aldrich Incorporated) in TBS or TBS/1% Triton-X100 for 1 hour at 4°C with gentle rotation.

2.7.4 *In vitro* dephosphorylation of immunoprecipitated DivIVA

DivIVA was dephosphorylated using lambda protein phosphatase (λ PPase; Sigma-Aldrich Incorporated, St. Louis, USA) according to the manufacturer's instructions and a modified protocol from (Peck, 2006). Preparation of cell extracts from liquid cultures of *S. coelicolor* and immunoprecipitations were carried out as described in **Section 2.8.1 to 2.8.3** using TBS as the buffer of choice. Immunoprecipitated DivIVA was eluted by 100 μ l 3x FLAG-peptide

solution (150 ng/ μ l; Sigma-Aldrich Incorporated, St. Louis, USA) and 21 μ l of the eluate was dephosphorylated using 100 U λ PPase for 10 minutes at 30°C. The reaction was stopped with 50 mM EDTA at 65°C for 60 minutes.

2.7.5 SDS-PAGE

Proteins were separated using 5% stacking and 12% separation SDS gels. Samples were mixed with 6x SDS loading dye (0.3 M SDS in 0.4 M Tris-HCl pH 6.8, 30% glycerol, 10% SDS, 0.6 M DTT, 0.012% bromophenol blue). Gels were run in 1x running buffer (3.02 g/l Tris base, 14.4 g/l glycine, 0.1% SDS, pH 8.3) using the BioRad Mini-Protean 3 Cell electrophoresis system (Bio-Rad Laboratories, Incorporated). Gels were run at 80 V until samples entered the separation gel, then at 150 V. Two types of protein standard markers were used; Precision Plus Protein Standard Dual Colour Marker (Bio-Rad Laboratories, Incorporated) or 7-175 kDa Broadrange Prestained Protein Marker (NEB) for general protein detection, and PeppermintStick Phosphoprotein molecular weight standard (Molecular Probes) for phosphorylation detection.

In general, gels were stained with 0.1% Coomassie brilliant blue G250 in 50% methanol/10% acetic acid and destained with 7% methanol/ 5% acetic acid or 20% ethanol/10% acetic acid. Images of such gels were captured using a digital imaging system.

2.7.6 ProQ-Diamond Staining of SDS-PA gels

Staining of gels for detection of phosphorylated proteins was done using Pro-Q[®] Diamond phosphoprotein gel stain (Molecular Probes) according to the manufacturer's instructions with some modifications. First, gels were fixed twice in 50% methanol/10% acetic acid for 30 minutes with gentle shaking. Then, they were washed 3 times in ultrapure deionised water for 10 minutes with gentle shaking. Thereafter, all steps were carried out in darkness to protect gels from strong light. Gels were stained for 60 to 90 minutes with gentle shaking. Destaining of the gels was done three times in 20% acetonitrile/50 mM sodium acetate pH 4.5 for 30 minutes with gentle shaking. Gels were washed once with ultrapure deionised water for 5 minutes and kept in water. Visualisation of

phosphorylation was done using a Typhoon 9410 Scanner (GE Healthcare) or Fujifilm FLA-7000 (Fujifilm) in fluorescence mode.

2.7.7 Immunoblotting

For immunoblotting, proteins were separated by SDS PAGE and transferred onto Immobilon™-P PVDF membrane (Millipore, USA) or Trans-Blot® 0.2 µm PVDF membrane (Bio-Rad Laboratories, Incorporated) as described previously (Flärdh, 2003). Transfer was done for 140 minutes at 100 V (300 mA) at 4°C (transfer buffer: 250 mM Tris base, 1.92 M glycine) using BioRad Mini-Protean 3 Cell electrophoresis system (Bio-Rad Laboratories, Incorporated). Membranes were blocked with 5% non-fat dry milk in 1x phosphate buffered saline (PBS; 137 mM NaCl, 2.7 mM KCl, 4.3 mM Na₂HPO₄·7H₂O, 1.4 mM KH₂PO₄, pH 7.4). Incubation with the primary antibody was done overnight with gentle shaking at 4°C using an anti-DivIVA_{SC} antiserum from rabbit (1:10,000 or 1:5,000). The membrane was washed three times with 5% non-fat dry milk in 1x PBS (1 time 1 minute, twice 20 minutes). Incubation with the secondary antibody was done for 30 minutes at room temperature with gentle shaking using swine anti-rabbit IgG linked to horseradish peroxidase (1:1,000; DakoCytomation Denmark A/S) or goat anti-rabbit IgG linked to horseradish peroxidase (1:10,000; Amersham Biosciences). Membranes were washed 5 times with 0.5% Tween 20 in 1x PBS (1 time 5 minutes, 4 times 30 minutes). Proteins were visualised by SuperSignal® West Pico Chemiluminescence (Pierce) and results were captured using a Kodak Digital Science™ Image Station 440CF (Kodak) or using the Amersham™ ECL™ Western Blotting detection kit (GE Healthcare) followed by exposure to X-ray film (Fujifilm).

2.7.8 *In vitro* phosphorylation of DivIVA

In vitro phosphorylation was carried out in 20 µl reactions containing the recombinant AfsK (1 µg), and/or DivIVA (4 µg) and 200 µCi/ml (65 nM) [γ -³³P]ATP (PerkinElmer, 3000 Ci/mmol) in phosphorylation buffer (25 mM Tris-HCl pH 6.8, 1 mM DTT, 5 mM MgCl₂, 1 mM EDTA). The reaction was carried out for 30 minutes at 37°C and stopped by addition of Laemmli sample loading

buffer and incubated at 100°C for 5 minutes before analysis by SDS-PAGE. After electrophoresis, gels were washed in 10% trichloroacetic acid for 10 minutes at 90°C then stained with Coomassie stain, dried and visualised by autoradiography overnight.

2.9 Proteomics

2.9.1 MALDI-ToF

Cell extraction and immunoprecipitation were performed as described in sections 2.9.1 – 2.9.3, except that Tris buffered saline (TBS; 25 mM Tris-HCl pH 8, 150 mM NaCl) supplemented with complete EDTA-free protease inhibitor cocktail (Roche) was used as the buffer, and bound proteins were eluted from the M2 beads by competition with 150 ng/ml 3x FLAG peptide (Sigma-Aldrich) in TBS containing 1% Triton-X100 for 1 hour at 4°C with gentle rotation. The immunoprecipitated DivIVA was digested with trypsin using magnetic trypsin beads (Clontech) for 10 minutes at 37°C in a vortex shaker. Without desalting or other concentration steps the resulting digest was mixed 1:1 with a saturated matrix solution of sinapinic acid (Fluka) in 30 % acetonitrile, 0.1 % TFA and 1 µl was spotted onto a polished stainless steel MALDI target and air dried. A portion of the digest was dephosphorylated for 1 hour at 37°C using glycerol-free calf intestinal alkaline phosphatase (NEB) and analyzed similarly. Co-crystallised spots of matrix and sample were washed briefly (<5 seconds) on the MALDI target where necessary using 10 mM ammonium phosphate, 0.1% TFA before analysis. Myoglobin was used for calibration.

Matrix-assisted laser desorption ionization-time of flight (MALDI-ToF) mass spectrometry was carried out on an UltraFlex™ MALDI-ToF ToF mass spectrometer (Bruker (UK) Ltd, Coventry, UK) in linear positive ionization mode using a 337 nm pulsed nitrogen laser with a 50 Hz repetition rate. The source voltage (IS1) was set to 25 kV, with IS2 at 23.4 kV, pulsed ion extraction delay at

80 ns and deflection of ions $m/z < 1000$. Linear detector voltage was 1.65 kV and 800 shots were collected per spectrum.

2.9.2 Nano-HPLC MALDI-ToF

Protein samples were digested with trypsin (sequencing grade, Roche, Basel, Switzerland) according to standard procedures. For limited trypsin digests, a trypsin:protein ratio of 1:100 and 30 minutes incubation time were used. The digestions were stopped by the addition of TFA (Rathburn Chemicals Ltd, Walkerburn, Scotland) to a final concentration of 0.5%.

For LC-MS/MS analysis, a sample aliquot was applied via a nanoAcquity™ (Waters, Manchester, UK) UPLC™-system running at a flow rate of 250 nL min⁻¹ to an LTQ-Orbitrap™ mass spectrometer (Thermo Fisher, Waltham, MA). Peptides were trapped using a pre-column (Symmetry® C18, 5 μm, 180 μm x 20 mm, Waters) which was then switched in-line to an analytical column (BEH C18, 1.7 μm, 75 μm x 250 mm, Waters) for separation. Peptides were eluted with a gradient of 3-40% acetonitrile in water/0.1% formic acid at a rate of 0.67% min⁻¹. The column was connected to a 10 μm SilicaTip™ nanospray emitter (New Objective, Woburn, MA, USA) attached to a nanospray interface (Proxeon, Odense, Denmark) for infusion into the mass spectrometer. The mass spectrometer was operated in positive ion mode at a capillary temperature of 200°C. The source voltage and focusing voltages were tuned for the transmission of MRFA peptide (m/z 524) (Sigma-Aldrich, St. Louis, MO). Data dependent analysis was carried out in orbitrap-IT parallel mode using CID fragmentation on the 5 most abundant ions in each cycle. For detection and analysis of phosphopeptides, multistage activation was used with neutral loss m/z of 48.99 and 32.66 (for 2+ and 3+ charged ions). For detailed analysis of specific potential phosphopeptides, their masses were included in an inclusion list for triggering MS2 fragmentation, and no dynamic exclusion was used.

The orbitrap was run with a resolution of 30,000 over the MS range from m/z 350 to m/z 1800 and an MS target of 10⁶ and 1 second maximum scan time. Collision energy was 35, and an isolation width of 2 was used. Only mono-isotopic 2+ and 3+ charged precursors were selected for MS2. The MS2 was triggered by a

minimal signal of 5000 with an AGC target of 3×10^4 ions and 150 milliseconds scan time. Dynamic exclusion was set to 1 or 2 counts and 60 seconds exclusion time with an exclusion mass window of ± 20 ppm. MS scans were saved in profile mode while MSMS scans were saved in centroid mode.

Tandem mass spectra were extracted by BioWorks version 3.3.1. (Thermo Fisher, Waltham, MA) or with MaxQuant version 1.1.1.36 (<http://maxquant.org>; Cox and Mann, 2008), and Mascot-mgf files were generated using suitable perl scripts. For peptide assignment, protein identification, and phosphorylation site identification, the Mascot search programme (Matrix Science, London, UK; version Mascot 2.3, in-house) was used. Searches were performed on the SPTreMBL database (taxonomy set to “*Streptomyces coelicolor*”) or a small database containing the target sequence in a background of 100 random *E. coli* sequences using 6 ppm precursor tolerance, 0.5 Da fragment tolerance, carbamidomethylation (C) as fixed modification, and oxidation (M) as well as phosphorylation (STY) as variable modifications. Mascot search results were imported and evaluated (especially regarding phosphorylation sites) in ScaffoldPTM (proteomsoftware.com, Portland, OR, USA).

The annotated spectra shown for visual inspection were generated using the Scaffold programme.

2.10 Microscopy

2.10.1 Light microscopy

Hyphae were prepared for microscopy as described previously (Flärdh, 2003a). For Differential interference contrast microscopy (DIC), phase-contrast and fluorescence microscopy, liquid cultures of *S. coelicolor* overnight were grown for 15 to 18 hours in YEME from pre-germinated spores. Samples of these cultures were spotted directly onto microscope slides coated with 1 % agarose in PBS and mounted with a cover slip. Photo documentation was done using a DIC 63x objective of a Nikon Eclipse 800 with an attached Pixera Pro600ES camera or

Leica DM6000 equipped with a Leica 100x/1.4 oil DIC immersion objective and optovar 0.7x and an attached Leica DFC420 camera. Images were acquired and analysed with Pixera software, Leica LAS AF7000 software (Leica) and ImageJ (National Institute of Health USA).

For fluorescence microscopy, equipment and imaging were as described previously (Salerno *et al.*, 2009). Deconvolution of fluorescence images used the iterative restoration algorithm in Volocity 3DM (Perkin Elmer) and a calculated point spread function, and was carried out on Z-stacks of over 50 images with 0.2 μm spacing, captured with a 100x NA 1.4 lens.

2.10.2 Analysis of hyphal branching data from still images

As described in more detail in Chapter 3 and Richards *et al.* (2012), it is important when measuring tip-to-branch distances to account for biases that might artificially skew the data. To do this we introduced a protocol that ensures that all measured hyphae have effectively the same length of 80 μm . Hyphae shorter than 80 μm were discarded and those longer than 80 μm were trimmed so that only the 80 μm nearest the tip remained. Since still images do not normally capture the exact instant at which a new branch emerges, it was necessary to infer the tip-to-branch distance at the moment of branching (failure to do so will result in biased tip-to-branch distances). Measurements from time-lapse microscopy have shown that an established tip extends at an approximately constant speed of $v_{\text{max}} = 8 \pm 4$ $\mu\text{m/hr}$. In contrast, newly developing branches initially extend at $v_0 = 4 \pm 2$ $\mu\text{m/hr}$, and then gradually increase in speed until they reach v_{max} after about $T = 90$ minutes (see Chapter 3 section 3.3). Using these values we inferred, for each measured branch, a distribution for the tip-to-branch distance at the moment of branching. We did this by allowing each of v_0 , v_{max} and T to fluctuate independently according to Gaussian distributions (which are truncated to ensure $0 < v_0 < v_{\text{max}}$ and $T > 0$). For each measured branch we randomly chose many sets $\{v_0, v_{\text{max}}, T\}$, each one leading to a tip-to-branch distance (impossible negative distances are discarded), which in turn led to a tip-to-branch distribution for that single branch measurement. Finally, the complete measured tip-to-branch

distribution was obtained by summing the normalized distributions of all the individual branch measurements.

2.10.3 Time-lapse microscopy

Live cell time-lapse microscopy was performed essentially as described in (Hempel *et al.*, 2008). In brief, hyphae of *S. coelicolor* strains were grown on 1% agarose pads with Oxoid antibiotic medium no. 3. Pads were sealed to the bottom by an oxygen-permeable Lumox Biofoil 25 membrane (Greiner Bio-One) and to the top by a coverslip. Samples were incubated at 24 to 27°C and observed using a Zeiss Axio Imager Z1 microscope, a 9100-02 EM-CCD camera (Hamamatsu Photonics), and Volocity 3DM software (Improvision). Images were captured every 6 minutes, processed by Volocity (adjustment of contrast and correction for photobleaching) and analysed using ImageJ. The brightness of DivIVA foci was measured using ImageJ and normalised to the background fluorescence of hyphae of *S. coelicolor* wild type that did not contain DivIVA-EGFP.

Chapter 3

Mechanistic basis of branch-site selection in *Streptomyces*

3.1	Introduction	82
3.2	Lateral polarisomes arise from splitting of apical polarisomes	83
3.3	Measurements of hyphal growth and lateral branching	86
3.3.1	Tip growth speed	86
3.3.2	Controlling for biases	88
3.4	How far behind the hyphal tip do new branches form	89
3.5	Development of a minimal mathematical model describing the growth of polarisomes	91
3.6	The tip-to-branch distribution is regulated by one aspect of the polarisome splitting mechanism	95
3.7	Verifying a prediction of the model concerning the tip-to-branch distribution	97
3.8	A different aspect of the polarisome splitting mechanism regulates the branch-to-branch distance	100
3.9	Full model: curvature-dependent polarisome splitting	104
3.10	Discussion	105
3.11	Summary Points	109

Statement of my work

This work was a collaboration project with David Richards and Martin Howard, Department of Computational and Systems Biology, John Innes Centre, and is now published as:

Richards, D. M.*, [A. M. Hempel*](#), K. Flårdh, M. J. Buttner & M. Howard, (2012) Mechanistic basis of branch-site selection in filamentous bacteria. *PLoS Comput Biol* **8**: e1002423. *Joint first authors

I performed all *Streptomyces* experiments and microscopy and analysed the raw data. Additional data analysis was done in collaboration with David Richards. My work is fully represented in **Figures 3.1, 3.2, 3.3** and **3.6** and proportionally represented in **Figures 3.4, 3.5** and **3.7** (*in-vivo Streptomyces* experiments).

3.1 Introduction

Hyphal growth has evolved independently in eukaryotic and prokaryotic microbes, including fungi and Gram-positive bacteria of the genus *Streptomyces*. This mode of growth depends on pronounced cellular polarity and the specific localisation of cell envelope assembly to one cell pole in order to achieve tip extension. New sites of growth arise by hyphal branching, which requires the re-orientation of cellular polarity and the *de novo* establishment of new zones of cell wall synthesis from which lateral branches emerge. The result is a mycelial network in which the regulation of branching largely determines the morphology and behaviour of the mycelium as it spreads through the environment. However, the general principles that control such cellular branching have remained unknown. In the current view, cell wall growth is directed by the polarity determinant DivIVA, which together with other proteins and cytoskeletal elements (for example Scy; Walshaw *et al.*, 2010) is suggested to form a tip-organising multi-protein complex – here referred to as the bacterial polarisome.

DivIVA is an essential component of this polarisome complex, so in this chapter I used the DivIVA-EGFP fusion protein as a marker to monitor the dynamics of the polarisome complex as a whole in *S. coelicolor* by live cell time-lapse imaging. These experiments revealed that lateral branches arise predominantly by a novel polarisome-splitting mechanism that bypasses the necessity for initial nucleation or a specific site-selection. In order to gain a deeper and more rigorous understanding of the regulation of hyphal branching, I then quantified hyphal branching patterns from still images, and in collaboration with David Richards and Martin Howard, Department of Computational and Systems Biology, John Innes Centre, we developed a mathematical model of the polarisome dynamics. This model demonstrates that this remarkably simple polarisome splitting mechanism is capable of quantitatively explaining all of the experimental branching pattern data, a result which is far from intuitive. Moreover, the model makes explicit predictions that have been experimentally verified. Since all hyphal bacteria are actinomycetes, this polarisome-splitting mechanism is likely to be widely relevant in this important phylum of bacteria, which account for the majority of commercially available antibiotics.

3.2 Lateral polarisomes arise from splitting of apical polarisomes

Previous studies have shown that DivIVA foci are always present at hyphal tips and at new branch points before outgrowth occurs (Flärdh, 2003a; Hempel *et al.*, 2008). However, the origin of such DivIVA foci and the factors that determine their localisation have remained unclear (Flärdh, 2010).

To further understand the branching process, I therefore studied more carefully how such polarisomes (marked with DivIVA-EGFP) are formed in *S. coelicolor* wild type (strain K112) and traced their origin from time-lapse images. These experiments revealed that new daughter polarisomes often arise from the existing polarisomes at growing hyphal tips, by a process we have termed polarisome splitting, in which a small cluster of the tip polarisome breaks off and is left behind on the lateral membrane. There it grows in size and, upon reaching a critical mass, initiates a new branch. An example is shown in **Figure 3.1**. The hyphal tip contains a large multi-protein polarisome (marked with DivIVA-EGFP) and established tips extend at an approximately constant speed. At about 12 minutes, the tip polarisome underwent splitting, leaving behind a small new daughter polarisome on the adjacent membrane (arrow). As the tip continued to extend, the new daughter polarisome remained in place on the membrane and grew in size and intensity. At about 42 minutes a new branch was formed with the daughter polarisome now at the tip of this new branch. Both the new branch and the original hyphal tip continue to extend in length.

In time-lapse imaging, polarisome splitting was only seen to occur from polarisomes associated with extending, growing tips; polarisomes that had not yet initiated a branch, such as the small daughter polarisome between 12 and 36 minutes in **Figure 3.1**, did not undergo splitting. I traced the origin of 52 nascent branches and found that 42 of them (81%) could be accounted for by polarisome splitting events. Since only sufficiently large and intense DivIVA-EGFP foci were visible above the background fluorescence, some foci could not be traced to their point of creation, and so this is likely to be an underestimate of the real proportion of branching arising from polarisome splitting. Thus, polarisome splitting, rather

than other potential mechanisms, such as spontaneous nucleation, appears to be the predominant method of branch-site selection in wild-type *Streptomyces* hyphae.

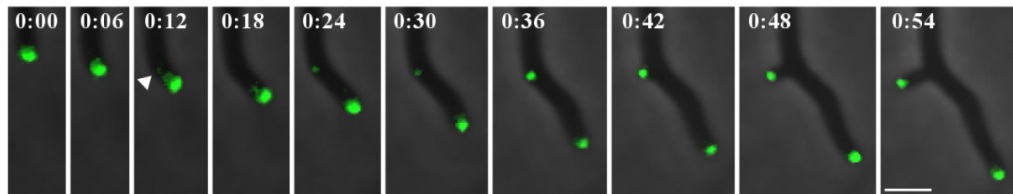


Figure 3.1 Evidence of polarisome splitting, growth of polarisomes and emergence of branches, in fluorescence-imaged *S. coelicolor* expressing *divIVA-egfp*.

For detailed information please refer to the text. Polarisomes are marked using DivIVA-EGFP and *S. coelicolor* strain K112 expressing *divIVA-EGFP*). The arrow head is pointing towards the split of the tip polarisome and thereby the break-off of the daughter polarisome. Time is shown in hours:minutes. Scale bar: 3 μm .

3.3 Measurements of hyphal growth and lateral branching

To understand *Streptomyces* branch-site selection quantitatively, I measured two categories of distances from still images: the distance between the tip and the points where new branches emerge, and the distance between the branches themselves. Whereas the branch-to-branch distance is fixed, the tip-to-branch distance is not, as the hyphae extend in length and so the tip-to-branch distances increase. Measurements from still images provided an extensive data set for statistical analysis. This is in contrast to the, in our case, relatively limited analysis possibilities of time-lapse imaging. But because still images do not normally capture the exact instant at which a new branch emerges, I measured the tip growth speed from time-lapse imaging, so that we were able to calculate the tip-to-branch distance at the moment when new branches emerged in still images.

3.3.1 Tip growth speed

I measured the extension rate of 45 established and 40 new branches. The initial growth speed for new branches was about half that of established branches, increasing linearly in time until full speed was reached after about ninety minutes. **Figure 3.2** shows the mean new branch growth speed against time (starting from when the branch first appears), and compares this to the mean growth speed of established hyphae. Using the same data the fluctuations in the initial and established extension speeds can also be estimated, from which I concluded that new branches initially grow at about $v_0 = 4 \pm 2 \mu\text{m hr}^{-1}$, and then gradually increase (approximately linearly) in speed until they reach $v_{\text{max}} = 8 \pm 4 \mu\text{m hr}^{-1}$ after about $T = 90$ minutes.

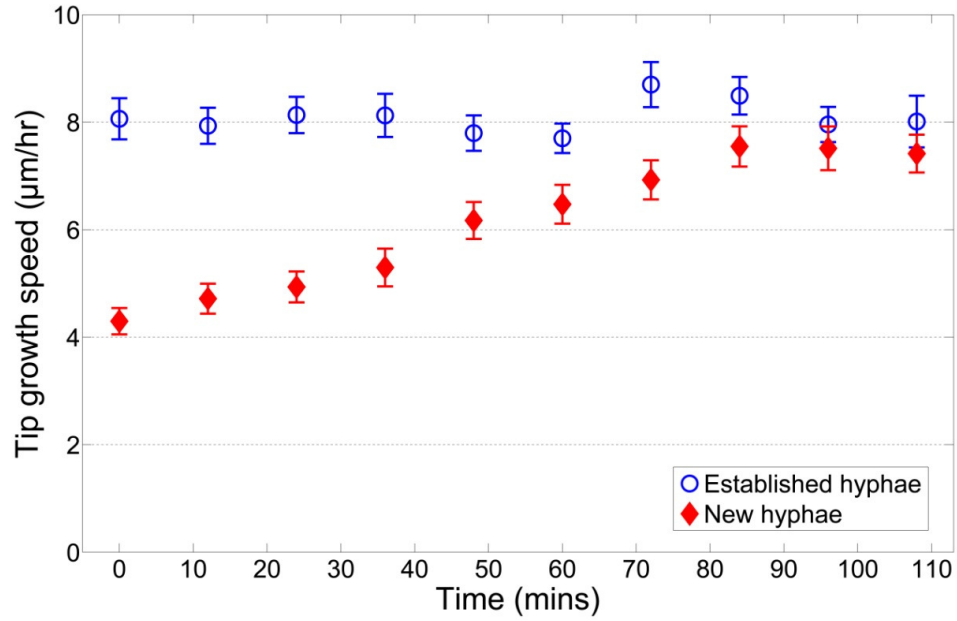


Figure 3.2 Tip growth speed against time for established hyphae and newly developed branches from time-lapse imaging of *Streptomyces* hyphae.

Error bars show the standard error of the mean.

3.3.2 Controlling for biases

Unless care is taken when measuring the distributions from still images, it is easy to introduce biases that uncontrollably skew the data. For example, if only branching events relatively close to hyphal tips are measured (as is inevitably the case for *Streptomyces* where individual hyphae cannot be traced into the dense mycelial clumps from which they emerge) then long branch-to-branch distances will never be recorded, even if they occur. This study controlled for this effect by introducing a protocol so that all measured hyphae had effectively the same length, a distance called the trim length. This was achieved by discarding hyphae which were shorter than the trim length. For all hyphae, which were longer than the trim length, only the segment within the trim distance of the tip was included in the data set. Thereby, all hyphae for which measurements were performed were trimmed to the fixed trim length.

The effect of trimming was necessary in order to ensure that all measured hyphae were effectively of the same length. As a consequence, both the tip-to-branch and branch-to-branch distributions explicitly depended on the trimming length. This protocol does not eliminate a measurement bias, but rather controls the bias so that the experimental measurements are unambiguous and can be precisely compared with data generated by the mathematical model (see below).

3.4 How far behind the hyphal tip do new branches form

Streptomycetes produce branches at a range of distances behind tips, leading to a distribution of tip-to-branch distances. To understand how far behind the hyphal tip new branches emerge, the average tip-to-branch distances were estimated from still images of growing *Streptomyces* hyphae, with the trimming protocol described above imposed on all measured data. The true average tip-to-branch distance was the average tip-to-branch distance extrapolated to infinite trim. Distributions at progressively smaller trims had progressively smaller average tip-to-branch distances. For the largest trim that a reasonable amount of data were obtained was 120 μm , with an average tip-to-branch distance of 67 μm . It was not obvious that this trim was high enough to give a good estimate of the true average tip-to-branch distance. However, by fitting the full distributions at 60 μm , 80 μm and 100 μm trims and extrapolating to infinite trim, this was seen to be a good approximation to the true average (data not shown, but see Richards *et al.*, 2012).

The measured tip-to-branch distributions with an 80 μm trim are shown in **Figure 3.3**. Instead of the expected Gaussian distribution, the tip-to-branch distance showed a bimodal distribution with two distinct peaks; one close to the origin between 0 – 5 μm and one at 40 – 45 μm . This might suggest that two distinct mechanisms are involved in the regulation of the tip-to-branch distance. Surprisingly, however, further analysis showed that a single mechanism could account for both peaks and all of the experimental data.

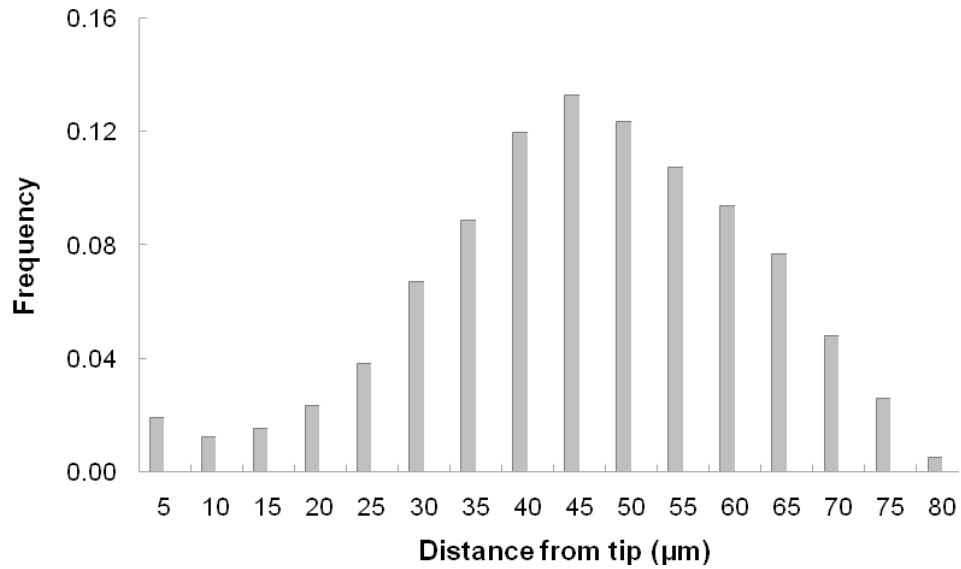


Figure 3.3 Histogram of tip-to-branch distribution of the experimental data at 80 µm trim.

For detailed information including the trimming protocol please refer to the text. 1097 experimental data points. Data analysis was done in collaboration with David Richards, Department of Computational and Systems Biology, John Innes Centre.

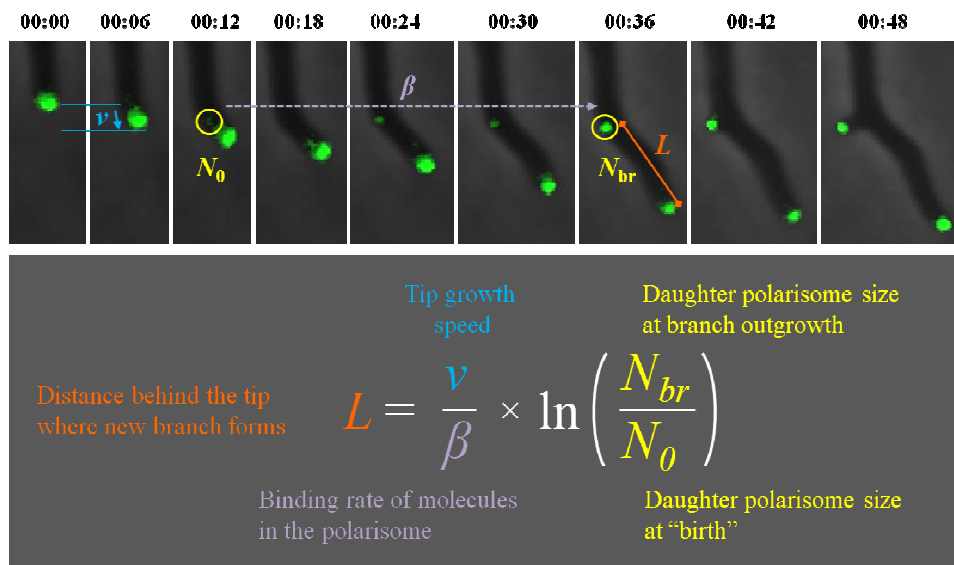
3.5 Development of a minimal mathematical model describing the growth of polarisomes

Polarisome splitting appears to be the predominant method of branch-site selection in wild-type *Streptomyces* hyphae (see section 3.2, page 83, **Figure 3.1**). In brief, while the hypha passes the future branch site, the tip polarisome splits and a small daughter polarisome breaks off and stays along the lateral wall. There it then grows in size and upon a critical size a new branch develops with this polarisome at the tip. In order to mechanistically understand how far behind the hyphal tip new branches form, it is necessary to understand how the number of molecules in a daughter polarisome changes over time – between the point where the small daughter polarisome split of the tip polarisome and the point when the new branch grows out with a bigger daughter polarisome at the tip. Most new daughter polarisomes do not immediately initiate a new branch. Instead, they sit on the lateral wall, grow in size and, upon reaching a critical mass, initiate a new branch. Implicit in this thinking is the assumption that the polarisome complex directs the cell wall biosynthetic machinery that extends hyphae and forms new branches. Although interaction with specific members of the *Streptomyces* cell wall biosynthetic machinery remain to be proven, it has been shown for the DivIVA homologue Wag 31 in *M. tuberculosis* that it interacts with PBP3 (Mukherjee *et al.*, 2009).

In collaboration with David Richards and Martin Howard, John Innes Centre, Norwich, a minimal mathematical model was developed that describes how *Streptomyces* develop branches (illustrated in **Equation 3.1**). Strikingly, this model is so simple that it was also solved analytically, but it was able to give mechanistic insights into how *Streptomyces* select new branch points. There follows a brief description of this model (for further details please refer to Richards *et al.*, 2012). The distance behind the hyphal tip (L) at which a new branch emerges equals the logarithm of the ratio of the size of the daughter polarisome at birth (N_0) to the size of the daughter polarisome at branch outgrowth (N_{br}) times the ratio of the rate of accumulation of molecules into the polarisome (β) to the tip growth speed (v). Simple cooperative binding was considered where the rate of molecules joining a polarisome is linearly dependent

on both the cytoplasmic concentration of DivIVA, and the polarisome size (N). In the minimal model it was assumed that polarisomes never lose any molecules; however, including this process in the full model made little or no difference. Also, it was assumed that the cytoplasmic concentration of DivIVA is uniform throughout the hyphae (this assumption was justified by the full model simulation; refer to Richards *et al.*, 2012).

The parameters listed in **Table 3.1** were used. By comparing images like **Figure 3.1** at 12 and 42 minutes, a typical value for $\frac{N_{br}}{N_0}$ [ratio of the size of the daughter polarisomes at birth (N_0) to the size of the daughter polarisomes at branch outgrowth (N_{br})] was estimated as between 5 and 10, so that, to a rough approximation, $L \approx \frac{2v}{\beta}$. The absolute value for the size of daughter polarisomes at branch outgrowth (N_{br}) is difficult to determine, but since the fluorescence of a typical DivIVA focus is not dissimilar to that of an FtsZ ring as quantified from still images of strains *S. coelicolor* strains expressing DivIVA-EGFP and FtsZ-EGFP (data not shown), and since an FtsZ ring contains on the order of 10,000 molecules (Lu *et al.*, 1998), N_{br} was taken to be of a similar order of magnitude. The growth speed of an established tip (v) was measured from time-lapse images to be about 8 $\mu\text{m}/\text{hr}$ (see **Figure 3.2**). Due to the trimming issues discussed above, measuring a typical value for the distance behind the tip where a new branch forms (L) is not straight forward. In particular, using the average of a trimmed distribution, such as that in **Figure 3.3**, will not give a good estimate. However, as explained above, by studying the distributions over a range of trims and extrapolating to infinite trim, a value of about 65 μm was estimated under the growth conditions used, which implies that the rate of accumulation of molecules (β) should be about $7 \times 10^{-5} \text{ s}^{-1}$. (See discussion and **Figure 3.8** for a schematic of the colony morphology for different values of β .) Streptomycetes produce branches at a range of distances behind tips, leading to a distribution of tip-to-branch distances. In this model, this is due to fluctuations in the parameters in **Equation 3.1**.



Equation 3.1

Illustration of the mathematical equation using **Figure 3.1**. For details please refer to the text and Richards *et al.* (2012).

Table 3.1 Main parameters and their values.

Parameter	Value
Tip growth speed, v	8 $\mu\text{m hr}^{-1}$
Binding parameter, β	$7 \times 10^{-5} \text{ s}^{-1}$
Mean initial focus size, $\langle N_0 \rangle$	1,700
Standard deviation in initial focus size, δN_0	1,000
Mean focus size for branch initiation, $\langle N_{\text{br}} \rangle$	10,000
Standard deviation in focus size for branch initiation, δN_{br}	2,600
Minimum polarisome size for polarisome splitting, N_{split}	10,000
Polarisome splitting probability per unit time, γ	$1 \times 10^{-3} \text{ s}^{-1}$

3.6 The tip-to-branch distribution is regulated by one aspect of polarisome splitting

In order to compare the minimal model with the experimental data, a simulation was developed which grows *Streptomyces* hyphae, implements polarisome splitting and focus growth, performs the trim to the required length, and extracts the distributions. For details of the minimal model simulation please refer to Richards *et al.* (2012). In brief, the parameters listed in **Table 3.1** were used and just N_0 and N_{br} were varied. This was sufficient to fit all the measured distributions. For simplicity, N_0 and N_{br} followed independent truncated Gaussian distributions, where the truncation ensured that N_0 and N_{br} were always positive. This was required since Gaussian distributions assign non-zero probabilities to all values, whereas biologically foci cannot contain fewer than zero molecules.

As **Figure 3.4** shows, there was excellent agreement between the data derived from the minimal model and the experimental data. For the trimmed tip-to-branch distributions, this model was sufficiently simple that this distribution could be calculated analytically without recourse to simulations. The analytic prediction is also shown in **Figure 3.4** (curved line) and agrees extremely well with the simulation data, as expected. Note that the reason the tip-to-branch distribution drops to zero at 80 μm is a consequence of the trimming protocol rather than any inherent property of *Streptomyces*. An 80 μm trim was chosen as a trade-off between the distribution width and the amount of data available for analysis, but it was also possible to compare the model and the experimental data at other trims (see Richards *et al.*, 2012).

It was confirmed that the tip-to-branch and the branch-to-branch distributions generated by the minimal model are robust to changes in all the parameters listed in **Table 3.1**. Further, it was also shown that adding fluctuations in the tip growth speed, v , and the on-rate parameter, β , do not qualitatively change these distributions.

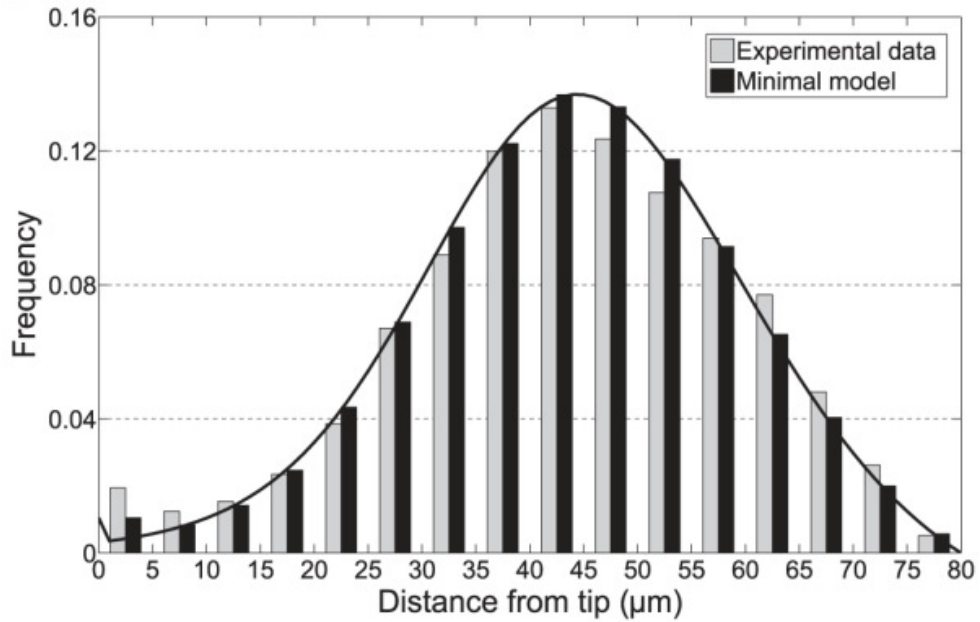


Figure 3.4 Comparison of histograms of the tip-to-branch distribution between minimal model and experimental data at 80 μm trim.

The analytic prediction is shown as a curved line. 1097 experimental data points were used. Data analysis of experimental data was done in collaboration with David Richards, Department of Computational and Systems Biology, John Innes Centre. Data derived from the minimal mathematical model and the analytical prediction were kindly provided by David Richards.

3.7 Verifying a prediction of the model concerning the tip-to-branch distribution

One of the most striking features of the experimentally measured tip-to-branch distribution was the peak at zero distance between 0 – 5 μm (**Figure 3.3**). Naïvely it may be thought that a second mechanism is required to account for this peak. However, the model predicts this peak without additional assumptions (**Figure 3.4**).

Since most new polarisomes must attract more molecules before they can initiate a new branch, the distributions of N_0 and N_{br} must be such that most new foci start with fewer than N_{br} molecules. However, there is a small tail to the distributions such that a few nascent polarisomes have N_0 above N_{br} , *i.e.* when they are formed these foci already have enough DivIVA molecules to initiate branch outgrowth. These foci will cause branching almost as soon as they are formed, very close to zero distance from the tip. I have directly observed such events and one example is shown in **Figure 3.6**. Furthermore, I also measured the total intensity of 25 newly produced foci from time-lapse images: 12 from cases where the new branch appears next to the tip and 13 from normal polarisome splitting events when the new branch appears much further back (data not shown). In the first case the average intensity is almost three times greater than in the second case, supporting the hypothesis that events where the branch appears next to the tip correspond to the initial focus size, N_0 , being much greater than average. The entire weight of the distribution with $N_0 \geq N_{\text{br}}$ will give effectively zero tip-to-branch distances, which then naturally explains the peak at the origin in **Figure 3.3 and 3.4**. Consequently, the model predicts that if the distribution is analysed with bins of smaller width, then the peak at the origin will become even more dramatic. After reanalysing the measured data, this prediction was strikingly confirmed, as shown in **Figure 3.5**. Although the peak in the 0 – 1 μm bin matched well, the agreement was not perfect in the range 1 – 6 μm . However, this feature is most likely an unavoidable artefact of how the data were analysed: the tip growth speed cannot be measured directly from still images, rather only the distribution of speeds is known, which necessarily slightly smears the data.

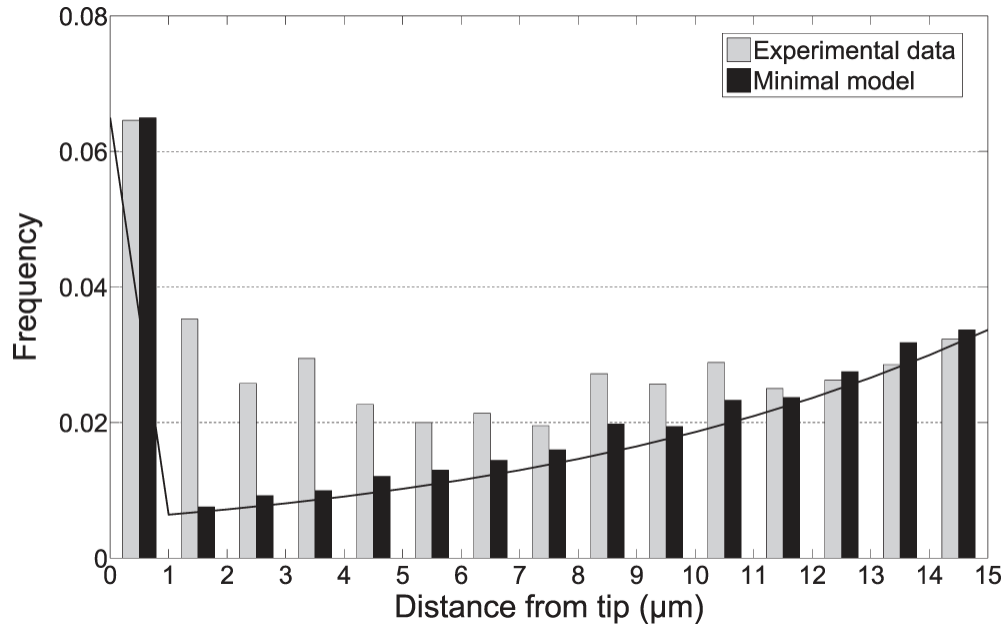


Figure 3.5 Comparison of tip-to-branch distribution at small distances between minimal model and experimental data at 80 μm trim.

The analytic prediction is shown as a curved line. Data analysis of experimental data was done in collaboration with David Richards, Department of Computational and Systems Biology, John Innes Centre. Data derived from the minimal mathematical model and the analytical prediction were kindly provided by David Richards.

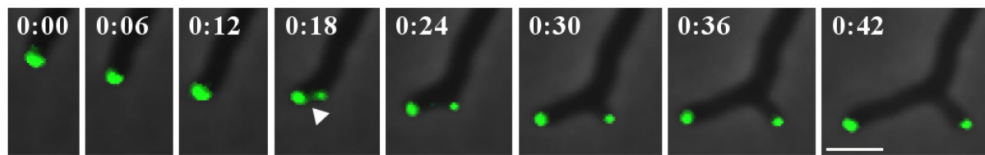


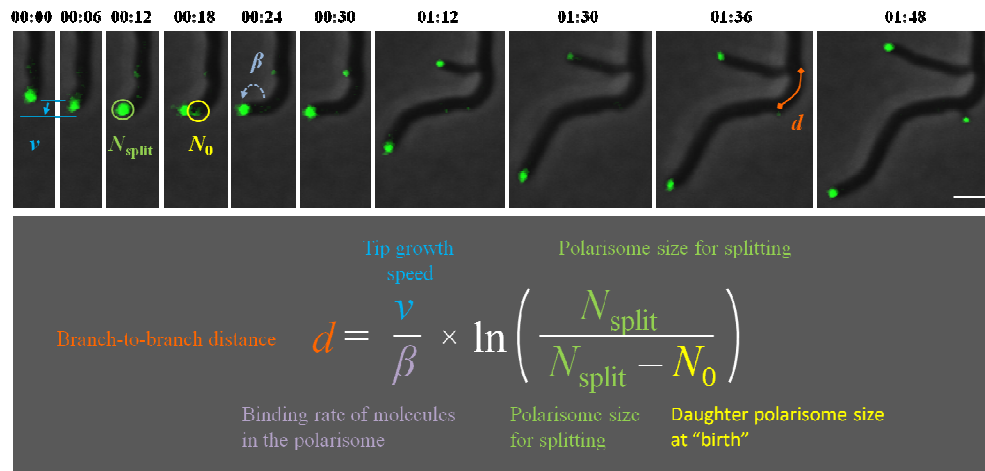
Figure 3.6 Example of branch development at almost zero distance from the hyphal tip in fluorescence-imaged *S. coelicolor* expressing *divIVA-egfp*. Polarisomes are marked using DivIVA-EGFP and *S. coelicolor* strain K112 expressing *divIVA-EGFP*). The arrow head is pointing towards the split of the tip polarisome and thereby the break-off of the daughter polarisome. This resulting daughter polarisome is already big enough to trigger branch outgrowth straight away and this is exactly what the model predicts; polarisome splitting events (arrow) where N_0 is greater than N_{br} . Thereby,. Time in hours:minutes. Scale bar: 3 μm .

3.8 A different aspect of the polarisome splitting mechanism regulates the branch-to-branch distance

So far we have been concerned with how daughter polarisomes grow and so the number of molecules in daughter polarisomes changes with time. However, the aspect of the polarisome splitting mechanism by which these new daughter polarisomes are formed was not discussed yet. Furthermore, after a tip polarisome has split, it is interesting to know the length of time before it can split again, because, after polarisomes have initiated new branches, this length of time translates into the distance between branches. It is important to emphasise that, whereas the growth of daughter polarisomes controls the tip-to-branch distribution, it is the frequency of tip polarisome splitting that controls the branch-to-branch distribution. The simplest assumption that could be made would be that the polarisome-splitting probability per unit time is constant, independent of when the polarisome last split. This would describe a Poisson process and so imply an exponential distribution for the branch-to-branch distribution. However, as **Figure 3.7** shows, for distances smaller than 10 μm , the branch-to-branch histogram is not described by a decaying exponential: these shorter distances are measured much less frequently than implied by a Poisson distribution.

This suppression of short branch-to-branch distances shows that tip polarisome-splitting events are not independent of each other: a polarisome that has just split is less likely to split again immediately. One potential explanation is that the probability of polarisome splitting depends on the polarisome size, such that smaller tip polarisomes are less likely to split. For this reason a minimum polarisome size (N_{split}), was implemented, below which the polarisome cannot split, with some constant polarisome-splitting probability per unit time (γ), for all tip polarisomes above N_{split} . Splitting events cause the polarisome to decrease in size and so, in some instances, such a splitting will cause the polarisome size to drop below N_{split} . In that case, only after the polarisome has absorbed more molecules from the cytoplasm will it have sufficient size to split again. This time delay effectively reduces the number of short branch-to-branch distances.

Although it is difficult to analyse polarisome splitting analytically, it is useful to note that, in the limit where γ is very large (compared to β), the branch-to-branch distance (d) is given by **Equation 3.2**, a result which follows the principles of **Equation 3.1**.



Equation 3.2

Illustration of the mathematical equation, which follows the principles of **Equation 3.1**. For details please refer to the text and Richards *et al.* (2012). Time is in hours:minutes. Scale bar: 3 μm .

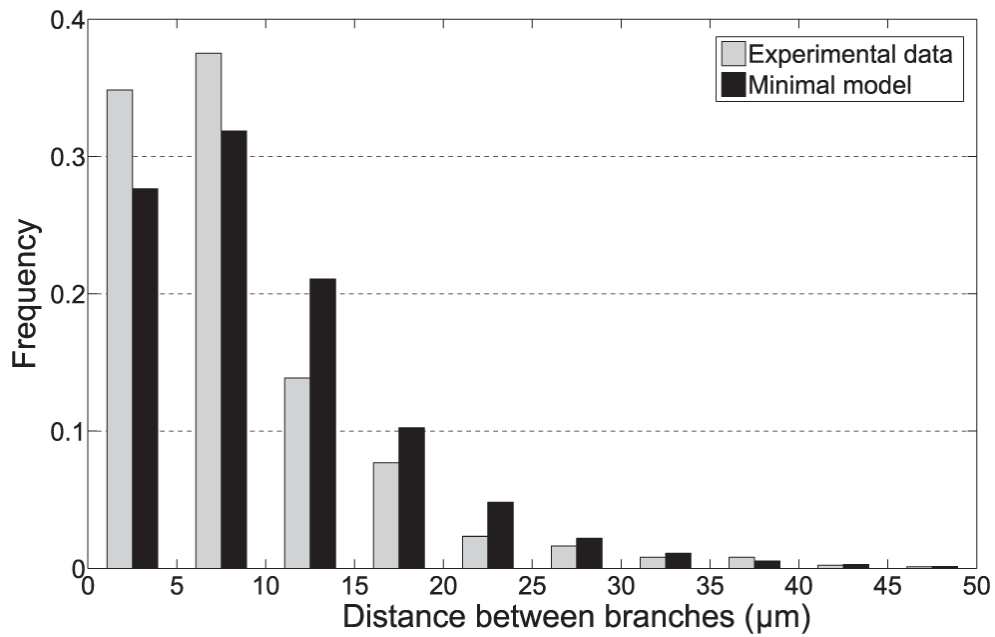


Figure 3.7 Comparison of histograms of the branch-to-branch distribution between minimal model and experimental data at 80 μm trim.

858 experimental data points were used. Data analysis of experimental data was done in collaboration with David Richards, Department of Computational and Systems Biology, John Innes Centre. Data derived from the minimal mathematical model were kindly provided by David Richards.

3.9 Full-model: curvature-dependent polarisome splitting

It has been shown that the DivIVA orthologue in *B. subtilis* preferentially assembles on negatively-curved membranes, and this appears to be an important factor in targeting of the *B. subtilis* DivIVA protein to cell poles and septation sites (Ramamurthi & Losick, 2009; Lenarcic *et al.*, 2009). Similarly, in *Streptomyces*, there is a marked preference for branches to emerge on the outer side of negatively-curved hyphae (Hempel *et al.*, 2008), which suggests that polarisomes are more likely to be deposited on the negatively-curved inner membrane. Neither the mechanism by which this occurs nor the specific need for local curvature for branch development are understood. During this study it was observed that the hyphal tip frequently turns while the polarisome splits (see for example **Figure 3.1**). However, the degree of local curvature is very variable and it is not clear whether turning of the hyphal tip generates a degree of local curvature and thereby promotes polarisome splitting or *vice versa*.

Therefore, we tested how local curvature would influence the model. To do so, a more detailed computational model was developed (for full details and parameters see Richards *et al.*, 2012), which implements hyphal growth in two-dimensional space. At each time step in the simulation, the direction of tip growth was randomly varied by a small amount, such that over sufficiently long distances of a few μm , memory of the previous growth direction was lost. It was postulated that polarisomes with sizes above the critical polarisome size for splitting (N_{split}) could only split when the degree of local curvature near the tip was sufficiently high. Hence, the previous polarisome-splitting parameter (γ) was understood as an effective parameter that could be replaced by variation of growth direction and curvature threshold.

However, it is worth noting that if curvature was the origin of γ it must be quite a sensitive effect since during growth the mean curvature near the tip only changes by about 10%. The full model produced colony dynamics that recapitulated the wild-type growth phenotype well. In particular, the tip-to-branch and branch-to-branch distributions were practically identical to the minimal model, thereby justifying the earlier simplifying assumptions.

3.10 Discussion

Streptomycetes, like other bacteria, lack the motor proteins, vesicle transport systems and polarisome components that are fundamental in eukaryotic cell biology. Thus, tip extension in *Streptomyces* is likely to be simpler than in, for example, filamentous fungi. Given that a complex of polarity proteins (including DivIVA) must presumably first gather at future branch sites, understanding branch-site selection in filamentous bacteria involves understanding where, when and how these proteins cluster together in sufficiently large groups. One surprising feature of *Streptomyces* is that this clustering of polarity proteins is not a random, spontaneous process. Rather, this study has shown that new branch sites are predominantly created from the tip protein complexes of previous branches by a novel polarisome splitting mechanism.

What is the benefit of producing new polarisomes, and hence branches, by polarisome splitting rather than spontaneous nucleation? One possibility is that it provides a more efficient method of acquiring nutrients. Spontaneous nucleation will produce new branches at positions well behind the tips. This outcome would be suboptimal since regions far behind the tips are likely to have already been well-exploited, with few remaining nutrients. Polarisome splitting, on the other hand, only generates new polarisomes at tips and so biases branching towards the growing ends of hyphae, where nutrients are still plentiful. Another potential advantage is that polarisome splitting allows for a greater level of control over exactly where branching occurs. Unlike spontaneous nucleation where branches can appear anywhere, polarisome splitting produces branches with an average tip-to-branch distance determined by parameters such as the initial polarisome size and the binding parameter. By modifying these parameters, it is possible to respond to external stimuli. For example, under conditions when branching further away from the tip would be favourable, this could be achieved by modifying DivIVA (or other proteins of the polarisome complex that affect its assembly) so that the binding parameter is decreased (this would correspond to a shift from the morphology shown in **Figure 3.8B** to that in **Figure 3.8A**).

The morphology of branching organisms can be characterised by the distance from the tip to where new branches appear and the inter-branch distance. Counter-intuitively, the model shows that these distances are controlled by two rather different aspects of the polarisome splitting mechanism (**Figure 3.9**). The tip-to-branch distance is governed by how long it takes for a new daughter polarisome to gather enough molecules to initiate a new branch. This is related to the initial daughter polarisome size (N_0), the size at which a new branch is initiated (N_{br}), the tip growth speed (v), and the binding parameter (β). In contrast, the branch-to-branch distance is governed by how often polarisomes are formed (how long polarisomes take to develop into branches is now irrelevant!). This is dependent on a partly overlapping, but nevertheless distinct set of parameters: the minimum polarisome size for splitting (N_{split}), the initial focus size (N_0), the tip growth speed (v), the binding parameter (β), and the polarisome splitting parameter (γ).

In conclusion, this study found that a remarkably simple model can quantitatively explain the statistical properties of a hyphal network. Even the bimodal nature of the tip-to-branch distribution originates from a single mechanism of forming new polarisomes, combined with variation in the parameter values. It is tempting to speculate that polarisome splitting might be used by many filamentous organisms amongst fungi and Actinobacteria. In fact, polarisome splitting could turn out to be a general mechanism in situations where discrete polar protein assemblies must be generated in a growing organism.

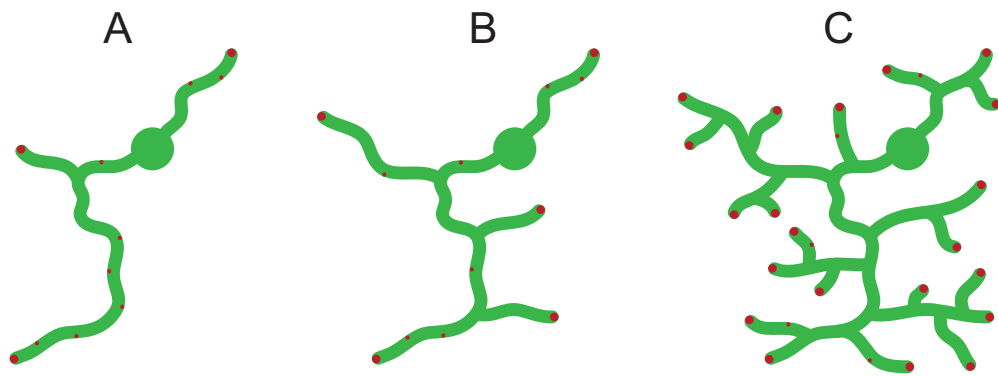


Figure 3.8 Schematic of colony morphology for various values of the binding rate parameter (β).

Red dots represent polarisomes. (A) Small value of β . (B) Wild-type value of β .

(C) Large value of β . **Figure 3.8** was kindly provided by David Richards.

TIP-BRANCH DISTANCE



= How long it takes daughter polarisomes to gather enough molecules to initiate a new branch

BRANCH-BRANCH DISTANCE



= How often polarisome splitting occurs
(how long daughter polarisomes take to develop into branches is irrelevant)

Figure 3.9 Two very different aspects of polarisome splitting regulate branch development in *Streptomyces*.

3.11 Summary Points

- Polarisome splitting is a novel mechanism that regulates branch formation in the filamentous bacteria *Streptomyces*: existing tip polarisomes split into two clusters; the larger cluster stays with the growing hyphal tip, while the smaller cluster is left on the lateral wall and initiates branch development.
- Polarisome splitting bypasses the need for initial *de-novo* nucleation and specific site-selection and thereby biases branching towards the growing ends of hyphae, where nutrients are still plentiful.
- Mathematical modelling predicts that this simple mechanism can quantitatively capture the statistical properties of the entire hyphal branching network.
- The model predicts a particular bimodal tip-to-branch distribution resulting from polarisome splitting; a prediction confirmed experimentally.
- The model also predicts that polarisome splitting events are dependent on one another, because the tip polarisome decreases in size during splitting and therefore needs time to reach a critical mass in order to be able to split again; a prediction confirmed experimentally.
- Counter-intuitively, the tip-to-branch distance and the branch-to-branch distance are regulated by two different aspects of polarisome splitting. The tip-to-branch distance is governed by how long new daughter polarisomes take to grow to the size required to initiate a new branch, whereas the branch-to-branch distance is governed by how often the tip polarisome splits.

Chapter 4

Polar growth in *Streptomyces* is regulated by a Ser/Thr protein kinase

4.1	Introduction	112
4.2	DivIVA phosphorylation increases dramatically when cell wall synthesis is blocked	113
4.3	Increased DivIVA phosphorylation upon cell envelope stress is not part of a general stress response	118
4.4	The C-terminal region of DivIVA is the target of multiple phosphorylations	120
4.5	DivIVA is not phosphorylated by PASTA-domain containing Ser/Thr protein kinases	123
4.6	The DivIVA protein kinase is AfsK	125
4.7	DivIVA is phosphorylated by AfsK <i>in vitro</i>	130
4.8	The AfsK kinase co-localises with its substrate DivIVA at the tips of growing vegetative hyphae	132
4.9	AfsK regulates the branching of growing hyphae	135
4.10	Constitutively active AfsK mutant protein profoundly affects apical growth, DivIVA localisation, and hyphal branching	141
4.11	Discussion	146
4.12	Summary Points	150

Statement of my work

The work of this chapter was a collaboration project between the research groups of Klas Flärdh (University of Lund, Sweden); Mark Buttner, Mike Naldrett and Martin Howard (John Innes Centre); and Virginie Molle (CNRS, University of Lyon 1, France) and was published as:

Hempel, A. M., S. Cantlay, V. Molle, S. B. Wang, M. J. Naldrett, J.L. Parker, D. M. Richards, Y. G. Jung, M. J. Buttner & K. Flärdh, (2012) A Ser/Thr protein kinase regulates polar growth and hyphal branching in the filamentous bacteria *Streptomyces*. *Proc Natl Acad Sci USA* **109**: e2371-2379.

The work presented in **Figure 4.1** I performed in Klas Flärdh's lab at Lund University, Sweden, as part of my "Diplomarbeit" for my University Degree "Diplom-Biologe" at the University of Heidelberg, Germany (Wollkopf, 2007). As part of my PhD project, I tested various antibiotics for their effect on DivIVA phosphorylation (**Figure 4.2**) and I performed the *in vivo* DivIVA phosphorylation assays of wild-type *Streptomyces*, *sigE* mutant and various Ser/Thr protein kinase mutants presented in **Figures 4.3, 4.5, 4.6, 4.7A and B**. I prepared the samples for mass spectrometry in **Figure 4.4**. The microscopic analysis and quantification of the phenotype of *Streptomyces* Δ *afsK* mutant and the complemented Δ *afsK* mutant was done by me and the final data analysis with help from David Richards, John Innes Centre (**Figures 4.10 – 4.12**). All strains and plasmids generated by me are included in the tables in **Section 2.1** in Materials and Methods.

4.1 Introduction

In Chapter 3, I showed that a novel polarisome splitting mechanism underlies the selection of new branch sites in *Streptomyces*. This work was done using a DivIVA-EGFP fusion as a marker to follow the dynamics of polarisomes in hyphae.

One obvious benefit of a polarisome splitting mechanism, is that it facilitates the regulation of hyphal branching, and that much of the regulation can occur at the actively growing hyphal tip, which is the part of the mycelium most likely to be exposed to relevant environmental stimuli (Richards *et al.*, 2012). Hyphal morphology is dependent on growth conditions, and the ability to control tip extension and branching in response to internal and external cues should be of large adaptive value both for streptomycetes and fungi (Harris, 2008). Still, such regulation of polarised growth has been very poorly understood in both types of organisms.

In this chapter, I investigate how DivIVA is regulated during hyphal growth and lateral branching and I show that cell polarity and branch-site selection is regulated by a Ser/Thr protein kinase AfsK. This kinase is located at hyphal tips and directly targets the cell polarity determinant DivIVA, affecting the development of new daughter polarisomes during normal growth. Further, I show that the kinase is activated by signals that arise when cell wall synthesis is blocked, and that high levels of kinase activity inhibit extension at existing tips and, by altering the sub-cellular localisation of DivIVA, trigger branching at multiple new sites. Thereby, the Ser/Thr protein kinase AfsK, which has previously only been implicated in control of secondary metabolism (Matsumoto *et al.*, 1994), plays a vital role in regulating cell polarity, apical growth, and branch-site selection in *Streptomyces*.

4.2 DivIVA phosphorylation increases dramatically when cell wall synthesis is blocked

The work presented in **Figure 4.1** of this section was part of my “Diplomarbeit” for my University Degree “Diplom-Biologe” at the University of Heidelberg, Germany (Wollkopf, 2007).

In the current view, DivIVA directs the cell wall biosynthetic machinery, thereby establishing apical growth and lateral branching, although how exactly they interact is not known. Assuming that mechanisms for regulating apical growth and hyphal branching may act directly on DivIVA, my strategy to identify regulatory mechanisms that control apical growth in *Streptomyces* was to perturb the system by exposing growing *S. coelicolor* hyphae to various stress conditions and to monitor how DivIVA responds.

Western blot analysis revealed a clear mobility shift of DivIVA when cell wall synthesis was blocked by bacitracin, which arrests the export of the peptidoglycan precursor lipid II (Stone & Strominger, 1971). One possible cause of this mobility shift could be a post-translational modification of DivIVA, such as phosphorylation.

To address this possibility, I introduced into the wild-type strain a thiostrepton-inducible *divIVA* allele encoding an N-terminally FLAG-tagged version of the protein, which is known to co-immunoprecipitate with the native DivIVA (Wang *et al.*, 2009). This allowed analysis of immunoprecipitated FLAG-DivIVA/DivIVA mixtures from growing and bacitracin-treated mycelium by staining with the phosphorylation-specific stain Pro-Q Diamond. The presence of DivIVA both with and without FLAG-tag gives rise to a double band in the Coomassie-stained SDS-PAGE gel (indicated by the open arrowheads in **Figure 4.1A**). A weak signal from Pro-Q Diamond staining of more slowly migrating species suggested a low level of DivIVA phosphorylation during growth (position of these bands indicated by the closed arrowheads in **Figure 4.1A**). Addition of bacitracin led within 5 minutes to phosphorylation of a large fraction of DivIVA, as shown by the relative amount of DivIVA that shifted mobility to the position coinciding with strong Pro-Q Diamond staining.

To confirm that the effect I observe was caused by phosphorylation, I treated immunoprecipitated FLAG-DivIVA/DivIVA from growing and bacitracin-treated mycelium with lambda protein phosphatase. This treatment abolished both the Pro-Q Diamond staining and the mobility shift (**Figure 4.1B**).

Next I determined whether extensive phosphorylation is triggered only in response to bacitracin. I tested a number of different antibiotics inhibiting different steps in cell wall synthesis (vancomycin, phosphomycin and penicillin G) and antibiotics inhibiting DNA and protein synthesis (novobiocin, kanamycin and thiostrepton) and analysed cell extracts by Western blotting. My results showed that both bacitracin and vancomycin induced a mobility shift of a large fraction of DivIVA, and that phosphomycin and penicillin G also caused some mobility shift (**Figure 4.2**) (*S. coelicolor* is relatively insensitive to both phosphomycin and penicillin G). In contrast, the antibiotics that inhibit DNA and protein synthesis did not induce phosphorylation of DivIVA.

These results demonstrate that DivIVA is indeed subject to phosphorylation, that there is a detectable basal level of DivIVA phosphorylation during undisturbed vegetative growth in liquid medium, and that DivIVA phosphorylation increases dramatically when cell wall synthesis is blocked.

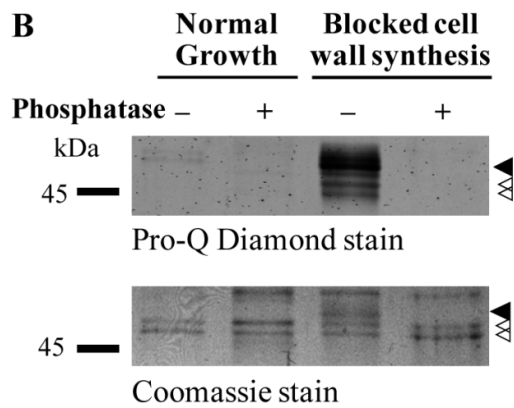
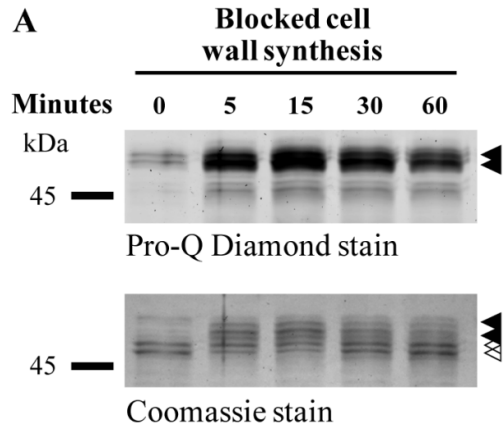


Figure 4.1 DivIVA is post-translationally regulated by phosphorylation.

(A) Time course of DivIVA phosphorylation in response to the arrest of cell wall synthesis induced by bacitracin. Bacitracin (50 µg/ml) was added to growing cultures of wild-type *S. coelicolor* expressing *FLAG-divIVA* from a thiostrepton-inducible promoter. At the times indicated, cells were lysed, cell extracts prepared, and FLAG-DivIVA/DivIVA was immunoprecipitated using anti-FLAG affinity gel. (B) Phosphatase treatment of DivIVA. Wild-type *S. coelicolor* expressing *FLAG-divIVA* was incubated with bacitracin (50 µg/ml) for 60 minutes before harvest, preparation of cell extracts and immunoprecipitation. The immunoprecipitated FLAG-DivIVA/DivIVA was analysed before and after treatment with lambda protein phosphatase. Closed arrowheads indicate phosphorylated DivIVA and open arrowheads indicate non-phosphorylated DivIVA. A molecular weight marker and its corresponding sizes are given on the sides of each gel. This work was part of my “Diplomarbeit” for my University Degree “Diplom-Biologe” at the University of Heidelberg, Germany (Wollkopf, 2007).

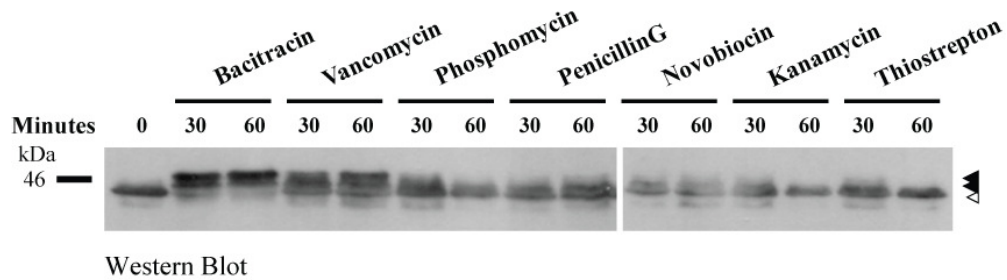


Figure 4.2 DivIVA is subject to increased phosphorylation specifically upon inhibition of cell wall synthesis.

The phosphorylation state of DivIVA indicated by mobility shift was analysed by Western blotting upon treatment with different antibiotics. Growing cultures of *S. coelicolor* wild-type strain were incubated for 30 minutes with bacitracin (50 $\mu\text{g/ml}$), vancomycin (50 $\mu\text{g/ml}$), phosphomycin (600 $\mu\text{g/ml}$), penicillin G (200 $\mu\text{g/ml}$), novobiocin (25 $\mu\text{g/ml}$), kanamycin (150 $\mu\text{g/ml}$), and thiostrepton (10 $\mu\text{g/ml}$) prior to harvest and cell extract preparation. Closed arrowheads indicate phosphorylated DivIVA and open arrowheads indicate non-phosphorylated DivIVA. A molecular weight marker and its corresponding sizes are given on the sides of the blot.

4.3 Increased DivIVA phosphorylation upon cell envelope stress is not part of a general stress response

Previous studies have shown that *Streptomyces* has a two-component signal transduction system, the CseB/CseC- σ^E system, which is involved in sensing and responding to changes in the integrity of the cell envelope, and that inducers of this system include antibiotics that inhibit cell wall synthesis such as bacitracin and vancomycin (Paget *et al.*, 1999a; Paget *et al.*, 1999b; Hong *et al.*, 2002). To test whether the CseB/CseC- σ^E system might be involved in mediating the increase in DivIVA phosphorylation observed when cell wall synthesis is blocked as part of this general cell envelope stress response, I analysed immunoprecipitated DivIVA material from a *sigE* null mutant (Paget *et al.*, 1999a). The results showed that the bacitracin-induced increased DivIVA phosphorylation does not depend on the general σ^E -mediated cell envelope stress response (**Figure 4.3**).

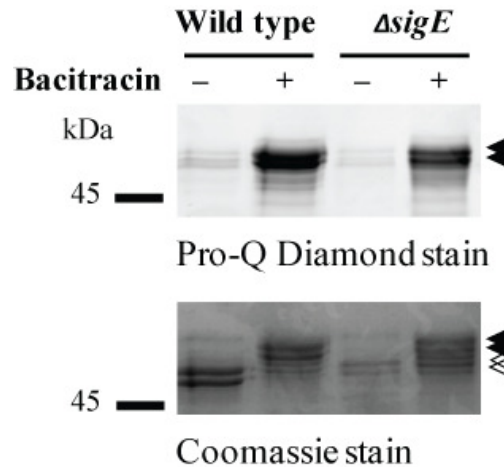


Figure 4.3 Increased DivIVA phosphorylation is not part of a general stress response.

The phosphorylation state of DivIVA, before and after bacitracin treatment, was analysed in a *sigE* mutant, lacking RNA polymerase sigma factor σ^E . Growing hyphae of wild-type and mutant strain expressing *FLAG-divIVA* were incubated with bacitracin (50 $\mu\text{g/ml}$) for 30 minutes before harvest, preparation of cell extracts and immunoprecipitation. Closed arrowheads indicate phosphorylated DivIVA and open arrowheads indicate non-phosphorylated DivIVA. A molecular weight marker and its corresponding sizes are given on the sides of the gel.

4.4 The C-terminal region of DivIVA is the target of multiple phosphorylations

To confirm and extend our results, we used mass spectrometry in collaboration with Mike Naldrett, Proteomics Facility, John Innes Centre, to characterise the phosphorylation of DivIVA further. I immunoprecipitated DivIVA from cultures that had been exposed to bacitracin to block cell wall synthesis, and the protein was subsequently digested with trypsin and analysed by MALDI-ToF. A 7.2 kDa tryptic peptide that contains most of the C-terminal region of DivIVA was found to be singly, doubly and triply phosphorylated, with the doubly phosphorylated species the most abundant (**Figure 4.4B**). After treatment with calf intestinal alkaline protein phosphatase, the three peaks corresponding to the phosphorylated forms of DivIVA disappeared leaving only the peak corresponding to the non-phosphorylated form (**Figure 4.4B**). Further analysis showed that another DivIVA tryptic peptide was also multiply phosphorylated (data not shown). This second peptide is 1.5 kDa in size and sits immediately N-terminal to the 7.2 kDa tryptic peptide in the primary amino acid sequence of DivIVA (**Figure 4.4A**). Thus, the C-terminal region of DivIVA becomes highly phosphorylated in response to the inhibition of cell wall synthesis in *S. coelicolor*. Further analysis of DivIVA phosphorylation is presented in **Chapter 5**.

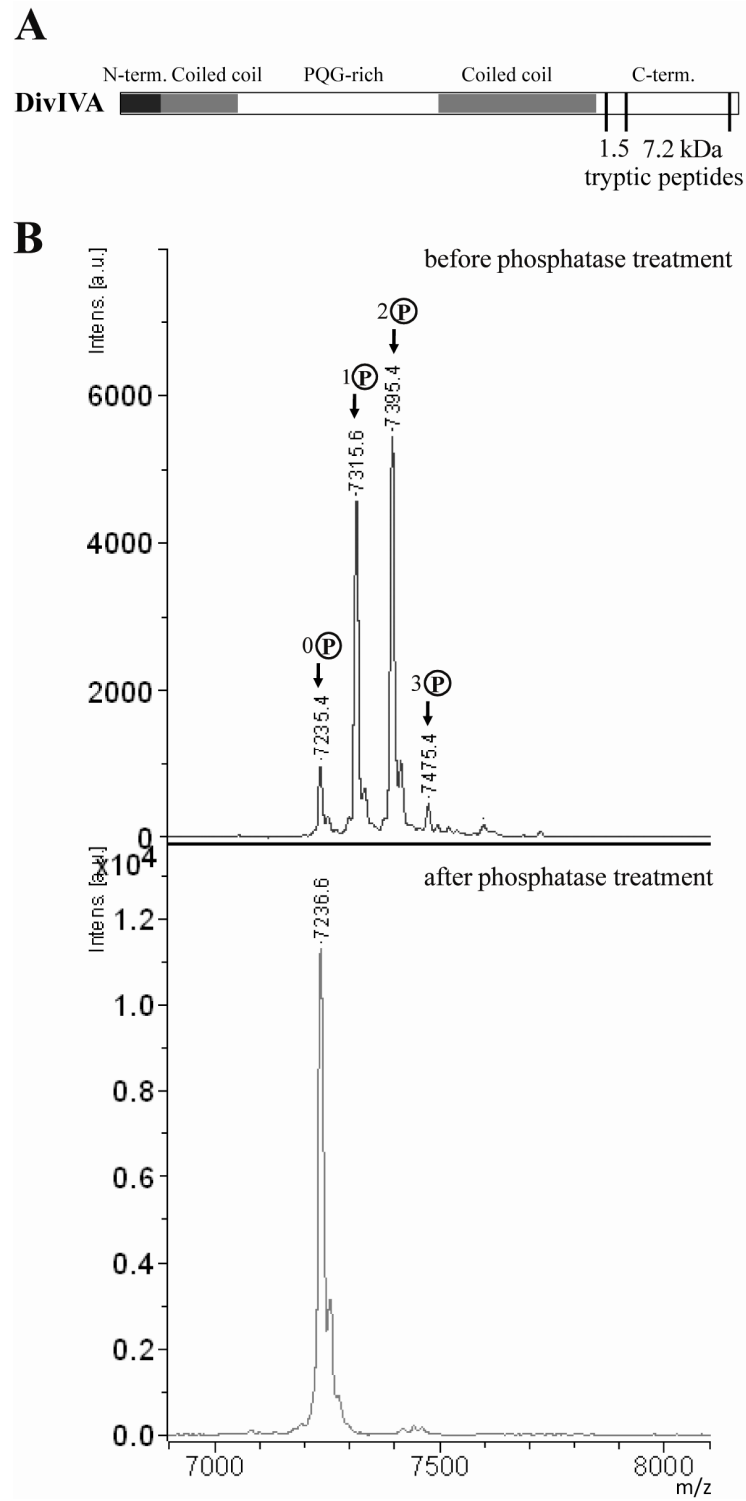


Figure 4.4 *S. coelicolor* DivIVA is multiply phosphorylated in the C-terminal region.

(A) Schematic showing the positions within the DivIVA primary sequence of the 7.2 kDa phosphorylated peptide (residues 315-389) relative to the 1.5 kDa phosphorylated peptide (residues 301-314) described in the text. (B) Upper panel: the MALDI-ToF mass spectrum of a 7.2 kDa tryptic fragment derived from the C-terminal region of DivIVA showing zero to three phosphorylations (+80, +160 and +240 Da). The lower panel shows the disappearance of the phosphorylated species upon treatment of the protein with calf intestinal alkaline phosphatase.

Figure 4.4B was kindly provided by Mike Naldrett, Proteomics Facility, John Innes Centre.

4.5 DivIVA is not phosphorylated by PASTA-domain containing Ser/Thr protein kinases

I next attempted to identify the kinase responsible for DivIVA phosphorylation. Multiple reports show that Ser/Thr protein kinases carrying PASTA domains play important regulatory roles in *Mycobacterium* and *Corynebacterium*. PASTA domains are known to bind peptidoglycan components and β -lactam antibiotics (Shah *et al.*, 2008; Maestro *et al.*, 2011), and actinobacterial Ser/Thr protein kinases carrying such domains (PknA and PknB) have been reported to phosphorylate several proteins involved in cell wall growth and cell division, including the mycobacterial DivIVA-orthologue Wag31 (see *e.g.* Kang *et al.*, 2005; Fiuza *et al.*, 2008; Schultz *et al.*, 2009; Molle & Kremer, 2010). These reports prompted me to investigate the three PASTA domain-containing Ser/Thr protein kinases in *S. coelicolor* (SCO2110, SCO3821 and SCO3848), of which SCO3848 shows microsynteny with mycobacterial *pknB*.

Accordingly, I tested null mutants of *SCO2110*, *SCO3821* and *SCO3848* (constructed by Yong-Gyun Jung, Department of Molecular Microbiology, John Innes Centre; Jung, 2007) and found that both the basal level of DivIVA phosphorylation during growth and the strongly increased level seen after bacitracin treatment occurred normally in each of the three mutants (**Figure 4.5**). To rule out the possibility of redundancy, I tested a triple mutant lacking all three of these kinases. Again, basal DivIVA phosphorylation during growth and the dramatic increase in phosphorylation caused by the inhibition of cell wall synthesis occurred normally, even in the absence of all three kinases (**Figure 4.5**). Thus, DivIVA phosphorylation in *S. coelicolor* is mediated by some route other than PknA/ PknB-like PASTA domain-containing Ser/Thr protein kinases.

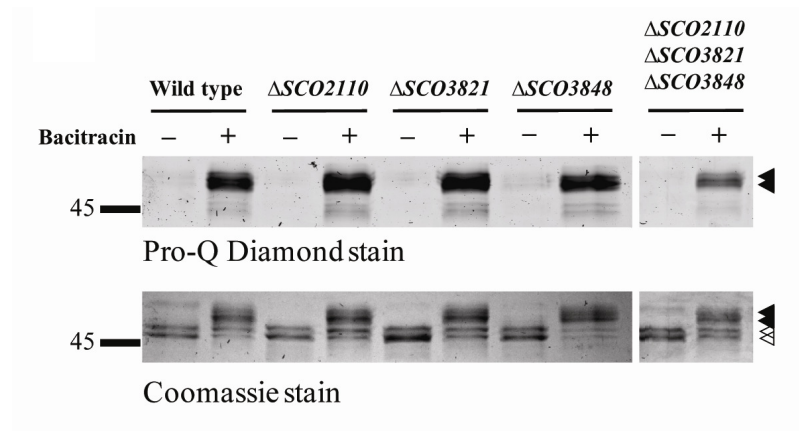


Figure 4.5 DivIVA is not phosphorylated by PASTA domain-containing Ser/Thr protein kinases.

The phosphorylation state of DivIVA, before and after the inhibition of cell wall synthesis with bacitracin (50 μ g/ml), was analysed in single, double and triple mutants of the three PASTA domain-containing Ser/Thr protein kinases of *S. coelicolor*, SCO2110, SCO3821 and SCO3848. Closed arrowheads indicate phosphorylated DivIVA and open arrowheads indicate non-phosphorylated DivIVA. A molecular weight marker and its corresponding sizes are given on the sides of each gel. The samples of the triple mutant were run on a different gel.

4.6 The DivIVA protein kinase is AfsK

The *S. coelicolor* genome carries at least 34 genes predicted to encode Ser/Thr protein kinases (Petrickova & Petricek, 2003). Accordingly, Yong-Gyun Jung and Jennifer Parker, Department of Molecular Microbiology, John Innes Centre, began systematically to disrupt these genes (Jung, 2007; Parker, 2010b). I then introduced the *divIVA* allele encoding the N-terminally FLAG-tagged version of the protein into the resulting mutants, and examined the pattern of DivIVA phosphorylation in FLAG-DivIVA/DivIVA mixtures immunoprecipitated from each strain. Including the three PASTA domain kinases described above, I tested 17 Ser/Thr protein kinases for their involvement in DivIVA phosphorylation (**Table 4.1**). In mutants for 16 of these kinases I observed the normal pattern of phosphorylation (**Figure 4.5** and **4.6**).

However, no DivIVA phosphorylation occurred in a constructed *afsK* mutant (*SCO4423*), neither during normal growth nor after cell wall synthesis was arrested with bacitracin (**Figure 4.7A**). When Stuart Cantlay, Department of Biology, University of Lund, Sweden, complemented the *afsK* mutant, DivIVA phosphorylation was restored to the wild-type pattern (**Figure 4.7B**).

AfsR (*SCO4426*) is a transcription factor phosphorylated by AfsK that influences secondary metabolism and antibiotic biosynthesis, and two other sensory kinases, PkaG (*SCO4487*) and AfsL (*SCO4377*), are also involved in signal transduction in secondary metabolism (**Figure 1.10**; reviewed by Umeyama *et al.*, 2002). Therefore, I checked the DivIVA phosphorylation level in a double mutant lacking *pkaG* and a kinase gene of unknown function lying upstream of *pkaG* (*SCO4488*) (mutant constructed by Jennifer Parker, Department of Molecular Microbiology, John Innes Centre; Parker, 2010b), and in an *afsR* single mutant (Floriano & Bibb, 1996). In both mutants DivIVA phosphorylation was still wild type, indicating that none of these members of the signalling cascade has any direct role in DivIVA phosphorylation (**Figure 4.7C**).

In summary, my results indicate that the *afsK*-encoded Ser/Thr protein kinase is required for both the basal level of DivIVA phosphorylation and the high levels induced by arresting peptidoglycan synthesis.

Table 4.1 Overview of 17 predicted Ser/Thr protein kinases in *S. coelicolor* that were tested for their involvement DivIVA phosphorylation.

Table is adapted from Petrickova & Petricek (2003).

Kinase	Name	Size (aa)	TM	Extra domains	Proposed role
SCO1468		774	–	–	RNA metabolism
SCO2110	PkaF	667	+	PASTA	DNA repair
SCO2244		686	+	WD-40	Metabolic regulation?
SCO3102	PkaE	510	–	–	DNA repair, glycan catabolism, growth
SCO3820		522	+	–	Energy metabolism
SCO3821	PksC	556	+	PASTA	Energy metabolism
SCO3848		673	+	PASTA	Cell division
SCO4423 ¹	AfsK	799	–	PQQ	Differentiation, secondary metabolism
SCO4487	PkaG	592	+	LamGL	Energy metabolism
SCO4488		626	+	Sugar-b.	Receptor kinase (sugar signals)
SCO4507		586	+	–	FA synthesis, cell division, cold shock
SCO4775	PkaH	717	+	–	Nucleotide, sugar metabolism
SCO4776		979	+	–	Nucleotide, sugar metabolism
SCO4777	PkaD	599	+	–	Nucleotide, sugar metabolism
SCO4778	PkaI	380	+	–	Nucleotide, sugar metabolism
SCO4779	PkaJ	548	+	–	Nucleotide, sugar metabolism
SCO7240		745	–	KLC	Respiration, electron transport

Abbreviations used in the table are as following; aa, amino acid; TM, trans-membrane domain; PASTA, PASTA β -lactam binding domain; WD-40, β -transducin repeat; PQQ, bacterial PQQ repeat; LamGL, LamG-like jellyroll fold domain; Sugar-b., ricin B sugar-binding domain; KLC, kinesin light-chain repeat; FA, fatty acid.

¹ SCO4423 is AfsK kinase and there is no DivIVA phosphorylation detectable in Δ *afsK* (see **Figure 4.7**).

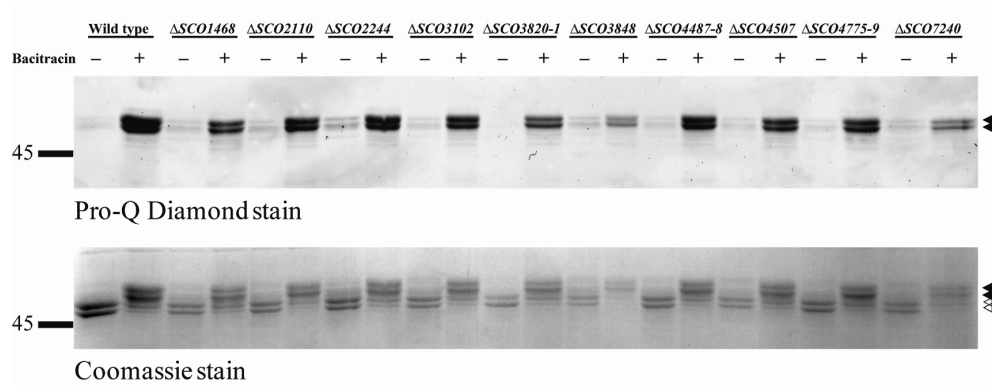


Figure 4.6 DivIVA is not phosphorylated by several Ser/Thr protein kinases. The phosphorylation state of DivIVA, before and after the inhibition of cell wall synthesis with bacitracin (50 μ g/ml), was analysed in various constructed Ser/Thr protein kinases mutants. Closed arrowheads indicate phosphorylated DivIVA and open arrowheads indicate non-phosphorylated DivIVA. A molecular weight marker and its corresponding sizes are given on the sides of each gel.

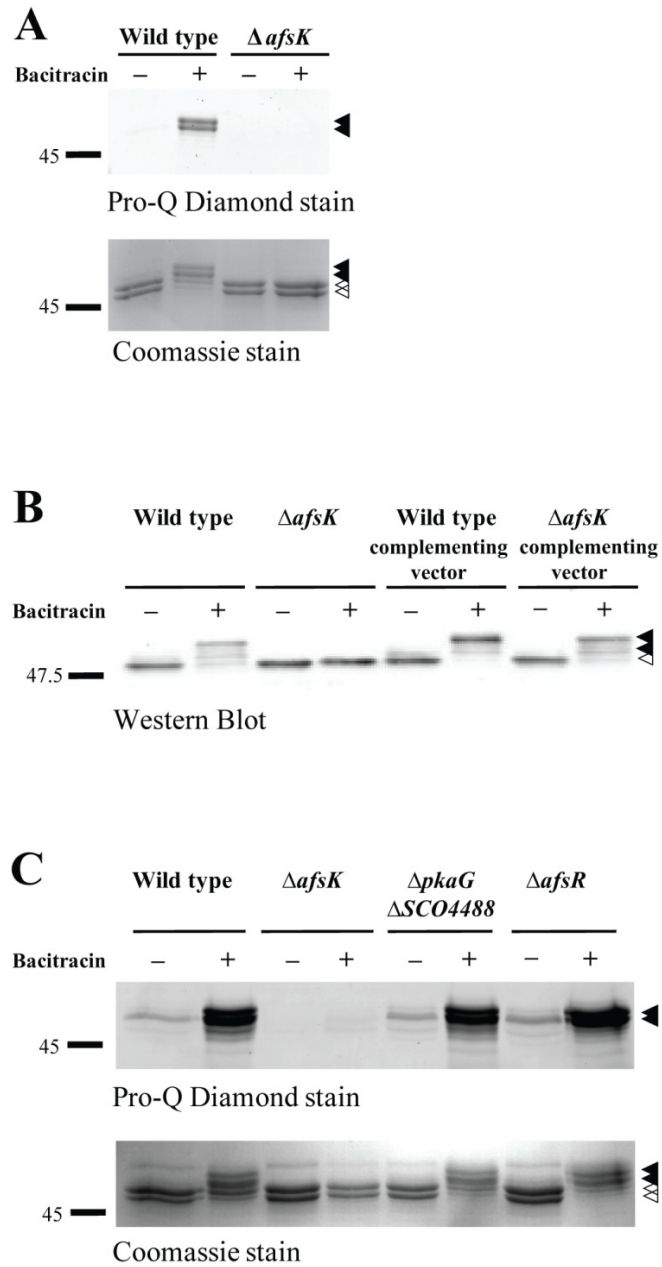


Figure 4.7 The DivIVA kinase is AfsK.

(A) The phosphorylation state of DivIVA, before and after the inhibition of cell wall synthesis, was analysed in a constructed *afsK* mutant. Growing cultures of wild-type *S. coelicolor* and of the Ser/Thr protein kinase mutants, each expressing *FLAG-divIVA*, were incubated with bacitracin (50 µg/ml) for 30 minutes before harvest, preparation of cell extracts, and immunoprecipitation of FLAG-DivIVA/DivIVA. (B) Complementation of the *afsK* null mutant restores DivIVA phosphorylation. *afsK* was cloned into the integrative vector pMS82 to create pKF256, which was introduced into the *afsK* null mutant and into wild-type *S. coelicolor*. The phosphorylation state of DivIVA, before and after the inhibition of cell wall synthesis, was analysed in each strain by Western blot analysis of crude cell extracts. (C) Analysis of the phosphorylation state of DivIVA, before and after the inhibition of cell wall synthesis in mutants of the *S. coelicolor* AfsR cluster each expressing *FLAG-divIVA*. Cultures were incubated with bacitracin (50 µg/ml) for 30 minutes before harvest, preparation of cell extracts, and immunoprecipitation of FLAG-DivIVA/DivIVA. Closed arrowheads indicate phosphorylated DivIVA and open arrowheads indicate non-phosphorylated DivIVA. Molecular weight markers and their corresponding sizes are given on the sides of each gel or blot.

4.7 DivIVA is phosphorylated by AfsK *in vitro*

These results led us to investigate as to whether AfsK directly phosphorylates DivIVA. To address this question, Virginie Molle, CNRS, University of Lyon 1, France, cloned, overexpressed and purified the kinase domain of AfsK (amino acids 1-311) and DivIVA as GST-tagged fusion proteins and used them to establish an *in vitro* phosphorylation system. When the kinase domain of AfsK was incubated with γ -labeled ATP, it underwent autophosphorylation, as revealed by autoradiography, and when this was mixed with purified DivIVA, the kinase was indeed able to phosphorylate DivIVA (**Figure 4.8**). DivIVA alone did not show any autophosphorylation activity (data not shown). Thus it can be concluded that the absence of DivIVA phosphorylation in the *afsK* mutant arises because DivIVA is a direct substrate for AfsK.

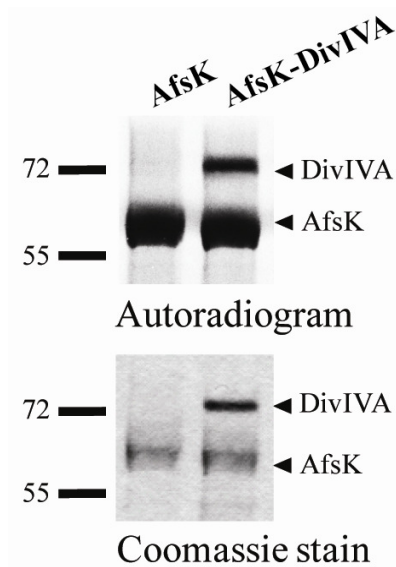


Figure 4.8 *In vitro* phosphorylation of DivIVA by AfsK.

The recombinant GST-tagged AfsK kinase domain (amino acids 1-311) and GST-tagged DivIVA were incubated with [γ - 33 P]ATP. Samples were separated by SDS-PAGE, visualised by autoradiography (upper panel) and Coomassie stain (lower panel). Lower bands in the autoradiogram illustrate the autokinase activity of AfsK, whereas upper bands reflect DivIVA phosphorylation. In control experiments, DivIVA did not show any autophosphorylation activity (data not shown). A molecular weight marker and its corresponding sizes are given on the sides of the gel. **Figure 4.8** was kindly provided by Virginie Molle, CNRS, University of Lyon 1, France.

4.8 The AfsK kinase co-localises with its substrate DivIVA at the tips of growing vegetative hyphae

DivIVA shows a distinct subcellular localisation, with strong accumulation at the tips of growing hyphae and lateral branches (Flärdh, 2003a). It was therefore of interest to determine whether AfsK would show a similar distribution and co-localise with its substrate. Stuart Cantlay, Department of Biology, University of Lund, Sweden, investigated this question by creating a fusion between AfsK and the red fluorescent protein mCherry. The translational fusion was expressed from the *afsK* promoter and was integrated at the chromosomal *att_{φBT1}* site in both the wild-type strain and its congenic *afsK* null mutant. The *afsK-mCherry* allele restored the ability to phosphorylate DivIVA to the *afsK* mutant, both the basal level seen during growth and the high level induced by bacitracin-treatment (**Figure 4.9A**), showing that the fusion protein is functional. In both strain backgrounds, this hybrid protein showed clear accumulation as foci at the tips of vegetative hyphae, although we also observed weak fluorescence along the hyphae (**Figure 4.9B**).

The co-localisation of AfsK with DivIVA at the hyphal tips was further confirmed by examining a strain expressing both *divIVA-egfp* and *afsK-mCherry* (**Figure 4.9C**). Thus, a substantial fraction of the AfsK kinase co-localises with its substrate DivIVA at hyphal tips.

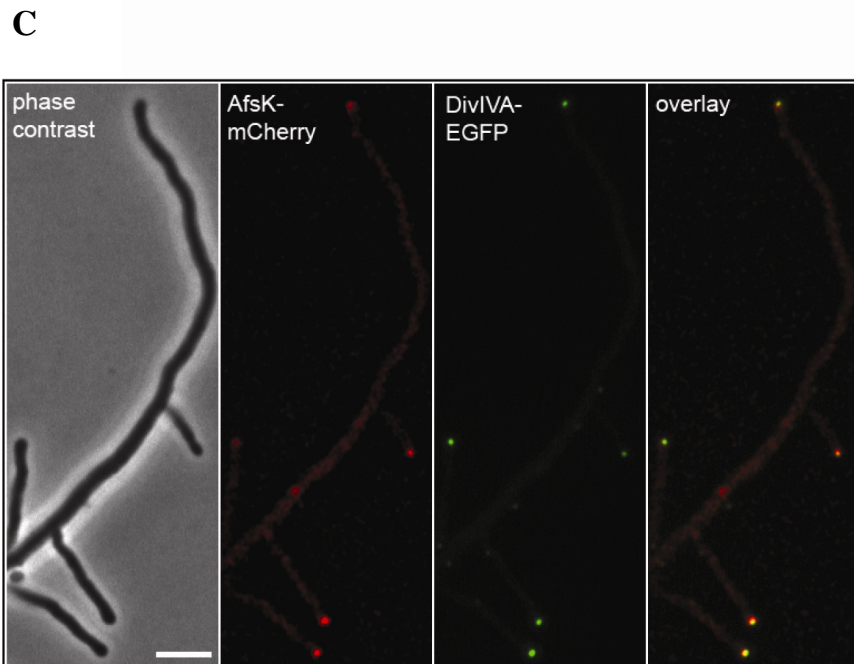
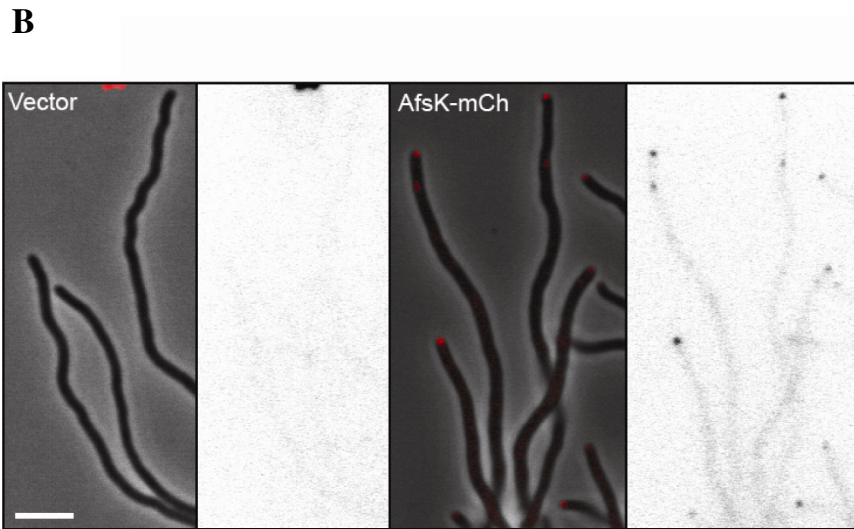
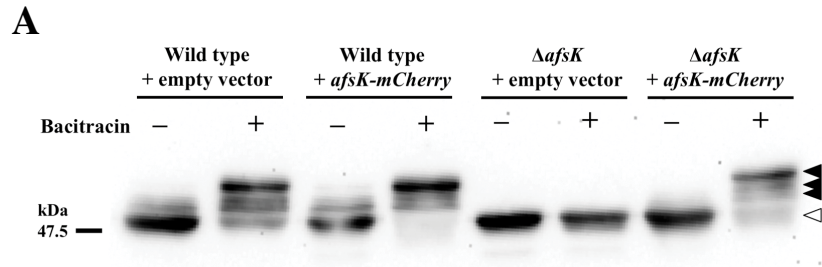


Figure 4.9 The DivIVA kinase AfsK localises to hyphal tips.

(A) Complementation of the *afsK* null mutant with *afsK-mCherry* restores DivIVA phosphorylation to wild-type levels. *afsK* was cloned into the integrative vector pKF210 with promoterless *mCherry* to create pKF256. pKF210 and pKF256 were introduced into the *afsK* null mutant and into wild-type *S. coelicolor*. The phosphorylation state of DivIVA, before and after the inhibition of cell wall synthesis with bacitracin (50 µg/ml) for 30 minutes, was analysed in each strain by Western blot of crude cell extracts. Closed arrowheads indicate phosphorylated DivIVA and open arrowheads indicate non-phosphorylated DivIVA. A molecular weight marker and its corresponding sizes are given on the sides of the blot. (B) *S. coelicolor* wild-type strain carrying empty vector pKF210 with promoterless *mCherry* (left-hand panels) or plasmid pKF255 expressing a translational *afsK-mCherry* fusion (right-hand panels). Representative images of growing hyphae are shown both as phase contrast image with overlaid fluorescence in red, and as the fluorescence image alone in inverted grey-scale. (C) Co-localisation of DivIVA and AfsK demonstrated using an *S. coelicolor* strain producing both DivIVA-EGFP (green) and AfsK-mCherry (red). A series of images were collected for each channel, moving focus 0.2 µm between each image. The Z-stacks were deconvolved using the Volocity software, and a central focal plane through the mid of the cells is shown as, from left to right, phase contrast image, mCherry fluorescence, EGFP fluorescence image, and overlay of the fluorescence channels. Size bars, 4 µm. **Figure 4.9** was kindly provided by Stuart Cantlay, Department of Biology, University of Lund, Sweden.

4.9 AfsK regulates the branching of growing hyphae

With the discovery that DivIVA is directly phosphorylated by AfsK, I wondered whether disruption of *afsK* would influence hyphal branching and the underlying polarisome splitting mechanism. Previously reported *afsK* mutant phenotypes in *S. coelicolor* have only concerned decreased synthesis of antibiotics (Matsumoto *et al.*, 1994). I analysed liquid cultures of the *S. coelicolor afsK* deletion mutant microscopically in comparison to the wild type and discovered that the *afsK* mutant strain does indeed have a previously unrecognised phenotype: it exhibits an altered tip-to-branch distribution, shifting the average to a longer distance than in the wild type (**Figure 4.10**). This effect is quantified in **Figure 4.10B**. The effect is also clearly apparent when comparing time-lapse image sequences of growing hyphae of the *afsK* mutant and its congenic *afsK*⁺ parent (Klas Flärdh, personal communication). To confirm that the effect on hyphal branching was due to the absence of *afsK*, Stuart Cantlay, Department of Biology, University of Lund, Sweden, complemented the *afsK* mutant and I analysed the resulting strain, finding that reintroducing the *afsK* gene largely restored wild-type branching behavior (**Figure 4.10C**).

To my surprise, the branch-to-branch distance is not changed in *afsK* mutant hyphae (**Figure 4.11**). These results show that loss of the AfsK kinase affects the normal regulation of branch-site selection and thereby lateral branch formation, and since the vast majority of hyphal branches emerge from DivIVA foci deposited by polarisome splitting (Richards *et al.*, 2012), this suggests that AfsK modulates some aspect of the development of new daughter polarisomes.

Using the mathematical model developed in Richards *et al.* (2012) and in collaboration with David Richards, Department of Computational and Systems Biology, John Innes Centre, we tried to determine which aspect of polarisome splitting might be affected in an *afsK* mutant. We attempted to recapitulate the *afsK* mutant branching phenotype by testing the variation of several parameter values from those in the wild type. The data derived from the minimal model capture the experimentally measured tip-to-branch distributions well by decreasing the binding affinity of molecules from the cytoplasm into the

polarisomes (β) and the initial polarisome size after splitting (N_0), as shown in **Figure 4.12**. (Decreasing only either one parameter could not fit both distributions.) This result suggests that the *afsK* mutant strain affects (at least indirectly) not only the binding affinity of DivIVA, but also the initial size of new daughter polarisomes. Importantly, this mathematical model is able to explain the quantitative *afsK* mutant branching phenotype data by straightforward reparameterisation, without the introduction of any new mechanisms.

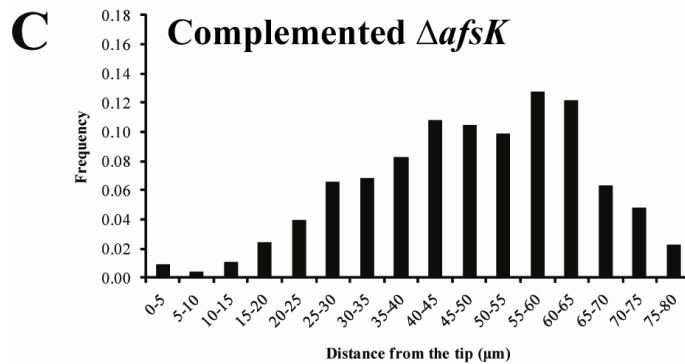
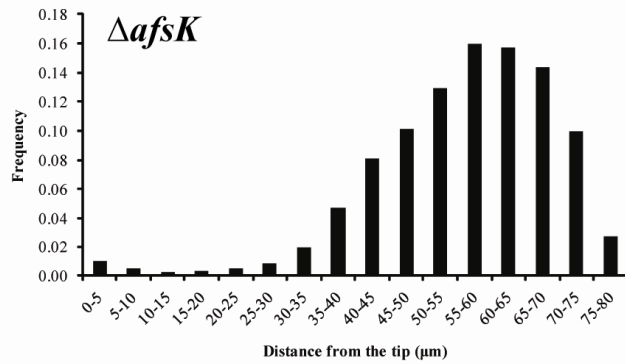
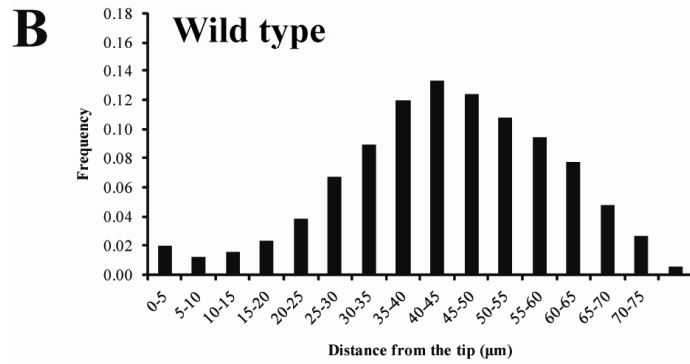
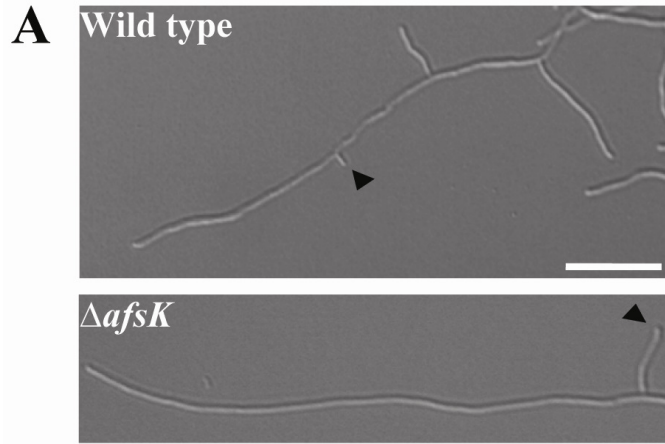


Figure 4.10 The *afsK* mutant has a branching phenotype.

(A) Representative DIC images of wild type *S. coelicolor* and the congenic *afsK* mutant grown in YEME. Arrows indicate the first lateral branch behind the hyphal tip. Size bar, 10 μm . (B) Histograms of distances between the tip and lateral branches at the moment of branch development in cultures of *S. coelicolor* wild type and the congenic *afsK* mutant, and (C) the complemented *afsK* mutant grown for 15-18 hours in YEME at 80 μm trim. The number of tip-to-branch distances measured per strain were 1097 (wild type), 875 (*afsK* mutant) and 281 (complemented mutant). Data analysis was done in collaboration with David Richards, Department of Computational and Systems Biology, John Innes Centre. For details of the data analysis see **Chapter 3**.

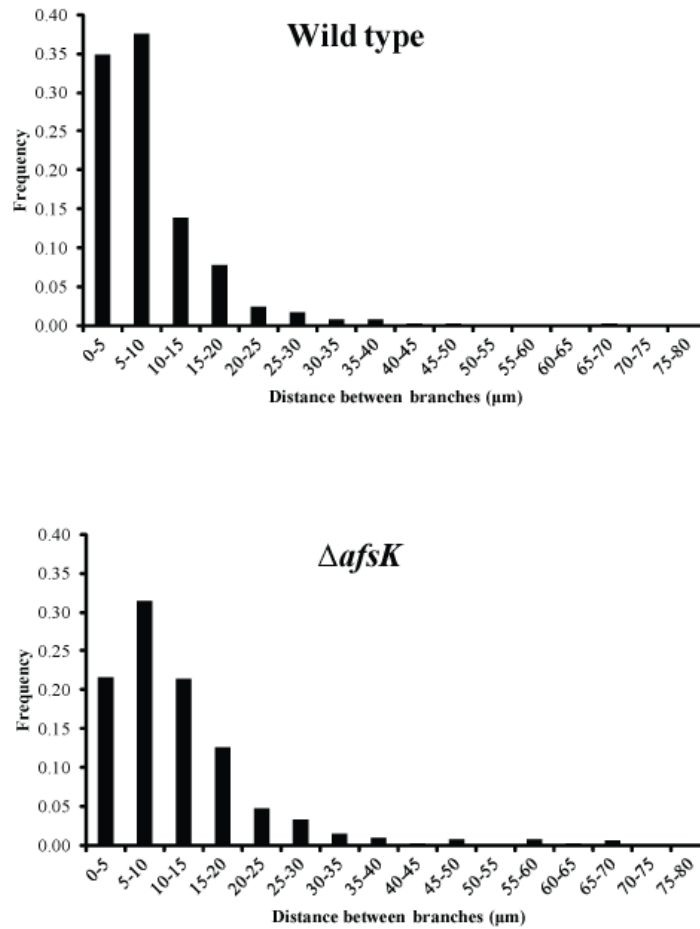


Figure 4.11 The branch-to-branch distance in the *afsK* mutant is unchanged. Histograms of distances between lateral branches in cultures of *S. coelicolor* wild type and the congenic *afsK* mutant grown for 15-18 hours in YEME at 80 μm trim. The number of branch-to-branch distances measured per strain were 858 (wild type) and 398 (*afsK* mutant). Data analysis was done in collaboration with David Richards, Department of Computational and Systems Biology, John Innes Centre. For details of the data analysis see **Chapter 3**.

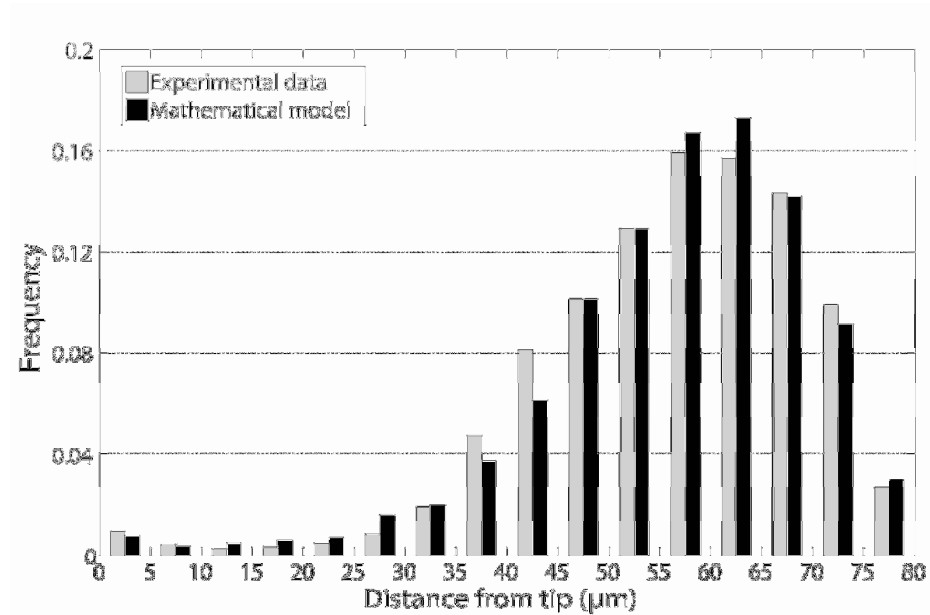


Figure 4.12 Histogram comparing the mathematical model and experimental data of the tip-to-branch distribution of the *afsK* mutant with a trim length of 80μm. Experimental data are the same as in **Figure 4.9**. Mathematical modeling was done by David Richards, Department of Computational and Systems Biology, John Innes Centre. For details of the mathematical model see **Chapter 3**.

4.10 Constitutively active AfsK mutant protein profoundly affects apical growth, DivIVA localisation, and hyphal branching

The data described above show that AfsK regulates branch-site selection and hyphal morphology during normal growth, when its activity, as reflected in the basal level of DivIVA phosphorylation, is relatively low. However, when peptidoglycan synthesis is blocked, there is a pronounced upregulation of AfsK-dependent DivIVA phosphorylation. This raised the question as to whether high levels of AfsK activity could profoundly affect hyphal growth and branching, but these effects cannot be evaluated when cell wall growth is simultaneously blocked by bacitracin.

Stuart Cantlay, Department of Biology, University of Lund, Sweden, therefore engineered a strain in which the AfsK kinase activity could be induced in normally growing hyphae. This was achieved by creating a constitutively active mutant version of AfsK in which two threonines in the activation loop of the kinase (T165 and T168) were changed to aspartates in order to mimic the autophosphorylation of AfsK that leads to its activation. As in other Ser/Thr protein kinases, the conserved residues T165 and T168 in the activation loop of *S. coelicolor* and *S. avermitilis* AfsK are required for activation of the kinase, and T168 has been shown to undergo autophosphorylation in *S. coelicolor* (Tomono *et al.*, 2006; Rajkarnikar *et al.*, 2007). Most importantly, in both species, T165D and T168D phosphomimic mutations result in a constitutively active kinase (Tomono *et al.*, 2006; Rajkarnikar *et al.*, 2007). The mutant *afsK* (T165D T168D) allele was placed under control of the thiostrepton-inducible *tipAp* promoter in the integrative vector pIJ6902 to create pKF275 (see Material and Methods, **Table 2.1**). When strains carrying pKF275 were grown in the absence of thiostrepton, they showed similar basal levels of DivIVA phosphorylation to control strains carrying only the empty vector pIJ6902 (**Figure 4.13A**). However, addition of thiostrepton to cultures of pKF275-carrying strains led to a dramatic increase in the level of phosphorylated DivIVA, as detected by the mobility shift of a major part of the DivIVA protein population seen in Western blots (**Figure 4.13A**).

Besides hyper-phosphorylation, the thiostrepton-induced expression of the constitutively active kinase also affected DivIVA localisation, as detected using the DivIVA-EGFP fusion. Prior to thiostrepton addition, the majority of hyphae carried detectable DivIVA-EGFP foci at the tips, but when expression of the constitutively active AfsK was induced, the majority of these foci dissolved or were strongly reduced in intensity (**Figure 4.13C**), leading to decreased average fluorescence intensity at the hyphal tip, and an increased fraction of hyphae without detectable apical foci. Cultures of pKF275-carrying strains that did not receive thiostrepton showed normal DivIVA localisation (**Figure 4.13C**), and similarly, the control strain carrying the empty vector pIJ6902 was not affected by addition of thiostrepton and showed normal DivIVA localisation to hyphal tips (data not shown). These observations show that strong upregulation of AfsK activity stimulates disassembly of polarisome structures and dissociation of DivIVA from hyphal tips.

When AfsK was activated using bacitracin or vancomycin, the arrest of peptidoglycan synthesis prevented studies of how a high level of AfsK activity affects hyphal growth and branching. However, the inducible expression system allowed us to examine such effects and revealed that induction of the constitutively active kinase caused dramatic changes in hyphal growth and morphology. When cultures containing the *tipAp-afsK* (T165D T168D) construct were incubated in the presence of the inducer thiostrepton, growth was impeded at existing hyphal tips (**Figure 4.13B**). However, despite the arrest of growth at existing hyphal tips, multiple new hyphal branches started to emerge from the lateral walls distal to these tips (**Figure 4.13D**). Such effects were not seen in control strains carrying the empty vector pIJ6902, which carried on growing without any detectable effect of thiostrepton (data not shown). It thus appears that induction of high AfsK activity causes growth inhibition at existing hyphal tips, and the subsequent initiation of multiple new lateral branches. This gave the cultures a conspicuous appearance, with unusually dense and compact hyphal pellets from which emerge hyperbranched and irregularly shaped hyphal structures (representative image in **Figure 4.13D**), strikingly different from the regular and loose hyphal pellets and long tip-to-branch distances seen in control cultures (representative image in **Figure 4.13D**). As a likely consequence of these

changes in growth and morphology, cultures expressing the constitutively active kinase accumulated biomass very slowly compared to the controls (data not shown). In summary, AfsK kinase activity has strong effects on cell polarity, tip extension, subcellular localisation of DivIVA, and initiation of new hyphal branches.

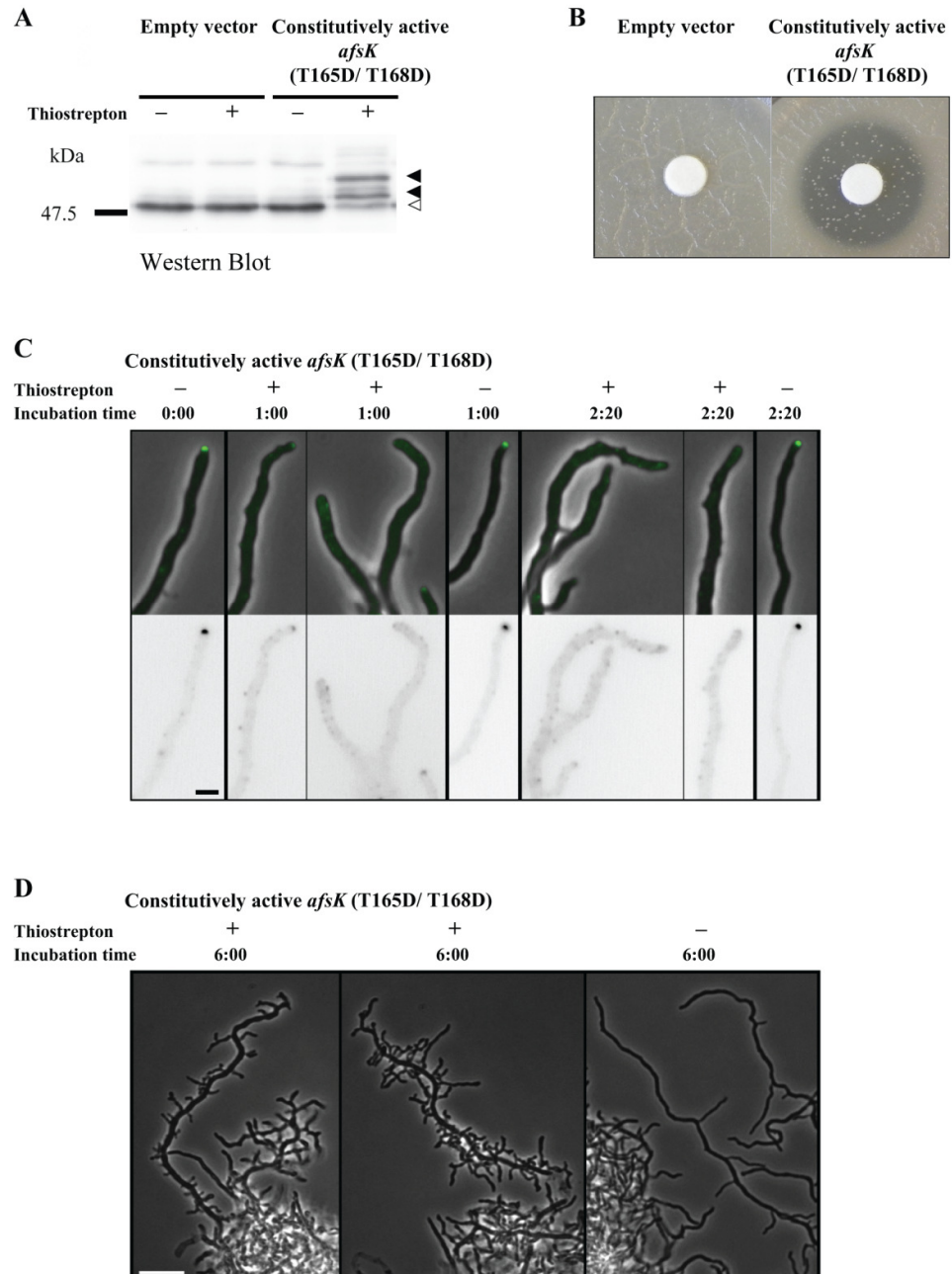


Figure 4.13 Engineered expression of a constitutively active version of the AfsK kinase induces high levels of DivIVA phosphorylation and profoundly affects hyphal tip extension and branching.

(A) Levels of DivIVA phosphorylation induced by expression of the *afsK* (T165D T168D) allele from the thiostrepton-inducible *tipAp* promoter in plasmid pKF275. A strain carrying empty vector pIJ6902 was used as control. Growing cultures were split in two and thiostrepton was added to one (+) while a mock addition of DMSO was made to the other (-). Extracts of cells harvested after 2.5 hours were separated by SDS-PAGE and DivIVA was detected by immunoblotting. Phosphorylated species of DivIVA (closed arrowheads) migrate more slowly than unphosphorylated DivIVA (open arrowhead). (B) Inhibition of growth caused by induced expression of the *afsK* (T165D T168D) allele. Spores of two bacterial strains were spread evenly TSB agar plates containing apramycin maintain selection for the integrated plasmids. The strains were derivatives of *S. coelicolor* strain M600 carrying plasmids integrated at the *attB_{φC31}* site with the thiostrepton-inducible promoter driving expression of constitutively active AfsK (strain K335) or control strain with empty vector (strain K336) A sterile paper disc was soaked with 15 µl of 0.1 mg/ml thiostrepton dissolved in DMSO. Plates were incubated at 30°C for 2 days, and then photographed. The clearing zone around the disc in the left-hand image demonstrates that induced expression of the constitutively active AfsK kinase inhibits growth. (C) The effects of overproduction of constitutively active AfsK (T165D T168D) on DivIVA-EGFP localisation. Images captured before addition of thiostrepton (10 µg/ml), the inducer of *tipAp-afsK* (T165D T168D) expression, 1 hour, and 2:20 hours after addition of thiostrepton or mock. EGFP fluorescence is shown in inverted grey scale (lower panels) or shown in green overlaid on phase contrast images (upper panels). Bar, 2 µm. (D) Typical examples of hyperbranched hyphal morphology developing after overexpression of *afsK* (T165D T168D) for 6 hours (left-hand and middle panels), compared to the uninduced control sample (right-hand panel). Bar, 10 µm. **Figure 4.13** was kindly provided by Klas Flärdh, Department of Biology, Lund University, Sweden.

4.11 Discussion

The work described in this chapter shows that the Ser/Thr protein kinase AfsK is part of the apparatus that controls polar growth in *Streptomyces*, and that it directly phosphorylates the cell polarity determinant DivIVA. These data indicate dual roles for the AfsK kinase. First, during normal growth it modulates the control of hyphal branching and the development of daughter polarisomes. Second, when cell wall synthesis is arrested, AfsK is strongly activated and causes the profound reconfiguration of DivIVA localisation, apical growth, and hyphal branching.

Induction of a constitutively active form of AfsK causes the disappearance of the DivIVA foci that normally mark growing hyphal tips. No concomitant degradation or decrease in cellular DivIVA content is observed, suggesting that high AfsK activity destabilises the DivIVA-containing apical polarisome. DivIVA is a self-assembling coiled-coil protein that forms oligomers and higher order complexes and is involved in polar targeting in a range of Gram-positive bacteria (Nguyen *et al.*, 2007; Letek *et al.*, 2008; Wang *et al.*, 2009; Lenarcic *et al.*, 2009; Oliva *et al.*, 2010). The AfsK-mediated phosphorylation of DivIVA in *Streptomyces* occurs on two trypsin-generated fragments in the C-terminal domain. Although this C-terminal domain is not conserved outside of *Streptomyces* orthologues (Flårdh, 2003), it lies just downstream of the conserved second coiled-coil domain, which is known to be important in the oligomerisation of *B. subtilis* DivIVA (Oliva *et al.*, 2010). It is therefore possible that the AfsK-mediated phosphorylation influences oligomerisation, acting as a means to control the assembly or disassembly of multimeric complexes or higher order structures formed by DivIVA in the cell. Such a role for Ser/Thr protein kinases in controlling assemblages of coiled-coil proteins is well known in eukaryotes, a classic example being the disassembly of the nuclear lamina mediated by cyclin-dependent kinases (Shimi *et al.*, 2011). In addition, it was recently reported that the assembly and subcellular localisation of the coiled-coil protein RsmP in *C. glutamicum* is affected by phosphorylation (Fiuza *et al.*, 2010). However, it cannot be excluded that phosphorylation may also influence other aspects of DivIVA behavior, such as its interaction with other proteins or the membrane. The

function of *B. subtilis* DivIVA depends on direct interactions with MinJ and the nucleoid-associated protein RacA (Bramkamp *et al.*, 2008; Lenarcic *et al.*, 2009), and the function of *S. coelicolor* DivIVA is also likely to depend on the direct recruitment of other proteins to the cell poles (Flärdh, 2010; Flärdh & Buttner, 2009). Further, crystal structures of *B. subtilis* DivIVA show how the oligomers may interact with the membrane via an exposed phenylalanine residue in the highly conserved N-terminal part of the protein (Oliva *et al.*, 2010), and the polar and septal targeting of the *B. subtilis* DivIVA appears to be explained by a preference of the oligomers for negatively curved membrane surfaces (Lenarcic *et al.*, 2009; Eswaramoorthy *et al.*, 2011).

The decreased branching observed in *afsK* mutants could be explained by an effect of AfsK-mediated phosphorylation on the stability of the apical DivIVA clusters. Most branches in *S. coelicolor* are formed by a polarisome splitting mechanism in which the DivIVA-containing apical polarisome splits to leave smaller daughter polarisomes behind along the lateral hyphal walls as the tip extends, foci which act as seeds for new branches (Richards *et al.*, 2012). Although only a small fraction of the DivIVA molecules in the cell are detectably phosphorylated during normal growth, this low basal activity obviously has significant impact on hyphal branching. Since AfsK co-localises with the DivIVA foci at hyphal tips, it is possible that the low level of DivIVA phosphorylation seen during normal growth affects polarisome splitting (perhaps by controlling the initial size of new daughter polarisomes) and thereby modulates the pattern of hyphal branching.

Hyperactivity of AfsK inhibits growth at the original hyphal tips, but paradoxically it also induces the subsequent formation of multiple short lateral branches distal to these tips. This observation, that growth can be initiated at new sites while being prevented at the original tip, could also be explained by the localisation of AfsK to hyphal tips. High levels of DivIVA phosphorylation might promote the complete disassembly of the apical protein complexes. The released DivIVA molecules could then diffuse away and gradually be dephosphorylated, allowing them to form new foci that are capable of establishing new branches distal to the original tips. This could provide *S. coelicolor* with a mechanism to

dismantle the apical growth apparatus at hyphal tips that encounter problems with cell wall synthesis.

AfsK was one of the first bacterial Ser/Thr protein kinases to be investigated, having been studied by Horinouchi and colleagues since the 1980s, particularly in *S. griseus* and *S. lividans*. An *afsK* disruption mutant of *S. coelicolor* was reported to grow and sporulate normally, while showing reduced production of blue-pigmented antibiotic actinorhodin (Matsumoto *et al.*, 1994). The effect on antibiotic production appears to be mediated by the transcription factor AfsR, which is directly phosphorylated by AfsK *in vitro* and activates transcription of *afsS*, encoding a small pleiotropic regulator of antibiotic synthesis in *Streptomyces* (Tanaka *et al.*, 2007; Lee *et al.*, 2002). This thesis reports a completely different role for AfsK in the control of hyphal growth and branching, one that does not involve AfsR (since an *afsR* mutant shows normal hyphal branching and normal levels of DivIVA phosphorylation). Strikingly, the conditions we employed to induce high AfsK activity (addition of bacitracin or the engineered expression of a constitutively active kinase) did not trigger overproduction of actinorhodin (unpublished data). In summary, the finding that AfsK plays a key role in controlling polar growth and branching is novel and is not obviously related to the previously inferred role of AfsK in secondary metabolism.

Overall, these findings show that communication between the polarity determinant DivIVA and the cell wall biosynthetic machinery is bidirectional (**Figure 4.14**), with DivIVA directing cell wall synthesis (Hempel *et al.*, 2008), and the biosynthetic machinery communicating back to DivIVA via AfsK-mediated phosphorylation. All three components – the cell wall biosynthetic machinery, AfsK and DivIVA - localise to growing hyphal tips.

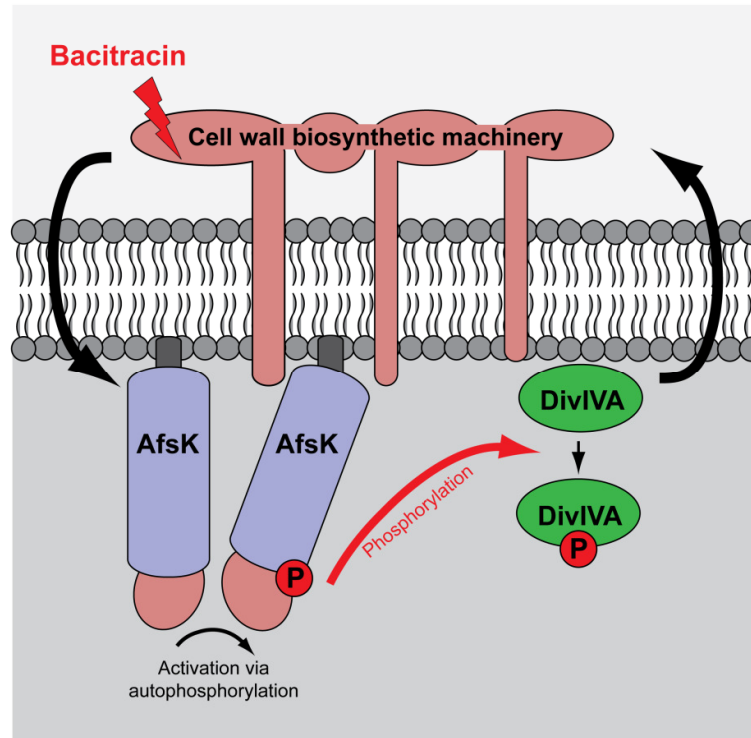


Figure 4.14 Communication between the polarity determinant DivIVA and the cell wall biosynthetic machinery in *Streptomyces* is bidirectional.

The cytoskeletal protein DivIVA directs cell wall synthesis at hyphal tips, but when the cell wall biosynthetic machinery is compromised, for example when it is inhibited by the antibiotic bacitracin, it communicates back to DivIVA via AfsK-mediated phosphorylation, leading to modulation of apical growth and branching.

4.12 Summary Points

- During undisturbed hyphal growth DivIVA is phosphorylated at a basal level.
- DivIVA phosphorylation increases dramatically when cell wall synthesis is blocked.
- The C-terminal region of DivIVA is the target of multiple phosphorylations.
- The DivIVA kinase is AfsK, previously known to be involved in secondary metabolism, and not a PASTA-domain containing Ser/Thr protein kinase.
- The AfsK kinase co-localises with its substrate DivIVA at the tips of growing vegetative hyphae.
- AfsK regulates branch development of growing hyphae by modulating the tip-to-branch distance.
- Constitutively-active AfsK profoundly affects apical growth, DivIVA localisation, and hyphal branching.

Chapter 5

Systematic characterisation of the Ser/Thr phosphorylation sites of the *Streptomyces* polarity determinant DivIVA using a combination of nano-LC and high-accuracy mass spectrometry

5.1	Introduction	153
5.2	MALDI-ToF mass spectrometric analysis of the DivIVA phosphorylation	153
5.3	Introduction of two additional tryptic cleavage sites into the 7.2 kDa C-terminal peptide	157
5.4	Mapping of the phosphorylation sites in the DivIVA C-terminus	159
5.5	Discussion and Conclusion	175
5.6	Summary Points	178

Statement of my work

This chapter is part of a collaborative project with Mike Naldrett and Gerhard Saalbach, Proteomics Facility, John Innes Centre, and is currently on the way to be written up as a manuscript for a proteomics journal. I provided the samples for mass spectrometry (**Figure 5.1A**) and constructed the allele encoding FLAG-DivIVA (Q343R Q360R).

5.1 Introduction

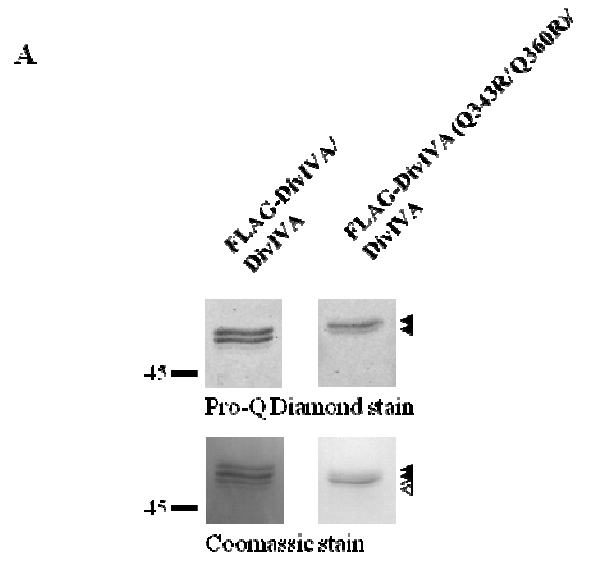
The work in Chapter 4 showed that the Ser/Thr protein kinase AfsK co-localises with the polarisome complex at the tips of growing *Streptomyces* hyphae and that AfsK modulates cell polarity, both during normal growth and during cell wall stress. One substrate of AfsK is DivIVA, which becomes multiply phosphorylated in the C-terminal part of the protein. In order to begin to understand how phosphorylation contributes to the regulation of DivIVA, polarisome splitting and branch development, the exact phosphorylation sites needed to be mapped.

Accordingly, in collaboration with Mike Naldrett and Gerhard Saalbach, Proteomics Facility, John Innes Centre, we attempted to characterise DivIVA phosphorylation further. Although identification of the precise phosphorylation sites is technically quite challenging in a large peptide containing multiple putative phosphorylation sites, we were able to pinpoint the exact sites using a combination of nano-liquid chromatography (nano-LC) peptide fractionation and high-accuracy mass spectrometry.

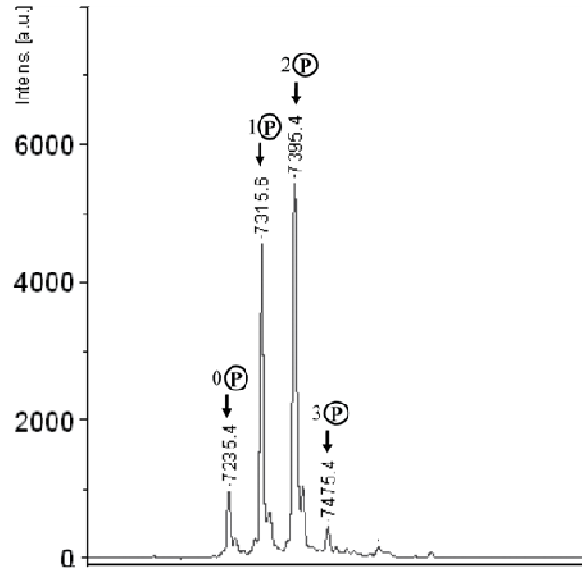
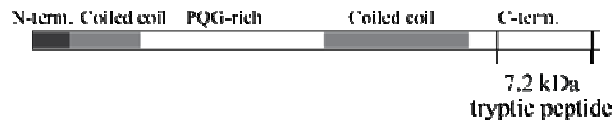
5.2 MALDI-ToF mass spectrometric analysis of DivIVA phosphorylation

Initially, I would briefly like to reiterate and extend the results from **Chapter 4 Section 4.4** that identified the phosphorylated region of DivIVA. The level of DivIVA phosphorylation during undisturbed growth is very low and is therefore difficult to analyse. As a consequence, I isolated DivIVA from cultures treated with bacitracin to block cell wall synthesis and thereby increase the level of phosphorylation. I used a strain that carried wild-type *divIVA* and a second *divIVA* allele encoding an N-terminally FLAG-tagged version of the protein. This FLAG-tagged allele was under the control of a thiostrepton-inducible promoter and was carried on a single-copy vector that integrates site-specifically into the *S. coelicolor* chromosome at the phage *attB*_{ϕC31} site. FLAG-DivIVA co-immunoprecipitates with the native DivIVA (Wang *et al.*, 2009) and this allowed me to analyse the immunoprecipitated FLAG-DivIVA/DivIVA mixtures. The conditions for protein

purification were optimised to preserve the native phosphorylation state and for mass spectrometric analysis (see Material and Methods **Section 2.9**). The presence of DivIVA both with and without FLAG-tag gives rise to a double band in the Coomassie-stained SDS-PAGE gel (indicated by the open arrowheads in **Figure 5.1A**) and the level of phosphorylation of the samples was determined using the phosphorylation-specific stain Pro-Q Diamond (**Figure 5.1A**). The DivIVA material was then digested with trypsin coupled to magnetic beads and analysed by Ultraflex MALDI-ToF-ToF. Tryptic digestion of DivIVA results in multiple fragments below 3.8 kDa in size, but also in two large, 9.2 and 7.2 kDa, peptides. The 9.2 kDa tryptic peptide contains mostly the PQG-rich linker separating the two coiled-coil domains. The 7.2 kDa tryptic peptide derives from the C-terminal part of the protein and, using MALDI-ToF mass spectrometry, we were able to show that this 7.2 kDa tryptic peptide becomes singly, doubly and triply phosphorylated (**Figure 5.1B**). When examining the amino acid sequence of this peptide for potential phosphorylation sites, it became clear that it carries a total of 14 serine and threonine residues (highlighted in red and green, respectively, in the DivIVA amino acid sequence in **Figure 5.1C**). However, determining which of these 14 residues were phosphorylated was not immediately possible because the 7.2 kDa tryptic peptide was too large to be analysed by MS/MS peptide sequencing. Attempts to get around this problem by cleaving DivIVA with chymotrypsin, a combination of trypsin and chymotrypsin, proteinase K or cyanogen bromide, were unsuccessful (Naldrett, Saalbach and Hempel unpublished data). Therefore, we decided to introduce additional tryptic cleavage sites into the 7.2 kDa peptide by site-directed mutagenesis of the *divIVA* gene.



B
DivIVA



C

```

1  MFLTPEDVPH  KCFITVPLPE  GYDEDEVDAF  LDSYBAELTE  LLRNEDLRA
51  KLAARTRAAA  GNCONMPKPF  EPPDGOOHG  GPFCHOCGPP  GGGGKPGGGK
101  PGGAPVPAE  IGGPPQCGMG  GPMGGPPQLP  GGAPQLPAGP  GGQGGCQGGC
151  PNGQGGPGMG  CCGSPNCGGM  GPGPMGGPMG  GPDGCGGPGG  PMPCGGGPG
201  GDSARVLSL  AQQTADQAZA  EARERANKIV  GEAPSPAEGL  EADARAKDA
251  LEPDAQENHR  VAMSSLESAP  ATLSREVEOL  PGTREYPTTE  LLSYLESQLE
301  QLETQADDSE  AEPRTPTAS  LPPSPAPSM  PAGASAPSYG  GNQSMGGGPG
351  QSGPSYGGQQ  QMSPANTQPM  APVRPQGPS  MGQAPSPMRG  FLIDEIDH
    
```

Figure 5.1 *S. coelicolor* DivIVA is multiply phosphorylated in the C-terminus. (A) DivIVA samples for mass spectrometric analysis. Bacitracin (50 µg/ml) was added for 30 minutes to growing cultures of wild-type *S. coelicolor* expressing *FLAG-divIVA* from a thiostrepton-inducible promoter or a strain expressing *afsK* from the constitutively active promoter *ermE** and *FLAG-divIVA (Q343R Q360R)* from a thiostrepton-inducible promoter. Cells were lysed, cell extracts prepared, and FLAG-DivIVA/DivIVA was immunoprecipitated using anti-FLAG affinity gel. Closed arrowheads indicate phosphorylated DivIVA and open arrowheads indicate non-phosphorylated DivIVA. A molecular weight marker and its corresponding sizes are given on the sides of the gel. Irrelevant lanes between the two samples have been excised from the image. (B) Schematic showing the position of the 7.2 kDa phosphorylated peptide (residues 315-389) within the DivIVA primary sequence. The MALDI mass spectrum of the 7.2 kDa tryptic peptide shows 0 to 3 phosphorylations (molecular mass of the peptide 7235.4 Da is shifted by multiples of 80 Da; $\text{HPO}_3 = 80$ Da; +80, +160 and +240 Da, respectively). (C) Sequence of the 7.2 kDa tryptic peptide is highlighted in yellow in the DivIVA amino acid sequence; potential phosphorylation sites are highlighted in red (serines) and green (threonines). **Figure 5.1** was adapted and extended from **Figure 4.4**.

5.3 Introduction of two additional trypsin cleavage sites into the 7.2 kDa C-terminal peptide

In order to determine which serine and threonine residues in the C-terminal 7.2 kDa peptide are phosphorylated *in vivo*, two additional tryptic cleavage sites were engineered into DivIVA using site-directed mutagenesis (**Figure 5.2A**). Two glutamines (Q343 and Q360) were strategically chosen for mutagenesis to arginines because they lie in regions in which structural secondary effects were predicted to be minimal (**Figure 5.2B**). Because *divIVA* is essential in *Streptomyces*, replacing the chromosomal allele with a mutant allele is technically challenging. For that reason, the *FLAG-divIVA (Q343R Q360R)* allele was cloned into the integrative vector pIJ10550 under control of the thiostrepton-inducible *tipA* promoter and introduced into the *S. coelicolor* wild-type strain M600 and into a strain carrying the *afsK* kinase gene under control of the strong, constitutively active promoter *ermE**. After immunoprecipitation, the mixtures of DivIVA and FLAG-DivIVA (Q343R Q360R) were examined using SDS-PAGE (**Figure 5.1**). Because of technical problems, only the sample from the strain carrying *afsK* under the control of *ermEp** was cleaved with trypsin and analysed further (**Figure 5.1** and data not shown). Although the 7.2 kDa peptide derived from the wild-type DivIVA was still present in the digestion mix, it was disregarded for the purpose of this experiment and instead the newly derived smaller peptides from digestion of FLAG-DivIVA (Q343R Q360R) were analysed.

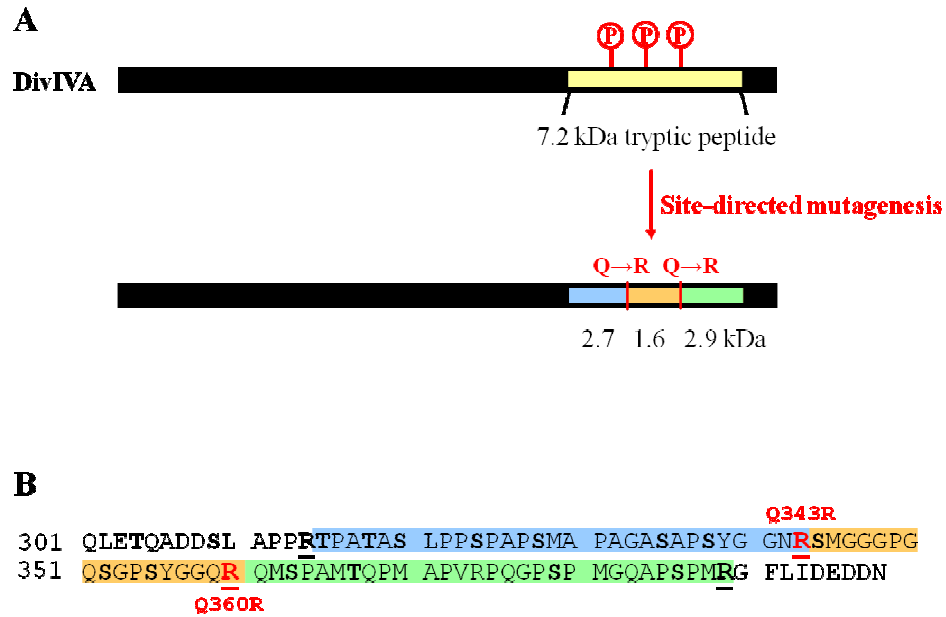


Figure 5.2 Schematic of the site-directed mutagenesis to introduce two additional trypsin cleavage sites in the DivIVA C-terminus.

The positions of the glutamine residues that were changed to arginines and the resulting peptides after trypsin cleavage are shown in a schematic (A) and are highlighted in the amino acid sequence of the C-terminus (B).

5.4 Mapping the phosphorylation sites in the DivIVA C-terminus

Our strategy to map the phosphorylation sites was to digest the purified protein mixture of DivIVA/FLAG-DivIVA (Q343R Q360R) with trypsin as before and then to separate the tryptic peptides chromatographically using nano-Liquid Chromatography (25 cm C18 reverse-phased chromatography column, 1.7 μ m BEH). Peptides were automatically injected into an Orbitrap mass spectrometer, where they were initially analysed using a standard “top5” DDA setup followed by a Mascot database search. Mascot identified a number of phosphopeptides and possible sites (**Table 5.1**). For a more detailed analysis, samples were re-run with targeted LC-MS/MS analysis using an inclusion list for the peptides of interest without dynamic exclusion. Special care was taken for the evaluation and interpretation of the data. All MS/MS spectra were analysed by Mascot and ScaffoldPTM as well as by visual inspection. Initial Mascot results showed sequence coverage of 46% including the complete 7.2 kDa fragment, but not the 9.2 kDa fragment which is completely free of tryptic cleavage sites. This fragment showed no phosphorylation in the MALDI-ToF experiments mentioned above (data not shown).

Table 5.1 Overview of initial Mascot results identifying various phosphopeptides and possible phosphorylation sites in the DivIVA C-terminus.

m/z (expt)	Mr (expt)	z (expt)	Mr (calc)	Delta	Score	Expect	Peptide amino acid sequence/ site of phosphorylation
810.8658	1619.7171	2	1619.7192	-0.0021	33.73	0.00042	QLETQADDpSLAPPR
810.8658	1619.7171	2	1619.7192	-0.0021	77.25	1.90E-08	QLETQADDpSLAPPR
810.8657	1619.7168	2	1619.7192	-0.0025	34.28	0.00037	QLEpTQADDSLAPPR
810.8652	1619.7159	2	1619.7192	-0.0033	27.34	0.0018	QLETQADDpSLAPPR
810.8652	1619.7159	2	1619.7192	-0.0033	47.87	1.60E-05	QLETQADDpSLAPPR
810.8662	1619.7179	2	1619.7192	-0.0013	22.75	0.0053	QLEpTQADDSLAPPR
810.8662	1619.7179	2	1619.7192	-0.0013	29.01	0.0013	QLEpTQADDSLAPPR
830.3310	1658.6473	2	1658.6508	-0.0035	26.45	0.0023	SMGGGPGQSGPpSYGGQR
830.3310	1658.6473	2	1658.6508	-0.0035	47.31	1.90E-05	SMGGGPGQpSGPSYGGQR
553.8899	1658.6479	3	1658.6508	-0.0029	16.15	0.024	SMGGGPGQSGSpYGGQR
830.3310	1658.6473	2	1658.6508	-0.0035	46.72	2.10E-05	SMGGGPGQpSGPSYGGQR
830.3310	1658.6473	2	1658.6508	-0.0035	61.09	7.80E-07	SMGGGPGQpSGPSYGGQR
830.3310	1658.6473	2	1658.6508	-0.0035	65.18	3.00E-07	pSMGGGPGQSGPSYGGQR
830.3310	1658.6473	2	1658.6508	-0.0035	55.49	2.80E-06	pSMGGGPGQSGPSYGGQR
921.0927	2760.2564	3	2760.2578	-0.0014	25.78	0.0026	TPATASLPPSPAPSMAPAGASAPpSYGGNR
921.0927	2760.2564	3	2760.2578	-0.0014	13.84	0.041	TPATASLPPSPAPSMAPAGASAPpSYGGNR
921.0927	2760.2564	3	2760.2578	-0.0014	39.34	0.00012	TPATASLPPSPAPSMAPAGASAPpSYGGNR
921.0927	2760.2564	3	2760.2578	-0.0014	26.22	0.0024	TPATASLPPSPAPSMAPAGASAPpSYGGNR

Abbreviations used in the **Table 5.1** are as following; m/z , mass-over-charge ratio; m/z (expt), experimentally observed mass-to-charge value; M_r (expt), experimental m/z transformed into a relative molecular mass; M_r (calc), calculated relative molecular mass of the matched peptide; Delta, difference (error) between experimental and calculated masses; Expect, comparison to a small in-house library based on various *E. coli* proteins.

These initial mass spectrometry results indicated a heterogeneous mixture of phosphopeptides with specific phosphopeptides being phosphorylated at different sites. These so-called isoforms of individual phosphopeptides were expected to have very different HPLC elution profiles. By using an inclusion list for the peptides of interest (targeted LC-MS/MS) and running the mass spectrometer without dynamic exclusion, extensive data for peptides and fragment ions were generated allowing the reliable assignment of the phosphorylation sites.

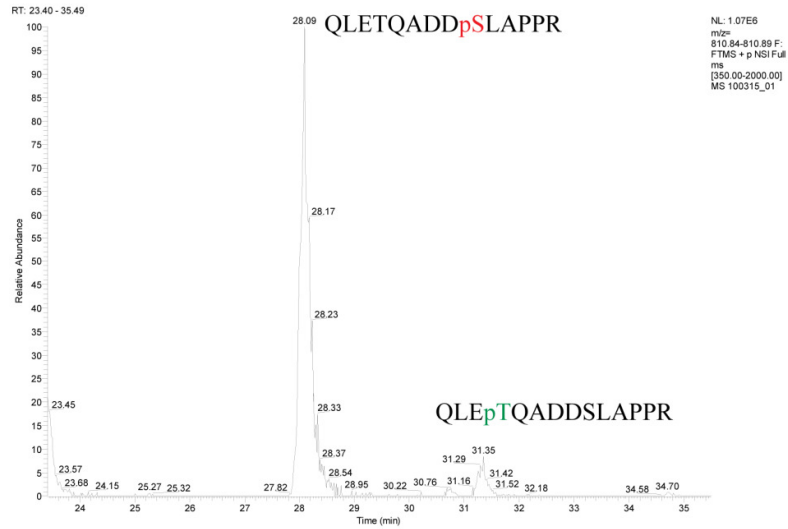
Initially, results were analysed in ScaffoldPTM, which allowed reliable assignment of phosphorylation sites to a 1.5 kDa peptide, (QLETQADDSLAPPR, amino acids 301 to 314, Figure 5.3A) that is immediately N-terminal to the 7.2 kDa peptide in the primary amino acid sequence. The extracted ion chromatogram (XIC) of the corresponding mass-to-charge ratio (m/z) of 810.8669 showed two distinct peaks (Figure 5.3B). As shown by the Mascot and ScaffoldPTM (Ascore) results (Table 5.2), these peaks correspond to two isoforms of the 1.5 kDa peptide; one abundant isoform phosphorylated on S309 and a minor abundant isoform phosphorylated on T304, with the S309 phosphopeptide eluting three minutes before the T304 phosphopeptide (Figure 5.3B). This is confirmed by visual inspection of the MS/MS spectra (Figures 5.3C and D), in which fragment ions $y_3 - y_6$ identify phosphorylation on T304 (Figure 5.3C) and fragment ions $y_6 - y_9$ identify phosphorylation on S309 (Figure 5.3D) No doubly phosphorylated species was detected.

A

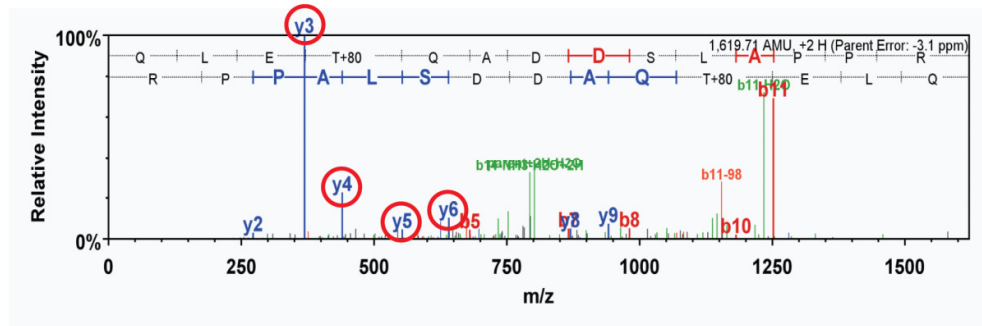
```

1  MPLTPEDVRN KQFTTVRLRE GYDEDEVDAF LDEVEAELTR LLRENEDLRA
51  KLAAATRAAA QNQONMRKPP EPPQDQQHQQ GPPQHQQGPP QGGGMPQQGM
101 RFGAPVPAG ISGPPQQMG GPMGGPQLP SGAPQLPAGP GGQGGPQGGP
151 PMGQGGPMPG QGPGPMQGM GPGPMGGPMG GPQGGPGPG PGMPGQGGPG
201 GDSAAARVLSL AQTADQAI AEARSEANKIV GEARSRAEGL ERDARAKADA
251 LERDAQEKHR VAMGSLESAR ATLERKVEDL RGFEREYRTR LKSYLESQLR
301 QLETQADDSL APERTPATAS LPPSPAPMA PAGASAPSYG GNRSMGGGPG
351 QSGPSYGGQR QMSPAMTQPM APVRPQGSP MGQAPSPMRG FLIDEDDN
    
```

B QLEpTQADDpSLAPPR (2+), m/z = 810.8669



C QLEpTQADDSLAPPR



QLETQADDpSLAPPR

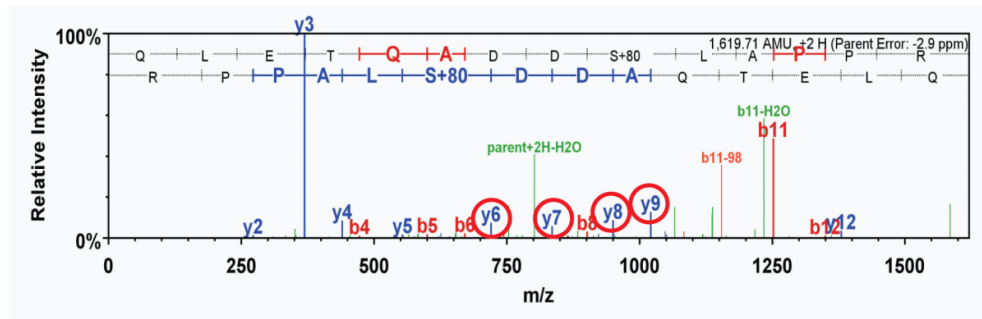


Figure 5.3 Identification of the phosphorylation sites on peptide QLETQADDSLAPPR (amino acids 301 to 314).

(A) The peptide and the identified phosphorylated serine and threonine are highlighted on the primary amino acid sequence (peptide in yellow, serine in red, threonine in green, tryptic cleavage sites in bold). (B) Extracted ion chromatogram of $m/z = 810.8669$ showing the elution profile of the two monophosphorylated phosphopeptide isoforms. (C) MS/MS spectra of the two fragmented phosphopeptide isoforms showing that the $y_3 - y_6$ -ions identify T304 as the phosphorylated residue (highlighted in green) in the first isoform and the $y_6 - y_9$ -ions identify S309 (highlighted in red) as the phosphorylated residue on the second isoform. Critical ions for identification of phosphosite are circled in red. **Figure 5.3** was kindly provided by Gerhard Saalbach, Proteomics Facility, John Innes Centre.

Table 5.2 Scaffold/Ascore results of the XIC of $m/z = 810.8669$ of the QLETQADDSLAPPR (amino acids 301 to 314) phosphopeptide isoforms. **Table 5.2** was provided by Gerhard Saalbach, Proteomics Facility, John Innes Centre.

Localisation of phosphorylation on peptide (on protein)	Localisation probability	Ascore	Peptide Score	Scaffold: Peptide probability	Spectrum Name
S9 (S309)	100%	76.42	82.09	0.9345	Scan 1891 (rt=27.9051)
S9 (S309)	100%	77.53	106.54	0.9965	Scan 1893 (rt=27.9218)
S9 (S309)	100%	115.97	125.82	0.9338	Scan 1895 (rt=27.9387)
S9 (S309)	100%	68.60	115.23	0.9977	Scan 1897 (rt=27.9558)
S9 (S309)	100%	100.21	148.50	0.9956	Scan 1899 (rt=27.9727)
S9 (S309)	100%	81.69	117.10	0.9965	Scan 1902 (rt=27.998)
S9 (S309)	100%	81.69	100.91	0.9984	Scan 1905 (rt=28.0235)
S9 (S309)	100%	107.29	131.58	0.9967	Scan 1908 (rt=28.0487)
S9 (S309)	100%	87.95	127.81	0.9962	Scan 1911 (rt=28.0739)
S9 (S309)	100%	107.29	150.31	0.9979	Scan 1914 (rt=28.0985)
S9 (S309)	100%	95.62	124.59	0.9965	Scan 1922 (rt=28.1654)
					Sum of 2 scans in range 1917 (rt=28.1239) to 1920 (rt=28.1489)
S9 (S309)	100%	96.85	123.29	0.9982	1920 (rt=28.1489)
T4 (T304)	100%	70.86	70.82	0.9257	Scan 2134 (rt=31.3252)
T4 (T304)	100%	60.87	90.92	0.9964	Scan 2136 (rt=31.3416)
T4 (T304)	100%	29.88	62.69	0.846	Scan 2140 (rt=31.3741)
T4 (T304)	100%	33.54	60.46	0.5858	Scan 2142 (rt=31.3907)
T4 (T304)	100%	35.03	60.38	0.8799	Scan 2144 (rt=31.4074)
T4 (T304)	100%	44.27	40.35	0.8017	Scan 2146 (rt=31.4242)
T4 (T304)	100%	35.03	59.34	0.6003	Scan 2148 (rt=31.4411)
T4 (T304)	100%	26.84	68.27	0.8536	Scan 2150 (rt=31.458)
T4 (T304)	100%	32.16	56.15	0.5858	Scan 2152 (rt=31.4749)

As expected, three tryptic peptides were derived from the original C-terminal 7.2 kDa tryptic peptide.

The first peptide (TPATASLPPSPAPSMAPAGASAPSYGGNR, amino acids 315 to 343) eluted as a single peak from the HPLC column, suggesting that this peptide is only phosphorylated on a single residue (**Figure 5.4A and B**). By analysis of the MS/MS spectra using Mascot and ScaffoldPTM, no definite conclusion as to which of the potential eight sites was phosphorylated could be obtained, although residues S338 and Y339 were favoured (**Table 5.3**). However, by visual inspection two specific fragment ions (y5 and y7) were detected in most of the MS/MS spectra that unambiguously identified S338 as the phosphorylated residue (**Figure 5.4C**). The y7-ion indicating that S338 or Y339 must be phosphorylated is present in 64 out of a total of 70 acquired spectra obtained from the peptide peak, and the y5-ion indicating that Y339 is not phosphorylated is present in 29 of the 70 spectra. Both fragment ions elute under the XIC of the phosphopeptide. To visualise this, a script was developed by Marielle Vigouroux, John Innes Centre, showing the LC elution profile of the indicative MS/MS fragments for specific phosphorylation sites, which can then be compared with the XIC of the peptide (**Figure 5.4D**).

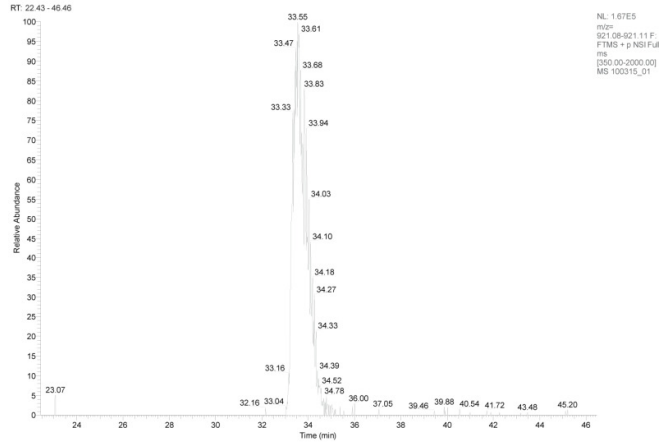
A

```

1  MPLTPEDVRN  KQFTTVRLRE  GYDEDEVDAF  LDEVEAELTR  LLRENEDLRA
51  KLAATRAAA  QNQNMKPP  EPPQDQHQQ  GPPQHQQGPP  QQGMPQQGM
101  RGPAPVPAG  ISGFPQQMG  GPMGGPQLP  SGAPQLPAGP  GGQGGPQGP
151  PMQGPGPMG  QGPGMQGM  GPGPMGGPMG  GPQGGPGPG  PGMPGQGGP
201  GDSAAVLSL  AQQTADQIA  EARSEANKIV  GEARSRAEGL  ERDARAKADA
251  LERDAQEKHR  VAMGSLESAR  ATLERKVEDL  RGFEREYRTR  LKSYLESQLR
301  QLETQADDSL  APPRTPATAS  LPPSPAPSPA  PAGASAPSYG  GNRSMGGGPG
351  QSGPSYGGQR  QMSPAMTQPM  APVVRPQGPS  MGQAPSPMRG  FLIDEDDE
    
```

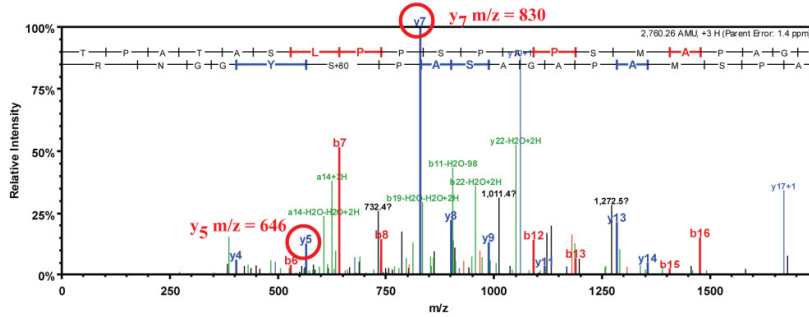
B

TPATASLPPSPAPSMAPAGASAPpSYGGNR (3+), m/z = 921.0932



C

TPATASLPPSPAPSMAPAGASAPpSYGGNR



D

TPATASLPPSPAPSMAPAGASAPpSYGGNR

TPATASLPPSPAPSMAPAGASAPpSYGGNR

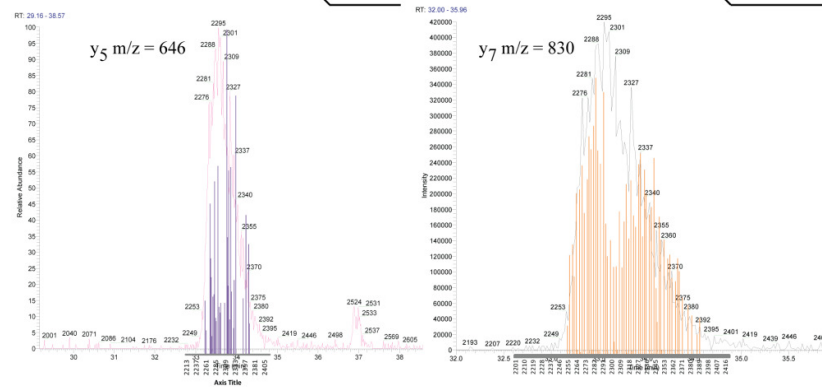


Figure 5.4 Identification of the phosphorylation site on peptide TPATASLPPSPAPSMAPAGASAPSYGGNR (amino acids 315 to 343). (A) The peptide and the identified phosphorylated serine are highlighted on the primary amino acid sequence (peptide in blue, serine in red, tryptic cleavage sites in bold). (B) Extracted ion chromatogram of $m/z = 921.0932$ showing the elution profile of the a monophosphorylated phosphopeptide. (C) MS/MS spectra of the fragmented phosphopeptide showing the unique $y5$ - and $y7$ -ions that identify S338 (highlighted in red) as the phosphorylated residue. Critical ions for identification of phosphosite are circled in red. (D) Extracted ion chromatogram of $y5$ $m/z = 646$ and $y7$ $m/z = 830$. Quantitatively, 29 spectra out of a total of 70 spectra were detected for the $y5$ -ion, and 64 spectra out of a total of 70 spectra were detected for the $y7$ -ion. **Figure 5.4** was kindly provided by Gerhard Saalbach, Proteomics Facility, John Innes Centre.

Table 5.3 Scaffold/Ascore results identifying the phosphorylated residues in the extracted ion chromatogram of $m/z = 921.0932$ of TPATASLPPSPAPSMAPAGASAPSYGGNR (amino acids 315 to 343). **Table 5.3** was kindly provided by Gerhard Saalbach, Proteomics Facility, John Innes Centre.

Localisation of phosphorylation on peptide (on protein)	Localisation probability	Ascore	Peptide Score	Scaffold: Peptide probability	Spectrum Name
S24 (S338)	81%	14.04	82.73	0.9933	229: Scan 2315 (rt=33.7359)
S24 (S338)	81%	14.04	54.70	0.9946	240: Scan 2336 (rt=33.9282)
S24 (S338)	76%	12.81	95.61	0.9945	231: Scan 2318 (rt=33.7625)
S24 (S338)	76%	12.81	36.03	0.9875	249: Scan 2353 (rt=34.0866)
S24 (S338)	68%	11.10	64.78	0.9913	211: Scan 2284 (rt=33.4582)
S24 (S338)	68%	11.10	42.82	0.9928	228: Scan 2313 (rt=33.7183)
S24 (S338)	68%	11.06	14.53	0.8636	219: Scan 2297 (rt=33.572)
S24 (S338)	59%	9.40	75.56	0.9892	234: Scan 2323 (rt=33.8063)
S24 (S338)	59%	9.40	70.02	0.9928	204: Scan 2272 (rt=33.3513)
S24 (S338)	53%	8.46	32.19	0.9945	254: Scan 2367 (rt=34.2406)
S24 (S338)	52%	8.22	53.53	0.9944	216: Scan 2292 (rt=33.528)
S24 (S338)	38%	8.18	50.65	0.9930	220: Scan 2299 (rt=33.5893)
S24 (S338)	49%	7.77	18.06	0.8915	213: Scan 2287 (rt=33.4849)
S24 (S338)	49%	7.71	57.39	0.9947	197: Scan 2260 (rt=33.2449)
S24 (S338)	47%	7.32	57.16	0.9831	238: Scan 2332 (rt=33.8939)
S24 (S338)	45%	7.09	41.39	0.9946	206: Scan 2275 (rt=33.3777)
S24 (S338)	39%	5.99	31.14	0.9831	222: Scan 2302 (rt=33.6146)
Y25 (Y339)	68%	11.1	49.42	0.9888	224: Scan 2305 (rt=33.6407)
Y25 (Y339)	51%	8.22	61.03	0.9947	218: Scan 2296 (rt=33.5632)
Y25 (Y339)	39%	5.99	57.23	0.9930	239: Scan 2334 (rt=33.9114)

The elution profile (XIC) of the second peptide (SMGGGPGQSGPSYGGQR, amino acids 344 to 360) derived from the original 7.2 kDa tryptic fragment showed two distinct peaks (**Figure 5.5B**), again demonstrating that two monophosphorylated peptide isoforms could be separated from each other on the HPLC column. With the help of the targeted LC-MS/MS analysis, the phosphosites on these two isoforms were identified as S344 and S355 (**Table 5.4**), with the S355 phosphopeptide being more abundant and eluting before the S344 phosphopeptide (**Table 5.4** and **Figure 5.5B**). To confirm those Mascot and ScaffoldPTM results, the occurrence of indicative fragments ions was analysed as described above. Phosphorylation of S355 was identified on the basis of the y5-, y8- and y9-ions, in particular with the assignment of the y8-ion, which excludes phosphorylation on Y356. The y8-ion was used to demonstrate co-elution with the major peptide peak (**Figure 5.5C**). In the case of phosphorylation of the N-terminal S344, all detected y-ions (up to y14) are unmodified, and the strong y-9 ion was used to demonstrate co-elution with the minor peptide peak (**Figure 5.5D**). No doubly phosphorylated species were detected.

No phosphorylation of the third tryptic peptide (QMSPAMTQPMAPVRPQGSPMGQAPSPMR, amino acids 361 to 388) derived from the 7.2 kDa peptide was detected (data not shown).

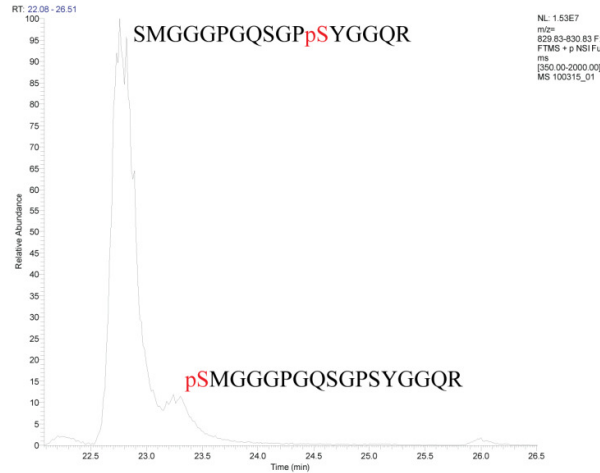
A

```

1  MPLTPEDVRN KQFTTVRLRE GYDEDEVDFAF LDEVEAELTR LLRENEDLRA
51  KLAATRAAA QNQNMKRPK EPPDQDQHQQ GPPQHQQGPP QGGGMPQQGM
101 RGPGAPVPAG ISGPPQQQMG GPMGGPQLP SGAPQLPAGP GGQGGPQGGP
151 PMGQGGPMPG QGPGPMQQGM GPGPMGGPMG GPQGGGGPGG FGMPPGQGGP
201 GDSAAARVLSL AQQTADQAI A EARSEANKIV GEARSRAEGL ERDARAKADA
251 LERDAQEKHR VAMGSLESAR ATLERKVEDL RGFEREYRTR LKSYLESQLR
301 QLETQADDL APPRTPATAS LPPSPAPSPA PAGASAPSYG GNRSMGGGPG
351 QSGPSYGGQR QMSPAMTQPM APVRPQGPSP MGQAPSPMRG FLIDEDDN
    
```

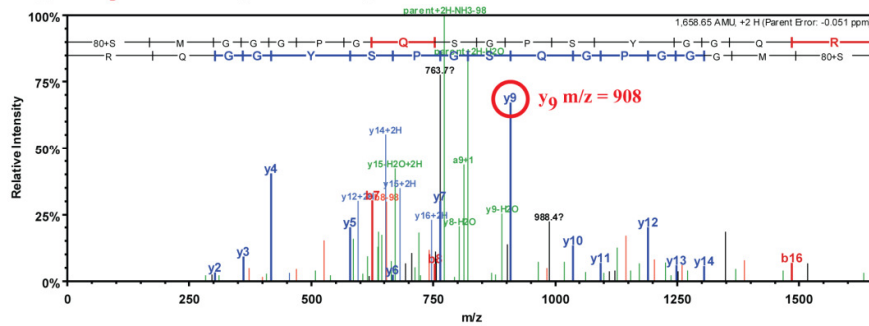
B

pSMGGGPGQSGPpSYGGQR (2+), m/z = 830.3327

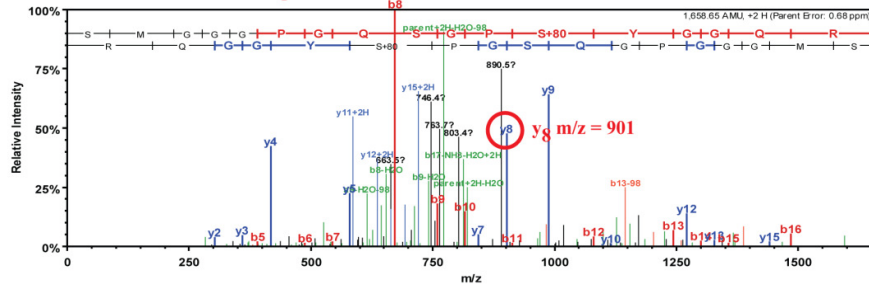


C

pSMGGGPGQSGPSYGGQR



SMGGGPGQSGPpSYGGQR



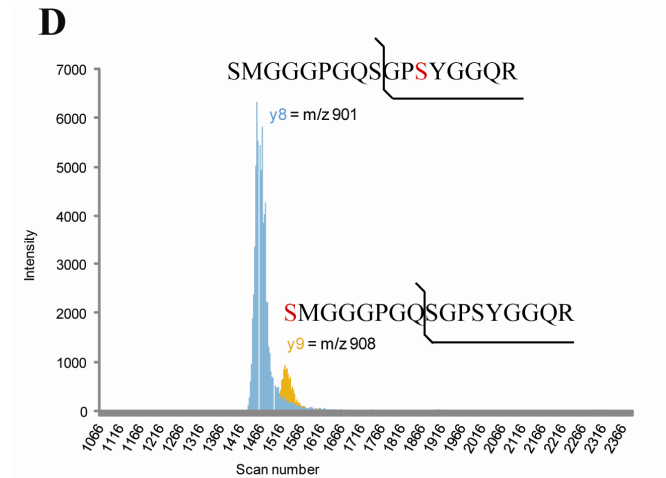


Figure 5.5 Identification of the phosphorylation sites on peptide SMGGGPGQSGPSYGGQR (amino acids 344 to 360).

(A) The peptide and the identified phosphorylated serines are highlighted on the primary amino acid sequence (peptide in blue, serines in red, tryptic cleavage sites in bold). (B) Extracted ion chromatogram of $m/z = 830.3327$. Quantitatively, 38 spectra were detected for the S344 phosphopeptide and 36 spectra were detected for the S355 phosphopeptide. (C) MS/MS spectra showing the y9-ion unique to the S344 phosphopeptide and the y8-ion unique to the S355 phosphopeptide (both highlighted in red). (D) Extracted ion chromatogram of y9-ion $m/z = 908$ unique to the S344 phosphopeptide and the y8-ion $m/z = 901$ unique to the S355 phosphopeptide, as determined by MS/MS.

Table 5.4 Scaffold/Ascore results identifying the phosphorylated residues in the extracted ion chromatogram of $m/z = 830.0932$ of SMGGPGQSGPSYGGQR (amino acids 344 to 360). **Table 5.4** was kindly provided by Gerhard Saalbach, Proteomics Facility, John Innes Centre.

Localisation of phosphorylation on peptide (on protein)	Localisation probability	Ascore	Peptide Score	Scaffold: Peptide probability	Spectrum Name
S12 (S355)	100%	30.46	107.43	0.9988	Scan 1468 (rt=22.8264)
S12 (S355)	100%	30.46	123.44	0.9992	Scan 1452 (rt=22.7081)
S12 (S355)	100%	30.46	101.96	0.9989	Scan 1448 (rt=22.6787)
S12 (S355)	100%	30.46	109.70	0.999	Scan 1506 (rt=23.1116)
S12 (S355)	100%	27.96	116.82	0.9993	Scan 1458 (rt=22.7524)
S12 (S355)	100%	27.96	103.01	0.9985	Scan 1498 (rt=23.0504)
S12 (S355)	100%	27.96	116.92	0.9992	Scan 1488 (rt=22.9753)
S12 (S355)	100%	27.07	81.08	0.9967	Scan 1638 (rt=24.1908)
S12 (S355)	100%	26.02	102.56	0.9990	Scan 1496 (rt=23.0353)
S12 (S355)	100%	26.02	84.03	0.9987	Scan 1456 (rt=22.7376)
S12 (S355)	100%	26.02	104.63	0.9983	Scan 1474 (rt=22.8708)
S12 (S355)	100%	26.02	104.45	0.9993	Scan 1502 (rt=23.081)
S12 (S355)	100%	26.02	85.01	0.9991	Scan 1470 (rt=22.8412)
S12 (S355)	100%	26.02	108.57	0.9993	Scan 1480 (rt=22.9155)
S12 (S355)	100%	26.02	107.02	0.9988	Scan 1438 (rt=22.6042)
S12 (S355)	100%	26.02	116.71	0.9991	Scan 1454 (rt=22.7228)
S12 (S355)	99%	24.44	115.91	0.9993	Scan 1460 (rt=22.7672)
S12 (S355)	99%	24.44	112.69	0.9992	Scan 1482 (rt=22.9304)
S12 (S355)	99%	24.44	91.65	0.9989	Scan 1490 (rt=22.9903)
S12 (S355)	99%	24.44	102.74	0.9991	Scan 1444 (rt=22.6491)
S12 (S355)	99%	24.44	112.59	0.9990	Scan 1464 (rt=22.7968)

Chapter 5 – Identification of the DivIVA phosphorylation sites

S12 (S355)	99%	24.44	120.92	0.9991	Scan 1472 (rt=22.856)
S12 (S355)	99%	24.44	117.61	0.9990	Scan 1442 (rt=22.6343)
S12 (S355)	99%	23.1	98.83	0.9986	Scan 1508 (rt=23.1272)
S12 (S355)	99%	23.1	100.53	0.9989	Scan 1440 (rt=22.6196)
S12 (S355)	99%	23.1	100.63	0.9987	Scan 1484 (rt=22.9454)
S12 (S355)	99%	21.94	125.29	0.9993	Scan 1476 (rt=22.8857)
S1 (S344)	100%	51.77	80.89	0.9993	Scan 1532 (rt=23.3123)
S1 (S344)	100%	49.25	91.45	0.9988	Scan 1540 (rt=23.3739)
S1 (S344)	100%	48.77	89.58	0.9992	Scan 1526 (rt=23.2662)
S1 (S344)	100%	40.28	62.74	0.9988	Scan 1534 (rt=23.3276)
S1 (S344)	100%	39.00	95.43	0.9993	Scan 1528 (rt=23.2815)
S1 (S344)	100%	36.31	82.50	0.9989	Scan 1538 (rt=23.3582)
S1 (S344)	100%	29.62	68.50	0.9965	Scan 1556 (rt=23.4993)
S1 (S344)	100%	29.52	91.74	0.9988	Scan 1548 (rt=23.4364)
S1 (S344)	100%	29.35	77.78	0.9984	Scan 1542 (rt=23.3893)
S1 (S344)	100%	28.36	72.70	0.9983	Scan 1544 (rt=23.405)
S1 (S344)	100%	26.56	75.58	0.9989	Scan 1522 (rt=23.2352)
S1 (S344)	100%	26.22	77.10	0.9989	Scan 1518 (rt=23.2042)
S1 (S344)	99%	25.75	83.82	0.9984	Scan 1554 (rt=23.4837)
S1 (S344)	99%	25.75	70.78	0.9989	Scan 1530 (rt=23.2968)
S1 (S344)	99%	24.87	76.47	0.9986	Scan 1536 (rt=23.3429)
S1 (S344)	99%	22.84	80.72	0.9991	Scan 1524 (rt=23.2508)

5.5 Discussion and Conclusion

Mass spectrometry is the technique of choice for direct identification of protein phosphorylation sites and phosphorylated peptides present in protein mixtures. However, the MS/MS sequencing of large peptides is often problematic and that was exactly our experience in this study. We were only able to map the DivIVA phosphorylation sites in the C-terminus of the protein by introducing two additional tryptic cleavage sites, allowing us to generate three tryptic peptides corresponding to the original 7.2 kDa fragment from the C-terminus of the protein.

The combination of nano-HPLC and MS/MS (nano-LC-MS/MS) is a standard technical approach in peptide analysis (see for example Winter *et al.*, 2009). In summary, our results demonstrate that DivIVA can be phosphorylated *in vivo* on five sites in the C-terminus of the protein (T304, S309, S338, S344 and S355, **Figure 5.6**). These sites are located on two tryptic peptides originating from the 7.2 kDa peptide and on a 1.5 kDa peptide that is immediately N-terminal to the 7.2 kDa peptide in the primary amino acid sequence of DivIVA. The C-terminus of DivIVA carries 16 potential phosphorylation sites (12 serines and 4 threonines), but the separation of the phosphopeptide isoforms by nano-LC and subsequent sequencing of the fragment ions by MS/MS allowed us to identify the phosphorylated residues with confidence. The quality of the data allowed us even to quantify the spectral information of the elution profiles of the MS/MS fragments.

The correct assignment of the phosphorylation sites is a critical aspect for phosphoproteomic analysis. This study proved to be a very useful test of the available software tools for identification of phosphorylation sites, especially Mascot and ScaffoldPTM (Ascore). In our experience, although these programmes provided clear support for some assignments, for other cases the time-consuming visual inspection of the various spectra was essential in order to confirm and validate the computational analysis and to assign the phosphorylation sites correctly.

The original MALDI analysis presented in **Figure 5.1** identified a low-abundance, triply phosphorylated 7.2 kDa species. Presumptively, based on our subsequent identification of the phosphosites, this species is likely to carry phosphate groups on S338, S344 and S355. Therefore, it is notable that, after the introduction of the additional tryptic cleavages sites, although single phosphorylations were detected on S344 and S355 in the SMGGGPGQSGPSYGGQR peptide (amino acids 344 to 360); no doubly phosphorylated species was detected. However, phosphorylation on S344 was much more abundant than on S355, as was phosphorylation on S309 compared to T304. Given the low abundance of the triply phosphorylated 7.2 kDa species in the original experiments, it is possible that the doubly phosphorylated SMGGGPGQSGPSYGGQR peptide species was not present in the later experiments (the extent of phosphorylation is somewhat variable from experiment to experiment), or that this species cannot be detected under the conditions used.

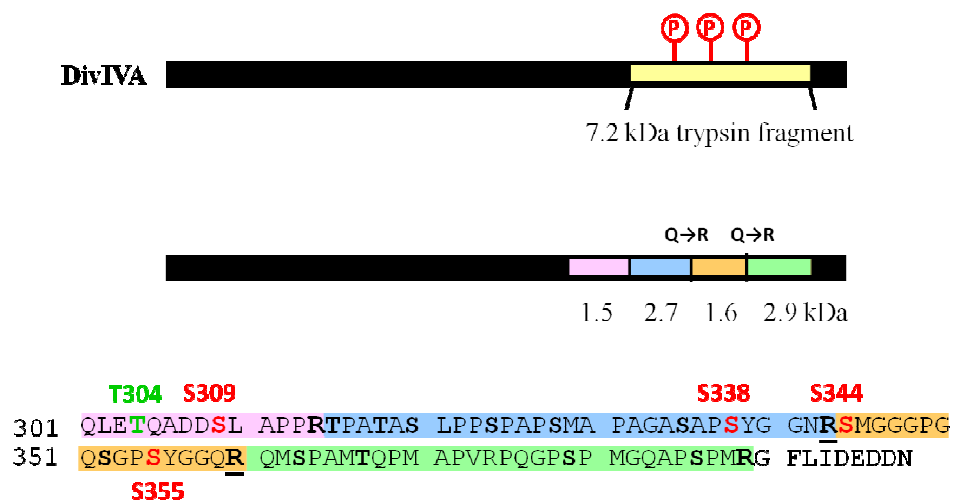


Figure 5.6 Overview schematic of the five identified phosphorylation sites in the tryptic peptides of the DivIVA C-terminus.

5.6 Summary Points

- The C-terminal region of DivIVA is multiply phosphorylated.
- Site-directed mutagenesis was used to introduce two additional tryptic cleavage sites to fragment the 7.2 kDa tryptic peptide further for better analysis.
- Nano-LC-MS/MS combined with major database search and peptide PTM assignment tools as well as detailed visual inspection of spectra identified five phosphorylation sites in the DivIVA C-terminus.
- Phosphopeptide isoforms differing only in the residue carrying the phosphate group can have very different HPLC elution profiles.

Chapter 6

Discussion

The ability to break symmetry and establish an axis of polarity is crucial for the function and development of almost all cell types. In bacteria, such symmetry-breaking is often mediated by cytoskeletal elements inside the cell that direct new cell wall synthesis. Many rod-shaped bacteria (including *E. coli* and *B. subtilis*) grow solely through the isotropic insertion of new cell wall material throughout the length of the lateral walls (de Pedro *et al.*, 1997; Daniel & Errington, 2003). In these rod-shaped bacteria, polarity systems are required to identify and differentiate cell poles that remain inert during cell elongation. However, many other organisms, including filamentous bacteria, enlarge by polar growth, a strategy that has proven successful for the exploitation of soil and other environments.

Streptomycetes, like other bacteria, lack the motor proteins, vesicle transport systems and polarisome components that are fundamental in eukaryotic cell biology. Thus, tip extension in *Streptomyces* is likely to be simpler than in, for example, filamentous fungi. Given that a complex of polarity proteins (including DivIVA) must presumably first gather at future branch sites, understanding branch-site selection in filamentous bacteria involves understanding where, when and how these proteins cluster together in sufficiently large groups. One surprising feature of *Streptomyces* is that this clustering of polarity proteins is not a random, spontaneous process.

Rather, in **Chapter 3** of this thesis I showed that branch sites in *Streptomyces* are selected by a novel polarisome splitting mechanism, in which this apical protein assembly at the existing hyphal tip, visualised as a focus of DivIVA-EGFP, splits to deposit a small daughter polarisome, which is left behind on the lateral

membrane as the tip grows away. Each daughter polarisome acts as a polarity mark, growing in size and ultimately initiating the outgrowth of a new hyphal tip.

This study focused on the control of branch development during vegetative growth. However, there is a parallel question about how the first germ tube emerges from a spore. By imaging germinating spores expressing functional *divIVA-EGFP*, it has been shown that, exactly as in vegetative growth, a focus of DivIVA is first observed on the spore envelope, which then grows in size before initiating the first germ tube (Flärdh, 2003a). To date, it is not understood how this first focus is formed, but it is clear that the polarisome splitting mechanism cannot be responsible since there are initially no previous DivIVA foci in a germinating spore. This raises the possibility that the spontaneous nucleation mechanism which plays a role when DivIVA is heavily overexpressed, is also responsible for the first DivIVA focus in a spore. If this is the case, then the DivIVA concentration within a spore would have to be elevated to a level that overcomes the nucleation barrier. Preliminary experiments, however, indicate that the DivIVA concentration within a spore is not raised preceding DivIVA focus formation (as determined by measuring the fluorescence intensity of DivIVA-EGFP signals in germinating spores; data not shown), indicating that spontaneous nucleation might not exclusively be involved. Alternatively, other proteins may aid DivIVA focus formation during spore germination. One candidate is SsgA, a small acidic protein, proposed to act as a chaperonin-like protein that affects cell division or specific stages of spore development (Traag & van Wezel, 2008; Willemsse *et al.*, 2011). A study by Noens *et al.* (2007) described that SsgA forms distinct foci in developing spores during sporulation septation and at the base of growing germ tubes in germinating spores. They proposed that SsgA marks the cell envelope and thereby determines the future sites of germ tube outgrowth. Future experiments are necessary to test this hypothesis.

In contrast to vegetative growth, the growth of aerial hyphae has previously been largely overlooked. Initially, aerial hyphae grow straight and relatively unbranched into the air with a polarisome cluster containing DivIVA at the hyphal tip. Upon an unknown trigger, this polarisome disappears, tip extension ceases and sporulation septation initiates (Flärdh & Buttner, 2009). It remains to be

investigated in the future whether the components of these polarisomes in aerial hyphae are the same as in vegetative hyphae and how aerial hyphal growth is regulated at the molecular level.

In fungi, branching also occurs at the cellular level and involves establishment of new cell poles at which apical growth will occur (Harris, 2008). An apical cluster of vesicles and cytoskeletal elements named the Spitzenkörper has a prominent role in fungal tip extension. During branching, a new Spitzenkörper structure is established at the nascent branch tip, aided by proteins that direct cell polarity, cytoskeletal reorganisation, vesicle transport, and exo- and endocytosis (for reviews, see *e.g.* Steinberg, 2007; Harris, 2008; Fischer *et al.*, 2008; Riquelme *et al.*, 2011). One of the components that appears to be involved in branch site selection prior to assembly of the Spitzenkörper structure is the protein complex termed the polarisome. Intriguingly, a recent study showed that the polarisome scaffold protein SPA-2 in *Neurospora crassa* also exhibits tip-focus splitting behavior. Homologues of the budding yeast polarisome component Spa2p have been detected at hyphal tips in several fungi, and, in *N. crassa*, small foci of SPA-2-GFP were observed to detach from the major SPA-2 assemblies at elongating hyphal tips, remain on the lateral wall and subsequently give rise to new lateral branches (Araujo-Palomares *et al.*, 2009). This observation strongly suggests that, in addition to streptomycetes, polarisome splitting mechanisms are also involved in the establishment of new hyphal branches in filamentous fungi. In fact, polarisome splitting could turn out to be widely applicable as a general mechanism in situations where discrete polar protein assemblies must be generated in a growing organism.

Chapters 4 and 5 extend our knowledge of how the key determinant of polarised growth, DivIVA, itself is regulated in *Streptomyces*, showing that a Ser/Thr protein kinase, AfsK, is part of the apparatus that controls polar growth and that it directly phosphorylates DivIVA. Dual roles have been shown for AfsK; it modulates the control of hyphal branching and the development of daughter polarisomes during normal growth, but it also causes profound reconfiguration of DivIVA localisation, apical growth, and hyphal branching when cell wall synthesis is arrested. We suggest that this stress response provides *Streptomyces*

with a mechanism to dismantle the apical growth apparatus at hyphal tips that encounter problems with cell wall synthesis, for example through exposure to an antibiotic or by hitting a physical obstacle in the soil, and instead direct emergence of new branches elsewhere. Such conditions would strongly activate AfsK, leading to disassembly of the apical DivIVA complex and liberation of DivIVA molecules that can then direct emergence of new branches elsewhere, leading, for example, to growth around an obstacle. In the simplest scenario, DivIVA molecules that are liberated from the original tip could join small daughter foci that have been deposited along the lateral wall, accelerating their maturation into polarisomes competent to trigger branch outgrowth. Alternatively, the release of large quantities of soluble DivIVA into the cytoplasm from the disassembly of apical foci could trigger the spontaneous nucleation of new DivIVA foci.

The phosphorylation of DivIVA by AfsK represents an intriguing prokaryotic parallel to the broadly conserved roles of Ser/Thr protein kinases in controlling cell polarity in eukaryotes (Nelson, 2003; McCaffrey & Macara, 2009) and particularly to the control of polar growth by kinases targeting polarisome components in fungi (see references in Moseley & Goode, 2006). Further, these findings show that communication between the polarity determinant DivIVA and the cell wall biosynthetic machinery is bidirectional, with DivIVA directing cell wall synthesis (Hempel *et al.*, 2008), and the biosynthetic machinery communicating back to DivIVA via AfsK-mediated phosphorylation of DivIVA.

The AfsK-mediated phosphorylation of *S. coelicolor* DivIVA differs in several important ways from the previously observed phosphorylation of the mycobacterial DivIVA orthologue, Wag31 (Kang *et al.*, 2005). First, the phosphorylation of mycobacterial Wag31 is poorly understood, but seems to promote its localisation to cell poles and stimulate polar growth and cell wall synthesis (Kang *et al.*, 2008; Jani *et al.*, 2010). In contrast, the activation of the DivIVA kinase in *S. coelicolor* has the opposite effect, promoting the disassembly of DivIVA foci and the inhibition of growth at existing hyphal tips. Second, different kinases are involved, which are likely to be activated by different stimuli. The essential PASTA-domain kinases PknA and PknB act on Wag31 in

mycobacteria and the reports so far only describe activity during undisturbed growth (Kang *et al.*, 2005; Kang *et al.*, 2008). In contrast, AfsK, the DivIVA kinase in *S. coelicolor*, is weakly active during vegetative growth and strongly activated in response to the arrest of cell wall synthesis as indicated by the levels of DivIVA phosphorylation. Third, the site of phosphorylation is different, with a single threonine close to the first coiled-coil domain being targeted in *M. tuberculosis*, while it is the C-terminal domain of *S. coelicolor* DivIVA that is phosphorylated on five residues.

What are the signals that lead to the activation of AfsK? AfsK has an N-terminal Ser/Thr protein kinase domain and a C-terminal putative sensory portion carrying PQQ domain repeats. These PQQ domain repeats are predicted to form a β -propeller structure similar to WD40 domains and may interact with a ligand, although the general function of PQQ domains is not known (Petrickova & Petricek, 2003). Further, AfsK does not have a predicted transmembrane segment, and is reported to be cytoplasmic but loosely associated with the membrane (Matsumoto *et al.*, 1994). AfsK activity (at least as reflected in the level of DivIVA phosphorylation) is strongly stimulated by antibiotics like bacitracin and vancomycin, which block the lipid II cycle of peptidoglycan biosynthesis, raising the possibility that AfsK can sense the accumulation of intermediates in peptidoglycan biosynthesis. This would provide a mechanism to sense the capacity of the hyphal tip to sustain extension during normal growth and during stress conditions, and, via AfsK-mediated phosphorylation, transduce this information to the polarisome that directs apical growth and branching. This function of AfsK may be reminiscent of the regulatory circuits controlling polarity proteins and polarisome components by Ser/Thr protein kinases in eukaryotes. A phosphatase regulating the balance between phosphorylated and unphosphorylated forms of DivIVA has been identified and is currently under investigation (Klas Flårdh, personal information).

References

- Amos, L. A., F. van den Ent & J. Löwe, (2004) Structural/ functional homology between the bacterial and eukaryotic cytoskeletons. *Curr Opin Cell Biol* **16**: 24-31.
- Araujo-Palomares, C. L., M. Riquelme & E. Castro-Longoria, (2009) The polarisome component SPA-2 localises at the apex of *Neurospora crassa* and partially colocalises with the Spitzenkörper. *Fungal Genet Biol* **46**: 551-563.
- Arthur, M., C. Molinas & P. Courvalin, (1992) Sequence of the *vanY* gene required for production of a vancomycin-inducible D,D-carboxypeptidase in *Enterococcus faecium* BM4147. *Gene* **120**: 111-114.
- Bagchi, S., H. Tomenius, L. M. Belova & N. Ausmees, (2008) Intermediate filament-like proteins in bacteria and a cytoskeletal function in *Streptomyces*. *Mol Microbiol* **70**: 1037-1050.
- Barreteau, H., A. Kovac, A. Boniface, M. Sova, S. Gobec & D. Blanot, (2008) Cytoplasmic steps of peptidoglycan biosynthesis. *FEMS Microbiol Rev* **32**: 168-207.
- Beilharz, K., L. Novakova, D. Fadda, P. Branny, O. Massidda & J. W. Veening, (2012) Control of cell division in *Streptococcus pneumoniae* by the conserved Ser/Thr protein kinase StkP. *Proc Natl Acad Sci USA* **109**: E905-913.
- Bentley, S. D., K. F. Chater, A. M. Cerdeno-Tarraga, G. L. Challis, N. R. Thomson, K. D. James, D. E. Harris, M. A. Quail, H. Kieser, D. Harper, A. Bateman, S. Brown, G. Chandra, C. W. Chen, M. Collins, A. Cronin, A. Fraser, A. Goble, J. Hidalgo, T. Hornsby, S. Howarth, C. H. Huang, T.

- Kieser, L. Larke, L. Murphy, K. Oliver, S. O'Neil, E. Rabinowitsch, M. A. Rajandream, K. Rutherford, S. Rutter, K. Seeger, D. Saunders, S. Sharp, R. Squares, S. Squares, K. Taylor, T. Warren, A. Wietzorrek, J. Woodward, B. G. Barrell, J. Parkhill & D. A. Hopwood, (2002) Complete genome sequence of the model *actinomycete* *Streptomyces coelicolor* A3(2). *Nature* **417**: 141-147.
- Bierman, M., R. Logan, K. O'Brien, E. T. Seno, R. N. Rao, & B. E. Schoner, (1992) Plasmid cloning vectors for the conjugal transfer of DNA from *Escherichia coli* to *Streptomyces* spp. *Gene* **116**: 43-49.
- Bouhss, A., A. E. Trunkfield, T. D. Bugg & D. Mengin-Lecreulx, (2008) The biosynthesis of peptidoglycan lipid-linked intermediates. *FEMS Microbiol Rev* **32**: 208-233.
- Bramkamp, M., R. Emmins, L. Weston, C. Donovan, R. A. Daniel & J. Errington, (2008) A novel component of the division-site selection system of *Bacillus subtilis* and a new mode of action for the division inhibitor MinCD. *Mol Microbiol* **70**: 1556-1569.
- Brown, P. J., D. T. Kysela & Y. V. Brun, (2011) Polarity and the diversity of growth mechanisms in bacteria. *Semin Cell Dev Biol* **22**: 790-798.
- Brown, P. J., M. A. de Pedro, D. T. Kysela, C. van der Henst, J. Kim, X. de Bolle, C. Fuqua & Y. V. Brun, (2012) Polar growth in the Alphaproteobacterial order Rhizobiales. *Proc Natl Acad Sci U S A* **109**:1697-1701.
- Bugg, T. D. & C. T. Walsh, (1992) Intracellular steps of bacterial cell wall peptidoglycan biosynthesis: enzymology, antibiotics, and antibiotic resistance. *Nat Prod Rep* **9**: 199-215.
- Cabeen, M. T. & C. Jacobs-Wagner, (2005) Bacterial cell shape. *Nat Rev Microbiol* **3**: 601-610.
- Carballido-Lopez, R. & J. Errington, (2003) A dynamic bacterial cytoskeleton. *Trends Cell Biol* **13**: 577-583.

- Carballido-Lopez, R., A. Formstone, Y. Li, S. D. Ehrlich, P. Noirot & J. Errington, (2006) Actin homolog MreBH governs cell morphogenesis by localisation of the cell wall hydrolase LytE. *Dev Cell* **11**: 399-409.
- Carballido-Lopez, R., (2006) The bacterial actin-like cytoskeleton. *Microbiol Mol Biol Rev* **70**: 888-909.
- Chater, K. F., (1998) Taking a genetic scalpel to the *Streptomyces* colony. *Microbiology* **144**: 1465-1478.
- Chater, K.F. (2000) Developmental decisions during sporulation in the aerial mycelium in *Streptomyces*. In *Prokaryotic Development*. Brun, Y.V., and Shimkets, L.J. (editors). Washington DC, USA: American Society for Microbiology Press.
- Chater, K. F., (2001) Regulation of sporulation in *Streptomyces coelicolor* A3(2): a checkpoint multiplex? *Curr Opin Microbiol* **4**: 667-673.
- Chauhan, A., H. Lofton, E. Maloney, J. Moore, M. Fol, M. V. Madiraju & M. Rajagopalan, (2006) Interference of *Mycobacterium tuberculosis* cell division by Rv2719c, a cell wall hydrolase. *Mol Microbiol* **62**: 132-147.
- Daniel, R. A. & J. Errington, (2003) Control of cell morphogenesis in bacteria: two distinct ways to make a rod-shaped cell. *Cell* **113**: 767-776.
- de Jong, W., H. A. Wosten, L. Dijkhuizen & D. Claessen, (2009) Attachment of *Streptomyces coelicolor* is mediated by amyloid fimbriae that are anchored to the cell surface via cellulose. *Mol Microbiol* **73**: 1128-1140.
- de Pedro, M. A., J. C. Quintela, J. V. Höltje & H. Schwarz, (1997) Murein segregation in *Escherichia coli*. *J Bacteriol* **179**: 2823-2834.
- Dominguez-Cuevas, P., R. Mercier, M. Leaver, Y. Kawai & J. Errington, (2012) The rod to L-form transition of *Bacillus subtilis* is limited by a requirement for the protoplast to escape from the cell wall sacculus. *Mol Microbiol* **83**: 52-66

- Dominguez-Escobar, J., A. Chastanet, A. H. Crevenna, V. Fromion, R. Wedlich-Soldner & R. Carballido-Lopez, (2011) Processive movement of MreB-associated cell wall biosynthetic complexes in bacteria. *Science* **333**: 225-228.
- Dworkin, J. & I. M. Shah, (2010) Exit from dormancy in microbial organisms. *Nat Rev Microbiol* **8**: 890-896.
- Edwards, D. H. & J. Errington, (1997) The *Bacillus subtilis* DivIVA protein targets to the division septum and controls the site specificity of cell division. *Mol Microbiol* **24**: 905-915.
- Edwards, D. H., H. B. Thomaides & J. Errington, (2000) Promiscuous targeting of *Bacillus subtilis* cell division protein DivIVA to division sites in *Escherichia coli* and fission yeast. *Embo J* **19**: 2719-2727.
- Errington, J., (2001) Septation and chromosome segregation during sporulation in *Bacillus subtilis*. *Curr Opin Microbiol* **4**: 660-666.
- Eswaramoorthy, P., M. L. Erb, J. A. Gregory, J. Silverman, K. Pogliano, J. Pogliano & K. S. Ramamurthi, (2011) Cellular architecture mediates DivIVA ultrastructure and regulates min activity in *Bacillus subtilis*. *MBio* **2**: e00257-00211.
- Fischer, R., N. Zekert & N. Takeshita, (2008) Polarised growth in fungi-interplay between the cytoskeleton, positional markers and membrane domains. *Mol Microbiol* **68**: 813-826.
- Fiuza, M., M. J. Canova, D. Patin, M. Letek, I. Zanella-Cleon, M. Becchi, L. M. Mateos, D. Mengin-Lecreulx, V. Molle & J. A. Gil, (2008) The MurC ligase essential for peptidoglycan biosynthesis is regulated by the serine/threonine protein kinase PknA in *Corynebacterium glutamicum*. *J Biol Chem* **283**: 36553-36563.
- Fiuza, M., M. Letek, J. Leiba, A. F. Villadangos, J. Vaquera, I. Zanella-Cleon, L. M. Mateos, V. Molle & J. A. Gil, (2010) Phosphorylation of a novel

cytoskeletal protein (RsmP) regulates rod-shaped morphology in *Corynebacterium glutamicum*. *J Biol Chem* **285**: 29387-29397.

Flårdh, K., (2003a) Essential role of DivIVA in polar growth and morphogenesis in *Streptomyces coelicolor* A3(2). *Mol Microbiol* **49**: 1523-1536.

Flårdh, K., (2003b) Growth polarity and cell division in *Streptomyces*. *Curr Opin Microbiol* **6**: 564-571.

Flårdh, K. & M. J. Buttner, (2009) *Streptomyces* morphogenetics: dissecting differentiation in a filamentous bacterium. *Nat Rev Microbiol* **7**: 36-49.

Flårdh, K., (2010) Cell polarity and the control of apical growth in *Streptomyces*. *Curr Opin Microbiol* **13**: 758-765.

Flett, F., V. Mersinias & C. P. Smith, (1997) High efficiency intergeneric conjugal transfer of plasmid DNA from *Escherichia coli* to methyl DNA-restricting Streptomycetes. *FEMS Microbiol Lett* **155**: 223-229.

Fleurie, A., C. Cluzel, S. Guiral, C. Freton, F. Galisson, I. Zanella-Cleon, A. M. Di Guilmi & C. Grangeasse, (2012) Mutational dissection of the S/T-kinase StkP reveals crucial roles in cell division of *Streptococcus pneumoniae*. *Mol Microbiol* **83**: 746-758.

Floriano, B. & M. Bibb, (1996) *afsR* is a pleiotropic but conditionally required regulatory gene for antibiotic production in *Streptomyces coelicolor* A3(2). *Mol Microbiol* **21**: 385-396

Galperin, M. Y., R. Higdon & E. Kolker, (2010) Interplay of heritage and habitat in the distribution of bacterial signal transduction systems. *Mol Biosyst* **6**: 721-728.

Garnak, M. & H. C. Reeves, (1979) Phosphorylation of Isocitrate dehydrogenase of *Escherichia coli*. *Science* **203**: 1111-1112.

- Garner, E. C., R. Bernard, W. Wang, X. Zhuang, D. Z. Rudner & T. Mitchison, (2011) Coupled, circumferential motions of the cell wall synthesis machinery and MreB filaments in *B. subtilis*. *Science* **333**: 222-225.
- Graumann, P. L., (2007) Cytoskeletal elements in bacteria. *Annu Rev Microbiol* **61**: 589-618.
- Gregory, M. A., R. Till & M. C. Smith, (2003) Integration site for *Streptomyces* phage phiBT1 and development of site-specific integrating vectors. *J Bacteriol* **185**: 5320-5323.
- Gust, B., G. L. Challis, K. Fowler, T. Kieser & K. F. Chater, (2003) PCR-targeted *Streptomyces* gene replacement identifies a protein domain needed for biosynthesis of the sesquiterpene soil odor geosmin. *Proc Natl Acad Sci USA* **100**: 1541-1546.
- Haiser, H. J., M. R. Yousef & M. A. Elliot, (2009) Cell wall hydrolases affect germination, vegetative growth, and sporulation in *Streptomyces coelicolor*. *J Bacteriol* **191**: 6501-6512.
- Hamasha, K., M. B. Sahana, C. Jani, S. Nyayapathy, C. M. Kang & S. J. Rehse, (2010) The effect of Wag31 phosphorylation on the cells and the cell envelope fraction of wild-type and conditional mutants of *Mycobacterium smegmatis* studied by visible-wavelength Raman spectroscopy. *Biochem Biophys Res Commun* **391**: 664-668.
- Hanahan, D., (1983) Studies on transformation of *Escherichia coli* with plasmids. *J Mol Biol* **166**: 557-580.
- Hanks, S. K. & T. Hunter, (1995) Protein kinases 6. The eukaryotic protein kinase superfamily: kinase (catalytic) domain structure and classification. *FASEB J* **9**: 576-596.
- Harris, S. D., (2008) Branching of fungal hyphae: regulation, mechanisms and comparison with other branching systems. *Mycologia* **100**: 823-832.

- Hempel, A. M., S. B. Wang, M. Letek, J. A. Gil & K. Flårdh, (2008) Assemblies of DivIVA mark sites for hyphal branching and can establish new zones of cell wall growth in *Streptomyces coelicolor*. *J Bacteriol* **190**: 7579-7583.
- Hempel, A. M., S. Cantlay, V. Molle, S. Wang, M. J. Naldrett, J. L. Parker, D. M. Richards, Y. G. Jung, M. J. Buttner, and K. Flårdh (2012). A Ser/Thr protein kinase regulates polar growth and hyphal branching in the filamentous bacteria *Streptomyces*. *Proc Natl Acad Sci USA* **109**: e2371-2379.
- Hong, H. J., M. S. Paget & M. J. Buttner, (2002) A signal transduction system in *Streptomyces coelicolor* that activates the expression of a putative cell wall glycan operon in response to vancomycin and other cell wall-specific antibiotics. *Mol Microbiol* **44**: 1199-1211.
- Hopwood, D. A., (1999) Forty years of genetics with *Streptomyces*: from *in vivo* through *in vitro* to *in silico*. *Microbiology* **145 (Pt 9)**: 2183-2202.
- Hopwood, D. A., (2006) Soil to genomics: the *Streptomyces* chromosome. *Annu Rev Genet* **40**: 1-23.
- Hopwood, D. A., (2007) *Streptomyces in Nature and Medicine: The Antibiotic Makers*. Oxford University Press, USA.
- Huang, J., J. Shi, V. Molle, B. Sohlberg, D. Weaver, M. J. Bibb, N. Karoonuthaisiri, C. J. Lih, C. M. Kao, M. J. Buttner & S. N. Cohen, (2005) Cross-regulation among disparate antibiotic biosynthetic pathways of *Streptomyces coelicolor*. *Mol. Microbiol.* **58**: 1276-1287.
- Hutchings, M. I., H. J. Hong, E. Leibovitz, I. C. Sutcliffe & M. J. Buttner, (2006) The sigma(E) cell envelope stress response of *Streptomyces coelicolor* is influenced by a novel lipoprotein, CseA. *J Bacteriol* **188**: 7222-7229.
- Jani, C., H. Eoh, J. J. Lee, K. Hamasha, M. B. Sahana, J. S. Han, S. Nyayapathy, J. Y. Lee, J. W. Suh, S. H. Lee, S. J. Rehse, D. C. Crick & C. M. Kang, (2010) Regulation of polar peptidoglycan biosynthesis by Wag31 phosphorylation in mycobacteria. *BMC Microbiol* **10**: 327.

- Jones, G. & P. Dyson, (2006) Evolution of transmembrane protein kinases implicated in coordinating remodeling of gram-positive peptidoglycan: inside versus outside. *J Bacteriol* **188**: 7470-7476.
- Jones, L. J., R. Carballido-Lopez & J. Errington, (2001) Control of cell shape in bacteria: helical, actin-like filaments in *Bacillus subtilis*. *Cell* **104**: 913-922.
- Jordan, S., M. I. Hutchings & T. Mascher, (2008) Cell envelope stress response in Gram-positive bacteria. *FEMS Microbiol Rev* **32**: 107-146.
- Jung, Y. G., (2007) *Resistance to daptomycin and study of cell wall-related proteins in Streptomyces coelicolor*. PhD Thesis, John Innes Centre, UK.
- Kang, C. M., D. W. Abbott, S. T. Park, C. C. Dascher, L. C. Cantley & R. N. Husson, (2005) The *Mycobacterium tuberculosis* serine/threonine kinases PknA and PknB: substrate identification and regulation of cell shape. *Genes Dev* **19**: 1692-1704.
- Kang, C. M., S. Nyayapathy, J. Y. Lee, J. W. Suh & R. N. Husson, (2008) Wag31, a homologue of the cell division protein DivIVA, regulates growth, morphology and polar cell wall synthesis in mycobacteria. *Microbiology* **154**: 725-735.
- Kieser, T., M. J. Bibb, M. J. Buttner, K. F. Chater & D. A. Hopwood, (2000) *Practical Streptomyces Genetics*. The John Innes Foundation, UK.
- Kruse, T., J. Bork-Jensen & K. Gerdes, (2005) The morphogenetic MreBCD proteins of *Escherichia coli* form an essential membrane-bound complex. *Mol Microbiol* **55**: 78-89.
- Leaver, M., P. Dominguez-Cuevas, J. M. Coxhead, R. A. Daniel & J. Errington, (2009) Life without a wall or division machine in *Bacillus subtilis*. *Nature* **457**: 849-853.
- Lee, P. C., T. Umeyama & S. Horinouchi, (2002) *afsS* is a target of AfsR, a transcriptional factor with ATPase activity that globally controls

- secondary metabolism in *Streptomyces coelicolor* A3(2). *Mol Microbiol* **43**: 1413-1430.
- Le Gouill, C., J.-L. Parent, M. Rola-Pleszcynski & J. Stankova, (1994) Analysis of recombinant plasmids by a modified alkaline lysis method. *Analytical Biochemistry* **164**: 164.
- Lenarcic, R., S. Halbedel, L. Visser, M. Shaw, L. J. Wu, J. Errington, D. Marenduzzo & L. W. Hamoen, (2009) Localisation of DivIVA by targeting to negatively curved membranes. *Embo J* **28**: 2272-2282.
- Letek, M., M. Fiuza, E. Ordonez, A. F. Villadangos, K. Flärdh, L. M. Mateos & J. A. Gil, (2009) DivIVA uses an N-terminal conserved region and two coiled-coil domains to localise and sustain the polar growth in *Corynebacterium glutamicum*. *FEMS Microbiol Lett* **297**: 110-116.
- Letek, M., E. Ordonez, J. Vaquera, W. Margolin, K. Flärdh, L. M. Mateos & J. A. Gil, (2008) DivIVA is required for polar growth in the MreB-lacking rod-shaped Actinomycete *Corynebacterium glutamicum*. *J Bacteriol* **190**: 3283-3292.
- Löwe, J. & L. A. Amos, (1998) Crystal structure of the bacterial cell-division protein FtsZ. *Nature* **391**: 203-206.
- Löwe, J., F. van den Ent & L. A. Amos, (2004) Molecules of the bacterial cytoskeleton. *Annu Rev Biophys Biomol Struct* **33**: 177-198.
- Lu, C., J. Stricker & H. P. Erickson, (1998) FtsZ from *Escherichia coli*, *Azotobacter vinelandii*, and *Thermotoga maritima* – quantitation, GTP hydrolysis, and assembly. *Cell Motil Cytoskeleton* **40**: 71-86.
- Maestro, B., L. Novakova, D. Heseck, M. Lee, E. Leyva, S. Mobashery, J. M. Sanz & P. Branny, (2011) Recognition of peptidoglycan and beta-lactam antibiotics by the extracellular domain of the Ser/Thr protein kinase StkP from *Streptococcus pneumoniae*. *FEBS Lett* **585**: 357-363.

- Margolin, W., (2005) FtsZ and the division of prokaryotic cells and organelles. *Nat Rev Mol Cell Biol* **6**: 862-871.
- Matsumoto, A., S. K. Hong, H. Ishizuka, S. Horinouchi & T. Beppu, (1994) Phosphorylation of the AfsR protein involved in secondary metabolism in *Streptomyces* species by a eukaryotic-type protein kinase. *Gene* **146**: 47-56.
- Mazza, P., E. E. Noens, K. Schirmer, N. Grantcharova, A. M. Mommaas, H. K. Koerten, G. Muth, K. Flårdh, G. P. van Wezel & W. Wohlleben, (2006) MreB of *Streptomyces coelicolor* is not essential for vegetative growth but is required for the integrity of aerial hyphae and spores. *Mol Microbiol* **60**: 838-852.
- McCaffrey, L. M. & I. G. Macara, (2009) Widely conserved signalling pathways in the establishment of cell polarity. *Cold Spring Harb Perspect Biol* **1**:a001370.
- McCormick, J. R., E. P. Su, A. Driks & R. Losick, (1994) Growth and viability of *Streptomyces coelicolor* mutant for the cell division gene *ftsZ*. *Mol Microbiol* **14**: 243-254.
- McCormick, J. R., (2009) Cell division is dispensable but not irrelevant in *Streptomyces*. *Curr Opin Microbiol* **12**: 689-698.
- McCormick, J. R. & K. Flårdh, (2012) Signals and regulators that govern *Streptomyces* development. *FEMS Microbiol. Rev.* **36**: 206-231.
- Mohammadi, T., V. van Dam, R. Sijbrandi, T. Vernet, A. Zapun, A. Bouhss, M. Diepeveen-de Bruin, M. Nguyen-Disteche, B. de Kruijff & E. Breukink, (2011) Identification of FtsW as a transporter of lipid-linked cell wall precursors across the membrane. *Embo J* **30**: 1425-1432.
- Molle, V. & L. Kremer, (2010) Division and cell envelope regulation by Ser/Thr phosphorylation: *Mycobacterium* shows the way. *Mol Microbiol* **75**: 1064-1077.

-
- Moseley, J. B. & B. L. Goode, (2006) The yeast actin cytoskeleton: from cellular function to biochemical mechanism. *Microbiol Mol Biol Rev* **70**: 605-645.
- Muchova, K., E. Kutejova, L. Pribisova, A. J. Wilkinson & I. Barak, (2002a) *Bacillus subtilis* division protein DivIVA – screen for stable oligomer state conditions. *Acta Crystallogr D Biol Crystallogr* **58**: 1542-1543.
- Muchova, K., E. Kutejova, D. J. Scott, J. A. Brannigan, R. J. Lewis, A. J. Wilkinson & I. Barak, (2002b) Oligomerisation of the *Bacillus subtilis* division protein DivIVA. *Microbiology* **148**: 807-813.
- Mukherjee, P., K. Sureka, P. Datta, T. Hossain, S. Barik, K. P. Das, M. Kundu & J. Basu, (2009) Novel role of Wag31 in protection of mycobacteria under oxidative stress. *Mol Microbiol* **73**: 103-119.
- Munoz-Dorado, J., S. Inouye & M. Inouye, (1991) A gene encoding a protein serine/threonine kinase is required for normal development of *M. xanthus*, a gram-negative bacterium. *Cell* **67**: 995-1006.
- Nelson, W. J., (2003) Adaptation of core mechanisms to generate cell polarity. *Nature* **422**: 766-774.
- Nguyen, L., N. Scherr, J. Gatfield, A. Walburger, J. Pieters & C. J. Thompson, (2007) Antigen 84, an effector of pleiomorphism in *Mycobacterium smegmatis*. *J Bacteriol* **189**: 7896-7910.
- Noens, E. E., V. Mersinias, J. Willemsse, B. A. Traag, E. Laing, K. F. Chater, C. P. Smith, H. K. Koerten & G. P. van Wezel, (2007) Loss of the controlled localisation of growth stage-specific cell-wall synthesis pleiotropically affects developmental gene expression in an *ssgA* mutant of *Streptomyces coelicolor*. *Mol Microbiol* **64**: 1244-1259.
- Nolen, B., S. Taylor & G. Ghosh, (2004) Regulation of protein kinases; controlling activity through activation segment conformation. *Mol Cell* **15**: 661-675.

-
- Oliva, M. A., S. Halbedel, S. M. Freund, P. Dutow, T. A. Leonard, D. B. Veprintsev, L. W. Hamoen & J. Löwe, (2010) Features critical for membrane binding revealed by DivIVA crystal structure. *EMBO J* **29**: 1988-2001.
- Ortiz-Lombardia, M., F. Pompeo, B. Boitel & P. M. Alzari, (2003) Crystal structure of the catalytic domain of the PknB serine/threonine kinase from *Mycobacterium tuberculosis*. *J Biol Chem* **278**: 13094-13100.
- Paget, M. S., L. Chamberlin, A. Atrih, S. J. Foster & M. J. Buttner, (1999a) Evidence that the extracytoplasmic function sigma factor sigmaE is required for normal cell wall structure in *Streptomyces coelicolor* A3(2). *J Bacteriol* **181**: 204-211.
- Paget, M. S., E. Leibovitz & M. J. Buttner, (1999b) A putative two-component signal transduction system regulates sigmaE, a sigma factor required for normal cell wall integrity in *Streptomyces coelicolor* A3(2). *Mol Microbiol* **33**: 97-107.
- Parker, J. L., A. M. Jones, L. Serazetdinova, G. Saalbach, M. J. Bibb & M. J. Naldrett, (2010a) Analysis of the phosphoproteome of the multicellular bacterium *Streptomyces coelicolor* A3(2) by protein/peptide fractionation, phosphopeptide enrichment and high-accuracy mass spectrometry. *Proteomics* **10**: 2486-2497.
- Parker, J. L., (2010b) *Investigation of the phosphoproteome of Streptomyces coelicolor* A3(2). PhD Thesis, John Innes Centre, UK.
- Peck, S. C., (2006) Analysis of protein phosphorylation: methods and strategies for studying kinases and substrates. *Plant J* **45**: 512-522.
- Pereira, S. F., L. Goss & J. Dworkin, (2011) Eukaryote-like serine/threonine kinases and phosphatases in bacteria. *Microbiol Mol Biol Rev* **75**: 192-212.
- Petrickova, K. & M. Petricek, (2003) Eukaryotic-type protein kinases in *Streptomyces coelicolor*: variations on a common theme. *Microbiology* **149**: 1609-1621.

- Prisic, S., S. Dankwa, D. Schwartz, M. F. Chou, J. W. Locasale, C. M. Kang, G. Bemis, G. M. Church, H. Steen & R. F. Husson, (2010) Extensive phosphorylation with overlapping specificity by *Mycobacterium tuberculosis* serine/threonine protein kinases. *Proc Natl Acad Sci USA* **107**: 7521-7526.
- Rajkarnikar, A., H. J. Kwon, Y. W. Ryu & J. W. Suh, (2007) Two threonine residues required for role of AfsKav in controlling morphogenesis and avermectin production in *Streptomyces avermitilis*. *J Microbiol Biotechnol* **17**: 1563-1567.
- Ramamurthi, K. S. & R. Losick, (2009) Negative membrane curvature as a cue for subcellular localisation of a bacterial protein. *Proc Natl Acad Sci U S A* **106**: 13541-13545.
- Ramos, A., M. P. Honrubia, N. Valbuena, J. Vaquera, L. M. Mateos & J. A. Gil, (2003) Involvement of DivIVA in the morphology of the rod-shaped actinomycete *Brevibacterium lactofermentum*. *Microbiology* **149**: 3531-3542.
- Richards, D. M., A. M. Hempel, K. Flärdh, M. J. Buttner & M. Howard, (2012) Mechanistic basis of branch-site selection in filamentous bacteria. *PLoS Comput Biol* **8**: e1002423.
- Rigden, M. D., C. Baier, S. Ramirez-Arcos, M. Liao, M. Wang & J. A. Dillon, (2008) Identification of the coiled-coil domains of *Enterococcus faecalis* DivIVA that mediate oligomerisation and their importance for biological function. *J Biochem* **144**: 63-76.
- Riquelme, M., O. Yarden, S. Bartnicki-Garcia, B. Bowman, E. Castro-Longoria, S. J. Free, A. Fleissner, M. Freitag, R. R. Lew, R. Mourino-Perez, M. Plamann, C. Rasmussen, C. Richthammer, R. W. Roberson, E. Sanchez-Leon, S. Seiler & M. K. Watters, (2011) Architecture and development of the *Neurospora crassa* hypha – a model cell for polarised growth. *Fungal Biol* **115**: 446-474.

- Ruban-Osmialowska, B., D. Jakimowicz, A. Smulczyk-Krawczynszyn, K. F. Chater & J. Zakrzewska-Czerwinska, (2006) Replisome localisation in vegetative and aerial hyphae of *Streptomyces coelicolor*. *J Bacteriol* **188**: 7311-7316.
- Sambrook, J. & D. W. Russel, (2001) *Molecular Cloning: A Laboratory Manual*. Cold Spring Harbor Laboratory Press, Cold Spring Harbor, NY, USA.
- Schultz, C., A. Niebisch, A. Schwaiger, U. Viets, S. Metzger, M. Bramkamp & M. Bott, (2009) Genetic and biochemical analysis of the serine/threonine protein kinases PknA, PknB, PknG and PknL of *Corynebacterium glutamicum*: evidence for non-essentiality and for phosphorylation of OdhI and FtsZ by multiple kinases. *Mol Microbiol* **74**: 724-741.
- Shah, I. M., M. H. Laaberki, D. L. Popham & J. Dworkin, (2008) A eukaryotic-like Ser/Thr kinase signals bacteria to exit dormancy in response to peptidoglycan fragments. *Cell* **135**: 486-496.
- Shih, Y. L. & L. Rothfield, (2006) The bacterial cytoskeleton. *Microbiol Mol Biol Rev* **70**: 729-754.
- Shimi, T., V. Butin-Israeli, S. A. Adam & R. D. Goldman, (2011) Nuclear lamins in cell regulation and disease. *Cold Spring Harb Symp Quant Biol* **75**: 525-531.
- Smokvina, T., P. Mazodier, F. Boccard, C. J. Thompson & M. Guérineau, (1990) Construction of a series of pSAM2-based integrative vectors for use in *Actinomyces*. *Gene* **94**: 53-59.
- Stahlberg, H., E. Kutejova, K. Muchova, M. Gregorini, A. Lustig, S. A. Muller, V. Olivieri, A. Engel, A. J. Wilkinson & I. Barak, (2004) Oligomeric structure of the *Bacillus subtilis* cell division protein DivIVA determined by transmission electron microscopy. *Mol Microbiol* **52**: 1281-1290.
- Steinberg, G., (2007) Hyphal growth: a tale of motors, lipids, and the Spitzenkörper. *Eukaryot Cell* **6**: 351-360.

- Stock, A. M., V. L. Robinson & P. N. Goudreau, (2000) Two-component signal transduction. *Ann Rev Biochem* **69**: 183-215.
- Stone, K. J. & J. L. Strominger, (1971) Mechanism of action of bacitracin: complexation with metal ion and C55-isoprenyl pyrophosphate. *Proc Natl Acad Sci USA* **68**: 3223-3227.
- Tanaka, A., Y. Takano, Y. Ohnishi & S. Horinouchi, (2007) AfsR recruits RNA polymerase to the *afsS* promoter: a model for transcriptional activation by SARPs. *J Mol Biol* **369**: 322-333.
- Thomaides, H. B., M. Freeman, M. El Karoui & J. Errington, (2001) Division site selection protein DivIVA of *Bacillus subtilis* has a second distinct function in chromosome segregation during sporulation. *Genes Dev* **15**: 1662-1673.
- Tomono, A., M. Mashiko, T. Shimazu, H. Inoue, H. Nagasawa, M. Yoshida, Y. Ohnishi & S. Horinouchi, (2006) Self-activation of serine/threonine kinase AfsK on autophosphorylation at threonine-168. *J Antibiot* **59**: 117-123.
- Traag, B. & G. P. van Wezel, (2008) The SsgA-like proteins in actinomycetes: small proteins up to a big task. *Antonie van Leeuwenhoek* **94**: 85-97.
- Trachtenberg, S., (1998) Mollicutes-wall-less bacteria with internal cytoskeletons. *J Struct Biol* **124**: 244-256.
- Tran, N. T., (2010) *The σE cell envelope stress signal transduction system of Streptomyces coelicolor*. PhD Thesis, John Innes Centre, UK.
- Ubersax, J. A. & J. E. Ferrel, (2007) Mechanisms of specificity in protein phosphorylation. *Nat Rev Mol Cell Biol* **8**: 530-541.
- Umeyama, T., P. C. Lee & S. Horinouchi, (2002) Protein serine/threonine kinases in signal transduction for secondary metabolism and morphogenesis in *Streptomyces*. *Appl Microbiol Biotechnol* **59**: 419-425.

- Urabe, H. & H. Ogawara, (1995) Cloning, sequencing and expression of serine/threonine kinase-encoding genes from *Streptomyces coelicolor* A3(2). *Gene* **153**: 99-104.
- van den Ent, F., L. Amos & J. Löwe, (2001a) Bacterial ancestry of actin and tubulin. *Curr Opin Microbiol* **4**: 634-638.
- van den Ent, F., L. A. Amos & J. Löwe, (2001b) Prokaryotic origin of the actin cytoskeleton. *Nature* **413**: 39-44.
- Veyron-Churlet, R., V. Molle, R. C. Taylor, A. K. Brown, G. S. Besra, I. Zanella-Cleon, K. Futterer & L. Kremer, (2009) The *Mycobacterium tuberculosis* β -ketoacyl-acyl carrier protein synthase III activity is inhibited by phosphorylation on a single threonine residue. *J Biol Chem* **284**: 6414-6424.
- Vogelmann, J., M. Ammelburg, C. Finger, J. Guezguez, D. Linke, M. Flotenmeyer, Y. D. Stierhof, W. Wohlleben & G. Muth, (2011) Conjugal plasmid transfer in *Streptomyces* resembles bacterial chromosome segregation by FtsK/SpoIIIE. *Embo J* **30**: 2246-2254.
- Vollmer, W. & U. Bertsche, (2008) Murein (peptidoglycan) structure, architecture and biosynthesis in *Escherichia coli*. *Biochim Biophys Acta* **1778**: 1714-1734.
- Walshaw, J., M. D. Gillespie & G. H. Kelemen, (2010) A novel coiled-coil repeat variant in a class of bacterial cytoskeletal proteins. *J Struct Biol* **170**: 202-215.
- Wang, S., S. Cantlay, N. Nordberg, M. Letek, J. A. Gil & K. Flärdh, (2009) Domains involved in the *in vivo* function and oligomerisation of apical growth determinant DivIVA in *Streptomyces coelicolor*. *FEMS Microbiol Lett* **297**: 101-109.
- Willemse, J., J. W. Borst, E. de Waal, T. Bisseling, G. P. van Wezel, (2011) Positive control of cell division: FtsZ is recruited by SsgB during sporulation of *Streptomyces*. *Genes Dev* **25**: 89-99.

- Winter, D., R. Pipkorn & W. D. Lehmann, (2009) Separation of peptide isomers and conformers by ultra performance liquid chromatography. *J Sep Sci* **32**: 1111-1119.
- Wolanski, M., R. Wali, E. Tilley, D. Jakimowicz, J. Zakrzewska-Czerwinska & P. Herron, (2011) Replisome trafficking in growing vegetative hyphae of *Streptomyces coelicolor* A3(2). *J Bacteriol* **193**: 1273-1275.
- Wollkopf, A. M., (2007) *Control of hyphal tip growth and branching by the coil-coiled protein DivIVA in Streptomyces coelicolor*. Diplomarbeit. University of Heidelberg, Germany.
- Xu, H., K. F. Chater, Z. Deng & M. Tao, (2008) A cellulose synthase-like protein involved in hyphal tip growth and morphological differentiation in *Streptomyces*. *J Bacteriol* **190**: 4971-4978.
- Yanisch-Perron, C., J. Vieira & J. Messing, (1985) Improved M13 phage cloning vectors and host strains: nucleotide sequences of the M13mp18 and pUC19 vectors. *Gene* **33**: 103-119.
- Young, T. A., B. Delagoutte, J. A. Endrizzi, A. M. Falick & T. Alber, (2003) Structure of *Mycobacterium tuberculosis* PknB supports a universal activation mechanism for Ser/Thr protein kinases. *Nat Struct Biol* **10**: 168-174.
- Young, K. D., (2003) Bacterial shape. *Mol Microbiol* **49**: 571-580.

Publications

Mechanistic Basis of Branch-Site Selection in Filamentous Bacteria

David M. Richards¹✉, Antje M. Hempel^{1,2}✉, Klas Flårdh^{2*}, Mark J. Buttner¹, Martin Howard^{1*}

1 John Innes Centre, Norwich Research Park, Norwich, United Kingdom, **2** Department of Biology, Lund University, Lund, Sweden

Abstract

Many filamentous organisms, such as fungi, grow by tip-extension and by forming new branches behind the tips. A similar growth mode occurs in filamentous bacteria, including the genus *Streptomyces*, although here our mechanistic understanding has been very limited. The *Streptomyces* protein DivIVA is a critical determinant of hyphal growth and localizes in foci at hyphal tips and sites of future branch development. However, how such foci form was previously unknown. Here, we show experimentally that DivIVA focus-formation involves a novel mechanism in which new DivIVA foci break off from existing tip-foci, bypassing the need for initial nucleation or *de novo* branch-site selection. We develop a mathematical model for DivIVA-dependent growth and branching, involving DivIVA focus-formation by tip-focus splitting, focus growth, and the initiation of new branches at a critical focus size. We quantitatively fit our model to the experimentally-measured tip-to-branch and branch-to-branch length distributions. The model predicts a particular bimodal tip-to-branch distribution results from tip-focus splitting, a prediction we confirm experimentally. Our work provides mechanistic understanding of a novel mode of hyphal growth regulation that may be widely employed.

Citation: Richards DM, Hempel AM, Flårdh K, Buttner MJ, Howard M (2012) Mechanistic Basis of Branch-Site Selection in Filamentous Bacteria. *PLoS Comput Biol* 8(3): e1002423. doi:10.1371/journal.pcbi.1002423

Editor: Christopher V. Rao, University of Illinois at Urbana-Champaign, United States of America

Received: November 28, 2011; **Accepted:** January 26, 2012; **Published:** March 8, 2012

Copyright: © 2012 Richards et al. This is an open-access article distributed under the terms of the Creative Commons Attribution License, which permits unrestricted use, distribution, and reproduction in any medium, provided the original author and source are credited.

Funding: We receive core support from the BBSRC. The funders had no role in study design, data collection and analysis, decision to publish, or preparation of the manuscript.

Competing Interests: The authors have declared that no competing interests exist.

* E-mail: klas.flardh@biol.lu.se (KF); martin.howard@jic.ac.uk (MH)

✉ These authors contributed equally to this work.

Introduction

The ability to break symmetry and establish an axis of polarity is crucial for the function and development of almost all cell types. In bacteria, such symmetry-breaking is often mediated by cytoskeletal elements inside the cell that direct new cell wall synthesis. Many rod-shaped bacteria (including *Escherichia coli*, *Bacillus subtilis* and *Caulobacter crescentus*) grow solely through the isotropic insertion of new cell wall material throughout the length of the lateral walls [1,2]. Here, cell wall growth is directed by MreB, the bacterial ortholog of eukaryotic actin [3–6], whereas cell division is mediated by the bacterial tubulin ortholog, FtsZ. In these rod-shaped bacteria, polarity systems are required to identify and differentiate cell poles that remain inert during cell elongation. However, many other organisms enlarge by hyphal growth, a strategy that has proved successful for the exploitation of soil and other environments. Hyphal growth has evolved independently in both eukaryotic and prokaryotic microbes, including fungi and Gram-positive bacteria of the genus *Streptomyces*. This mode of growth depends on pronounced cellular polarity and the specific localization of cell envelope assembly to one cell pole in order to achieve tip extension. New sites of growth arise by hyphal branching, which requires the re-orientation of cellular polarity and the *de novo* establishment of new zones of cell wall synthesis from which lateral branches emerge. The result is a mycelial network in which the regulation of branching largely determines the morphology and behaviour of the mycelium as it spreads through the environment. However, the general principles that

control such cellular branching have remained unknown. Here we report a novel mechanistic basis for branch-site selection in the mycelial actinomycete bacterium *Streptomyces coelicolor*. Since all hyphal bacteria are actinomycetes, this mechanism is likely to be widely relevant in this important phylum of bacteria, which account for the majority of commercial antibiotics.

Tip extension and hyphal branching in *Streptomyces* are independent of both MreB and FtsZ, and depend instead on the coiled-coil cytoskeletal-like protein DivIVA [7,8]. A functional DivIVA-EGFP fusion localizes to tips and marks new branch points well before visible lateral outgrowth [9,10]. Deletion of *divIVA* is lethal, whereas overexpression leads to greatly increased numbers of DivIVA foci along the lateral wall and *de novo* cell wall outgrowth at these foci [8–10]. These data suggest that DivIVA can direct cell polarity and recruit the machinery for cell wall synthesis. Additional cytoskeletal components may also be involved (for example, Scy [11]), together forming a tip-organizing complex. However, regardless of whether there are additional components, we can use DivIVA-EGFP as a marker to monitor the dynamics of the tip-organizing complex as a whole.

The branch-site selection mechanism that localises DivIVA to new sites along the lateral wall, from which branches subsequently emerge, was previously unknown. We therefore used the DivIVA-EGFP fusion to monitor the dynamics of the tip-organizing complex in *S. coelicolor* by live cell time-lapse imaging. These experiments revealed that the new DivIVA foci that initiate lateral branches arise predominantly by a novel tip focus-splitting mechanism that bypasses the necessity for initial nucleation or

Author Summary

Amongst the great variety of shapes that organisms assume, many grow in a filamentous manner and develop at least partly into a network of branches. Examples include plant roots, fungi and some bacteria. Whereas the mechanisms of filamentous growth are partially understood in fungi, the same cannot be said in filamentous bacteria, where our knowledge of hyphal growth regulation is very limited. To rectify this we have studied the bacteria *Streptomyces*, which are an excellent model for all hyphal bacteria. The protein DivIVA is known to play a critical role in controlling filamentous growth in *Streptomyces*, forming large foci at branch tips and smaller foci that mark sites of future branch outgrowth. However, until now nothing was known about how these foci first appear. We have shown experimentally that new foci appear via a novel mechanism, whereby existing tip-foci split into two clusters. The larger cluster remains at the growing tip, while the smaller cluster fixes onto the adjacent lateral membrane, where it grows in size, eventually initiating a new branch. By mathematically modelling how DivIVA foci grow, we show how this one simple mechanism of focus formation can quantitatively capture the statistical properties of the entire hyphal branching network.

site-selection. In order to gain a deeper and more rigorous understanding of the regulation of hyphal branching, we then quantified hyphal branching patterns from still images, and developed a mathematical model of the DivIVA dynamics. As we will see, the model demonstrates that a remarkably simple tip-focus splitting mechanism is capable of quantitatively explaining all of our experimental branching pattern data, a result which is far from intuitive. Moreover, the model makes explicit predictions that we have experimentally verified. Intriguingly, a similar splitting mechanism has recently been reported in hyphal growth in fungi (*Neurospora crassa*) [12], raising the possibility that this simple mechanism may be widely applicable.

Results

Lateral DivIVA foci arise from splitting of apical foci

Our previous studies have shown that DivIVA foci are always present at new branch points before outgrowth occurs [9,10]. However, the origin of such DivIVA foci and the factors that determine their localisation have remained unclear [8]. To further understand the branching process, we have therefore studied more carefully how such foci are formed and traced their origin from time-lapse images. These experiments revealed that new small foci often arise from existing DivIVA foci at hyphal tips, by a process where a small cluster of DivIVA separates from the tip-focus and is left on the membrane just behind the tip. An example is shown in Figure 1 (see Video S1 for a movie of this figure). At around 12–18 minutes the focus of DivIVA at the tip splits and leaves behind a small focus on the adjacent membrane. As the tip continues to extend, the new focus remains fixed in place on the membrane and grows in size and intensity. In between 42 and 48 minutes a new branch is formed at the position of the new focus. Tip-focus splitting is only seen to occur from foci associated with extending tips; foci which have not yet initiated a branch, such as the smaller focus between 12 and 36 minutes in Figure 1, do not undergo splitting. We traced the origin of 52 nascent branches in time-lapse images and found that 42 of them (81%) were accounted for by tip-focus splitting events. Since only sufficiently large and intense

DivIVA-EGFP foci are visible above the background fluorescence, some foci cannot be traced to their point of creation, and so this is likely to be an underestimate of the real proportion of branching arising from tip-focus splitting [10]. Thus, tip-focus splitting, rather than other potential mechanisms, such as spontaneous nucleation, appears to be the predominant method for focus initiation in wild-type cells.

Measurements of hyphal growth and lateral branching

In order to quantitatively understand *Streptomyces* branch-site selection, we have measured two categories of distances from still images: the distance between the tip and the points where branches emerge, and the spacing between the branches themselves. Unlike the branch spacing, the tip-to-branch distance is not fixed: as the hyphae extend in length, the tip-to-branch distances increase. To avoid this difficulty we use our measurements to work out the tip-to-branch distance at the moment when the new branches appear, as discussed in *Materials and Methods*.

Unless care is taken when measuring the distributions from still images, it is easy to introduce biases that uncontrollably skew the data. For example, if only branching events relatively close to hyphal tips can be measured (as is inevitably the case for *Streptomyces* where individual hyphae cannot be traced into the dense mycelial clumps from which they emerge), then long branch-to-branch distances will never be recorded, even if they occur. As explained in *Materials and Methods*, we control for this effect by introducing a protocol so that all measured hyphae have effectively the same length, a distance we call the trim length. This is achieved by discarding hyphae which are shorter than the trim length and trimming those which are longer. This protocol does not eliminate measurement bias, but rather controls the bias so that our experimental measurements are unambiguous and can be precisely compared with data generated by our mathematical model (see below).

The measured tip-to-branch and branch-to-branch distributions with a 80 μm trim are shown in Figure 2. The tip-to-branch distribution has two distinct peaks, one between 0–5 μm and one at 40–45 μm (Figure 2A). This might suggest that two distinct mechanisms are involved in producing new branches. Surprisingly, however, our later analysis will show that a single mechanism can account for both peaks.

Minimal mathematical model of the growth of DivIVA foci

We assume that DivIVA foci, either on their own or as part of a tip-organizing complex, assemble the cell wall synthesis machinery to both extend hyphae and form new branches. Most new DivIVA foci do not immediately initiate a new branch (Figure 1). We assume this is a result of the small starting sizes of most foci. Foci must instead grow in size by accumulating DivIVA molecules from the cytoplasm until they contain enough molecules to initiate a new branch. To understand where new branches emerge we must therefore understand how the number of molecules, N , in a focus changes with time. We will refer to this number N as the tip-focus size. We consider simple cooperative binding where the rate of DivIVA molecules joining a focus is linearly dependent on both the cytoplasmic DivIVA density, ρ , and the focus size, N (alternative growth rules are considered in Supporting Text S1, but these alternatives give qualitatively similar results, with no better fit to the experimental data). Thus we have $\dot{N} = \beta\rho N$, where β is a parameter independent of N and ρ . Although, in the minimal model, we assume foci never lose DivIVA molecules, including this process again makes little or no difference (see Supporting Text S1). We also assume that the cytoplasmic DivIVA

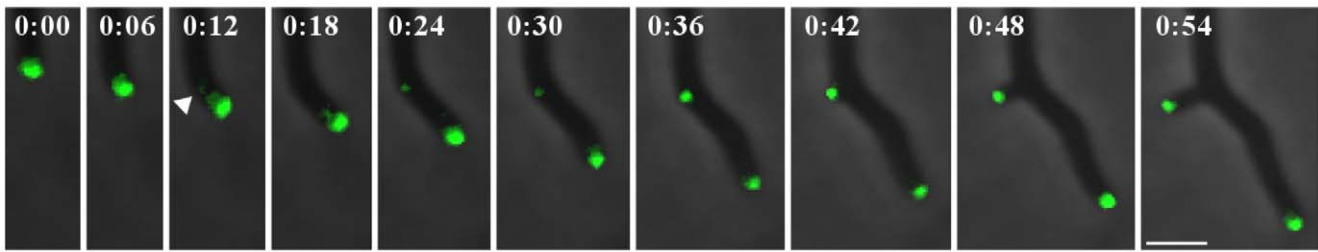


Figure 1. Evidence of tip-focus splitting, growth of foci and emergence of branches, in fluorescence-imaged *Streptomyces coelicolor* expressing *divIVA-egfp*. The tip always contains a large DivIVA focus and established tips extend at an approximately constant speed. At about 12 minutes, the DivIVA tip-focus undergoes splitting, leaving behind a new focus (arrow). As the tip continues to extend, the new focus remains in place on the membrane and grows in intensity. After about 42 minutes a new branch is formed at the position of the new focus, with the new focus now sitting at the tip of the new branch. Both the new branch and the original branch now continue to extend in length. Time in hours:minutes. Scale bar: 3 μm . doi:10.1371/journal.pcbi.1002423.g001

density appearing in the above equation is the same for all foci (this assumption is justified by our full simulations, see Supporting Text S1). Thus we can replace $\tilde{\beta}\rho$ by the single parameter β , which we call the binding parameter, and consider $\tilde{N} = \beta N$. We assume that a focus starts with N_0 molecules and must reach N_{br} molecules before it can form a branch. We can easily solve the above equation for N to find the time taken, τ , for this growth from N_0 to N_{br} . With an extension speed v for established tips, the distance $L = v\tau$ behind the tip where a branch appears is

$$L = \frac{v}{\beta} \ln \frac{N_{\text{br}}}{N_0}. \quad (1)$$

By comparing images like Figure 1 at 12 and 42 minutes, we estimate a typical value for $\frac{N_{\text{br}}}{N_0}$ as between 5 and 10, so that, to a rough approximation, $L \approx \frac{2v}{\beta}$. The absolute value of N_{br} is difficult to determine, but since the fluorescence of a typical DivIVA focus is not dissimilar to that of an FtsZ ring, and since an FtsZ ring contains on the order of 10,000 molecules [13], we take N_{br} to be of a similar order of magnitude. The growth speed of an established tip, v , is measured from time lapse images to be about 8 $\mu\text{m}/\text{hr}$. Due to the trimming issues discussed above, measuring a typical value for L is not straightforward. In particular, using the average of a trimmed distribution, such as that in Figure 1A, will

not give a good estimate. However, as explained in *Materials and Methods*, by studying the distributions over a range of trims, we estimate a value of about 65 μm under the growth conditions used, which implies that β should be about $7 \times 10^{-5} \text{s}^{-1}$. (See Figure S10 for a schematic of the colony morphology for different values of β .)

Streptomyces produces branches at a range of distances behind tips, producing a distribution of tip-to-branch distances. In our model, this is due to fluctuations in the parameters in Eq. (1). Note that, although we vary these parameters, we do not model the growth of foci themselves stochastically (instead using a deterministic differential equation) due to the large number (thousands) of molecules involved. Each binding event will itself be stochastic but the overall process involving many thousands of such binding events will be well described deterministically.

The tip-focus splitting mechanism

So far we have been concerned with how the number of molecules in a pre-existing focus changes with time. We have not yet discussed the mechanism by which new foci are formed, the tip-focus splitting mechanism. Furthermore, after a tip-focus has undergone splitting, we are interested in the length of time before the focus can split again, which, after both foci have initiated new branches, will translate into the distance between branches. It is important to emphasise that, whereas the growth of foci controls the tip-to-branch distribution, it is the focus-splitting rules that control the branch-to-branch distribution.

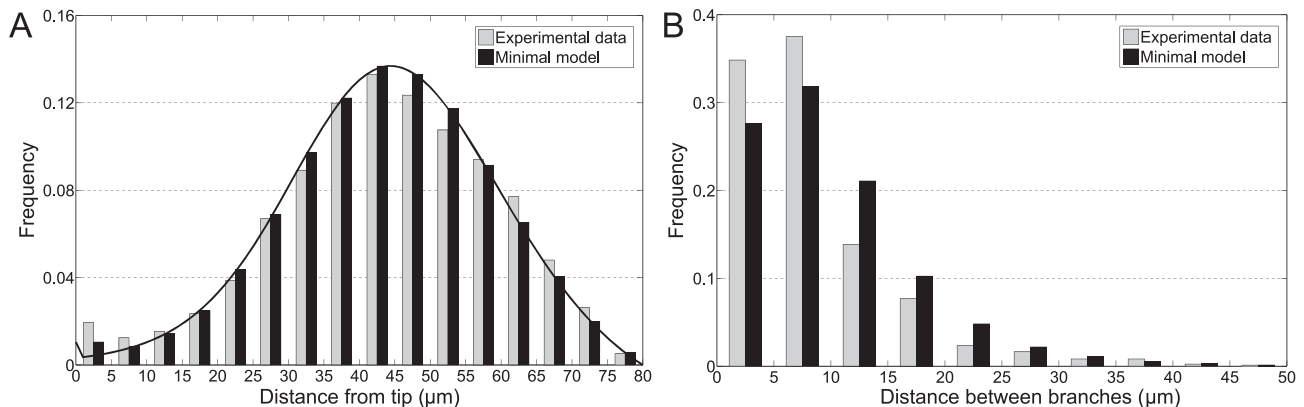


Figure 2. Comparison of histograms between minimal model and experimental data at 80 μm trim. (A) Tip-to-branch distribution. Analytic prediction is also shown (curved line). 1097 experimental data points. (B) Branch-to-branch distribution. 858 experimental data points. doi:10.1371/journal.pcbi.1002423.g002

The simplest assumption that could be made would be that the focus-splitting probability per unit time is constant, independent of when the tip-focus last split. This would describe a Poisson process and so imply an exponential distribution for the branch-to-branch distribution. However, as Figure 1B shows, for distances smaller than 10 μm the branch-to-branch histogram is not described by a decaying exponential: these shorter distances are measured much less frequently than implied by a Poisson distribution.

This suppression of short branch-to-branch distances shows that focus-splitting events are not independent of each other: a tip-focus that has just split is less likely to immediately split again. One potential explanation is that the probability of tip-focus splitting depends on the tip-focus size, such that smaller tip-foci are less likely to split. For this reason we implement a minimum tip-focus size (a critical mass), N_{split} , below which the tip-focus cannot split, with some constant focus-splitting probability per unit time, characterised by the parameter γ , for all tip-foci above N_{split} . Splitting events cause the tip-focus to decrease in size and so, in some instances, such a splitting will cause the tip-focus size to drop below N_{split} . In that case, only after the tip-focus has absorbed more DivIVA from the cytoplasm will it have sufficient size to split again. This time delay effectively reduces the number of short branch-to-branch distances.

Although it is difficult to analyse tip-focus splitting analytically, it is useful to note that, in the limit where γ is very large (compared to β), the branch-to-branch distance, d , is given by

$$d = \frac{v}{\beta} \ln \frac{N_{\text{split}}}{N_{\text{split}} - N_0}, \quad (2)$$

a result which follows in a very similar way to Eq. (1).

Fitting the minimal model

In order to compare the minimal model with the experimental data, we developed a simulation which grows *Streptomyces* hyphae, implements tip-focus splitting and focus growth, performs the trim to the required length, and extracts the distributions (see *Materials and Methods*). We used the parameters listed in Table 1 with v , β , the mean initial focus size $\langle N_0 \rangle$, and the mean focus size for branch initiation $\langle N_{\text{br}} \rangle$ inferred from experiments (see above), and with the standard deviations in N_0 and N_{br} , that is δN_0 and δN_{br} , and γ fitted to the experimentally determined tip-to-branch and branch-to-branch distributions at 80 μm trim. We find that variations in just N_0 and N_{br} are sufficient to fit all the measured distributions. For simplicity we take N_0 and N_{br} to follow independent truncated Gaussian distributions, where the truncation ensures that N_0 and N_{br} are always positive. This is required since Gaussian distributions assign non-zero probabilities to all values, whereas biologically foci cannot contain fewer than zero molecules. The means ($\langle N_0 \rangle$ and $\langle N_{\text{br}} \rangle$) and standard deviations (δN_0 and δN_{br}) are those for the truncated distributions, rather than the full Gaussians. However, as shown in Supporting Text S1, other distributions do not qualitatively change our results.

In our fitting, it was not immediately clear whether $\langle N_{\text{br}} \rangle$ should be larger or smaller than N_{split} . Note that although we allow the possibility that N_{split} is less than $\langle N_{\text{br}} \rangle$ in the model, this does not mean that foci can split before they have initiated branches; DivIVA foci have only been observed to split when they are associated with a growing tip. However, $\langle N_{\text{br}} \rangle$ smaller than N_{split} would imply that newly formed branches cannot normally produce their own branches until the tip-focus has grown further to size N_{split} . This in turn results in a gap between where a branch emerges from its parent hypha and the position of its first offshoot.

Table 1. Main parameters and their values.

Parameter	Value
Tip growth speed, v	8 $\mu\text{m hr}^{-1}$
Binding parameter, β	$7 \times 10^{-5} \text{ s}^{-1}$
Mean initial focus size, $\langle N_0 \rangle$	1,700
Standard deviation in initial focus size, δN_0	1,000
Mean focus size for branch initiation, $\langle N_{\text{br}} \rangle$	10,000
Standard deviation in focus size for branch initiation, δN_{br}	2,600
Minimum tip-focus size for tip-focus splitting, N_{split}	10,000
Tip-focus splitting probability per unit time, γ	$1 \times 10^{-3} \text{ s}^{-1}$

doi:10.1371/journal.pcbi.1002423.t001

We measured this distribution of distances and found no evidence for such a gap (see Supporting Text S1 and Figure S2), which implies that N_{split} is equal to (or smaller than) $\langle N_{\text{br}} \rangle$. In our model we choose $N_{\text{split}} = \langle N_{\text{br}} \rangle$, although smaller values of N_{split} make little qualitative difference.

As shown in Figure 2, there is excellent agreement between the minimal model fits and the experimental data. For the trimmed tip-to-branch distributions, our model is sufficiently simple that this distribution can be calculated analytically (see Supporting Text S1) without recourse to simulations. The analytic prediction is also shown in Figure 2A and agrees extremely well with the simulation data, as expected. Note that the reason the tip-to-branch distribution drops to zero at 80 μm is a consequence of the trimming protocol rather than any inherent property of *Streptomyces*. We chose a 80 μm trim as a trade-off between distribution width and amount of data, but it is also possible to compare the model and the experimental data at other trims. Figures S8 and S9 show that there is also good agreement at trims of 60 μm and 100 μm .

We have checked that the tip-to-branch and branch-to-branch distributions generated by the minimal model are robust to changes in all the parameters in Table 1. Further, we tested that adding fluctuations in the tip growth speed, v , and the on-rate parameter, β , also do not qualitatively change these distributions (see Supporting Text S1). There is little to be gained by also considering fluctuations in N_{split} since the stochastic nature of tip-focus splitting is already included via γ , the tip-focus splitting parameter.

Verifying a model prediction in the tip-to-branch distribution

One of the most striking features of the experimentally measured tip-to-branch distribution, Figure 2A, is the peak at small distances. Naïvely it may be thought that a novel tip-focus splitting mechanism is required to account for this peak. However, our model predicts that this peak can be simply explained without additional assumptions. Since most new foci must attract more DivIVA molecules before they can initiate a new branch, the distributions of N_0 and N_{br} must be such that most new foci start with fewer than N_{br} molecules. However, there is a small tail to the distributions that causes a few foci to have N_0 above N_{br} , i.e. when they are formed these foci already have enough DivIVA molecules to initiate branch outgrowth. These foci will cause branching

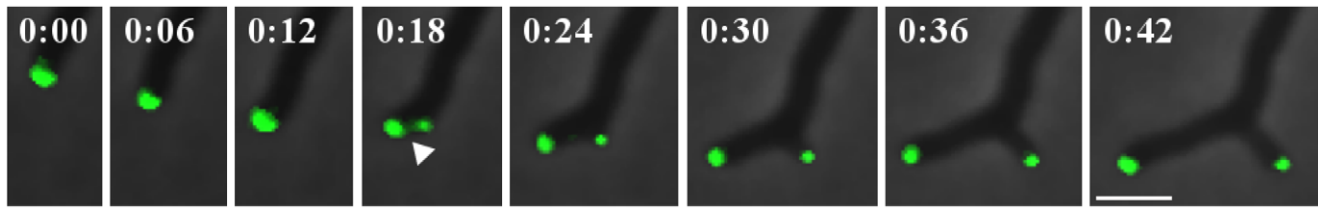


Figure 3. Example of branching at almost zero distance from the tip. The model indicates that this is due to tip-focus splitting events (arrow) where N_0 is greater than N_{br} . Time in hours:minutes. Scale bar: $3\ \mu\text{m}$. doi:10.1371/journal.pcbi.1002423.g003

almost as soon as they are formed, very close to zero distance from the tip. We have directly observed such events and an example is shown in Figure 3 (see Video S2 for a movie of this figure). Furthermore, we also measured the total intensity of 25 newly-produced foci from time-lapse images: 12 from cases where the new branch appears next to the tip and 13 from normal tip-focus splitting events when the new branch appears much further back. In the first case the average intensity is almost three times greater than in the second case, supporting the hypothesis that events where the branch appears next to the tip correspond to the initial focus size, N_0 , being much greater than average. The entire weight of the distribution with $N_0 \geq N_{br}$ will give effectively zero tip-to-branch distances, which then naturally explains the peak at the origin in Figure 2A. Consequently, our model predicts that if the distribution is analysed with bins of smaller width, then the peak at the origin will become even more dramatic. After reanalysing the measured data, this prediction is strikingly confirmed, as shown in Figure 4. Although the peak in the $0-1\ \mu\text{m}$ bin matches well, the agreement is not perfect in the range $1-6\ \mu\text{m}$. However, we believe this feature is an unavoidable artifact of how the data is analysed: the tip growth speed cannot be measured directly from still images, rather only the distribution of speeds is known, which necessarily slightly smears the data (see *Materials and Methods* and Supporting Text S1).

Full model: curvature-dependent tip-focus splitting

It has been shown that the DivIVA orthologue in *B. subtilis* preferentially assembles on negatively-curved membranes, and this appears to be an important factor in targeting of the *B. subtilis* protein to cell poles and septation sites [14,15]. Similarly, in *Streptomyces*, a preference for branches to emerge on the outer side of curved hyphae has been reported [10], which suggests, for example, that for tips that bend to the left, foci are more likely to form on the right inner membrane. Although the mechanism by which this occurs is not yet fully understood, it is possible to ask how such an effect impacts our model. To do so we developed and simulated a more detailed computational model (see Supporting Text S1), which implements hyphal growth in two-dimensional space. At each time step in the simulation, the direction of tip growth is randomly varied by a small amount, such that over sufficiently long distances (a few μm), memory of the previous growth direction is lost. We postulate that tip-foci with sizes above N_{split} can split only when the local curvature near the tip is sufficiently high. Hence the earlier focus-splitting parameter, γ , is understood as an effective parameter that can be replaced by growth direction variation and a curvature threshold. However, it is worth noting that if curvature is the origin of γ , it must be quite a sensitive effect since during growth the mean curvature near the tip only changes by about 10%. The full model (see Supporting Text S1 for full details and parameters) produces colony dynamics that match well with the wild-type

phenotype (for example, see Videos S3 and S4). In particular, the tip-to-branch and branch-to-branch distributions are practically identical to the minimal model, thereby justifying our earlier simplifying assumptions.

Under- and overexpression of *divIVA*

Since DivIVA is an essential protein, it cannot be completely removed. However, we can consider mild underexpression and various levels of overexpression. We first consider heavy overexpression. Previous work has examined hyphal morphology when *divIVA* was overexpressed in preformed hyphae to approximately twenty-five times its usual level [9,10]. Such overexpression resulted in increased levels of cytoplasmic DivIVA, swollen hyphal tips and lateral hyperbranching. Interestingly, after inducing increased DivIVA production, many of the new branches developed well behind the tip positions at the moment of induction. This observation is unexpected since, in the minimal model, foci can only be produced from the splitting of tip-foci. It is possible that these new branches are due to foci that were already present at the time of induction but that were too small to be seen, and that overexpression subsequently caused them to develop into branches much more rapidly than normal. However, if this explanation were correct, wild-type *Streptomyces* would form many branches hundreds of microns behind the tips, a strategy which would be very inefficient in terms of nutrition acquisition. For this reason, we favour an alternative explanation, namely that these new branches arise from a separate mechanism of focus formation: spontaneous nucleation. In this process, due to the stochastic dynamics of molecules within the cytoplasm, occasionally a sufficient number of DivIVA molecules come together on the membrane and spontaneously form a cluster.

As is standard for nucleation dynamics [16], and as we confirmed by stochastic simulations, for cytoplasmic DivIVA densities below some threshold, the probability of spontaneous nucleation (involving the near simultaneous binding of multiple DivIVA molecules to overcome a nucleation barrier) is close to zero. Above this threshold, however, we find that the rate of nucleation rises approximately linearly with increasing cytoplasmic density. We assume that for the parameters chosen in Table 1, the DivIVA concentrations during wild-type growth fall well below this threshold and hence spontaneous nucleation does not occur. However, at 25-fold overexpression, this threshold is exceeded. In this latter case, we implemented spontaneous nucleation in our full model in the simplest possible way, by having a probability per unit length and time for spontaneously creating a new focus on the membrane, with a linear increase in nucleation probability with increasing cytoplasmic density above the threshold (see Supporting Text S1 for full details and parameters). We were then able to produce simulated colony dynamics which successfully matched the observed phenotype of 25-fold overexpression (for example, see Video S5).

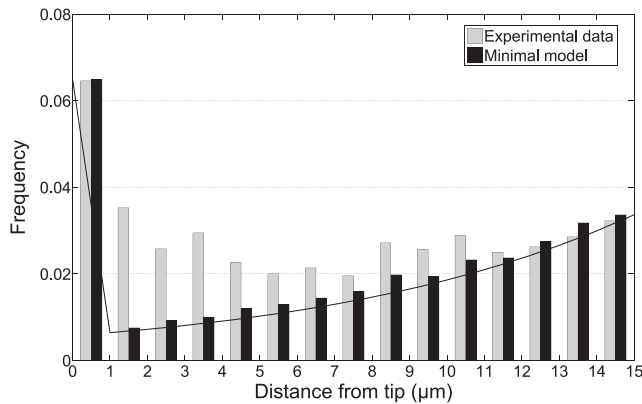


Figure 4. Comparison of tip-to-branch distribution at small distances between minimal model and experimental data at 80 μm trim. Analytic prediction is also shown (curved line). doi:10.1371/journal.pcbi.1002423.g004

In addition to heavy overexpression, we can also consider mild under- and overexpression. It was observed in [9] that under-expression seems to reduce the average tip-to-branch distance. It is important to realise that a change in DivIVA expression will probably not only affect the binding parameter β (since $\beta \equiv \beta\rho$, with ρ the cytoplasmic DivIVA density and β a constant), but also the tip growth speed v . This is because DivIVA is a critical component of the tip-organizing complex, which is present at all growing tips, and which is presumably important for tip extension. Since N_0 and N_{br} are unlikely to depend strongly on DivIVA levels, Eq. (1) shows that it is actually the ratio v/β which controls the average tip-to-branch distance. When DivIVA is underexpressed it is likely that both v and β decrease. Since in this case the average tip-to-branch distance decreases, this result suggests that v proportionally decreases by more than β . In the case of overexpression β will increase. However, it is less likely that v will also increase. This is because the tip-organizing complex, which is responsible for tip extension, is likely to consist of many components, of which DivIVA is only one. Unless other components in addition to DivIVA are overexpressed, the effect on tip growth speed could be small, with v remaining approximately constant. Thus we predict that mild overexpression of DivIVA will reduce v/β and so decrease the average tip-to-branch distance. If this is the case, then both mild under- and overexpression of DivIVA will reduce the average tip-to-branch distance, with wild-type levels corresponding to the longest tip-to-branch distance.

Discussion

Streptomyces, like other bacteria, lack the motor proteins, vesicle transport systems, and polarisome components that are fundamental in eukaryotic cell biology. Thus, tip extension in *Streptomyces* is likely to be simpler than in, for example, filamentous fungi. Given that a complex of polarity proteins (including DivIVA) must presumably first gather at future branch sites, understanding branch-site selection in filamentous bacteria involves understanding where, when and how these proteins cluster together in sufficiently large groups. One surprising feature of wild-type *Streptomyces* is that this clustering of polarity proteins is not a random, spontaneous process. Rather, we have shown that new branch sites are predominantly created from the tips of previous branches, by a tip-focus splitting mechanism.

One important question concerns the benefit of producing foci, and hence branches, by tip-focus splitting rather than spontaneous nucleation. One possibility is that this provides a more efficient

method of acquiring nutrients. Spontaneous nucleation will produce new branches at positions well behind the tips. This outcome would be suboptimal since regions far behind the tips are likely to have already been well-exploited, with few remaining nutrients. Tip-focus splitting, on the other hand, only generates new foci at tips and so biases branching towards the growing ends of hyphae, where nutrients are still more plentiful. Another potential advantage is that tip-focus splitting allows for a greater level of control over exactly where branching occurs. Unlike spontaneous nucleation where branches can appear anywhere, tip-focus splitting produces branches with an average tip-to-branch distance determined by parameters such as the initial tip-focus size and the binding parameter. By modifying these parameters, it is possible to respond to external stimuli. For example, under conditions when branching further from the tip would be favourable, we speculate that this could be achieved by modifying DivIVA (or other proteins that affect its assembly) so that the binding parameter is decreased (this would correspond to a shift from the morphology shown in Figure S10B to that in Figure S10A).

The morphology of branching organisms can be characterized by both the distance from the tip that new branches appear and the inter-branch distance. Counter-intuitively, our model shows that these distances are controlled by rather different processes. The tip-to-branch distance is governed by how long it takes new foci to gather enough molecules to initiate a new branch. This is related to the initial focus size, N_0 , the size at which a new branch is initiated, N_{br} , the tip growth speed, v , and the binding parameter, β . In contrast, the branch-to-branch distance is governed by how often foci are formed (how long foci take to develop into branches is now irrelevant). This is dependent on a partly overlapping, but nevertheless distinct set of parameters: the minimum tip-focus size for splitting, N_{split} , the initial focus size, N_0 , the tip growth speed, v , the binding parameter, β , and the tip-focus splitting parameter, γ .

We have focused on the control of branching during vegetative growth. However, there is a parallel question about how the first germ tube emerges from a spore. By imaging germinating spores expressing functional *divIVA-EGFP*, it has been shown that, exactly as in vegetative growth, a focus of DivIVA is first observed on the spore envelope, which then grows in size before initiating the first branch [9]. It is interesting to inquire how this first focus is formed. It is clear that the tip-focus splitting mechanism cannot be responsible since there are no previous DivIVA foci from which the first focus could arise. It is possible that other proteins, such as SsgA [17], aid DivIVA focus formation during spore germination. However, there is another possibility, that the spontaneous nucleation mechanism which plays a role when DivIVA is heavily overexpressed, is also responsible for the first DivIVA focus in a spore. If this is the case, then the DivIVA concentration within a spore would have to first rise high enough to overcome the nucleation barrier, an effect which may well be testable.

In fungi, branching also occurs at the cellular level and involves establishment of new cell poles at which apical growth will occur [18]. An apical cluster of vesicles and cytoskeletal elements named the Spitzenkörper has a prominent role in fungal tip extension. During branching, a new Spitzenkörper structure is established at the nascent branch tip, aided by proteins that direct cell polarity, cytoskeletal reorganisation, vesicle transport, and exo- and endocytosis (for reviews, see e.g. [18–21]). One of the components that appears to be involved in branch site selection prior to assembly of the Spitzenkörper structure is the protein complex termed the polarisome. Homologs of the budding yeast polarisome component Spa2p have been detected at hyphal tips in several fungi, and intriguingly, in *Neurospora crassa*, small foci of SPA-2-GFP were observed to detach from the major SPA-2 assemblies at elongating hyphal tips and subsequently give rise to new lateral

branches [12]. This observation strongly suggests that, in addition to streptomycetes, tip-focus splitting mechanisms are also involved in the establishment of new hyphal branches in filamentous fungi.

Streptomycetes appear to regulate hyphal growth and branching in a simple way. Indeed, we have found that a remarkably simple model can quantitatively explain the statistical properties of the entire hyphal network. Even the bimodal nature of the tip-to-branch distribution originates from a single mechanism of forming new foci, combined with variation in the parameter values. It is tempting to speculate that tip-focus splitting might be used by many filamentous organisms amongst fungi and Actinobacteria. In fact, focus splitting could turn out to be a general mechanism in situations where discrete foci must be generated in a growing organism.

Materials and Methods

Strains, general methods and microscopy

S.coelicolor A3(2) strains M600 (SCP1⁻ SCP2⁻), M145 (SCP1⁻ SCP2⁻) and K112 [*divIVA*⁺/ Φ (*divIVA*–*egfp*)Hyb], which produces DivIVA-EGFP, were pregerminated and cultivated at 30°C in YEME medium [22]. Hyphae were prepared for microscopy as described previously [9]. Samples were observed through a DIC 63 \times objective of a Nikon Eclipse 800 microscope equipped with a Pixera ProES600 camera and still images were taken with Pixera software and processed with ImageJ (National Institute of Health USA).

Time-lapse imaging

Live cell time-lapse microscopy was performed essentially as described in [10]. In brief, hyphae of *S.coelicolor* strains were grown on 1% agarose pads with Oxoid antibiotic medium no. 3. Pads were sealed to the bottom by an oxygen-permeable Lumox Biofoil 25 membrane (Greiner Bio-One) and to the top by a coverslip. Samples were incubated at 24 to 27°C and observed using a Zeiss Axio Imager Z1 microscope, a 9100-02 EM-CCD camera (Hamamatsu Photonics), and Volocity 3DM software (Improvision). Images were captured every 6 minutes, processed by Volocity and analysed using ImageJ.

Measurement of tip-to-branch distances

Still images do not normally capture the exact instant at which a new branch emerges. To find the tip-to-branch distance at the moment the branch emerged, we measure the length of the new branch, calculate how long it has been growing for, and determine where the tip was when the new branch emerged. The calculation incorporates an initial speed for new branch growth of about half that of established branches, increasing linearly in time until full speed is reached after about ninety minutes (see Figure S1). For details see the Supporting Text S1.

Controlling for biases

When measuring tip-to-branch and branch-to-branch distances from still images, it is important to control biases that artificially skew the data. For example, as an extreme case, if the measured hyphae segments were all less than 60 μm in length, it would then be impossible to measure any branch-to-branch distance greater than 60 μm . To control this problem we use the following protocol. Before any measurements are performed, all hyphae must be trimmed to some fixed length Λ : any hyphae shorter than this are discarded and, for those which are longer, only the segment within a distance Λ of the tip is included in the data set. The effect of trimming is to ensure that all measured hyphae are effectively of length Λ . As a consequence, both the tip-to-branch and branch-to-branch distributions explicitly depend on the trimming length Λ .

Estimation of average tip-to-branch distance

Estimating the average tip-to-branch distance from still images is complicated by the need to impose the trimming protocol on all measured data. The true average tip-to-branch distance is the average tip-to-branch distance at infinite trim. Distributions at progressively smaller trims have progressively smaller average tip-to-branch distances. The largest trim that we have a reasonable amount of data for is 120 μm , with an average tip-to-branch distance of 67 μm . It is not obvious that this trim is sufficiently high to give a good estimate of the true average tip-to-branch distance. However, by fitting the full distributions at 60 μm , 80 μm and 100 μm trims and extrapolating to infinite trim, this is seen to be a good approximation to the true average.

Simulation details

We give details of the minimal model simulation here; details of the full model simulation can be found in Supporting Text S1. We simulate the growth of a single hypha starting with a single DivIVA focus at the tip (initially of size N_{br}) and keeping track of where branches appear. At each time step ($\Delta t = 10^{-4}$ s), the hypha length is increased by $v\Delta t$, the tip-focus is increased in size according to $\Delta N = \beta N \Delta t$, and the tip-focus splitting rules are implemented (i.e. a tip-focus above N_{split} has a probability $\gamma \Delta t$ of splitting). If a new focus is created then its initial and final sizes, N_0 and N_{br} , are chosen at random from truncated normal distributions, after which Eq. (1) gives the tip-to-branch distance. After the hypha has grown to sufficient length (we grow the hypha to twice the trim length in order to effectively randomise the initial conditions), the tip-to-branch and branch-to-branch distances are measured if they satisfy the trimming protocol with trim Λ , i.e. tip-to-branch distances are recorded only if the branch appears within a distance Λ of the tip, and branch-to-branch distances are recorded only if both branches are within a distance Λ of the tip.

Supporting Information

Figure S1 Tip growth speed against time in Oxoid antibiotic medium for an established hypha and a newly formed branch. Error bars show the standard error of the mean. (EPS)

Figure S2 Experimental distribution of distances from parent hypha to first offshoot at 35 μm trim. 44 data points. (EPS)

Figure S3 Comparison of model histograms at 80 μm trim with $\langle N_0 \rangle = 1,700$ and $\langle N_0 \rangle = 3,000$. (A) Tip-to-branch distribution. (B) Branch-to-branch distribution. (EPS)

Figure S4 Comparison of histograms at 80 μm trim for linear growth model ($\dot{N} = \beta N$, parameters in Table 1) and constant growth model ($\dot{N} = \beta_0$, $v = 8 \mu\text{m hr}^{-1}$, $\beta_0 = 0.29 \text{ s}^{-1}$, $\langle N_0 \rangle = 1,300$, $\delta N_0 = 850$, $\langle N_{\text{br}} \rangle = 10,000$, $\delta N_{\text{br}} = 3,000$, $\gamma = 2.5 \times 10^{-3} \text{ s}^{-1}$, $N_{\text{split}} = 10,000$). (A) Tip-to-branch distribution. (B) Branch-to-branch distribution. (EPS)

Figure S5 Analytic tip-to-branch distribution with infinite trim. This represents the “true” underlying distribution which can never be directly measured experimentally. (EPS)

Figure S6 Requirement for a branch to be included in the data set. (A) A growing branch which will be measured when it has grown another $\Lambda \mu\text{m}$. (B) A new focus is created at distance x from the base. (C) This focus develops into a branch after the tip has

grown a further $L\mu\text{m}$, i.e. this branch has a tip-to-branch distance of $L\mu\text{m}$. (D) Only branches within Λ of the tip are used to collect data. So this branch will only be recorded if $x + L < \Lambda$. (EPS)

Figure S7 Behaviour of the mode of the tip-to-branch distance distribution as a function of various model parameters, for both an infinite trim (blue line) and an $80\mu\text{m}$ trim (red line). The infinite trim line is always higher than the $80\mu\text{m}$ trim line. The black dotted line shows the wild-type parameter value. (A) As a function of the binding parameter, β . (B) As a function of the mean initial focus size, $\langle N_0 \rangle$. (C) As a function of the mean focus size for branch initiation, $\langle N_{\text{br}} \rangle$. (EPS)

Figure S8 Comparison of distributions between the minimal model and experimental data at $60\mu\text{m}$ trim. Analytic tip-to-branch distribution is also shown (curved line). (A) Tip-to-branch distribution. 1876 experimental data points. (B) Zoomed tip-to-branch distribution. (C) Branch-to-branch distribution. 1215 experimental data points. (EPS)

Figure S9 Comparison of distributions between the minimal model and experimental data at $100\mu\text{m}$ trim. Analytic tip-to-branch distribution is also shown (curved line). (A) Tip-to-branch distribution. 297 experimental data points. (B) Zoomed tip-to-branch distribution. (C) Branch-to-branch distribution. 257 experimental data points. (EPS)

Figure S10 Schematic of colony morphology for various values of the binding parameter, β . Red dots represent DivIVA foci. (A) Small value of β . (B) Wild-type value of β . (C) Large value of β . (EPS)

Text S1 Supporting text. (PDF)

References

- DePedro MA, Quintela JC, Holtje JV, Schwarz H (1997) Murein segregation in *Escherichia coli*. J Bacteriol 179: 2823–2834.
- Daniel RA, Errington J (2003) Control of cell morphogenesis in bacteria: two distinct ways to make a rod-shaped cell. Cell 113: 767–776.
- Margolin W (2009) Sculpting the Bacterial Cell. Curr Biol 19: R812–822.
- Young KD (2010) Bacterial shape: two-dimensional questions and possibilities. Annu Rev Microbiol 64: 223–240.
- Domínguez-Escobar J, Chastanet A, Crevenna AH, Fromion V, Wedlich-Söldner R, et al. (2011) Processive movement of MreB-associated cell wall biosynthetic complexes in bacteria. Science 333: 225–228.
- Garner EC, Bernard R, Wang W, Zhuang X, Rudner DZ, et al. (2011) Coupled, circumferential motions of the cell wall synthesis machinery and MreB filaments in *B. subtilis*. Science 333: 222–225.
- Flårdh K, Buttner MJ (2009) *Streptomyces* morphogenetics: dissecting differentiation in a filamentous bacterium. Nat Rev Microbiol 7: 36–49.
- Flårdh K (2010) Cell polarity and the control of apical growth in *Streptomyces*. Curr Opin Microbiol 13: 758–765.
- Flårdh K (2003) Essential role of DivIVA in polar growth and morphogenesis in *Streptomyces coelicolor* A3(2). Mol Microbiol 49: 1523–1536.
- Hempel AM, Wang S, Letek M, Gil JA, Flårdh K (2008) Assemblies of DivIVA mark sites for hyphal branching and can establish new zones of cell wall growth in *Streptomyces coelicolor*. J Bacteriol 90: 7579–7583.
- Walshaw J, Gillespie MD, Kelemen GH (2010) A novel coiled-coil repeat variant in a class of bacterial cytoskeletal proteins. J Struct Biol 170: 202–215.
- Araujo-Palomares CL, Riquelme M, Castro-Longoria E (2009) The polarisome component SPA-2 localizes at the apex of *Neurospora crassa* and partially colocalizes with the Spitzenkörper. Fungal Genet Biol 46: 551–563.
- Lu C, Stricker J, Erickson HP (1998) FtsZ from *Escherichia coli*, *Azotobacter vinelandii*, and *Thermotoga maritima*—quantitation, GTP hydrolysis, and assembly. Cell Motil Cytoskeleton 40: 71–86.
- Ramamurthi KS, Losick R (2009) Negative membrane curvature as a cue for subcellular localization of a bacterial protein. Proc Natl Acad Sci U S A 106: 13541–13545.
- Lenarcic R, Halbedel S, Visser L, Shaw M, Wu LJ, et al. (2009) Localisation of DivIVA by targeting to negatively curved membranes. EMBO J 28: 2272–2282.
- Howard J (2001) Mechanics of Motor Proteins and the Cytoskeleton. Massachusetts: Sinauer Associates. 384 p.
- Noens, et al. (2009) Loss of the controlled localization of growth stage-specific cell-wall synthesis pleiotropically affects developmental gene expression in an *ssgA* mutant of *Streptomyces coelicolor*. Mol Microbiol 64: 1244–1259.
- Harris SD (2009) Branching of fungal hyphae: regulation, mechanisms and comparison with other branching systems. Mycologia 100: 823–832.
- Fischer R, Zekert N, Takeshita (2008) Polarized growth in fungi – interplay between the cytoskeleton, positional markers and membrane domains. Mol Microbiol 68: 813–826.
- Steinberg G (2007) Hyphal growth: a tale of motors, lipids, and the Spitzenkörper. Eukaryotic Cell 6: 351–360.
- Riquelme, et al. (2011) Architecture and development of the *Neurospora crassa* hypha – a model cell for polarized growth. Fungal Biol 115: 446–474.
- Kieser T, Bibb MJ, Buttner MJ, Chater KF, Hopwood DA (2000) Practical *Streptomyces* Genetics. Norwich (UK): The John Innes Foundation. 613 p.

Video S1 Movie version of Figure 1. Evidence of tip-focus splitting, growth of foci and emergence of branches, in fluorescence-imaged *Streptomyces coelicolor* expressing *divIVA-egfp*. Time in hours:minutes:seconds. (MOV)

Video S2 Movie version of Figure 3. Example of branching at almost zero distance from the tip. Time in hours:minutes:seconds. (MOV)

Video S3 Example of the full model simulation output, showing *Streptomyces* starting from a spore and growing for about fourteen hours. Hyphae in green; DivIVA foci in red. (GIF)

Video S4 Large-scale example of the full model simulation output, showing *Streptomyces* starting from a spore and growing for about eleven hours. Hyphae in green; DivIVA foci in red; cross-walls in yellow. (GIF)

Video S5 Large-scale example of the full model simulation output with 25-fold overexpression of DivIVA. Simulation lasts for about seven hours with overexpression occurring after 14,000 s. Hyphae in green; DivIVA foci in red; cross-walls in yellow. (GIF)

Acknowledgments

We thank Liam Dolan for useful discussion.

Author Contributions

Conceived and designed the experiments: DMR AMH KF MJB MH. Performed the experiments: DMR AMH. Analyzed the data: DMR AMH. Wrote the paper: DMR AMH KF MJB MH.

Supporting Text S1

Data analysis

Tip growth speed

New branches do not grow at the same speed as established branches. Instead the tips of new branches initially extend more slowly and gradually increase in speed before attaining full speed. To quantitatively analyse this increase, we used our time-lapse imaging to measure the extension rate of 45 established and 40 new branches. Figure S1 shows the mean new branch growth speed against time (starting from when the branch first appears), and compares this to the mean growth speed of established hyphae. Using the same data we can also estimate the fluctuations in the initial and established extension speeds, from which we conclude that new branches initially grow at about $v_0 = 4 \pm 2 \mu\text{mhr}^{-1}$, and then gradually increase (approximately linearly) in speed until they reach $v_{\text{max}} = 8 \pm 4 \mu\text{mhr}^{-1}$ after about $T = 1.5$ hours.

Subtraction of branch lengths

As explained in *Materials and Methods*, the experimental data do not show new branches at the exact moment that they emerge. Instead it is necessary to infer the tip-to-branch distance, L , at the moment of branching. This involves knowledge of the tip growth speed of new branches, v_0 , the tip growth speed of established branches, v_{max} , and how long new branches take to reach full speed, T . However, these three parameters will differ from branch to branch. If fixed values are used then this will lead to incorrect tip-to-branch distances; in extreme cases, this can even lead to negative distances for tip-to-branch distances. Ideally it would be necessary to determine v_0 , v_{max} and T for each branch, although this is not possible from still images. Instead, we determine a distribution of tip-to-branch distances for each measured branch. To do this we allow all three parameters to fluctuate according to Gaussian distributions (which are truncated to ensure $0 < v_0 < v_{\text{max}}$ and $T > 0$). Each set $\{v_0, v_{\text{max}}, T\}$ leads to a tip-to-branch distance and the variations in the parameters leads to a distribution for L . Negative values of L are unphysical and so the distributions are truncated to remove negative distances and rescaled so that they still have unit area. The complete measured tip-to-branch distribution is obtained by summing the distributions derived from all the individual measured branches. The means and standard deviations for v_0 , v_{max} and T are taken from the above data in Oxoid antibiotic

medium. Although these values are likely to be altered in YEME medium, we have tried a wide range of values for each and discovered that changing the values of some or all of v_0 , v_{\max} and T by 100% or more makes little difference to the final histogram. Although this may appear counter-intuitive, the absolute tip growth speed cancels out of the branch-subtraction procedure; it is only the difference between v_0 and v_{\max} over the relatively short period T that is relevant.

Hyphal-base to first-offshoot distribution

In order to constrain the value of N_{split} , we measured the distance between the base of hyphae (where the hypha originates from its parent hypha) and the first (i.e. nearest) offshoot branch. If $N_{\text{split}} > \langle N_{\text{br}} \rangle$ then there should be a gap, during which the tip-focus of the new branch is growing in size, before it can form its own offshoot branches. As with measuring the tip-to-branch and branch-to-branch distributions, it is important to impose a trimming protocol. The results at $35\mu\text{m}$ trim are shown in Figure S2. The data is well fit by a decaying exponential. This is the behaviour expected if N_{split} is equal to (or less than) $\langle N_{\text{br}} \rangle$ since then new tip-foci have the potential to split almost straight away after branching initiation. Since there is no evidence for a gap before new hyphae can form their own branches, we conclude that $N_{\text{split}} \leq \langle N_{\text{br}} \rangle$.

Model robustness

Robustness to changes in mean parameter values and in size of fluctuations

Our model is robust to changes in all eight parameters in Table 1. For example, if we take $\langle N_0 \rangle$ as 3,000 rather than 1,700, then, although the distributions and their averages are changed to some extent, there is no overall qualitative difference (Figure S3). The same applies if we decrease $\langle N_0 \rangle$, or if we vary the other parameters by up to 30% of their size.

The minimal model only considers fluctuations in N_0 and N_{br} , which are sufficient to capture the observed distributions. However, there is no reason why the other parameters, in particular the tip growth speed, v , and the on-rate parameter, β , should not also vary. If these are also allowed to vary, even by up to 25% each, then there is no qualitative difference in either the tip-to-branch or branch-to-branch distributions.

Robustness to distribution of fluctuations

In the simplest version of the model, we assume a truncated normal distribution for N_0 with mean $\langle N_0 \rangle = 1,700$ and standard deviation $\delta N_0 = 1,000$. Although simple, this leads to a large, potentially unrealistic, weight for producing foci of very small size. To rectify this it is possible to consider other distributions where the distribution drops towards zero for small initial foci sizes. We considered three types of distribution: log-normal, gamma, and a distribution that is triangular for small foci and Gaussian for large foci. Each distribution had a similar mean and standard deviation to the original truncated Gaussian distribution. In each case there was little qualitative difference from the truncated Gaussian case, showing that the exact shape of the N_0 distribution is not important for our results. We also considered log-normal and gamma distributions for N_{br} , which again made little difference.

Robustness to foci growth dynamics and foci evaporation

In the main text we implemented a rule where a focus containing N DivIVA molecules increases in size at a rate proportional to its size: $\dot{N} = \beta N$. However, we can consider other rules, such as a constant on-rate ($\dot{N} = \beta_0$), or even some combination of the two ($\dot{N} = \beta_0 + \beta N$). Also, we have assumed that foci can capture DivIVA molecules from the cytoplasm but can never return them, i.e. there is no off-rate. However, if we assume that the off-rate is either constant, linear in N , or some combination of the two, then including an off-rate just implies that β_0 and β are rescaled. In any case, we find that these alternative growth laws do not qualitatively change any of our results, and do not lead to a better fit with the experimental data. For example, Figure S4 shows the distributions when a constant growth rule ($\dot{N} = \beta_0$) is implemented.

It is possible that foci can spontaneously evaporate by detaching into the cytoplasm. However, it is difficult to directly observe this potential effect since foci often move out of the focal plane, thereby disappearing. We considered a simple extension to the minimal model where developing foci (i.e. those which have not yet initiated a branch) have a fixed probability per second of evaporating. Even with a probability such that over half of all foci evaporate before initiating a branch, there is little change to the model distributions. This is because the tip-to-branch distribution is determined only by those foci which eventually initiate branches, whereas any change in the branch-to-branch distribution can be compensated by increasing the tip-focus splitting parameter, γ .

Analytic results

Analytic expression for the tip-to-branch distribution

Starting from Eq. (1) and by varying both N_0 and N_{br} , we can derive an analytic expression for the distribution of the tip-to-branch distance, L . We assume that both N_0 and N_{br} follow independent truncated normal distributions with means μ_0 and μ_{br} and standard deviations σ_0 and σ_{br} respectively¹. The probability density function (pdf) for N_0 is given by

$$f_0(N_0) = \begin{cases} 0 & \text{if } N_0 \leq 0, \\ \frac{1}{\sqrt{2\pi}\sigma_0\Phi\left(\frac{\mu_0}{\sigma_0}\right)} e^{-\frac{(N_0-\mu_0)^2}{2\sigma_0^2}} & \text{if } N_0 > 0, \end{cases} \quad (\text{S1})$$

where $\Phi(x)$ is the standard normal cumulative distribution function,

$$\Phi(x) = \frac{1}{\sqrt{2\pi}} \int_{-\infty}^x e^{-\frac{1}{2}t^2} dt.$$

A similar expression holds for $f_{\text{br}}(N_{\text{br}})$, the pdf for N_{br} . First, we determine the distribution of $u \equiv \frac{N_{\text{br}}}{N_0}$, which we write as $g(u)$. The ratio of two distributions is a standard result:

$$g(u) = \int_{-\infty}^{\infty} |x| f_0(x) f_{\text{br}}(ux) dx.$$

Since f_0 and f_{br} vanish for negative values, the lower limit can be replaced by 0 and the $|x|$ by x . Evaluating the integral gives

$$g(u) = \begin{cases} 0 & \text{if } u \leq 0, \\ \frac{e^{-\frac{c}{2}}}{\sqrt{2\pi}\sigma_0\sigma_{\text{br}}\Phi\left(\frac{\mu_0}{\sigma_0}\right)\Phi\left(\frac{\mu_{\text{br}}}{\sigma_{\text{br}}}\right)\tilde{a}(u)^{\frac{3}{2}}} \left(\sqrt{\frac{\tilde{a}(u)}{2\pi}} + \tilde{b}(u) e^{\frac{\tilde{b}(u)^2}{2\tilde{a}(u)}} \Phi\left(\frac{\tilde{b}(u)}{\sqrt{\tilde{a}(u)}}\right) \right) & \text{if } u > 0, \end{cases}$$

where

$$\begin{aligned} \tilde{a}(u) &= \frac{1}{\sigma_0^2} + \frac{1}{\sigma_{\text{br}}^2} u^2, \\ \tilde{b}(u) &= \frac{\mu_0}{\sigma_0^2} + \frac{\mu_{\text{br}}}{\sigma_{\text{br}}^2} u, \\ c &= \frac{\mu_0^2}{\sigma_0^2} + \frac{\mu_{\text{br}}^2}{\sigma_{\text{br}}^2}. \end{aligned}$$

¹Here μ_0 and μ_{br} are the means of the full Gaussians, rather than those of the truncated Gaussians. The same also applies to the standard deviations, σ_0 and σ_{br} .

Finally, we can determine the distribution of L , $h(L)$, by using $L = \frac{v}{\beta} \ln u$ and the fact that $|h(L)dL| = |g(u)du|$. Negative values of L imply that $N_0 > N_{\text{br}}$ and so, as discussed in the main text, these branches will emerge at zero distance from the tip and so should really contribute at $L = 0$. So the entire weight of $h(L)$ for negative L should be placed at $L = 0$. We achieve this by using a delta function at the origin of u . Then our final expression for the tip-to-branch distribution, $\bar{h}(L)$, becomes

$$\bar{h}(L) = \begin{cases} 0 & \text{if } L < 0, \\ \delta(L) \int_{-\infty}^0 h(\tilde{L}) d\tilde{L} + h(L) & \text{if } L \geq 0, \end{cases} \quad (\text{S2})$$

where

$$h(L) = \frac{\beta e^{\frac{\beta}{v}L - \frac{c}{2}}}{\sqrt{2\pi}v\sigma_0\sigma_{\text{br}}\Phi\left(\frac{\mu_0}{\sigma_0}\right)\Phi\left(\frac{\mu_{\text{br}}}{\sigma_{\text{br}}}\right)a(L)^{\frac{3}{2}}} \left(\sqrt{\frac{a(L)}{2\pi}} + b(L)e^{\frac{b(L)^2}{2a(L)}}\Phi\left(\frac{b(L)}{\sqrt{a(L)}}\right) \right),$$

and where

$$a(L) = \frac{1}{\sigma_0^2} + \frac{1}{\sigma_{\text{br}}^2} e^{2\frac{\beta}{v}L},$$

$$b(L) = \frac{\mu_0}{\sigma_0} + \frac{\mu_{\text{br}}}{\sigma_{\text{br}}} e^{\frac{\beta}{v}L}.$$

To compare this analytic solution to the numerical simulations, we must convert $\langle N_0 \rangle$, $\langle N_{\text{br}} \rangle$, δN_0 and δN_{br} (the means and standard deviations of the truncated Gaussians) to μ_0 , μ_{br} , σ_0 and σ_{br} (the means and standard deviations of the full Gaussians). Using the values in Table 1, where $\langle N_0 \rangle = 1,700$, $\langle N_{\text{br}} \rangle = 10,000$, $\delta N_0 = 1,000$ and $\delta N_{\text{br}} = 2,600$, we find that $\mu_0 \approx 1,500$, $\mu_{\text{br}} \approx 10,000$, $\sigma_0 \approx 1,200$ and $\sigma_{\text{br}} \approx 2,600$.

The resulting distribution (Figure S5) can never be measured experimentally since it corresponds to measuring tip-to-branch distances at infinite trim. However, it is in many ways the “true” underlying distribution, a distribution which is unbiased by experimental limitations.

Analytic expression for the trimmed tip-to-branch distribution

To compare Eq. (S2) with the measured data we must impose the same trimming protocol. By trimming all branches to some trim length Λ , it becomes less likely that we observe branches with longer tip-to-branch distances. This is because such branches emerge from foci which take longer to develop into branches and thus the associated tip-focus splitting event has a smaller time

frame in which it must have occurred. This is illustrated in Figure S6, where a branch with tip-to-branch distance L will only be measured if it was created within $\Lambda - L$ of the base of the hypha; if it is created nearer the tip than this, then the focus will not have originated a new branch by the time it is measured. Thus, assuming a constant probability per unit time of tip-focus splitting (which will be true when a sufficiently large number of hyphae are analysed), the probability of observing such a branch is scaled by a factor of $\Lambda - L$. This implies that the probability density function in Eq. (S2) should be scaled by the same factor. This gives the Λ -trimmed tip-to-branch distribution, $\bar{h}_\Lambda(L)$, as

$$\bar{h}_\Lambda(L) = \begin{cases} 0 & \text{if } L < 0, \\ \left(\frac{\Lambda-L}{\Lambda-\mu_{\bar{h}}}\right) \bar{h}(L) & \text{if } 0 \leq L < \Lambda, \\ 0 & \text{if } L \geq \Lambda, \end{cases} \quad (\text{S3})$$

where $\mu_{\bar{h}} = \int_0^\infty L \bar{h}(L) dL$ is the mean of $\bar{h}(L)$, and the $\Lambda - \mu_{\bar{h}}$ denominator is required to fix the normalisation.

The tip-to-branch distance as a function of the model parameters

In Figure S7 we show how the mode of the tip-to-branch distribution varies with (i) the binding parameter, β , (ii) the mean initial focus size, $\langle N_0 \rangle$, and (iii) the mean focus size for branch initiation, $\langle N_{\text{br}} \rangle$. With an infinite trim the behaviour is given by Eq. (1), which shows that $\langle L \rangle \sim 1/\beta$, $\langle L \rangle \sim \text{const} - \ln \langle N_0 \rangle$ and $\langle L \rangle \sim \text{const} + \ln \langle N_{\text{br}} \rangle$, where $\langle L \rangle$ here represents the mode of L . However, the behaviour is less intuitive when the trimming protocol is imposed. The most interesting case is when β is varied. At large values of β , the modal trimmed tip-to-branch distance tends to the untrimmed value. However, as β is reduced, the trimmed modal value reaches a maximum and begins to drop to zero as β is further reduced. This counter-intuitive behaviour is related to the trim length being much smaller than the true (i.e. infinite trim) modal tip-to-branch distance. It is worth recalling that it is only possible to directly measure the trimmed distribution and so, for any measured trimmed modal tip-to-branch distance, there are two possible values of β . However, it is easy to distinguish the correct value by the number of discarded hyphae (due to imposing the trimming protocol): the smaller β corresponds to a much greater true (i.e. infinite trim) modal distance and so results in a far greater number of discarded hyphae. We do not observe such a large number of discarded hyphae and so our wild-type β is the larger of the two possible values.

The full model

Despite the success of the minimal model described above and in the main paper, it is nevertheless useful to develop a full model including effects such as spatial and temporal gradients of the DivIVA concentration. This is important for two reasons: firstly, it justifies our claims that the extra parts of the full model play only a minor role, and secondly, the full model includes spontaneous nucleation which we need to understand heavy DivIVA overexpression.

Basic components

The full model is a one-dimensional simulation of an entire *Streptomyces* colony. Although there are stochastic elements, the diffusion, production and degradation of DivIVA is handled deterministically (see Table S1 for parameter values). This is justified since DivIVA for our parameters is present at high copy number (hundreds of copies per micron). Each hypha is represented by a 1D array specifying the cytoplasmic DivIVA density at that position, with a focus at the tip. Each site may or may not contain a focus on either the adjacent upper or lower membrane. After a new branch develops, an additional 1D array representing the new branch is generated. At each lattice site and time step, DivIVA is produced, degraded and diffuses using an Euler discretisation of the corresponding partial differential equation, with lattice spacing of $\Delta x = 0.1\mu\text{m}$ and a time step of $\Delta t = 10^{-4}\text{s}$. Diffusion is entirely one-dimensional apart from at points where branches meet, where two-dimensional diffusion occurs. Also, if there is an adjacent focus on the membrane, then DivIVA molecules can be recruited from the cytoplasm to the focus (and also in principle detach from the focus back to the cytoplasm). The number of molecules being recruited to a focus is linearly dependent on both the cytoplasmic DivIVA density at that point, ρ , and the number of molecules in the focus, N , such that $\Delta N = \tilde{\beta}\rho N\Delta t$, where $\tilde{\beta}$ is the binding constant. At each time step, the tip of each branch is extended by $v\Delta t$. Whenever the branch length (as measured in lattice steps) increases through an integer value, an extra lattice site is inserted (with the tip-focus now being adjacent to the newly-inserted site). Furthermore, tip-foci which contain more than N_{split} molecules have a constant probability at each time step of splitting to create new foci, which are placed on the membrane adjacent to the neighbouring cytoplasmic lattice site. When they do so the size of the focus left behind, N_0 , is chosen from a truncated Gaussian distribution of the form given in Eq. (S1). At the same time, the size that a focus needs to reach before a new branch is initiated, N_{br} , is chosen from a second truncated

Gaussian distribution of the same form. When that focus finally grows to a size N_{br} , a new branch is formed with the focus now sitting adjacent to the cytoplasmic site at the tip of that branch.

Additional processes

To the above form of the model we added various other effects. Firstly, spontaneous nucleation was included, where new foci could now arise at any membrane site along any hypha. This was implemented as a stochastic process where the probability of nucleation per unit time, η , on a membrane adjacent to each lattice site is dependent on the cytoplasmic DivIVA density, ρ , at that adjacent site and on a threshold concentration, ρ_{SN} (see [16]):

$$\eta = \begin{cases} 0 & \text{if } \rho \leq \rho_{\text{SN}}, \\ \tilde{\eta}(\rho - \rho_{\text{SN}}) & \text{if } \rho > \rho_{\text{SN}}, \end{cases} \quad (\text{S4})$$

where $\tilde{\eta}$ is a constant that is independent of ρ . Below the threshold, nucleation is assumed not to occur, whereas, above the threshold, the nucleation probability per unit time is assumed to increase linearly with the DivIVA concentration above the threshold. After nucleation, foci begin with a fixed size of $N_0 = 5$ and with N_{br} chosen in the same way as before, with the DivIVA for the new focus taken from the lattice site directly adjacent to the new focus. Parameter values for this and the other processes discussed here are listed in Table S1. Secondly, we included cross-walls which sometimes appear during vegetative growth and which can be visualised by fluorescently tagging FtsZ [S1]. For our purposes, the main effect of FtsZ is to isolate different compartments, preventing DivIVA from diffusing between them. It was shown in [S2] that FtsZ rings tend to form in a progressive manner, with subsequent Z-rings appearing closer to the tip. Rather than modelling the detailed dynamics of FtsZ and the formation of cross-walls, for each branch we simply included a constant probability per unit time ($1 \times 10^{-4}\text{s}^{-1}$) of forming a cross-wall; if a cross-wall is formed then its position is chosen randomly between the previous cross-wall and the tip. Thirdly, new branches initially extended at only half the speed of established branches, as found experimentally, thereafter gradually increasing in speed in a linear fashion, to achieve full speed after ninety minutes. Previously, in the minimal model, this effect was included only in the experimental extraction of tip-to-branch distances, rather than in the simulation itself.

Curved branch growth

We next consider non-straight tip-growth and allow the tip-growth direction to vary. It is possible that the curvature of the membrane just next to the tip is a factor influencing when tip-focus splitting occurs. Rather than trying to understand the details of what controls the tip-growth direction (not currently a tractable problem), at each time step we simply choose the new growth direction as the previous growth direction plus a Gaussian-distributed correction with zero mean. The width of this Gaussian (3.5° per new lattice site) is determined by the persistence length ($1.6\mu\text{m}$), which is the distance over which correlations in the growth direction are maintained. Once curved tip-growth is implemented, we can replace the tip-focus splitting parameter with a rule based on curvature: since DivIVA may preferentially form foci on negatively-curved membranes, we implement a rule where tip-foci split only if the local curvature near the tip (the change in tip direction over the last $1\mu\text{m}$ of growth) is sufficiently high (greater than 15°). This curvature threshold is chosen to reproduce the tip-focus splitting probability per unit time and to correctly match the branch-to-branch distribution. We also allow for a small probability of focus deposition on the membrane with the “wrong” local curvature (positive rather than negative; see Table S1).

Results

The full model (which uses the parameters in Table S1) produces output such as Videos S3 and S4, which match well with the observed *Streptomyces* phenotypes both in the wild type and when DivIVA is overexpressed. Despite the addition of effects such as cross-walls, DivIVA gradients and curvature-dependent tip-focus splitting, the full model is practically indistinguishable from the minimal model. In particular, there is no significant change in the tip-to-branch or branch-to-branch distributions. Thus the minimal model outlined in the main paper is sufficient to capture branching dynamics in *Streptomyces*. The full model is only needed when spontaneous nucleation becomes an important effect, such as when DivIVA is heavily overexpressed.

Table S1: Additional model parameters and their values

Parameter	Value
DivIVA cytoplasmic diffusion constant, D	$5\mu\text{m}^2\text{s}^{-1}$
DivIVA cytoplasmic production, μ	$0.2\mu\text{m}^{-1}\text{s}^{-1}$
DivIVA cytoplasmic degradation rate, ν	$5 \times 10^{-4}\text{s}^{-1}$
Binding constant, $\tilde{\beta}$	$3 \times 10^{-7}\mu\text{m}\text{s}^{-1}$
Spontaneous nucleation threshold, ρ_{SN}	$400\mu\text{m}^{-1}$
Spontaneous nucleation parameter, $\tilde{\eta}$	$5 \times 10^{-8}\mu\text{m}\text{s}^{-1}$
FtsZ ring creation probability per unit time	$1 \times 10^{-4}\text{s}^{-1}$
Distribution width for new growth direction	3.5°
Local curvature length	$1\mu\text{m}$
Tip-focus splitting curvature threshold	15°
Probability of “wrong”-side splitting	0.05

Supporting Text S1 References

- [S1] Grantcharova N, Lustig U, Flärdh K (2005) Dynamics of FtsZ Assembly during Sporulation in *Streptomyces coelicolor* A3(2) *J. Bacteriol.* 187:3227-3237.
- [S2] Jyothikumar V, Tilley EJ, Wali R, Herron PR (2008) Time-lapse microscopy of *Streptomyces coelicolor* growth and sporulation. *Appl. Environ. Microbiol.* 74:6774-6781.

Supporting Figure Legends

Figure S1: Tip growth speed against time in Oxoid antibiotic medium for an established hypha and a newly formed branch. Error bars show the standard error of the mean.

Figure S2: Experimental distribution of distances from parent hypha to first offshoot at $35\mu\text{m}$ trim. 44 data points.

Figure S3: Comparison of model histograms at $80\mu\text{m}$ trim with $\langle N_0 \rangle = 1,700$ and $\langle N_0 \rangle = 3,000$. (A) Tip-to-branch distribution. (B) Branch-to-branch distribution.

Figure S4: Comparison of histograms at $80\mu\text{m}$ trim for linear growth model ($\dot{N} = \beta N$, parameters in Table 1) and constant growth model ($\dot{N} = \beta_0$, $v = 8\mu\text{mhr}^{-1}$, $\beta_0 = 0.29\text{s}^{-1}$, $\langle N_0 \rangle = 1,300$, $\delta N_0 = 850$, $\langle N_{\text{br}} \rangle = 10,000$, $\delta N_{\text{br}} = 3,000$, $\gamma = 2.5 \times 10^{-3}\text{s}^{-1}$, $N_{\text{split}} = 10,000$). (A) Tip-to-branch distribution. (B) Branch-to-branch distribution.

Figure S5: Analytic tip-to-branch distribution with infinite trim. This represents the “true” underlying distribution which can never be directly measured experimentally.

Figure S6: Requirement for a branch to be included in the data set. (A) A growing branch which will be measured when it has grown another $\Lambda\mu\text{m}$. (B) A new focus is created at distance x from the base. (C) This focus develops into a branch after the tip has grown a further $L\mu\text{m}$, i.e. this branch has a tip-to-branch distance of $L\mu\text{m}$. (D) Only branches within Λ of the tip are used to collect data. So this branch will only be recorded if $x + L < \Lambda$.

Figure S7: Behaviour of the mode of the tip-to-branch distance distribution as a function of various model parameters, for both an infinite trim (blue line) and an $80\mu\text{m}$ trim (red line). The infinite trim line is always higher than the $80\mu\text{m}$ trim line. The black dotted line shows the wild-type parameter value. (A) As a function of the binding parameter, β . (B) As a function of the mean initial focus size, $\langle N_0 \rangle$. (C) As a function of the mean focus size for branch initiation, $\langle N_{\text{br}} \rangle$.

Figure S8: Comparison of distributions between the minimal model and experimental data at $60\mu\text{m}$ trim. Analytic tip-to-branch distribution is also shown (curved line). (A) Tip-to-branch distribution. 1876 experimental data points. (B) Zoomed tip-to-branch distribution. (C) Branch-to-branch distribution. 1215 experimental data points.

Figure S9: Comparison of distributions between the minimal model and experimental data at $100\mu\text{m}$ trim. Analytic tip-to-branch distribution is also shown (curved line). (A) Tip-to-branch distribution. 297 experimental data points. (B) Zoomed tip-to-branch distribution. (C) Branch-to-branch distribution. 257 experimental data points.

Figure S10: Schematic of colony morphology for various values of the binding parameter, β . Red dots represent DivIVA foci. (A) Small value of β . (B) Wild-type value of β . (C) Large value of β .

Video Legends

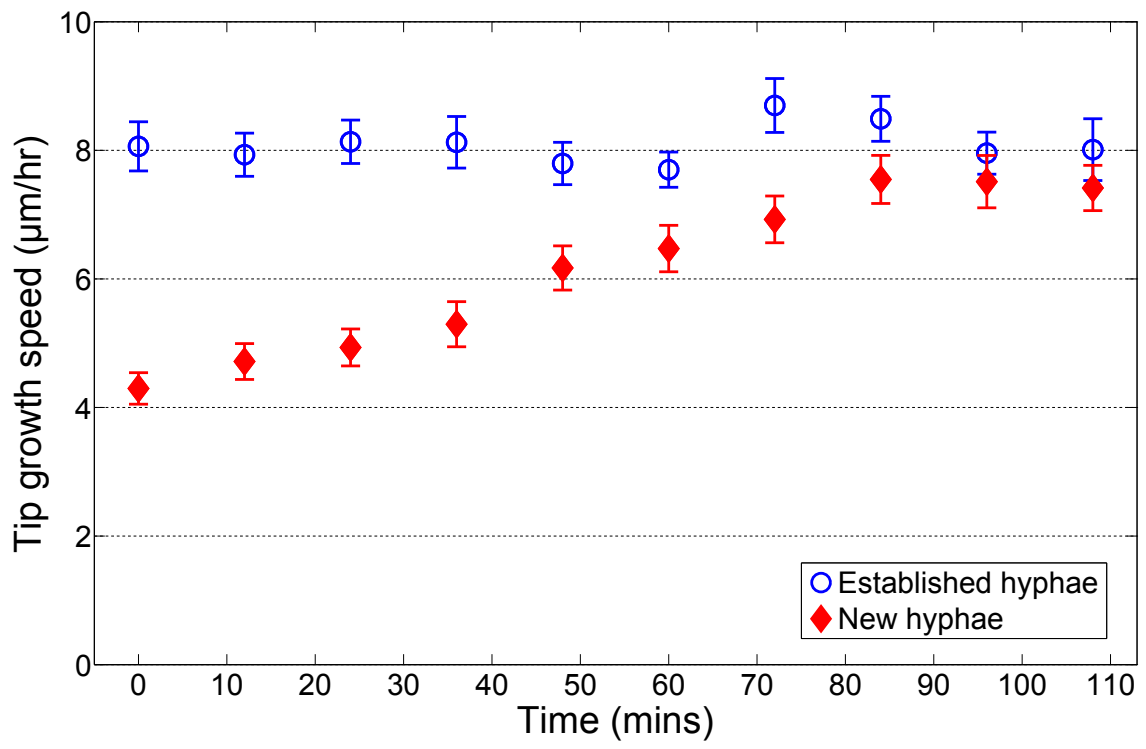
Video S1: Movie version of Figure 1. Evidence of tip-focus splitting, growth of foci and emergence of branches, in fluorescence-imaged *Streptomyces coelicolor* expressing *divIVA-egfp*.

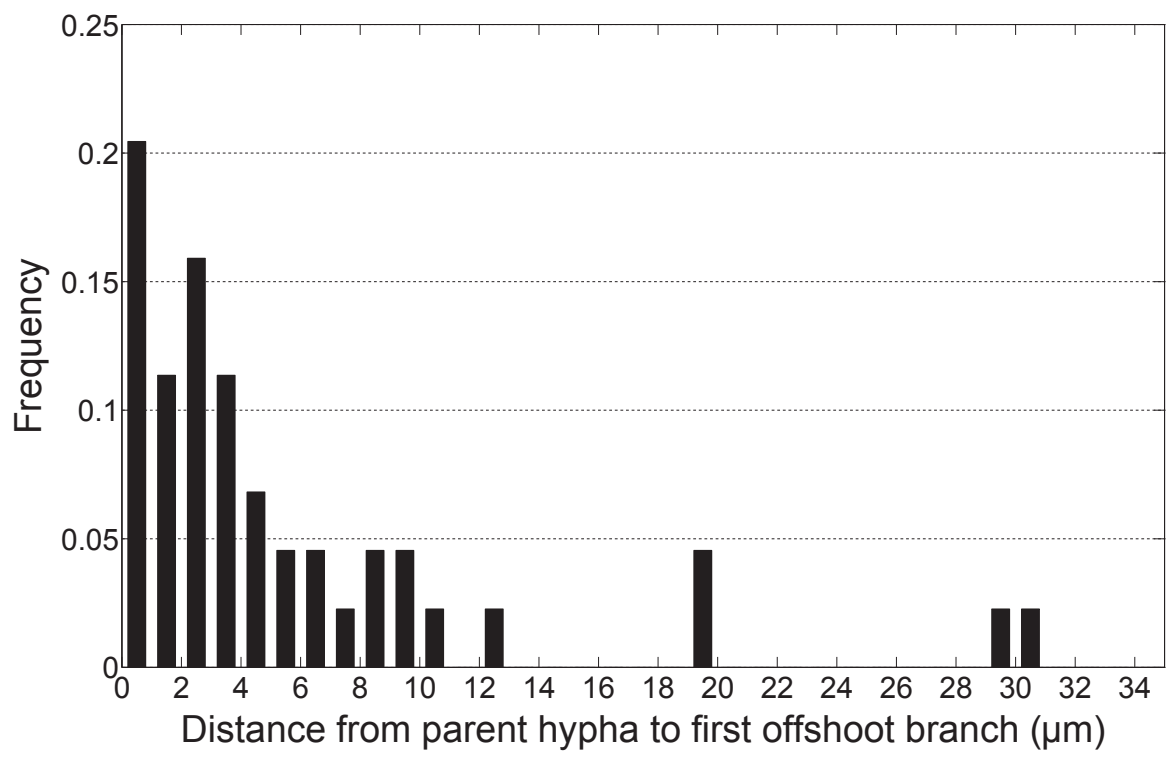
Video S2: Movie version of Figure 3. Example of branching at almost zero distance from the tip.

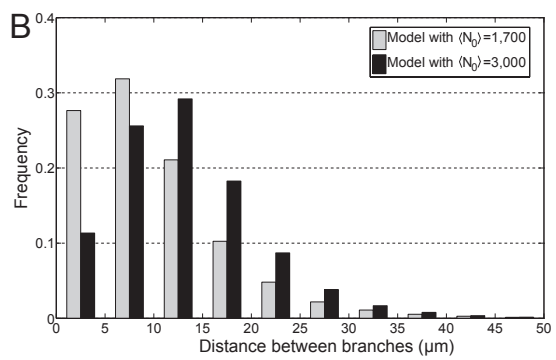
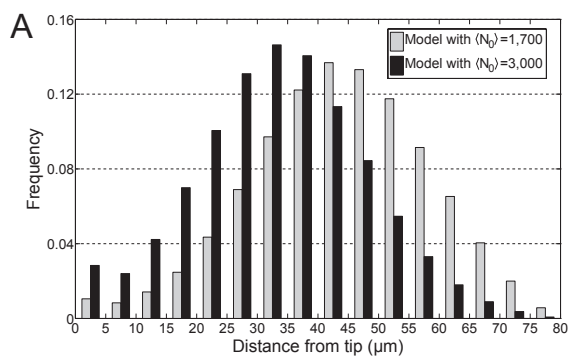
Video S3: Example of the full model simulation output, showing *Streptomyces* starting from a spore and growing for about fourteen hours. Hyphae in green; DivIVA foci in red.

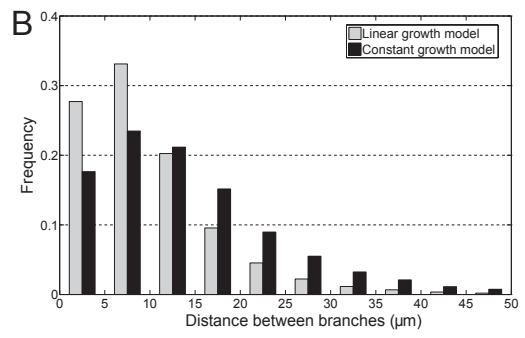
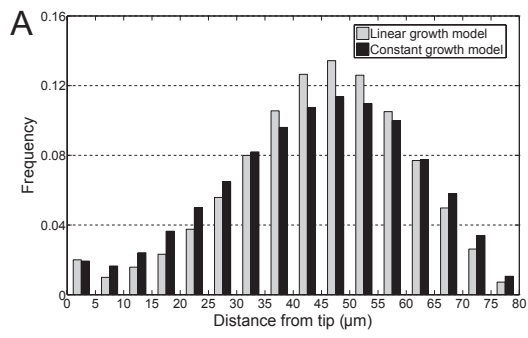
Video S4: Large-scale example of the full model simulation output, showing *Streptomyces* starting from a spore and growing for about eleven hours. Hyphae in green; DivIVA foci in red; cross-walls in yellow.

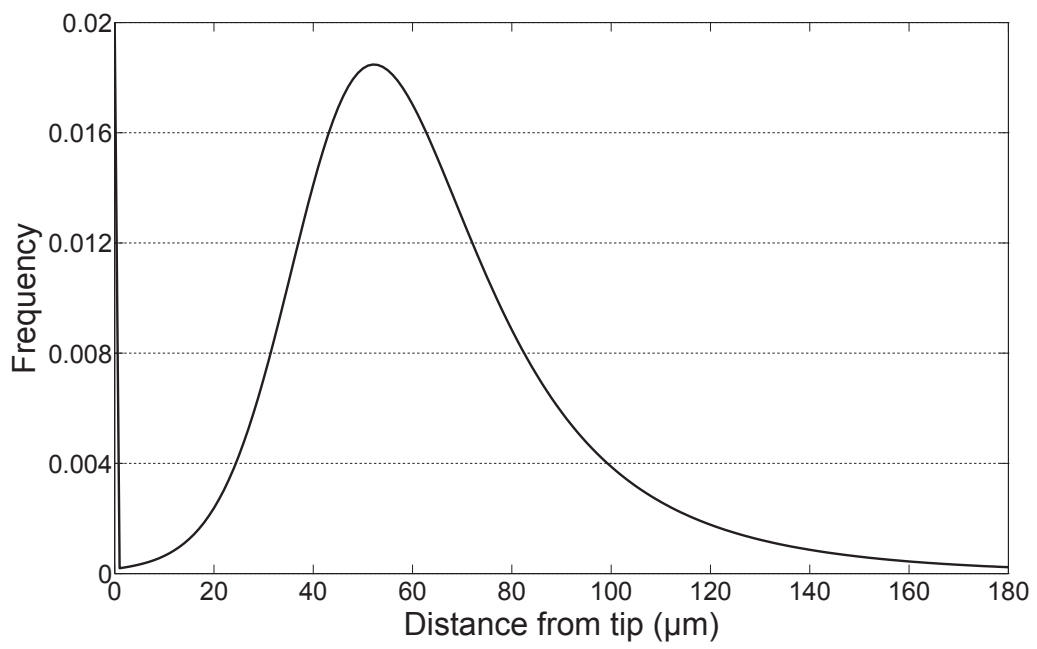
Video S5: Large-scale example of the full model simulation output with 25-fold overexpression of DivIVA. Simulation lasts for about seven hours with overexpression occurring after 14,000s. Hyphae in green; DivIVA foci in red; cross-walls in yellow.

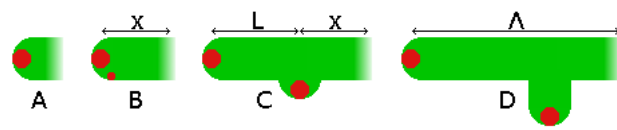


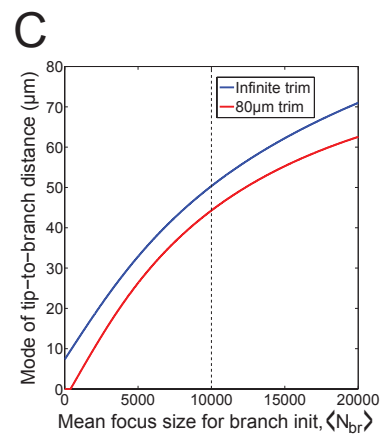
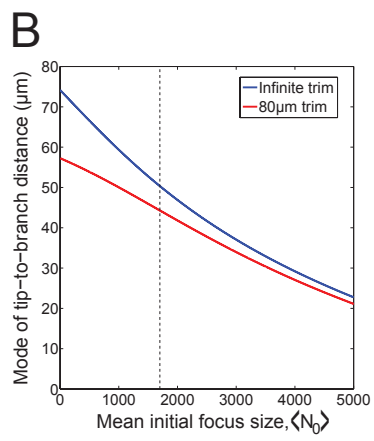
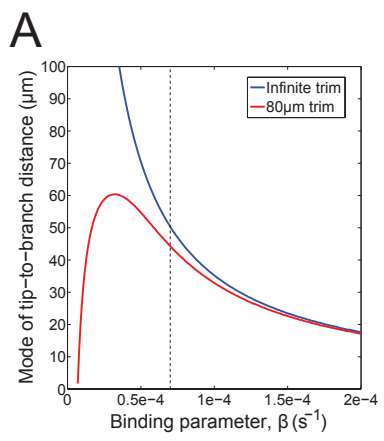


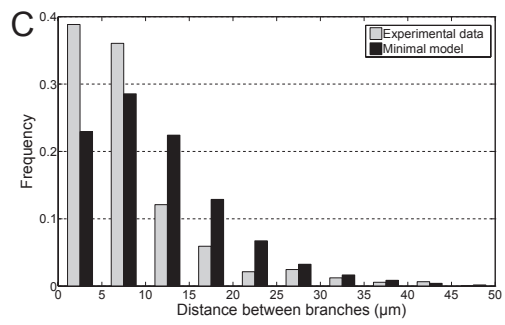
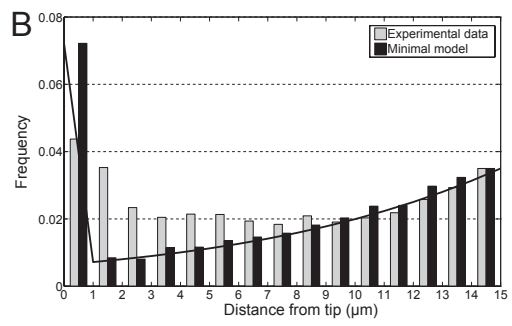
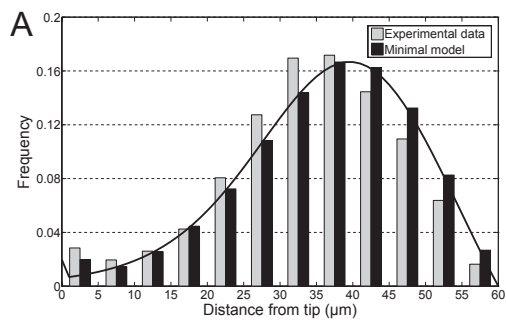


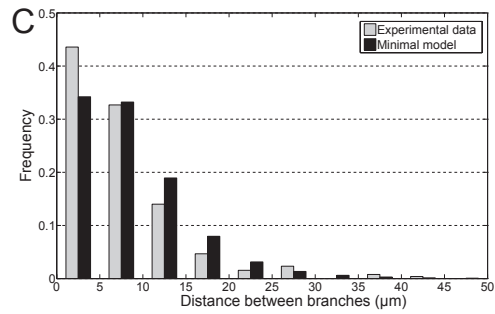
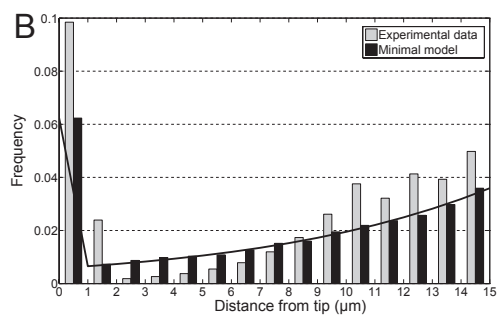
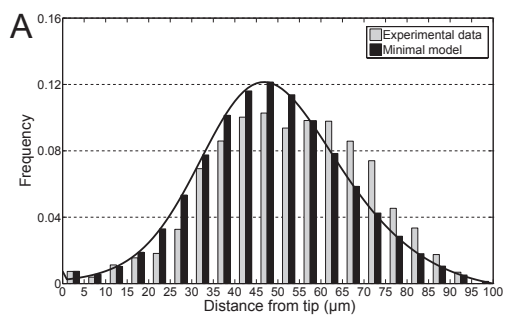




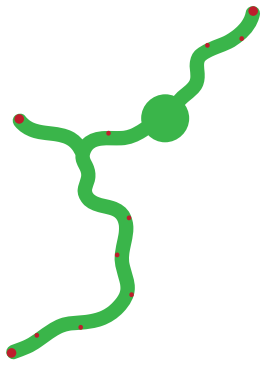




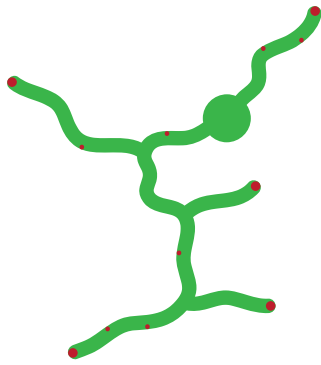




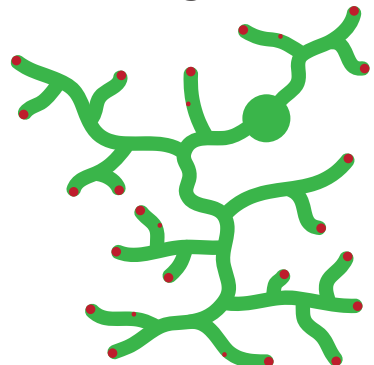
A



B



C



The Ser/Thr protein kinase AfsK regulates polar growth and hyphal branching in the filamentous bacteria *Streptomyces*

Antje M. Hempel^{a,b}, Stuart Cantlay^{a,1}, Virginie Molle^c, Sheng-Bing Wang^{a,2}, Mike J. Naldrett^b, Jennifer L. Parker^b, David M. Richards^b, Yong-Gyun Jung^b, Mark J. Buttner^b, and Klas Flärdh^{a,3}

^aDepartment of Biology, Lund University, 223 62 Lund, Sweden; ^bMolecular Microbiology, John Innes Centre, Norwich Research Park, Norwich NR4 7UH, United Kingdom; and ^cLaboratoire de Dynamique des Interactions Membranaires Normales et Pathologiques, Université de Montpellier II, Centre National de la Recherche Scientifique, 34095 Montpellier, France

Edited by Susan S. Golden, University of California at San Diego, La Jolla, CA, and approved June 28, 2012 (received for review May 15, 2012)

In cells that exhibit apical growth, mechanisms that regulate cell polarity are crucial for determination of cellular shape and for the adaptation of growth to intrinsic and extrinsic cues. Broadly conserved pathways control cell polarity in eukaryotes, but less is known about polarly growing prokaryotes. An evolutionarily ancient form of apical growth is found in the filamentous bacteria *Streptomyces*, and is directed by a polarisome-like complex involving the essential protein DivIVA. We report here that this bacterial polarization machinery is regulated by a eukaryotic-type Ser/Thr protein kinase, AfsK, which localizes to hyphal tips and phosphorylates DivIVA. During normal growth, AfsK regulates hyphal branching by modulating branch-site selection and some aspect of the underlying polarisome-splitting mechanism that controls branching of *Streptomyces* hyphae. Further, AfsK is activated by signals generated by the arrest of cell wall synthesis and directly communicates this to the polarisome by hyperphosphorylating DivIVA. Induction of high levels of DivIVA phosphorylation by using a constitutively active mutant AfsK causes disassembly of apical polarisomes, followed by establishment of multiple hyphal branches elsewhere in the cell, revealing a profound impact of this kinase on growth polarity. The function of AfsK is reminiscent of the phosphorylation of polarity proteins and polarisome components by Ser/Thr protein kinases in eukaryotes.

hyphal growth | protein phosphorylation | peptidoglycan | cytoskeleton | tip extension

How cells establish polarity is a fundamental question in developmental biology. It typically involves the initial deposition of a landmark protein at a cellular locus, followed by reinforcement of the polarization mark by assembly of larger multiprotein complexes. In eukaryotes, these complexes include broadly conserved proteins involved in the reorganization and polarization of the cytoskeleton and other cellular constituents (1, 2). Among the most pronounced cases of cell polarity are those in which growth or extension of the cell is targeted to a specific subcellular site, resulting in polar or apical growth. Important examples of polarized growth in eukaryotic cells include neuronal dendrites in animals, root hairs and pollen tubes in plants, bud emergence in *Saccharomyces cerevisiae*, the hyphal growth of filamentous fungi, and the elongation of fission yeast. However, in evolutionary terms, the most ancient forms of polarized growth are found in Bacteria (3, 4), most strikingly in the filamentous bacteria *Streptomyces*, which, in analogy to filamentous fungi, grow as branching hyphae and ramify into mycelial networks (5, 6).

The shape and integrity of *Streptomyces* hyphae are, like for most bacteria, maintained by the peptidoglycan cell wall, but the spatial control of cell wall assembly differs from other groups of bacteria. Conventional rod-shaped bacteria like *Escherichia coli* and *Bacillus subtilis* grow by intercalating new peptidoglycan along the lateral cell wall, and this cell elongation is orchestrated by a cytoskeleton formed by the actin-homologous MreB proteins,

which interact directly with the cell wall biosynthetic machinery (reviewed in, e.g., refs. 7, 8). In sharp contrast, streptomycetes grow by tip extension and hyphal branching. This apical mode of growth is independent of MreB (9), and instead depends on the coiled-coil protein DivIVA, which is localized in large assemblies at growing hyphal tips (10). *divIVA* is essential for growth, and overexpression of *divIVA* is sufficient to trigger hyper-branching, showing that DivIVA is a key determinant of polarized growth in *Streptomyces* (10, 11). Together with the nonessential coiled-coil protein Scy (12), DivIVA forms an apical multiprotein complex, here termed the bacterial polarisome by analogy with the polarisome complex that directs cell polarity in yeasts and filamentous fungi (13).

It was previously demonstrated that small foci of DivIVA mark the sites of new branches before visible outgrowth occurs (11), although it remained unclear how such polarity marks are established (5). However, we have recently shown that the foci of DivIVA that trigger branching are primarily created by a unique polarisome splitting mechanism, in which the apical polarisome, visualized as a tip focus of DivIVA-EGFP, splits to deposit a small daughter polarisome, which is left behind on the lateral membrane as the tip grows away (14). Each daughter focus acts as a polarity mark, growing in size and ultimately initiating the outgrowth of a new hyphal tip. An obvious benefit of the polarisome splitting mechanism is that it appears to bypass kinetic barriers and other constraints that may be associated with de novo nucleation of new DivIVA clusters (5, 14–16). Intriguingly, a recent study showed that the polarisome scaffold protein SPA-2 in *Neurospora crassa* also exhibits tip-focus splitting behavior, in which small foci of SPA-2 detach from the main apical cluster, remain on the lateral wall, and mark the sites of new lateral branches (17). This observation suggests that branch site selection in filamentous fungi could be determined by a polarisome splitting mechanism similar to the one we have characterized in *Streptomyces*.

A polarisome splitting mechanism for branch-site selection may also facilitate regulation of cell polarity and hyphal branching.

Author contributions: A.M.H., S.C., V.M., M.J.N., M.J.B., and K.F. designed research; A.M.H., S.C., V.M., S.-B.W., M.J.N., J.L.P., and K.F. performed research; A.M.H., S.C., S.-B.W., J.L.P., and Y.-G.J. contributed new reagents/analytic tools; A.M.H., S.C., V.M., M.J.N., D.M.R., M.J.B., and K.F. analyzed data; and A.M.H., M.J.B., and K.F. wrote the paper.

The authors declare no conflict of interest.

This article is a PNAS Direct Submission.

¹Present address: Department of Biological Sciences, Duquesne University, Pittsburgh, PA 15282.

²Present address: Division of Cardiology, Department of Medicine, School of Medicine, Johns Hopkins University, Baltimore, MD 21224.

³To whom correspondence should be addressed. E-mail: klas.flardh@biol.lu.se.

See Author Summary on page 13906 (volume 109, number 35).

This article contains supporting information online at www.pnas.org/lookup/suppl/doi:10.1073/pnas.1207409109/-DCSupplemental.

Previous studies have shown that *Streptomyces* has a signal transduction system, the CseB/CseC- σ^E system, which is involved in sensing and responding to changes in the integrity of the cell envelope, and that inducers of this system include antibiotics that inhibit cell wall synthesis such as bacitracin and vancomycin (31). To test whether the CseB/CseC- σ^E system might be involved in mediating the increase in DivIVA phosphorylation observed when cell wall synthesis is blocked as part of this general cell envelope stress response, we analyzed immunoprecipitated DivIVA material from a *sigE*-null mutant. The results showed that bacitracin-induced DivIVA phosphorylation does not depend on the σ^E -mediated cell envelope stress response (Fig. S1B).

C-Terminal Region of DivIVA Is Target of Multiple Phosphorylations.

To confirm and extend our results, we used MS to further characterize the phosphorylation of DivIVA. DivIVA was immunoprecipitated from cultures that had been exposed to bacitracin to block cell wall synthesis, and the protein was digested with trypsin and analyzed by MALDI-TOF. A 7.2-kDa tryptic peptide that contains most of the C-terminal region of DivIVA was found to be singly, doubly, and triply phosphorylated, with the doubly phosphorylated species the most abundant (Fig. 2B). After treatment with calf intestinal alkaline protein phosphatase, the three peaks corresponding to the phosphorylated forms of DivIVA disappeared, leaving only the peak corresponding to the nonphosphorylated form (Fig. 2B). Further analysis showed that another DivIVA tryptic peptide was also multiply phosphorylated. This second peptide is 1.5 kDa in size and sits immediately N-terminal to the 7.2-kDa tryptic peptide in the primary amino acid sequence of DivIVA (Fig. 2A). Thus, the C-terminal region of DivIVA becomes highly phosphorylated in response to the inhibition of cell wall synthesis in *S. coelicolor*.

DivIVA Kinase Is AfsK. We next attempted to identify the kinase responsible for DivIVA phosphorylation. Multiple reports show that STKs carrying PASTA domains play important regulatory roles in *Mycobacterium* and *Corynebacterium*. PASTA domains are known to bind peptidoglycan components and β -lactam antibiotics (21, 32), and actinobacterial STKs carrying such domains (PknA and PknB) have been reported to phosphorylate several proteins involved in cell wall growth and cell division, including the mycobacterial DivIVA-orthologue Wag31 (e.g., refs. 24, 33–35). These reports prompted us to investigate the three PASTA domain-containing STKs in *S. coelicolor* (SCO2110, SCO3821, and SCO3848), of which SCO3848 shows microsynteny with mycobacterial *pknB*. Accordingly, we constructed SCO2110-, SCO3821-, and SCO3848-null mutants and found that both the basal level of DivIVA phosphorylation during growth and the strongly increased level seen after bacitracin treatment occurred normally in each of the three mutants (Fig. 3A). To rule out the possibility of redundancy, we constructed a triple mutant lacking all three of these kinases. Again, basal DivIVA phosphorylation during growth and the dramatic increase in phosphorylation caused by the inhibition of cell wall synthesis occurred normally, even in the absence of all three kinases (Fig. 3A). Thus, DivIVA phosphorylation in *S. coelicolor* is mediated by some route other than PknA/PknB-like PASTA domain-containing STKs.

The *S. coelicolor* genome carries at least 34 genes predicted to encode STKs (25). Accordingly, we began systematically disrupting these genes, introducing the *divIVA* allele encoding the N-terminally FLAG-tagged version of the protein into the resulting mutants, and examining the pattern of DivIVA phosphorylation in FLAG-DivIVA/DivIVA mixtures immunoprecipitated from each strain. Including the three PASTA domain kinases described earlier, we examined 17 STKs for their involvement in DivIVA phosphorylation (Table S1 and Fig. 3). In mutants for 16 of these kinases, we observed the normal pattern of phosphorylation (Fig. 3A and B). However, no DivIVA phosphorylation

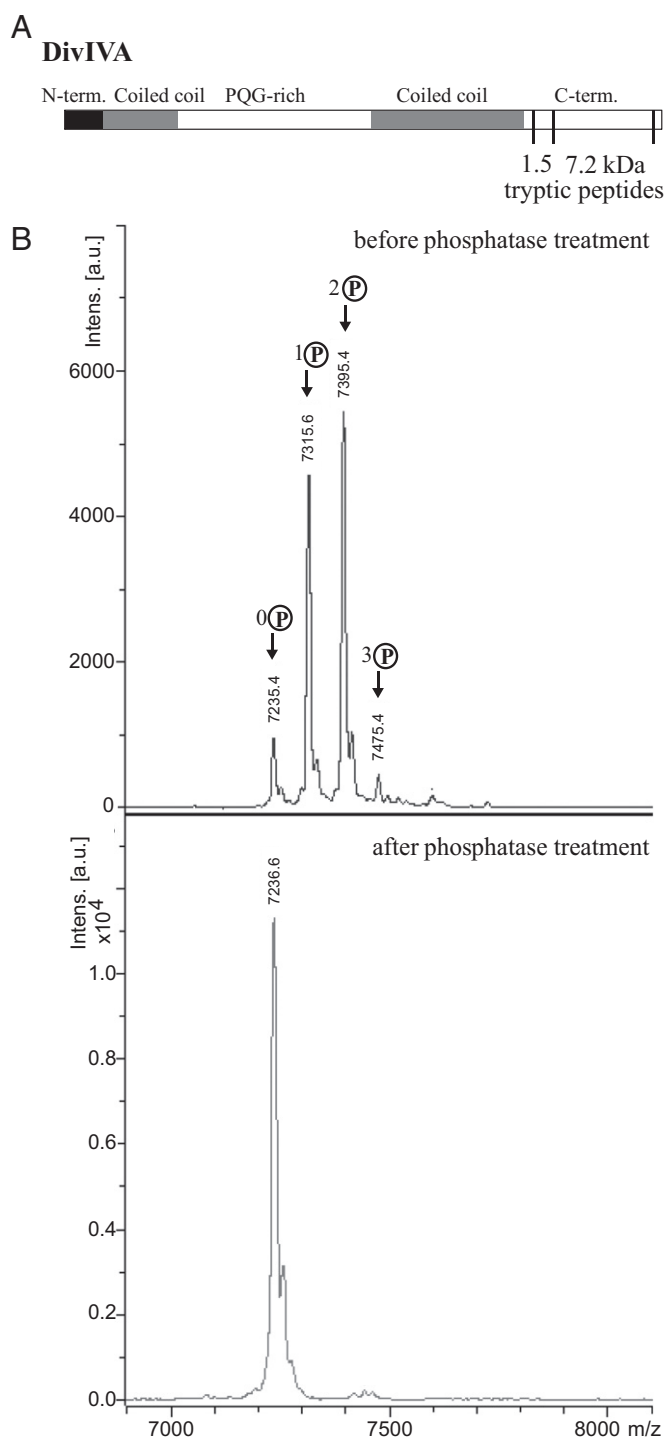


Fig. 2. *S. coelicolor* DivIVA is multiply phosphorylated in the C-terminal region. (A) Schematic showing the positions within the DivIVA primary sequence of the 7.2-kDa phosphorylated peptide (residues 315–389) relative to the 1.5-kDa phosphorylated peptide (residues 301–314) described in the text. (B) Upper: MALDI mass spectrum of a 7.2-kDa tryptic fragment derived from the C-terminal region of DivIVA showing 0 to 3 phosphorylations (+80, +160, and +240 Da). Lower: Disappearance of the phosphorylated species upon treatment of the protein with calf intestinal alkaline phosphatase.

occurred in a constructed *afsK* mutant (SCO4423) during normal growth or after cell wall synthesis was arrested with bacitracin (Fig. 3C). Complementation of the *afsK* mutant restored DivIVA phosphorylation to the WT pattern (Fig. 3D), showing that the

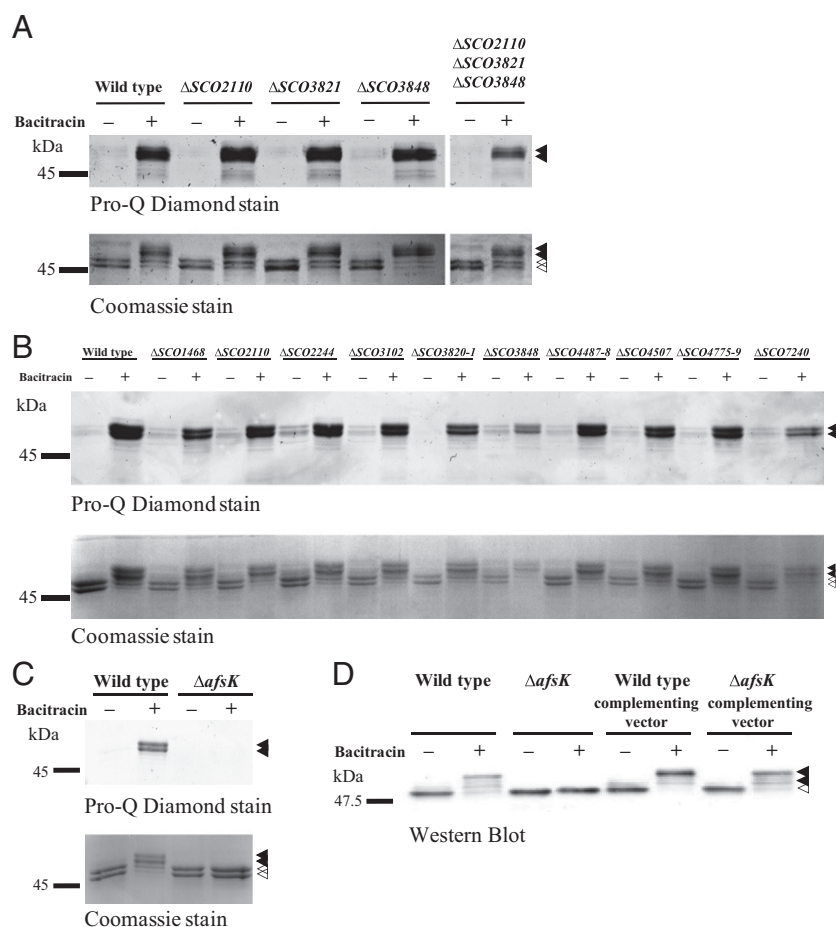


Fig. 3. The DivIVA kinase is AfsK. The phosphorylation state of DivIVA, before and after the inhibition of cell wall synthesis, was analyzed in (A) single, double, and triple mutants corresponding to three PASTA domain-containing STKs of *S. coelicolor*, SCO2110, SCO3821, and SCO3848, (B) 13 other constructed STK mutants, and (C) a constructed *afsK* mutant. Growing cultures of WT *S. coelicolor* and of the STK mutants, each expressing FLAG-*divIVA*, were incubated with 50 μ g/mL bacitracin for 30 min before harvest, preparation of cell extracts, and immunoprecipitation of FLAG-*DivIVA/DivIVA*. (D) Complementation of the *afsK*-null mutant restores DivIVA phosphorylation. *afsK* was cloned into the integrative vector pMS82 to create pKF256, which was introduced into the *afsK* null mutant and into WT *S. coelicolor*. The phosphorylation state of DivIVA, before and after the inhibition of cell wall synthesis, was analyzed in each strain by Western blot analysis of crude cell extracts. Closed arrowheads indicate phosphorylated DivIVA and open arrowheads indicate non-phosphorylated DivIVA.

afsK-encoded kinase is required for the basal level of DivIVA phosphorylation and the high levels induced by arresting peptidoglycan synthesis.

DivIVA Is Phosphorylated by AfsK in Vitro. These results led us to investigate whether AfsK directly phosphorylates DivIVA. To address this question, we cloned, overexpressed, and purified the kinase domain of AfsK (amino acids 1–311) and DivIVA as GST-tagged fusion proteins and used them to establish an in vitro phosphorylation system. When the kinase domain of AfsK was incubated with γ -labeled ATP, it underwent autophosphorylation, as revealed by autoradiography, and, when this was mixed with purified DivIVA, the kinase was indeed able to phosphorylate DivIVA (Fig. 4). Thus, we conclude that the absence of DivIVA phosphorylation in the *afsK* mutant arises because DivIVA is a direct substrate for AfsK.

AfsK Kinase Colocalizes with Its Substrate DivIVA at Tips of Growing Vegetative Hyphae. DivIVA shows a distinctive subcellular localization, with strong accumulation at the tips of growing hyphae (10). It was therefore of interest to determine whether AfsK would show a similar distribution and colocalize with its substrate. We investigated this question by creating a fusion between

AfsK and the red fluorescent protein mCherry. The translational fusion was expressed from the *afsK* promoter and was integrated at the chromosomal *att*_{φBT1} site in the WT strain and its congenic *afsK*-null mutant. The *afsK*-mCherry allele restored the ability to phosphorylate DivIVA to the *afsK* mutant—both the basal level seen during growth and the high level induced by bacitracin-treatment (Fig. S2)—showing that the fusion protein is functional. In both strain backgrounds, this hybrid protein showed clear accumulation as foci at the tips of vegetative hyphae, although we also observed weak fluorescence along the hyphae (Fig. 5A). The colocalization of AfsK with DivIVA at the hyphal tips was further confirmed by examining a strain expressing *divIVA-egfp* and *afsK*-mCherry (Fig. 5B). Thus, a substantial fraction of the AfsK kinase colocalizes with its substrate DivIVA at hyphal tips.

AfsK Regulates Branching of Growing Hyphae. With the discovery that DivIVA is directly phosphorylated by AfsK, we wondered whether disruption of *afsK* would influence hyphal branching and the underlying polarisome splitting mechanism. Previously reported *afsK* mutant phenotypes in *S. coelicolor* have only concerned decreased synthesis of antibiotics (28). We analyzed liquid cultures of our *S. coelicolor afsK* deletion mutant microscopically in comparison with the WT and discovered that the *afsK* mutant strain

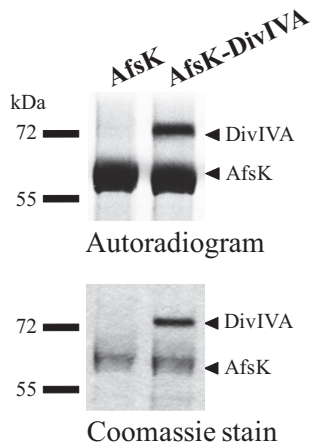


Fig. 4. In vitro phosphorylation of DivIVA by AfsK. Recombinant AfsK and DivIVA were incubated with [γ - 32 P]ATP. Samples were separated by SDS/PAGE, visualized by autoradiography (Upper), and Coomassie-stained (Lower). Lower bands in the autoradiogram illustrate the autokinase activity of AfsK, whereas upper bands reflect DivIVA phosphorylation. In control experiments, DivIVA alone did not show any autophosphorylation activity.

does indeed have a previously unrecognized phenotype: it exhibits an altered tip-to-branch distribution, shifting the average to a longer distance than in the WT (Fig. 6). This effect is quantified in Fig. 6B. The effect is also clearly apparent when comparing time-lapse image sequences of growing hyphae of the *afsK* mutant and its congenic *afsK*⁺ parent (Movies S1 and S2). To confirm that the effect on hyphal branching was caused by the absence of *afsK*, we complemented the *afsK* mutant strain and found that reintroducing the *afsK* gene largely restored WT branching behavior (Fig. 6C). These results show that loss of the AfsK kinase affects the normal regulation of lateral branch formation, and because the vast majority of hyphal branches emerge from DivIVA foci deposited by polarisome splitting (14), this suggests that AfsK modulates this mechanism for the development of new daughter polarisomes.

Constitutively Active AfsK Profoundly Affects Apical Growth, DivIVA Localization, and Hyphal Branching. The data described earlier show that AfsK regulates branch-site selection and hyphal morphology during normal growth, even when its activity, as reflected in the basal level of DivIVA phosphorylation, is relatively low. However, when peptidoglycan synthesis is blocked, there is a pronounced up-regulation of AfsK-dependent DivIVA phosphorylation (as described earlier). This raised the possibility that such high levels of AfsK activity would strongly affect hyphal growth and branching, but these effects cannot be evaluated when growth is simultaneously blocked by bacitracin. We therefore engineered a strain in which AfsK kinase activity could be induced in normally growing hyphae. This was achieved by creating a constitutively active mutant version of AfsK in which two threonines in the activation loop of the kinase (T165 and T168) were changed to aspartates to mimic the autophosphorylation of AfsK that leads to its activation. As in other STKs, the conserved residues T165 and T168 of *S. coelicolor* and *Streptomyces avermitilis* AfsK are required for activation of the kinase, and T168 has been shown to undergo autophosphorylation in *S. coelicolor* (36, 37). Most importantly, in both species, T165D and T168D phosphomimic mutations result in a constitutively active kinase (36, 37). The mutant *afsK*(T165D,T168D) allele was placed under control of the thioestrepton-inducible *tipAp* promoter in the integrative vector pIJ6902 to create pKF275 (Table S1). When strains carrying pKF275 were grown in the absence of thioestrepton, they showed basal levels of DivIVA phosphorylation similar to those of control

strains that carried only the empty vector pIJ6902 (Fig. 7A). However, addition of thioestrepton to cultures of pKF275-carrying strains led to a dramatic increase in the level of phosphorylated DivIVA, as detected by the mobility shift of a major part of the DivIVA protein population seen in Western blots (Fig. 7A).

The thioestrepton-induced hyperphosphorylation strongly affected DivIVA localization, as detected by using the DivIVA-EGFP fusion. Before thioestrepton addition, the majority of hyphae carried detectable DivIVA-EGFP foci at the tips, but when expression of the constitutively active AfsK was induced, the majority of these foci dissolved or were strongly reduced in intensity (Fig. 7B), leading to decreased average fluorescence intensity at the hyphal tip, and an increased fraction of hyphae without detectable apical foci. Cultures of pKF275-carrying strains that did not receive thioestrepton showed normal DivIVA localization (Fig. 7B), and, similarly, the control strain carrying the empty vector pIJ6902 was not affected by addition of thioestrepton and showed normal DivIVA localization to hyphal tips. These observations show that strong up-regulation of AfsK activity stimulates disassembly of polarisome structures and dissociation of DivIVA from hyphal tips.

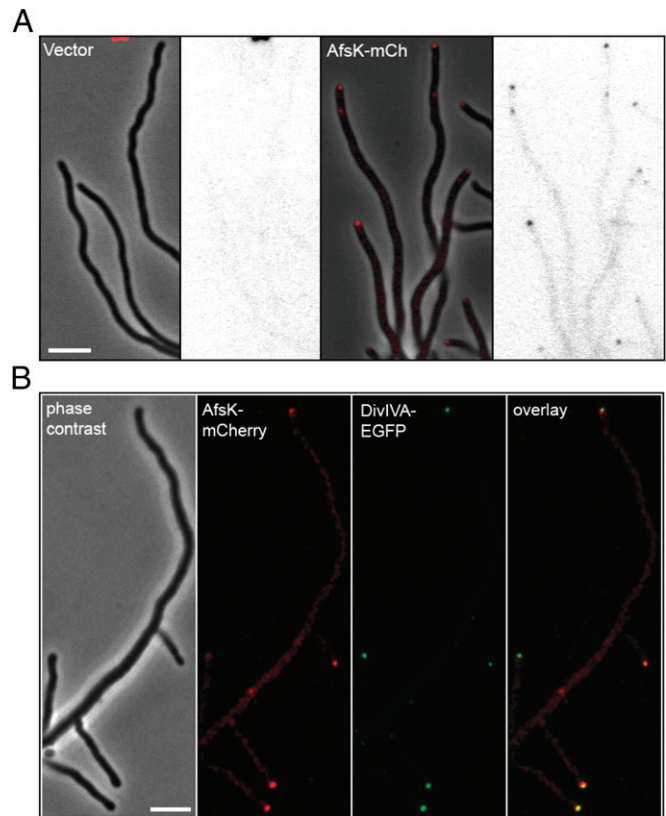


Fig. 5. The DivIVA kinase AfsK localizes to hyphal tips. (A) *S. coelicolor* WT strain carrying empty vector pKF210 with promoterless *mCherry* (Left) or plasmid pKF255 expressing a translational *afsK*-*mCherry* fusion (Right). Representative images of growing hyphae are shown as phase-contrast image with overlaid fluorescence in red, and as the fluorescence image alone in inverted grayscale. (B) Colocalization of DivIVA and AfsK demonstrated by using an *S. coelicolor* strain producing both DivIVA-EGFP (green) and AfsK-*mCherry* (red). A series of images were collected for each channel, moving focus 0.2 μ m between each image. The z-stacks were deconvolved by using Velocity software, and a central focal plane through the middle of the cells is shown as (from left to right) phase-contrast image, *mCherry* fluorescence, EGFP fluorescence image, and overlay of the fluorescence channels. (Scale bar, 4 μ m.)

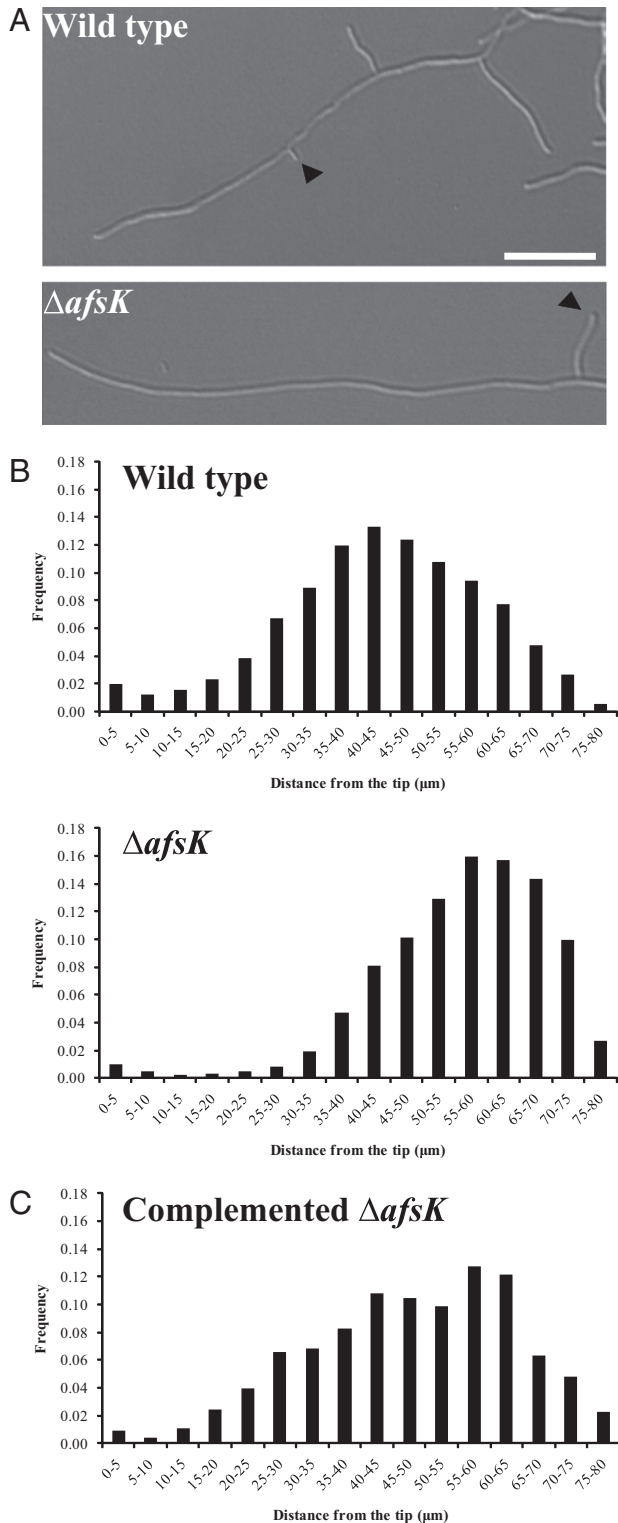


Fig. 6. The *afsK* mutant has a branching phenotype. (A) Representative DIC images of WT *S. coelicolor* and the congenic *afsK* mutant grown in YEME. Arrows indicate the first lateral branch behind the hyphal tip. (Scale bar, 10 μm.) (B) Histograms of distances between the tip and lateral branches at the moment of branch development in cultures of *S. coelicolor* WT and the congenic *afsK* mutant, and (C) the complemented *afsK* mutant grown for 15 to 18 h in YEME at 80 μm trim (*Experimental Procedures*). The number of tip-to-branch distances measured per strain were 1,097 (WT), 875 (*afsK* mutant), and 281 (complemented mutant).

The induction of the constitutively active AfsK further caused dramatic changes in hyphal growth and morphology. When cultures containing the *tipAp-afsK*(T165D,T168D) construct were incubated in the presence of the inducer thiostrepton, growth was impeded (Fig. S3). However, despite the arrest of growth at existing hyphal tips, multiple new hyphal branches started to emerge from the lateral walls distal to these tips, giving rise to conspicuous hyphal structures decorated by multiple branch initials (Fig. 7C). Such effects were not seen in control strains carrying the empty vector pIJ6902, which carried on growing without any detectable effect of thiostrepton (Fig. S3). Thus, induction of high AfsK activity causes disappearance of apical DivIVA foci, growth inhibition, and subsequent initiation of multiple new lateral branches. This gave the cultures a characteristic appearance, with unusually dense and compact hyphal pellets, from which emerge hyperbranched and irregularly shaped hyphal structures (representative images in Fig. 7C), strikingly different from the regular and loose hyphal pellets and long tip-to-branch distances seen in control cultures (representative image in Fig. 7C). In summary, AfsK kinase activity has strong effects on cell polarity, tip extension, subcellular localization of DivIVA, and initiation of new hyphal branches.

Discussion

This study shows that the Ser/Thr kinase AfsK is part of the apparatus that controls polar growth in *Streptomyces*, and that it directly phosphorylates the cell polarity determinant DivIVA. Our data indicate dual roles for the AfsK kinase. First, during normal growth, it modulates the control of hyphal branching and the development of daughter polarisomes. Second, AfsK is involved in a stress response when cell wall synthesis is arrested; under such conditions, AfsK is strongly activated and causes profound reconfiguration of DivIVA localization, apical growth, and hyphal branching. This discovery represents an intriguing prokaryotic parallel to the widespread and broadly conserved roles of STKs in controlling cell polarity in eukaryotes (1, 2), and particularly to the control of polar growth by kinases targeting polarisome components in fungi (references in ref. 13).

Induction of a constitutively active form of AfsK causes the disappearance of the DivIVA foci that normally mark growing hyphal tips (Fig. 7). No concomitant degradation or decrease in cellular DivIVA content is observed, suggesting that high AfsK activity causes disassembly of the DivIVA-containing apical polarisome. DivIVA is a self-assembling coiled-coil protein that forms oligomers and higher-order complexes and is involved in polar targeting in a range of Gram-positive bacteria (15, 30, 38–40). The AfsK-mediated phosphorylation of DivIVA in *Streptomyces* occurs on two trypsin-generated fragments in the C-terminal domain (Fig. 2). Although this C-terminal domain is not conserved outside of *Streptomyces* orthologues (10), it lies just downstream of the conserved second coiled-coil segment, which is known to be important in the oligomerization of *B. subtilis* DivIVA (40). It is therefore possible that the AfsK-mediated phosphorylation influences oligomerization, acting as a means to control the assembly or disassembly of multimeric complexes or higher-order structures formed by DivIVA in the cell. Such a role for STKs in controlling assemblages of coiled-coil proteins is well known in eukaryotes, a classic example being the disassembly of the nuclear lamina mediated by cyclin-dependent kinases (41). In addition, it was recently reported that the assembly and subcellular localization of the coiled-coil protein RsmP in *Corynebacterium glutamicum* is affected by phosphorylation (42). However, it cannot be excluded that phosphorylation may also influence other aspects of DivIVA behavior, such as its interaction with other proteins or the membrane. The function of *B. subtilis* DivIVA depends on direct interactions with MinJ and the nucleoid-associated protein RacA (15, 43), and the function of *S. coelicolor* DivIVA is also likely to depend on the direct

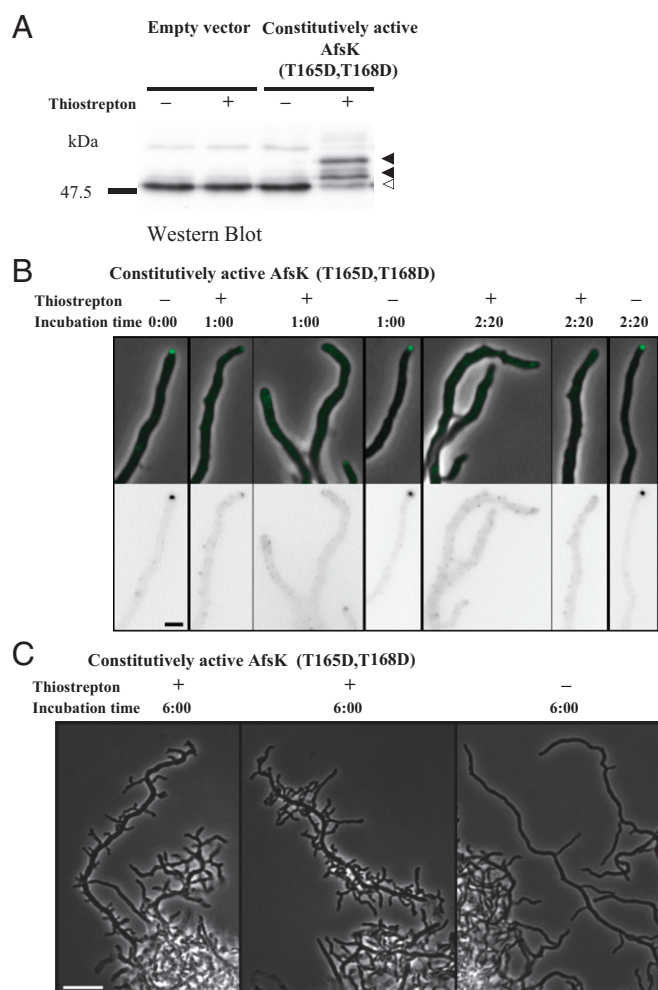


Fig. 7. Engineered expression of a constitutively active version of the AfsK kinase induces high levels of DivIVA phosphorylation and profoundly affects hyphal tip extension and branching. (A) Levels of DivIVA phosphorylation induced by expression of the *afsK*(T165D, T168D) allele from the thioestrepton-inducible *tipAp* promoter in plasmid pKF275. A strain carrying empty vector pJ16902 was used as control. Growing cultures were split in two, and thioestrepton was added to one (+) whereas a mock addition of DMSO was made to the other (-). Extracts of cells harvested after 2.5 h were separated by SDS/PAGE, and DivIVA was detected by immunoblotting. Phosphorylated species of DivIVA (closed arrowheads) migrate more slowly than unphosphorylated DivIVA (open arrowhead). (B) The effects of overproduction of constitutively active AfsK(T165D, T168D) on DivIVA-EGFP localization are illustrated by typical examples of hyphae from strain K338. Images captured before addition of thioestrepton (10 μ g/mL), the inducer of *tipAp-afsK*(T165D, T168D) expression, 1 h and 2 h 20 min after addition of thioestrepton or mock. EGFP fluorescence is shown in inverted grayscale (Lower) or shown in green overlaid on phase-contrast images (Upper). (Scale bar, 2 μ m.) (C) Typical examples of hyperbranched hyphal morphology developing after overexpression of *afsK*(T165D, T168D) for 6 h (Left) compared with the uninduced control sample (Right). (Scale bar, 10 μ m.)

recruitment of other proteins to the cell poles (5, 6). Further, crystal structures of *B. subtilis* DivIVA show how the oligomers may interact with the membrane via an exposed phenylalanine residue in the highly conserved N-terminal part of the protein (40), and the polar and septal targeting of the *B. subtilis* DivIVA appears to be explained by a preference of the oligomers for negatively curved membrane surfaces (15, 44).

The decreased branching observed in *afsK* mutants could be explained by an effect of AfsK-mediated phosphorylation on the stability of the apical DivIVA clusters. Most branches in *S.*

coelicolor are formed by a tip-focus splitting mechanism in which the DivIVA-containing apical polarisome splits to leave smaller foci behind along the lateral hyphal walls as the tip extends—foci that act as seeds for new branches (14). Although only a small fraction of the DivIVA molecules in the cell are detectably phosphorylated during normal growth (Fig. 1A), this low basal activity obviously has significant impact on hyphal branching. As AfsK colocalizes with the DivIVA foci at hyphal tips, it is possible that the low level of DivIVA phosphorylation seen during normal growth affects polarisome splitting (perhaps by controlling the initial size of new daughter polarisomes) and thereby modulates the pattern of hyphal branching.

Hyperactivity of AfsK inhibits growth at the original hyphal tips, but, paradoxically, it also induces the subsequent formation of multiple short lateral branches distal to these tips (Fig. 7). This observation, that growth can be initiated at new sites while being prevented at the original tip, could also be explained by the localization of AfsK to hyphal tips. A high level of DivIVA phosphorylation promotes the complete disassembly of the apical protein complexes. The released DivIVA molecules could then diffuse away and gradually be dephosphorylated, allowing them to form new foci that are capable of establishing new branches distal to the original tips. We suggest this provides *S. coelicolor* with a mechanism to dismantle the apical growth apparatus at hyphal tips that encounter problems with cell wall synthesis, for example through exposure to an antibiotic or by hitting a physical obstacle in the soil. Such conditions would strongly activate AfsK, leading to disassembly of the apical DivIVA complex and liberation of DivIVA molecules that can then direct emergence of new branches elsewhere, leading, for example, to growth around an obstacle. In the simplest scenario, DivIVA molecules that are liberated from the original tip could join small daughter foci that have previously been deposited along the lateral wall by polarisome splitting (14), accelerating their maturation into polarisomes competent to trigger branch outgrowth. Alternatively, the release of large quantities of soluble DivIVA from the disassembly of apical foci could trigger the spontaneous nucleation of new DivIVA foci.

Orthologues of AfsK are found among only streptomycetes and a few closely related mycelial actinomycetes, suggesting that its function is related to the filamentous or hyphal growth habit. Further, the AfsK-mediated phosphorylation of *S. coelicolor* DivIVA differs in several important ways from the previously observed phosphorylation of the mycobacterial DivIVA ortholog, Wag31 (34). First, the role of phosphorylation of mycobacterial Wag31 is poorly understood, but it seems to promote localization of Wag31 to cell poles and stimulate polar growth and cell wall synthesis (45, 46). In contrast, the activation of the DivIVA kinase in *S. coelicolor* has the opposite effect, promoting the disassembly of DivIVA foci and the inhibition of growth at existing hyphal tips. Second, different kinases are involved, which are likely to be activated by different stimuli. The essential PASTA-domain kinases PknA and PknB act on Wag31 in mycobacteria, and the reports so far describe activity only during undisturbed growth (34, 46). In contrast, AfsK, the DivIVA kinase in *S. coelicolor*, is weakly active during vegetative growth and strongly activated in response to the arrest of cell wall synthesis. Third, the site of phosphorylation is different, with a single threonine close to the first coiled-coil domain being targeted in *M. tuberculosis*, whereas it is the C-terminal domain of *S. coelicolor* DivIVA that is phosphorylated on multiple residues.

AfsK was one of the first bacterial STKs to be investigated, and an *afsK* disruption mutant of *S. coelicolor* was reported to grow and sporulate normally, while showing reduced production of blue-pigmented antibiotic actinorhodin (28). The effect on antibiotic production appears to be mediated by the transcription factor AfsR, which is directly phosphorylated by AfsK in vitro and activates transcription of *afsS*, encoding a small pleiotropic regulator of antibiotic synthesis in *Streptomyces* (47, 48). In this

study, we report a completely different role for AfsK in the control of hyphal growth and branching, one that does not involve AfsR (as an *afsR* mutant shows normal hyphal branching and normal levels of DivIVA phosphorylation). Strikingly, the conditions we used to induce high AfsK activity (i.e., addition of bacitracin or the engineered expression of a constitutively active kinase) did not trigger overproduction of actinorhodin (Fig. S3). In summary, the function of AfsK in controlling polar growth and branching is not obviously related to the previously inferred role of AfsK in secondary metabolism.

Overall, our findings show that communication between the polarity determinant DivIVA and the cell wall biosynthetic machinery is bidirectional, with DivIVA directing cell wall synthesis (11), and the biosynthetic machinery communicating back to DivIVA via AfsK-mediated phosphorylation. All three components—the cell wall biosynthetic machinery, AfsK, and DivIVA—localize to growing hyphal tips. What, then, are the signals that lead to the activation of AfsK? AfsK has an N-terminal STK domain and a C-terminal putative sensory portion carrying PQQ domain repeats. These PQQ domain repeats are predicted to form a β -propeller structure similar to WD40 domains and may interact with a ligand, although the general function of PQQ domains is not known (25). Further, AfsK does not have a predicted transmembrane segment, and is reported to be cytoplasmic but loosely associated with the membrane (28). AfsK activity (at least as reflected in the level of DivIVA phosphorylation) is strongly stimulated by antibiotics like bacitracin and vancomycin, which block the lipid II cycle of peptidoglycan biosynthesis, raising the possibility that AfsK can sense the accumulation of intermediates in peptidoglycan biosynthesis. This would provide a mechanism to sense the capacity of the hyphal tip to sustain extension during normal growth and during stress conditions, and via AfsK-mediated phosphorylation transduce this information to the polarisome that directs apical growth and branching.

Experimental Procedures

Bacterial Strains, Plasmids, and General Methods. Properties of bacterial strains and plasmids used in this study are described in Table S1. Details of plasmid construction are described in *SI Experimental Procedures*. Oligonucleotide primers are listed in Table S2. Media, culture conditions, and general genetic manipulations were as described previously for *E. coli* (49) and *Streptomyces* (50).

Analysis of DivIVA Phosphorylation by Immunoprecipitation, Pro-Q Diamond Staining, and MS. The appropriate *S. coelicolor* strains were grown in yeast extract–malt extract (YEME) medium for 15 to 22 h. For expression of FLAG-divIVA from the thiostrepton-inducible promoter *tipAp*, strains were grown in the presence of 0.1 μ g/mL of thiostrepton. The exact details of the following procedures are described in *SI Experimental Procedures*. Briefly, hyphae were harvested by centrifugation, washed twice, and resuspended in appropriate buffer. Cell extracts were prepared in a buffer designed to reduce phosphatase activity, and cell lysates were prepared by sonication or by bead beating. Cell lysates were cleared by centrifugation. The cleared cell lysates were used for immunoprecipitation by using anti-FLAG M2 affinity beads (Sigma-Aldrich), essentially as described by Wang et al. (30). Eluted

proteins were separated by SDS-PAGE, and phosphorylated proteins were detected by using Pro-Q Diamond phosphoprotein gel stain (Molecular Probes). When appropriate, the material eluted from the affinity beads was dephosphorylated for 10 min at 30 °C by using lambda protein phosphatase (Sigma-Aldrich). Identification of phosphorylated trypsin fragments of DivIVA was done by using MALDI-TOF MS.

In Vitro Phosphorylation of DivIVA. In vitro phosphorylation was carried out in 20- μ L reactions containing the recombinant AfsK (1 μ g) and/or DivIVA (4 μ g) and 200 μ Ci/mL (65 nM) [γ - 33 P]ATP (3,000 Ci/mmol; PerkinElmer) in phosphorylation buffer (25 mM Tris-HCl, pH 6.8, 1 mM DTT, 5 mM MgCl₂, 1 mM EDTA). The reaction was carried out for 30 min at 37 °C and stopped by addition of Laemmli sample loading buffer and incubated at 100 °C for 5 min before analysis by SDS-PAGE. After electrophoresis, gels were washed in 10% (wt/vol) trichloroacetic acid for 10 min at 90 °C and then stained with Coomassie stain, dried, and visualized by autoradiography overnight.

Western Blotting. Cell lysates from *S. coelicolor* cultures grown in YEME (17% sucrose) were prepared by bead beating (six times, 6.0 m/s, 30 s; FastPrep-24; MP Biomedicals) in lysate buffer (10 mM Tris-HCl, pH 7.5, 150 mM NaCl, 1 mM EDTA) supplemented with complete EDTA-free protease inhibitor mixture (Roche). Proteins were separated by SDS/PAGE and transferred onto Immobilon-P PVDF membrane (Millipore) as described previously (10). The membrane was incubated overnight at 4 °C with anti-DivIVA_{sc} antiserum from rabbit, diluted 1:5,000 (30), then washed three times with 5% (wt/vol) nonfat dry milk in PBS solution before incubation for 1 h at room temperature with pig anti-rabbit IgG linked to horseradish peroxidase (1:1,000; DakoCytomation). The membrane was washed six times in PBS solution with 0.05% Tween, proteins were visualized by SuperSignal West Pico chemiluminescence substrate (Pierce), and results were captured by using a Digital Science Image Station 440CF (Kodak).

Microscopy. Hyphae were prepared for microscopy as described previously (10). For differential interference contrast, phase-contrast, and fluorescence microscopy, liquid cultures of *S. coelicolor* were grown for 15 to 18 h in YEME from pregerminated spores. Samples of these cultures were spotted directly onto microscope slides coated with 1% (wt/vol) agarose in PBS solution and mounted with a coverslip. To obtain images for measuring the distance between the hyphal tip and lateral branches, samples were observed through a DIC 63 \times objective of a Nikon Eclipse 800 microscope equipped with a Pixera ProES600 camera and images were taken with Pixera software and processed with ImageJ (National Institutes of Health). The analysis of hyphal branching is further described in *SI Experimental Procedures*.

For fluorescence microscopy, equipment and imaging were as described previously (51). Deconvolution of fluorescence images used the iterative restoration algorithm in Velocity 3DM (Perkin-Elmer) and a calculated point spread function, and was carried out on z-stacks of more than 50 images with 0.2- μ m spacing, captured with a 100 \times NA 1.4 lens. Live-cell time-lapse microscopy was performed as described previously (11).

ACKNOWLEDGMENTS. The authors thank Erik Andreasson and Marit Lenman for invaluable assistance and advice on the analysis of phosphoproteins; Elisabeth Olsson, Jade Leiba, and Natalia Berges for excellent technical assistance; Paul Dyson and Katerina Petrickova for gifts of strains; and Keith Chater, Joe McCormick, and Nora Ausmees for critically reading the manuscript. This work was supported by postdoctoral stipends from the Carl Trygger Foundation (to S.C.) and Wenner-Gren Foundation (to S.-B.W.), John Innes Centre doctoral studentships (to A.M.H., J.L.P., and Y.-G.J.), Biotechnology and Biological Sciences Research Council Institute Strategic Programme Grant BB/J004561/1 (to M.J.B.), the John Innes Foundation (M.J.B.), Swedish Research Council Grants 621-2007-4767 and 621-2010-4463 (to K.F.), the O. E. och Edla Johansson Foundation (K.F.), and the Crafoord Foundation (K.F.).

- Nelson WJ (2003) Adaptation of core mechanisms to generate cell polarity. *Nature* 422:766–774.
- McCaffrey LM, Macara IG (2009) Widely conserved signaling pathways in the establishment of cell polarity. *Cold Spring Harb Perspect Biol* 1:a001370.
- Brown PJ, Kysela DT, Brun YV (2011) Polarity and the diversity of growth mechanisms in bacteria. *Semin Cell Dev Biol* 22:790–798.
- Brown PJ, et al. (2012) Polar growth in the Alphaproteobacterial order Rhizobiales. *Proc Natl Acad Sci USA* 109:1697–1701.
- Flårdh K (2010) Cell polarity and the control of apical growth in *Streptomyces*. *Curr Opin Microbiol* 13:758–765.
- Flårdh K, Buttner MJ (2009) *Streptomyces* morphogenetics: dissecting differentiation in a filamentous bacterium. *Nat Rev Microbiol* 7:36–49.
- Margolin W (2009) Sculpting the bacterial cell. *Curr Biol* 19:R812–R822.
- Cabeen MT, Jacobs-Wagner C (2010) The bacterial cytoskeleton. *Annu Rev Genet* 44:365–392.
- Heichlinger A, et al. (2011) The MreB-like protein Mbl of *Streptomyces coelicolor* A3 (2) depends on MreB for proper localization and contributes to spore wall synthesis. *J Bacteriol* 193:1533–1542.
- Flårdh K (2003) Essential role of DivIVA in polar growth and morphogenesis in *Streptomyces coelicolor* A3(2). *Mol Microbiol* 49:1523–1536.
- Hempel AM, Wang SB, Letek M, Gil JA, Flårdh K (2008) Assemblies of DivIVA mark sites for hyphal branching and can establish new zones of cell wall growth in *Streptomyces coelicolor*. *J Bacteriol* 190:7579–7583.
- Walshaw J, Gillespie MD, Kelemen GH (2010) A novel coiled-coil repeat variant in a class of bacterial cytoskeletal proteins. *J Struct Biol* 170:202–215.
- Moseley JB, Goode BL (2006) The yeast actin cytoskeleton: From cellular function to biochemical mechanism. *Microbiol Mol Biol Rev* 70:605–645.
- Richards DM, Hempel AM, Flårdh K, Buttner MJ, Howard M (2012) Mechanistic basis of branch-site selection in filamentous bacteria. *PLOS Comput Biol* 8:e1002423.

15. Lenarcic R, et al. (2009) Localisation of DivIVA by targeting to negatively curved membranes. *EMBO J* 28:2272–2282.
16. Ramamurthi KS, Losick R (2009) Negative membrane curvature as a cue for subcellular localization of a bacterial protein. *Proc Natl Acad Sci USA* 106:13541–13545.
17. Araujo-Palomares CL, Riquelme M, Castro-Longoria E (2009) The polarisome component SPA-2 localizes at the apex of *Neurospora crassa* and partially colocalizes with the Spitzenkörper. *Fungal Genet Biol* 46:551–563.
18. Harris SD (2008) Branching of fungal hyphae: Regulation, mechanisms and comparison with other branching systems. *Mycologia* 100:823–832.
19. Stock AM, Robinson VL, Goudreau PN (2000) Two-component signal transduction. *Annu Rev Biochem* 69:183–215.
20. Pereira SF, Goss L, Dworkin J (2011) Eukaryote-like serine/threonine kinases and phosphatases in bacteria. *Microbiol Mol Biol Rev* 75:192–212.
21. Shah IM, Laaberki MH, Popham DL, Dworkin J (2008) A eukaryotic-like Ser/Thr kinase signals bacteria to exit dormancy in response to peptidoglycan fragments. *Cell* 135:486–496.
22. Beilharz K, et al. (2012) Control of cell division in *Streptococcus pneumoniae* by the conserved Ser/Thr protein kinase StkP. *Proc Natl Acad Sci USA* 109:E905–E913.
23. Galperin MY, Higdon R, Kolker E (2010) Interplay of heritage and habitat in the distribution of bacterial signal transduction systems. *Mol Biosyst* 6:721–728.
24. Molle V, Kremer L (2010) Division and cell envelope regulation by Ser/Thr phosphorylation: *Mycobacterium* shows the way. *Mol Microbiol* 75:1064–1077.
25. Petricková K, Petricek M (2003) Eukaryotic-type protein kinases in *Streptomyces coelicolor*: Variations on a common theme. *Microbiology* 149:1609–1621.
26. Prsic S, et al. (2010) Extensive phosphorylation with overlapping specificity by *Mycobacterium tuberculosis* serine/threonine protein kinases. *Proc Natl Acad Sci USA* 107:7521–7526.
27. Parker JL, et al. (2010) Analysis of the phosphoproteome of the multicellular bacterium *Streptomyces coelicolor* A3(2) by protein/peptide fractionation, phosphopeptide enrichment and high-accuracy mass spectrometry. *Proteomics* 10:2486–2497.
28. Matsumoto A, Hong SK, Ishizuka H, Horinouchi S, Beppu T (1994) Phosphorylation of the AfsR protein involved in secondary metabolism in *Streptomyces* species by a eukaryotic-type protein kinase. *Gene* 146:47–56.
29. Stone KJ, Strominger JL (1971) Mechanism of action of bacitracin: complexation with metal ion and C 55 -isoprenyl pyrophosphate. *Proc Natl Acad Sci USA* 68:3223–3227.
30. Wang SB, et al. (2009) Domains involved in the *in vivo* function and oligomerization of apical growth determinant DivIVA in *Streptomyces coelicolor*. *FEMS Microbiol Lett* 297:101–109.
31. Hong HJ, Paget MS, Buttner MJ (2002) A signal transduction system in *Streptomyces coelicolor* that activates the expression of a putative cell wall glycan operon in response to vancomycin and other cell wall-specific antibiotics. *Mol Microbiol* 44:1199–1211.
32. Maestro B, et al. (2011) Recognition of peptidoglycan and β -lactam antibiotics by the extracellular domain of the Ser/Thr protein kinase StkP from *Streptococcus pneumoniae*. *FEBS Lett* 585:357–363.
33. Fiuza M, et al. (2008) The MurC ligase essential for peptidoglycan biosynthesis is regulated by the serine/threonine protein kinase PknA in *Corynebacterium glutamicum*. *J Biol Chem* 283:36553–36563.
34. Kang CM, et al. (2005) The *Mycobacterium tuberculosis* serine/threonine kinases PknA and PknB: substrate identification and regulation of cell shape. *Genes Dev* 19:1692–1704.
35. Schultz C, et al. (2009) Genetic and biochemical analysis of the serine/threonine protein kinases PknA, PknB, PknG and PknL of *Corynebacterium glutamicum*: Evidence for non-essentiality and for phosphorylation of OdhI and FtsZ by multiple kinases. *Mol Microbiol* 74:724–741.
36. Tomono A, et al. (2006) Self-activation of serine/threonine kinase AfsK on auto-phosphorylation at threonine-168. *J Antibiot (Tokyo)* 59:117–123.
37. Rajkarnikar A, Kwon HJ, Ryu YW, Suh JW (2007) Two threonine residues required for role of AfsK in controlling morphogenesis and avermectin production in *Streptomyces avermitilis*. *J Microbiol Biotechnol* 17:1563–1567.
38. Letek M, et al. (2008) DivIVA is required for polar growth in the MreB-lacking rod-shaped actinomycete *Corynebacterium glutamicum*. *J Bacteriol* 190:3283–3292.
39. Nguyen L, et al. (2007) Antigen 84, an effector of pleiomorphism in *Mycobacterium smegmatis*. *J Bacteriol* 189:7896–7910.
40. Oliva MA, et al. (2010) Features critical for membrane binding revealed by DivIVA crystal structure. *EMBO J* 29:1988–2001.
41. Shimi T, Butin-Israeli V, Adam SA, Goldman RD (2010) Nuclear lamins in cell regulation and disease. *Cold Spring Harb Symp Quant Biol* 75:525–531.
42. Fiuza M, et al. (2010) Phosphorylation of a novel cytoskeletal protein (RsmP) regulates rod-shaped morphology in *Corynebacterium glutamicum*. *J Biol Chem* 285:29387–29397.
43. Bramkamp M, et al. (2008) A novel component of the division-site selection system of *Bacillus subtilis* and a new mode of action for the division inhibitor MinCD. *Mol Microbiol* 70:1556–1569.
44. Eswaramoorthy P, et al. (2011) Cellular architecture mediates DivIVA ultrastructure and regulates Min activity in *Bacillus subtilis*. *mBio* 2:e00257-11.
45. Jani C, et al. (2010) Regulation of polar peptidoglycan biosynthesis by Wag31 phosphorylation in mycobacteria. *BMC Microbiol* 10:327.
46. Kang CM, Nyayapathy S, Lee JY, Suh JW, Husson RN (2008) Wag31, a homologue of the cell division protein DivIVA, regulates growth, morphology and polar cell wall synthesis in mycobacteria. *Microbiology* 154:725–735.
47. Tanaka A, Takano Y, Ohnishi Y, Horinouchi S (2007) AfsR recruits RNA polymerase to the *afsS* promoter: a model for transcriptional activation by SARPs. *J Mol Biol* 369:322–333.
48. Lee PC, Umeyama T, Horinouchi S (2002) *afsS* is a target of AfsR, a transcriptional factor with ATPase activity that globally controls secondary metabolism in *Streptomyces coelicolor* A3(2). *Mol Microbiol* 43:1413–1430.
49. Sambrook J, Russel DW (2001) *Molecular Cloning: A Laboratory Manual* (Cold Spring Harbor Laboratory Press, Cold Spring Harbor, NY), 3rd Ed.
50. Kieser T, Bibb MJ, Buttner MJ, Chater KF, Hopwood DA (2000) *Practical Streptomyces Genetics* (John Innes Foundation, Norwich, UK).
51. Salerno P, et al. (2009) One of the two genes encoding nucleoid-associated HU proteins in *Streptomyces coelicolor* is developmentally regulated and specifically involved in spore maturation. *J Bacteriol* 191:6489–6500.

Supporting Information

Hempel et al. 10.1073/pnas.1207409109

SI Experimental Procedures

Construction of *Streptomyces coelicolor* Kinase Mutants. STK mutants of *S. coelicolor* M600 were generated by replacing the entire coding sequence of individual genes (*SCO1468*, *SCO2110*, *SCO2244*, *SCO3102*, *SCO3821*, *SCO3848*, *SCO4507*, *SCO7240*), or pairs of adjacent genes (*SCO3820* and *SCO3821*, *SCO4487* and *SCO4488*), or five adjacent genes (*SCO4775*–*SCO4779*) with an apramycin-resistance cassette (*apr*) deriving from pIJ773, using the PCR-targeting method of Gust et al. (1). The double and triple mutants corresponding to the three PASTA domain-containing STK genes (*SCO2110*, *SCO3821*, and *SCO3848*) were built up by converting *apr*-marked mutations into in-frame deletions as described by Gust et al. (1), and then reusing the *apr* cassette to replace the next gene. All STK mutant strains were verified by PCR and by Southern blot hybridization.

Construction of Plasmids. Phusion DNA polymerase (Finnzymes) was used in PCR for construction of plasmids, and the inserts of constructed plasmids were confirmed by DNA sequencing. Oligonucleotide primers are listed in Table S2.

For complementation of the *afsK* mutant, *afsK* and the entire 217-bp intergenic region upstream of *afsK*, including the mapped transcription start site (2), was amplified by using the primers KF549, which introduced a SpeI restriction site, and KF547, allowing the amplified fragment to be digested and ligated into the EcoRV-SpeI-cut pMS82. The resulting plasmid, pKF256, was introduced into *S. coelicolor* strains by conjugation and integrated into the chromosome at the Φ BT1 attachment site.

To fuse AfsK to a fluorescent protein, the *afsK* gene, including the promoter region, was amplified using the primers KF547 and KF548, which introduced BamHI and NdeI restriction sites, and replaced the stop codon with four glycine codons. This PCR product was ligated into BamHI-NdeI-cut pKF210 resulting in an in-frame fusion of *afsK* with *mCherry* connected by a tetraglycine linker. The resulting plasmid, pKF255, was introduced into *S. coelicolor* strains by conjugation and integrated into the chromosome at the Φ C31 attachment site.

To create an *afsK* allele that would encode a constitutively active AfsK, site-directed mutagenesis was performed by using primers KF658 and KF659 and pIJ10551 as the template. Briefly, the primers led to amplification of the entire plasmid as a linear fragment incorporating the desired mutations (T165D and T168D), which were built into primers KF658 and KF659, respectively. The primers were phosphorylated before the PCR, and the PCR product was purified and religated. To create an inducible construct, the *afsK*(T165D,T168D) allele was cut out from the resulting plasmid, and subcloned into NdeI-EcoRI-cut pIJ6902, placing the *afsK*(T165D,T168D) allele directly downstream of the thiostrepton-inducible promoter *tipAp* (3). The resulting plasmid, pKF275, was introduced into *S. coelicolor* strains by conjugation and integrated into the chromosome at the Φ C31 attachment site.

Analysis of DivIVA Phosphorylation by Immunoprecipitation and Pro-Q Diamond Staining. The appropriate *S. coelicolor* strains were grown in yeast extract-malt extract medium for 15 to 22 h. For expression of *FLAG-divIVA* from the thiostrepton-inducible promoter *tipAp*, strains were grown in the presence of 0.1 μ g/mL of thiostrepton. Hyphae were harvested by centrifugation, washed twice in 10.3% (wt/vol) sucrose, and resuspended in appropriate buffer. Cell extracts were prepared in immunoprecipitation (IP) buffer (100 mM Tris-HCl, pH 8, 5% (vol/vol) glycerol, 50 mM sodium pyrophosphate, 1 mM sodium molybdate, 25 mM sodium

fluoride, 25 mM glycerophosphate, 15 mM EGTA, 5 mM EDTA, 150 mM NaCl, 1 mM PMSF, 10 μ M leupeptin, 1 nM calyculin A, 1 mM sodium orthovanadate). Cell lysates were prepared by sonication or by bead beating. After lysis, Triton X-100 was added to a final concentration of 1% (vol/vol) and cell lysates were cleared by centrifugation (16,000 \times g for 30 min at 4 $^{\circ}$ C) and, when appropriate, subsequent ultracentrifugation (100,000 \times g for 1 h at 4 $^{\circ}$ C). Protein concentrations were determined by using a Bio-Rad DC Kit.

The cleared cell lysates were used for IP essentially as described by Wang et al. (4). Briefly, pre-equilibrated anti-FLAG M2 affinity beads (Sigma-Aldrich) were mixed with equal amounts of total cell extracts and incubated from 1 h to overnight at 4 $^{\circ}$ C with gentle shaking. After three washes with IP buffer containing 1 M NaCl and then two with IP buffer containing 1 mM PMSF, bound proteins were eluted by boiling for 3 min in 2 \times elution buffer (125 mM Tris-HCl, pH 8, 4% (wt/vol) SDS, 20% (vol/vol) glycerol, 0.004% bromophenol blue). When appropriate, samples were dephosphorylated for 10 min at 30 $^{\circ}$ C by using lambda protein phosphatase (Sigma-Aldrich).

Eluted proteins were separated by SDS-PAGE, and phosphorylated proteins were detected by using Pro-Q Diamond phosphoprotein gel stain (Molecular Probes). Gels were fixed twice in 50% (vol/vol) methanol/10% (vol/vol) acetic acid for 30 min and then washed three times in ultrapure water for 10 min. Gels were stained for 60 to 90 min in the dark, then destained three times in 20% (vol/vol) acetonitrile/50 mM sodium acetate, pH 4.5, for 30 min before washing in ultrapure water. Phosphorylated species were visualized by using a Typhoon 9410 Scanner (GE Healthcare) or FLA-7000 system (Fujifilm) in fluorescence mode. Subsequently, the gels were also stained with Coomassie brilliant blue.

MS. Cell extraction and IP were performed as described earlier, except that Tris-buffered saline solution (25 mM Tris-HCl, pH 8, 150 mM NaCl) supplemented with complete EDTA-free protease inhibitor mixture (Roche) was used as the buffer, and bound proteins were eluted from the M2 beads by competition with 150 ng/mL 3 \times FLAG peptide (Sigma-Aldrich) in Tris-buffered saline solution containing 1% (vol/vol) Triton X-100 for 1 h at 4 $^{\circ}$ C with gentle rotation. The immunoprecipitated DivIVA was digested for 10 min at 37 $^{\circ}$ C in a vortex shaker by using magnetic trypsin beads (Clontech). Without desalting or other concentration steps, the resulting digest was mixed 1:1 with a saturated matrix solution of sinapinic acid (Fluka) in 30% (vol/vol) acetonitrile, 0.1% TFA, and 1 μ L was spotted onto a polished stainless steel MALDI target and air dried. A portion of digest was also dephosphorylated for 1 h at 37 $^{\circ}$ C by using glycerol-free calf intestinal alkaline phosphatase (NEB) and analyzed similarly. CocrySTALLIZED spots of matrix and sample were washed briefly (<5 s) on the MALDI target when necessary by using 10 mM ammonium phosphate, 0.1% TFA before analysis. Myoglobin was used for calibration.

MALDI-TOF MS was carried out on an UltraFlex MALDI-TOF/TOF mass spectrometer (Bruker) in linear positive ionization mode by using a 337-nm pulsed nitrogen laser with a 50-Hz repetition rate. The source voltage (IS1) was set to 25 kV, with IS2 at 23.4 kV, pulsed ion extraction delay at 80 ns, and deflection of ions <1,000. Linear detector voltage was 1.65 kV, and 800 shots were collected per spectrum.

Analysis of Hyphal Branching Patterns. As described in more detail in elsewhere (5), it is important when measuring tip-to-branch

Constitutively active AfsK
(T165D, T168D)

Empty vector

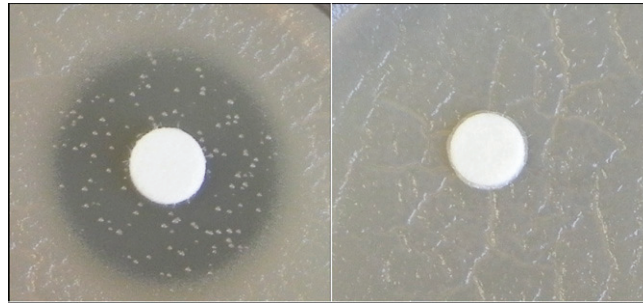


Fig. S3. Inhibition of growth caused by induced expression of the *afsK*(T165D, T168D) allele. Spores of two bacterial strains were spread evenly on TSB agar plates containing apramycin to maintain selection for the integrated plasmids. The strains were derivatives of *S. coelicolor* strain M600 carrying plasmids integrated at the ϕ C31 *attB* site with the thiostrepton-inducible promoter driving expression of constitutively active AfsK (strain K335) or a control strain with empty vector (strain K336). A sterile paper disk was soaked with 15 μ L of 0.1 mg/mL thiostrepton dissolved in DMSO. Plates were incubated at 30 °C for 2 d and then photographed. The clearing zone around the disk (*Left*) demonstrates that induced expression of the constitutively active AfsK kinase inhibits growth.

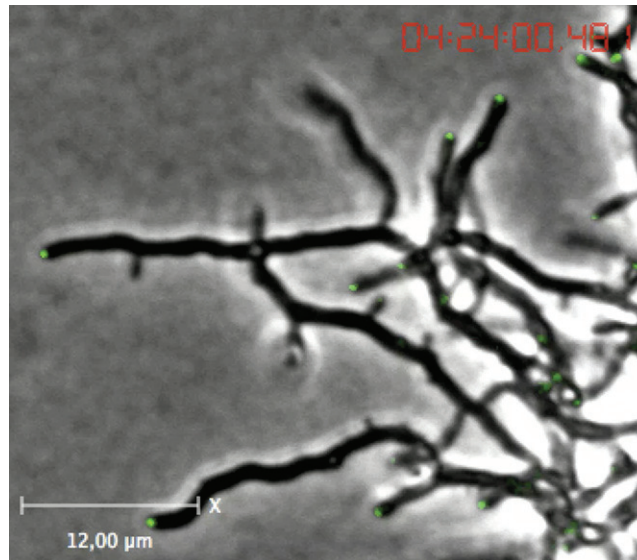
Table S2. Oligonucleotide primers used in this study

Primer	Sequence*	Introduced restriction site
afsK		
Forward	AAAAACATatggtggatcagctgacg	NdeI
Reverse	TTTTTAAGCTTtcacgtcgtacgggc	HindIII
KF547	CTGGTTAACCGGATCCcccggcgccacggcgccgac	BamHI
KF548	GGAATTCATAT GCCGCCGCCCG cgtcgtacggcggtccccgt [†]	NdeI
KF549	TGGTTAACCACTAGttcacgtcgtacggcggtccccgt	SpeI
KF658	CTGGACATGACGAACGTCGCCG [‡]	—
KF659	ACGGTCGTTTCGAGACGCCGG [‡]	—
VM712	TATGGATCCgtggtggatcagctgacgcagcac	BamHI
VM739	TATAAGCTTtcacggcgcccgccggtggtggc	HindIII
VM748	TATGGATCCatgcccgttgacccccgaggac	BamHI
VM749	TATAAGCTTtcagttgctcctcgtcgat	HindIII

*Sequence matching the template is shown in lowercase, whereas added or changed nucleotides in the 5'-ends of oligonucleotides that did not correspond to the template are shown in capitals. Added restriction sites are underlined.

[†]In bold is a sequence added to incorporate a four-glycine linker region in the recombinant AfsK-mCherry.

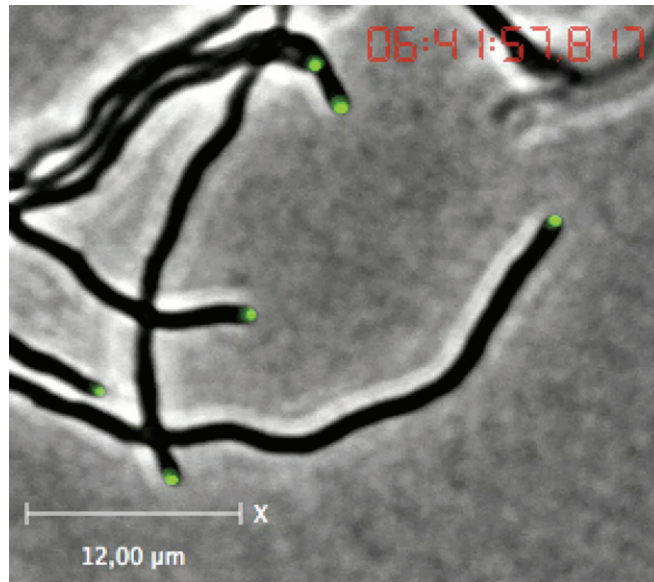
[‡]The specific point mutations that were introduced are underlined in the primer sequences. They gave rise to the *afsK* mutations T168D and T165D, respectively.



Movie S1. Time-lapse imaging of *S. coelicolor afsK*⁺ strain K325. Hyphae were grown on agarose pads, and images were captured every 6 min as described previously (1). Fluorescence signals from DivIVA-EGFP are shown overlaid on the phase-contrast images. (Scale bar, 12 μm.)

[Movie S1](#)

- Hempel AM, Wang SB, Letek M, Gil JA, Flärdh K (2008) Assemblies of DivIVA mark sites for hyphal branching and can establish new zones of cell wall growth in *Streptomyces coelicolor*. *J Bacteriol* 190:7579–7583.



Movie S2. Time-lapse imaging of *S. coelicolor* *afsK* mutant strain K324. Hyphae were grown on agarose pads, and images were captured every 6 min as described previously (1). Fluorescence signals from DivIVA-EGFP are shown overlaid on the phase-contrast images. (Scale bar, 12 μ m.)

[Movie S2](#)

1. Hempel AM, Wang SB, Letek M, Gil JA, Flårdh K (2008) Assemblies of DivIVA mark sites for hyphal branching and can establish new zones of cell wall growth in *Streptomyces coelicolor*. *J Bacteriol* 190:7579–7583.